Western Graduate&PostdoctoralStudies

Electronic Thesis and Dissertation Repository

10-23-2018 2:00 PM

# Spectral and Energy Efficient Communication Systems and Networks

Abdulbaset Hamed, *The University of Western Ontario*

Follow this and additional works at: https://ir.lib.uwo.ca/etd

 Part of the Power and Energy Commons, and the Systems and Communications Commons

# Abstract

In this thesis, design and analysis of energy- and spectral-efficient communication and cellular systems in micro wave and millimeter wave bands are considered using the following system performance metrics: $i$) Energy efficiency; $ii$) Spectral efficiency; $iii$) Spatial spectral efficiency; $iv$) Spatial energy efficiency, and $v$) Bit error rate. Statistical channel distributions, Nakagami-$m$ and Generalized-$K$, and path loss models, Line of Sight (LOS) and Non-Line of Sight (NLOS), are used to represent the propagation environment in these systems. Adaptive $M$-QAM and $M$-CPFSK communication systems are proposed to enhance their efficiency metrics as a function of Signal-to-Noise Ratio (SNR) over the channel. It is observed that in the adaptive $M$-QAM system energy efficiency can be improved by 0.214 bits/J whereas its spectral efficiency can be enhanced by 40%, for wide range of SNR compared to that of conventional $M$-QAM system. In case of adaptive $M$-CPFSK system, spectral and energy efficiencies can be increased by 33% and 76%, respectively. A framework for design and analysis of a cellular system, with omni and sectorized antenna systems at Base Station (BS), using its efficiency metrics and coverage probability is presented assuming wireless channel is Nakagami-$m$ fading coupled with path loss and co-channel interference. It is noted that sectorized antenna system at BS enhances energy and spectral efficiencies by nearly 109% and 1.5 bits/s/Hz, respectively, compared to conventional omni antenna system. A Multi-User MIMO cellular system is then investigated and closed-form expressions for its uplink efficiency metrics are derived for fading and shadowing wireless channel environment. It is observed that increasing number of antennas in MIMO system at BS can significantly improve efficiency metrics of cellular system. Finally, a framework for design and analysis of dense mmWave cellular system, in 28 and 73 GHz bands, is presented for efficient utilization of spectrum

and power of the system. The efficiency metrics of the system are evaluated for LOS and NLOS links. It is observed that while 28 GHz band is expedient for indoor cellular systems, the 73 GHz band is appropriate for outdoor systems.

# Acknowledgements

All the praises, and foremost thanks are due to Allah for being my refuge and strength's source in time of ease and hardship. Without His guidance and blessings, nothing is possible.

I would like to express my deep appreciation to my thesis supervisor Dr. Raveendra Rao. His office door is always open for discussion, encouragement, insightful guidance, consistent support, invaluable advice, and constructive criticism.

I would also like to show my sincere gratitude and deep thanks to my mother, my wife, my siblings and my children. Their dua'a, support, encouragement, smile, and countless sacrifice are the basis of my continuing personal development.

# Dedication

*To the Soul of my Father and To the Dear Mother*

*In memory of Dr. Mohamed Almosrati and Dr. Hasein Sigiuk*

# Table of Contents

# List of Figures

# List of Tables

# List of Acronyms

| | |
|---|---|
| **3GPP** | $3^{rd}$ Generation Partnership Project |
| **AWGN** | Additive White Gaussian Noise |
| **BER** | Bit Error Rate |
| **BS** | Base Station |
| **BW** | Bandwidth |
| **CAGR** | Compound Annual Growth Rate |
| **CO$_2$** | Carbon Dioxide |
| **CO$_{2e}$** | Carbon Dioxide equivalent emissions |
| **CPM** | Continuous Phase Modulation |
| $M$**-CPFSK** | $M$-ary Continuous Phase Frequency Shift Keying |
| **CSI** | Channel Side Information |
| **EARTH** | Energy Aware Radio and neTwork tecHnologies |
| **ECONET** | low Energy COnsumption NETworks |
| **EE** | Energy Efficiency |
| **FDMA** | Frequency Division Multiple Access |
| **FP7** | Seventh Framework Programme |
| **IoT** | Internet of Things |
| **IPCC** | International Panel on Climate Change |
| **IR-UWB** | Impulse Radio-Ultra Wide Band |

| | |
|---|---|
| **ITU** | International Telecommunication Union |
| **LMDS** | Local Multi-point Distribution System |
| **LOS** | Line of Sight |
| **M2M** | Machine-to-Machine |
| **MGF** | Moment Generation Function |
| **MIMO** | Multi Input Multi Output |
| **MMSE** | Minimum Mean Square Error |
| **mmWave** | millimeter Wave |
| $\mu$**Wave** | micro Wave |
| **MRC** | Maximal Ratio Combining |
| **MU** | Mobile User |
| **MU-MIMO** | Multi User Multi Input Multi Output |
| **NLOS** | Non Line of Sight |
| **PP** | Power Penalty |
| **PPP** | Poisson Point Processes |
| **QoS** | Quality of Service |
| **SE** | Spectral Efficiency |
| **SEE** | Spatial Energy Efficiency |
| **SSE** | Spatial Spectral Efficiency |
| **SNR** | Signal to Noise Ratio |
| **SINR** | Signal to Noise plus Interference Ratio |
| **SISO** | Single Input Single Output |

*List of Tables*

**TDMA**          Time Division Multiple Access

**UHDV**          Ultra High Definition Video

**ZF**            Zero Forcing

# List of Symbols

| | |
|---|---|
| $\mathbb{E}$ | Expected value |
| $m$ | fading figure |
| $c$ | Shadowing figure |
| $\upsilon$ | Path loss exponent |
| $d$ | User's distance |
| $\lambda$ | Wave length |
| $\sigma_s^2$ | Shadowing variance |
| $\varepsilon$ | Roll-off factor |
| $P(n)$ | probability of estimated SNR |
| $\gamma_n$ | SNR boundaries |
| $N$ | Number of adaptive regions |
| $M$ | Constellation size |
| $\widehat{\mathbb{M}}$ | Truncated Moment generation function |
| $\mathbb{M}$ | Moment generation function |
| $P_M(\epsilon\|\gamma)$ | Probability of error for AWGN |
| $P_{M,A}(\epsilon)$ | Average probability of error |
| $R_n$ | Adaptive Region |
| $\gamma$ | Instantaneous SNR |
| $\overline{\gamma}$ | Average SNR |

| | |
|---|---|
| $P_o$ | Outage probability |
| $E_s$ | Symbol energy |
| $T_s$ | Symbol duration |
| $f_c$ | carrier frequency |
| $\phi_o$ | Starting signal phase |
| $\theta$ | User's angle |
| $h$ | Modulation index |
| $\rho(l,j)$ | Normalized correlation coefficient |
| $n$ | Observation length |
| $I$ | Number of small cells |
| $J$ | Number of base stations |
| $K$ | Number of mobile users |
| $P_i$ | BS transmitted power |
| $NF$ | Noise figure |
| $\varrho$ | Propagation environment density |
| $l_t$ | Transmitter antenna length |
| $l_r$ | Receiver antenna length |
| $P_c$ | Circuit power |
| $P_t$ | Total power |
| $\mathcal{M}$ | Antenna array size |
| $R$ | Cell radius |
| $\eta_S$ | Bounds on spectral efficiency |

| | |
|---|---|
| $\eta_E$ | Bounds on energy efficiency |
| $\eta_{S_M}$ | Spectral efficiency for modulation system |
| $\eta_{E_M}$ | Energy efficiency for modulation system |
| $BT_s$ | Normalized Bandwidth |
| $N_o$ | Noise power spectral density |
| $D$ | Reuse distance |
| $A_{aff}$ | Affected area |
| $\alpha$ | Channel gain |
| $D_k$ | Transmission delay per bit |
| $Q_k$ | Quantity of information |
| $P_{cov}$ | Coverage probability |

# Chapter 1

# Introduction to Thesis

## 1.1 Wireless Communication and Cellular Systems

Wireless communications is one of the most rapidly growing industries on the globe in the $21^{st}$ century, and indications are that this trend will continue. Since it comprises of a large variety of devices, applications and services, it has become an essential part of our daily lives. The large scale development of portable communication devices provides users with the ability to communicate from anywhere to anywhere on the globe at anytime. The telecommunication industry is perhaps one of the largest industries worldwide with more than $ 1 trillion in annual revenues for service and equipment. In the last decade, the Internet has been extended to include wireless users and connections; such as users of smart phones, tablets, laptops etc. connecting to the Internet. The Internet of Things (IoT) paradigm is the trend in the coming years, which means most electronic devices will be connected to the Internet using wired/wireless communication technology. The expected number of IoT connected devices is likely to be 36 billion by the year 2021 [1]. Machine-to-Machine (M2M) communication is also rapidly growing and is expected to grow much more rapidly than the mobile devices. Optimistic predictions envision 3.3 billion connected devices by the year 2021 [1]. Despite low activity level and small

capacity required per device per link, the overall traffic and power consumption are going to be considerable due to huge number of devices connected to the system. This requires more bandwidth and results in more power consumption. A study of expected number of mobile devices and the associated growth of data traffic for 2016-2021 shows that globally the number of mobile devices has increased by almost half a billion in 2016 compared to the number of mobile devices in 2015 [2]. Also, the study mentions that the number of mobile devices is expected to rise to 8.4 billion by the year 2021, at 47% of Compound Annual Growth Rate (CAGR). Figure 1.1 [2] shows that the growth in the number of mobile devices is linearly increasing at the rate of about 1 billion devices per year. Mobile operators have predicated that the mobile data traffic is doubled every year
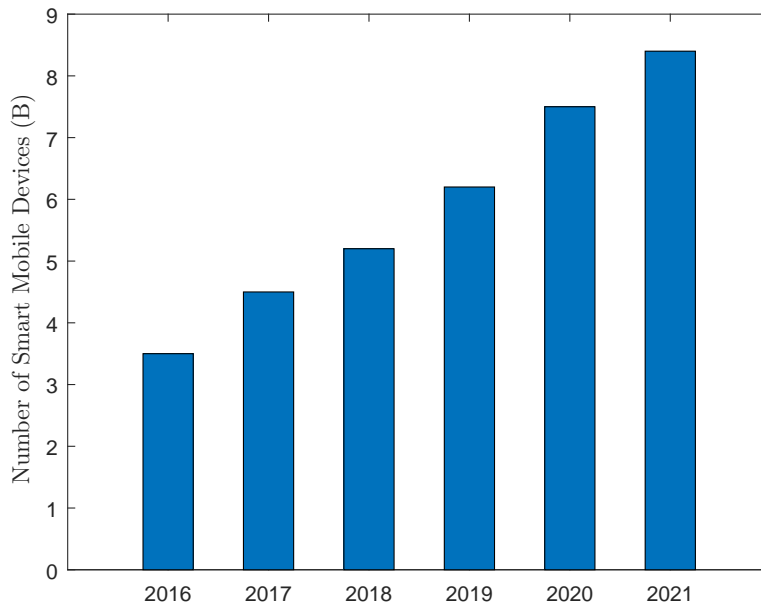


**Figure 1.1:** Global growth of smart mobile devices [2]

and in 2030 it is likely to increase 1000 times the traffic in 2011 [3]. The study in [2] indicates that the global mobile data traffic grew 63% in 2016 and reached 7.2 Exabytes

($2^{60}$ bytes) per month, and is expected to increase by seven folds between 2016 and 2021.

The predictions of global mobile data traffic for 2016 to 2021 are shown in Figure 1.2 [2],
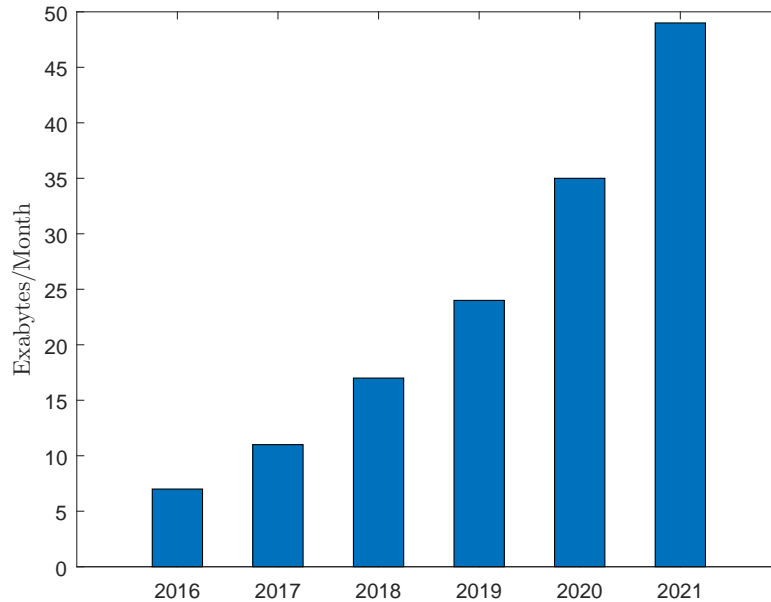


**Figure 1.2:** Global smarthphone data traffic forecast [3]

which shows that the traffic increases exponentially and is expected to reach 49 Exabytes per month in 2021. As a result of adding more and more new mobile devices and the increasing demand for data traffic, a huge expansion of the existing wireless system is inevitable. A study on infrastructure for future cellular systems [4] reported that in 2021 the number of macrocells will grow by 10% while the number of small cells in the cellular system will increase 10 times compared with data of 2016. The design and analysis of next generation of communication and cellular systems, with increasing number of mobile devices and data traffic, poses a serious challenge for engineers and system designers and requires careful considerations of system resources.

## 1.2 Conflicting System Resources: Energy and Bandwidth

As the number of mobile users and the demand for mobile services continue to increase, it is important to design systems that are efficient, reliable and offer high quality services. The mobile operators, therefore, have to fulfill certain requirements such as sufficient cellular system coverage, capacity, and reliable high speed connections. One way is to increase the number of cells in the system by splitting each cell into number of smaller cells and by increasing the frequency reuse factor in the system. However, this will increases the number of Base Stations (BSs) and hence will increase the energy consumption and complexity of the system. Study in [5] reported that the majority of increase in energy consumption is at BSs in a cellular system and about 50% of it is used for signal transmission and processing. Also, it has been noted that consumption of energy at BSs increases linearly with number of antennas and operating bandwidth. In order to meet expected demand for large traffic in cellular systems, spectral resource needs to be assigned appropriately. However, this is a limited resource which makes mobile users' plans expensive. Thus, improving system spectral efficiency is a method to increase user data rate. This can be done by using bandwidth efficient modulation techniques and MIMO systems at BSs. Shannan's formula predicts that increasing the spectral efficiency from 4 bit/s/Hz to 8 bit/s/Hz requires nearly 17 times more power. Consequently, a price has to be paid in terms of energy consumption of the system, which constitutes a considerable increase in the global power consumption. It is predicated that the annual increase in electrical energy consumption by communication and cellular systems is exponential in

nature for the next few decades [6], [7]. As shown in Figure 1.3, the global electricity usage of communication technology is estimated to be about 7500 TWh in 2022 which could use as much as 25% of global electricity generation. The ecological impact of
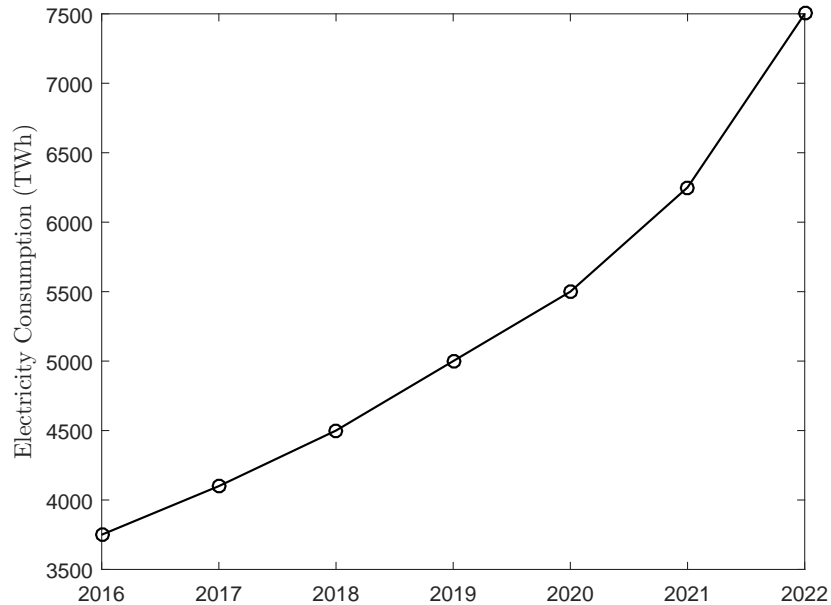


**Figure 1.3:** Global electricity demand of communication systems [8]

power consumption by communication and cellular systems has attracted the attention of environmental organizations and governments and are enforcing regulations on global energy consumption. International Panel on Climate Change (IPCC), in this context, specifies overall carbon footprint measured in $CO_2$ equivalent ($CO_2e$) emissions [9]. The estimated carbon footprint of global mobile communication systems is depicted in Figure 1.4 for the years 2014-2021. A major observation is that overall gas emissions increase linearly at the rate of 11 $CO_2e$ M ton/year, which is equivalent to carbon footprint per average mobile user of nearly 30 Kg of $CO_2e$ in 2021. In the worst case, electricity usage of communication systems could contribute up to 20% of the global greenhouse gas
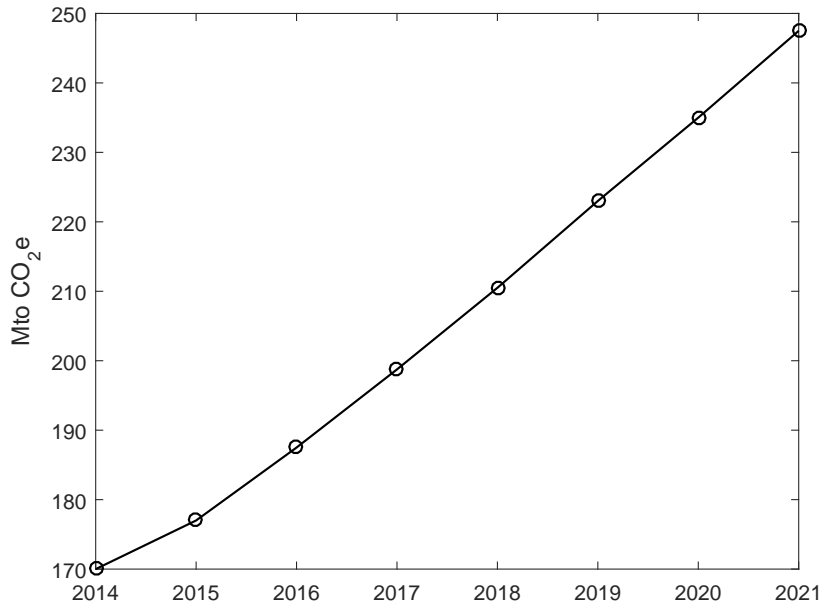
**Figure 1.4:** Global carbon footprint of communication systems [10]

emissions in the next decade [8]. The cost of energy and bandwidth determines financial

bottom line for wireless services providers. Conservative estimates are that cost of global

wireless services will increase for many years to come [11], [12]. International bodies have

addressed these issues and have introduced energy saving concepts for communication

and cellular systems. International Telecommunication Union (ITU), for example, issued

resolution ITU-R-60-1 in 2015 for reduction in energy consumption for environmental pro-

tection and to mitigate climate change [13]. Also, $3^{rd}$ Generation Partnership Project

(3GPP) has produced a technical report 3GPP TR 32.826 for energy management to

reduce energy consumption in cellular systems [14]. Recommendations in these reports

pose a big challenge for communication and cellular system researchers and engineers to

focus on design and implementation of energy- and spectral-efficient systems, not only

to save energy, but also to meet global warming standards and to maintain sustainable

development.

## 1.3   Literature Survey and Motivations for the Thesis

The intent of this thesis is to introduce a comprehensive framework for design and analysis of energy- and spectral-efficient communication and cellular systems. The framework includes investigation of systems using metrics such as Energy Efficiency (EE), Spectral Efficiency (SE), Spatial Spectral Efficiency (SSE), Spatial Energy Efficiency (SEE), Bit Error Rate (BER), coverage probability, outage probability and system latency. In particular the following systems are considered: $i$) $M$-QAM and $M$-CPFSK communication systems; $ii$) hexagonal cellular system with several antenna configurations at BS; $iii$) mmWave cellular systems in 28 and 73 GHz bands; $iv$) Multi-Users Multiple Input Multiple Output (MU-MIMO) system at BS in cellular systems. The impact of propagation environment on efficiency metrics are examined and suggestions are offered for efficient design of communication and cellular systems.

### 1.3.1   SE and EE Metrics of a Communication System

The SE metric is a critical performance metric of any Digital Communication System (DCS), and its EE metric can be used to measure energy usage in the system. The SE metric is defined as the maximum achievable data rate over a given channel bandwidth while maintaining an arbitrarily low probability of BER, without any delay or complexity

constraints [15]. Therefore, it represents an upper bound for practical communication systems. Until recently, researchers have used SE as a metric for optimum design of communication systems. The main concern has been to improve spectral efficiency of a DCS. A space-time signal processing technique is used in a multi-element antenna array system to enhance SE of a DCS [16]. Communication coordination is another method that can be used to minimize out-of-cell interference and hence can be used to increase SE of a cellular system [17]. To boost SE in harsh propagation environment, such as multipath fading and shadowing channel, Channel State Information (CSI) is often used at transmitter/receiver. Power adaptation strategy is proposed in [18] and [19] to increase this efficiency metric. The modulation technique has been conventionally used for design of spectrally efficient communication system. The SE metric is examined for multi-level and multi-phase modulation for a Discrete Memoryless Channel (DMC) in [20]. A bound on SE for $M$-ary digital modulations over an Additive White Gaussian Noise (AWGN) channel is examined using the Shannon's capacity formula for an $N$-dimensional signal set in [21]. The SE metric of an $M$-QAM system is investigated in [22] for land mobile propagation environment. Performance and implementation of spectrally efficient modulation techniques are summarized in [23].

It is also important to efficiently utilize the energy resource of a DCS. The fundamentals of energy efficient transmission for a point-to-point link can be traced back to [24], where EE metric is defined as number of *bits-per-Joule* of energy. The performance metrics of a DCS such as SE and BER are functions of SNR and depend on transmitted signal power. Due to recent government regulations, it has become mandatory to reduce energy consumption of a communication system and hence EE metric has become a key

performance metric in the design of such a system. Maximizing both EE and SE of a DCS is a conflicting objective which implies the existence of trade-off between EE and SE metrics of the system. A study of these metrics for a communication system is presented in [25] for an AWGN channel. The EE-SE trade-off is introduced for a wideband power-limited communication system in [26]. It is shown that it is possible to obtain analytically a fundamental limit on EE metric for a class of additive noise channels for a wideband signal with SE low but nonzero. For a point-to-point communication link, the trade-off between SE and EE metrics over a fading channel is examined in [27], where a power model used consists of fixed circuit power, $P_c$, and transmit power, $P_t$, a function of efficiency of power amplifier in the system. It is shown that SE-EE trade-off curve is steeper; hence, a small sacrifice in EE leads to significant gain in SE metric. An approximate closed-form expression has been derived in [28] to examine EE-SE trade-off for Single Input Single Output (SISO) communication system for a Rayleigh flat fading channel . It is shown that this expression is quite accurate for a wide range of SNR and SE metric values. The primary goal of the study is to examine in depth the trade-off between SE and EE metrics and provide general perspectives on efficient design of communication systems, particularly, over fading and shadowing channels with path losses and interferences. Since modulation is an essential part of any communication system, its design and analysis should be based on EE and SE metrics for a given modulation used in the system. These metrics for an $M$-QAM system are presented in [29] for an AWGN channel. It is shown that the system achieves maximum EE for specific regions of SNR for each constellation size, $M$, used in the system. The SE and EE metrics for an $M$-ary Continuous Phase Frequency Shift Keying ($M$-CPFSK) are presented in [30], where a

simple approximation for SE is given and is shown to be sufficiently accurate and can be used for design of efficient $M$-CPFSK system. General expression for SE of Continuous Phase Modulation (CPM) is given in [31], and is used for analysis of a multi-user system that uses CPM considering the inter-channel interference and channel spacing. The SE and EE metrics of $M$-CPFSK system are discussed in [32] as a function of system parameters such as modulation index, alphabet size and bandwidth. The channel is assumed to be conventional AWGN, and EE metric is not addressed in the design of the system. However, it is important to consider both SE and EE metrics in the design and analysis of $M$-CPFSK system, particularly over fading and shadowing communication channels, as they are the most frequently occurring channels in practice.

## 1.3.2 SE and EE Metrics of a Cellular System

The ever increasing demand for a variety of mobile communication systems and services has resulted in huge expansion of existing cellular network infrastructure. This in turn has resulted in a huge increase in energy consumption, particularly at BSs which are regarded as huge contributers to total energy consumption of a cellular system. In order to control this high consumption of energy, strict regulations have been imposed. This has necessitated energy-efficient designs of cellular systems. Towards this goal, European Commission has initiated projects such as Seventh Framework Programme (FP7) that include Energy Aware Radio and neTwork tecHnologies (EARTH) and low Energy COnsumption NETworks (ECONET) [33]. These projects are aimed at integrating activities of manufacturers, operators, and research centers, to quantitatively assess energy

demand of current and future telecommunication infrastructure, and to come up with energy-efficient, scalable and sustainable cellular systems for the future. Thus, many researches are motivated to study spectral- and energy-efficient communication and cellular systems. Fundamental trade-offs among system performance metrics for energy-efficient design of cellular systems are investigated in [34]. The trade-offs considered include deployment vs. EE, SE vs. EE, bandwidth vs. energy and delay vs. power. The impact of BS deployment strategies on EE of a cellular system is investigated in [35], by introducing the concept of area power efficiency of the system. Energy-efficient deployment strategy subject to coverage performance constraints has been investigated for both homogeneous and heterogeneous cellular systems in [36]. The SE and EE metrics of a cellular system are examined for a simple interference model and Rayleigh fading environment in [37]. A theoretical framework for studying SE vs. EE trade-off in a cellular system is proposed in [38], which is based on optimal allocation of BS transmit power and bandwidth. The framework can be used to evaluate EE metric for single- and multi-cell cellular systems. In [39], a new technique is presented to study SE vs. EE trade-off in a cellular system. This technique has been applied to Orthogonal Frequency Division Multiple Access (OFDMA) system, and it is shown that good balance can be achieved between consumption of power and bandwidth of the system. The trade-off between SE and EE for an interference limited wireless system using an optimal power allocation algorithm is examined in [40], as a function of circuit power, $P_c$, in log-normal shadowing channel [41]. The relationship between SE and EE metrics is evaluated by first obtaining a parametric expression for Signal-to-Interference plus Noise Ratio (SINR), and then using Monte-Carlo simulation technique. The relationship between SE and EE metrics for a

Poisson Point Process (PPP) in a cellular system is presented using standard stochastic geometry tools for a variety of multiple access technologies such as Time Division Multiple Access (TDMA), Frequency Division Multiple Access (FDMA) etc. in [42]. Besides SE and EE metrics, SSE and SEE metrics are being considered, in recent years, in the design of efficient cellular systems [43]. These spatial efficiency metrics have been used to investigate performance of a hierarchical cellular system in [44]. The metrics SSE and SEE are analyzed in [45] for a cellular system in Rayleigh fading channel. However, these efficiency metrics are not thoroughly investigated in literature for propagation environment with path loss, co-channel interference, fading and shadowing effects that are typical in a cellular system.

### 1.3.3   SE and EE Metrics of a MU-MIMO Cellular System

The MIMO-based communication system can significantly increase throughput, EE and reliability compared to a SISO system and hence is a promising technology for application in the next generation of cellular systems [46]. An MU-MIMO system at BS has the potential to realize promising benefits of MIMO system and hence has gained considerable attention and is proposed for next generation cellular systems such as $5G$ and LTE [47]. In such an MU-MIMO cellular system, BSs are equipped with a large number of antennas to serve simultaneously a number of users that share the same channel. Recently, considerable attention has been paid to a very large MU-MIMO system at BS in a multi-cell cellular system, in which a large number of antennas are used at BS receiver to significantly diminish effects of co-channel interference and fading over

the channel [48]. Such a technique can enhance EE and SE metrics of the system by reducing BS power. The MU-MIMO system at BS is examined in [49], and it is shown that increasing number of antennas in the system is beneficial in increasing considerable improvement in SE metric of the system, even for low values of SINR, for $\mathcal{M} \geq 16$, where $\mathcal{M}$ is number of antennas at BS. Such a system is proposed and examined in [50], where an MRC diversity technique is used at BS for combining signals received from users. The SEs of both uplink and downlink are examined as the number of antennas at BS approach infinity. The uplink throughput and EE metric of a large MU-MIMO system at BS are evaluated using Zero Forcing (ZF) receiver, for both perfect and imperfect CSI in [51]. It is shown that user's transmitted power in the system can be scaled by a factor of $1/\sqrt{\mathcal{M}}$ and $1/\mathcal{M}$ for $\mathcal{M}/K_i \geq 6$, for perfect and imperfect CSI, respectively, where $K_i$ is number of users in the system. The trade-off between uplink EE and SE metrics for this system is studied in [52], for a variety of detection techniques. Also, linear precoding and transmit antenna selection [53] are considered using a power consumption model and large-scale fading over the channel. An expression for downlink SE metric of an MU-MIMO system with beamforming ZF receiver for random number of users in a cell is derived in [54] for a Rayleigh fading and shadowing composite channel. When the channel impairments and co-channel interference exist, MU-MIMO system at BS is more practical and realistic in nature. However, when channel fading and shadowing exist, the performance evaluation of system metrics are quite complex and typically MGF technique is used to simplify their evaluation. In [55], downlink SE and EE metrics of an MU-MIMO system with finite number of antennas at BS are investigated for a single cell scenario, assuming perfect CSI for Rayleigh fast-fading channel. In [53], downlink SE and EE metrics of such a system

13

are examined for multi-cell scenario using MRC and ZF receivers, assuming number of antennas at BS is large. In [56], SE metrics of single- and a multi-cell distributed MU-MIMO system are examined for ZF receivers, for small-scale and large-scale fading channels with path loss. The efficiency metrics of MU-MIMO system at BS in a cellular system are not throughly investigated for fading and shadowing channel with path loss and co-channel interference. Thus, it is important to examine system metrics in presence of fading and shadowing over the channel coupled with cochannel interference due to inter- and intra-cell radiations. In this thesis, a gamma-gamma distribution is used to model fading and shadowing over the channel.

## 1.3.4 SE and EE Metrics of a mmWave Cellular System

The mmWave spectrum is known to offer tremendous bandwidth and can be utilized to meet not only the ever increasing demand for high data rate services, but also to accommodate a large number of users. This spectrum is also a serious contender for Ultra High Definition Video (UHDV) transmission. Several well-known cellular system standards such as ECMA-387, IEEE 802.11ad and IEEE 802.15.3c are being redefined to fit this spectrum. Despite the massive bandwidth potential in mmWave band, there exist a number of challenges: $i$) modelling and characterization of propagation environment; $ii$) design of antenna system; $iii$) transceiver integration; and $iv$) Digital Signal Processing (DSP) technology. The mmWave bands suffer from high path loss and hence techniques are required to enhance power received at receiver in the system. The modelling of propagation environment in mmWave band plays an important role in the design and analysis

of communication and cellular systems. In [57], characteristics of mmWave propagation environment are studied and it is observed that some bands in this spectrum offer lower delay spread and therefore it is possible to effectively suppress Inter-Symbol Interference (ISI) in these bands. Wells [58] has shown that 28 GHz and 73 GHz bands are the most natural choices for deployment in mmWave spectrum. Also, 28 GHz band is being actively pursued for Local Multi-point Distribution System (LMDS) and is very attractive for use in mmWave cellular system, although this band occupies relatively lower range of frequencies within mmWave spectrum. In recent years, there have been many efforts to accurately model mmWave channel for LOS and NLOS transmission links. The communication industry has devoted extensive resources to development of accurate channel models. For instance, Samsung conducted channel measurements in 28 GHz band and came up with a model to fit ITU-R and FITU-R standards [59]. This model can be used for a mmWave communication link over distances of up to 200 meters. In addition, Nokia, Huewei and Deutsch Telekom have shown keen interest in 73 GHz band and have developed prototype hardware using Multiple Input Multiple Output (MIMO) system to support throughput of up to 20 Gbps. A channel model based on stochastic path loss has been studied for urban propagation environment in [60]. A spatial statistical model of mmWave channel has been developed as a function of channel parameters, including path loss, in [61]. This model has been derived based on measurements in New York City in 28 and 78 GHz bands for LOS and NLOS links. A general framework has been proposed for evaluation of coverage probability and BER metrics of a mmWave cellular system in [62]. The short wave length of mmWave signals can accommodate a very large number of antennas at receiver and at transmitter, which makes beamforming a key

15

enabler technology in obtaining high antenna gain. Beamforming antenna systems for mmWave bands have been studied for 5G cellular system and a novel hybrid beamforming algorithm is proposed for indoor and outdoor transmission links in [63]. The design and implementation of mmWave antennas for wireless links are discussed in [64], [65]. Also, Madhow has addressed opportunities and challenges of utilizing MIMO system in LOS mmWave communications. An overview of Impulse Radio-Ultra Wide Band (IR-UWB) technology for design of transmitters and receivers is presented in [66]. In [67], coverage and capacity of a dense mmWave cellular system are analyzed using a theoretical model as a function of blocking probability and beamforming bandwidth. Also, SE metric of a mmWave cellular system is investigated for LOS and NLOS links in 28 and 73 GHz mmWave bands. Since minimal power consumption has received significant attention in recent years, due to governmental regulations, it is important to address this issue for mmWave cellular systems. This issue has not received much attention in literature. Tan *et al.* have investigated achievable downlink SE of a multi-user mmWave cellular system considering both small- and large-scale fading effects in [68]. In [69], an expression for energy coverage probability is derived for a mmWave system as a function of network density, beamforming bandwidth and channel parameters.

The trade-off between EE and SE metrics is examined for different types of access networks in [70]. It is demonstrated that for best utilization of mmWave bands, it is important to understand the trade-off between tolerable delay and power consumption. The delay-power trade off is examined for designing an energy-efficient cellular system in [34]. Levanen *et al.* have proposed technologies to reduce delay in mmWave communication systems in [71]. The challenges of designing an energy-efficient mmWave cellular

16

system are discussed in [72], where EE metric is presented and evaluated for 28 and 73 GHz mmWave bands for LOS and NLOS links, as a function of BS power, SNR, system parameters, and mmWave channel parameters. The spatial characteristics of a cellular system play a significant role on its performance. Thus, SSE and SEE metric are important and need to be considered in the design of a mmWave cellular system, which is one of the intents of this thesis as well.

## 1.4  Overview of Contributions of Thesis

The primary objective of this thesis is to use efficiency metrics in the design and analysis of communication and cellular systems. The key contributions of this thesis are summarized below:

- **Derivation of upper bounds on SE and EE metrics over fading and shadowing channels**

  The SE and EE metrics for an arbitrary communication system are investigated by deriving upper bounds on them for: $i$) Nakagami-$m$ fading and $ii$) GK fading and shadowing channels. These channel distributions represent real-world propagation environment in $\mu$Wave bands and their parameters can be adjusted to fit a variety of propagation conditions. Closed-form expressions for upper bound on SE and EE matrics are obtained as a function of SNR, channel distribution function parameters using MGF approach. These bounds are used for designing spectral-and energy-efficient communication and cellular systems.

- **Design and analysis of an adaptive $M$-QAM system using SE and EE metrics for Nakagami-$m$ and GK channels**

  The SE and EE metrics are examined for an $M$-QAM system using the concept of average system mutual information for Nakagami-$m$ and GK channels. These metrics are illustrated and an adaptive $M$-QAM system is proposed to enhance SE and EE metrics of the system, for severe propagation conditions over the channel. It is demonstrated that EE and SE metrics of the system can be enhanced for a wide range of SNR in the proposed adaptive $M$-QAM system.

- **Design and analysis of $M$-CPFSK system using SE and EE metrics for Nakagami-$m$ and GK channels**

  Closed from expressions for SE and EE metrics of an $M$-CPFSK system are derived based on the concept of mutual system information and are investigated for their behavior as a function of modulation index, observation length of receiver, normalized bandwidth and parameters of fading and shadowing distributions representing the channel. It is observed that memory inherent in an $M$-CPFSK system can be exploited to improve efficiency metrics. For example, it is shown that increasing observation length of receiver in $M$-CPFSK system can provide improved SE and EE metrics; however, at the cost of increased complexity of the system.

- **Investigation of BER Metric of $M$-QAM and $M$-CPFSK communication systems over Nakagami-$m$ and GK channels.**

  The BER metric of any communication system defines the quality of data transmission over a given channel. This metric for an $M$-QAM system in urban shadowed

18

propagation environment is investigated using MGF technique as a function of modulation and channel statistical parameters. Closed-form expressions for BER metric and system outage probability are derived and illustrated for an $M$-QAM system. An adaptive $M$-QAM system is proposed to improve its BER metric over fading and shadowing channel. It is shown that proposed adaptive system enhances system performance even when channel conditions are severe. Also, the BER metric is derived in closed-form for $M$-CPFSK system for Nakagami-$m$ and GK channels. It is shown that observation length of receiver plays a major role in determination of BER metric of $M$-CPFSK system. Power Penalties (PPs) required for an $M$-CPFSK system for various fading and shadowing conditions over the channel are determined.

- **Design and analysis of a cellular system limited by co-channel interference and path loss in Nakagami-$m$ fading environment**

  A comprehensive framework for design and analysis of hexagonal cellular system using SE, EE SSE, SEE and coverage probability metrics is presented. The propagation environment in the system is assumed to be Nakagami-$m$ fading coupled with a simplified path loss model and co-channel interference. Three antenna configurations at BS, namely, omni, $120^o$ and $60^o$ are considered. Closed-form expressions for SE and EE and coverage probability metrics are derived and illustrated as a function of SNR, cell radius, reuse distance, path loss exponent factor and fading figure. A discussion of trade-offs among SSE, SEE and coverage probability metrics as a function of cellular system parameters and propagation environment is also

provided. It is shown that antenna sectorization technique at BS provides significant improvement in efficiency metrics; however, at the cost of increased system complexity.

- **Design and analysis of MU-MIMO cellular system using SE and EE metrics in fading and shadowing channel**

  An MU-MIMO system, with large number of antennas, at BS is considered in a cellular system. This system employs low-complexity MRC receiver technique and is efficient at low values of SNR. The received signals at BS from users are assumed to experience path loss and fading and shadowing over the channel and is modelled as Gamma-Gamma distribution. The SINR is modelled considering intercell and intracell interferences. Closed-form expressions for SE and EE metrics of this system for uplink transmission are derived using MGF technique and are illustrated as a function of: $i$) number of BSs in the system, $(J)$; $ii$) number of users in each BS, $(K_i)$; $iii$) the size of antenna array in MU-MIMO system at BS, $(\mathcal{M})$; and $iv$) the fading figure. It is demonstrated that both SE and EE metrics of the system can be improved for low values of transmitted power by users for large antenna system at BS. Also, It is noted that increasing number of users in the system affects the efficiency metrics due to result of increased co-channel interference.

- **Design and analysis of SE and EE metrics of a mmWave cellular system**

  A dense mmWave hexagonal cellular system with each cell consisting of number of smaller cells with their own BSs is presented as a solution to meet the increasing

demand for a variety of high data rate services and growing number of users of cellular system. A framework for design of mmWave cellular system is presented using efficiency metrics, EE, SE, SSE, SEE and network latency, for LOS and NLOS links in 28 and 73 GHz bands. These efficiency metrics are analyzed as a function of SNR, channel and system parameters, user distance from BS, and BS power. It is observed that 73 GHz band achieves better SE; however, the 28 GHz band is superior in terms of EE.

## 1.5   Thesis Organization

The thesis is structured as follows:

In Chapter 2, fundamental concepts and definitions of efficiency metrics, SE, EE, SSE, SEE and BER, of communication and cellular systems are presented. A discussion of system resources such as power and spectrum and their connection to system performance metrics is also given. The trade-offs among efficiency metrics for efficient design and analysis of communication and cellular systems are also provided.

Chapter 3 provides a brief overview of channel models used in the thesis. The statistical descriptions of Nakagami-$m$ and GK models are given. While the former is used to represent multipath fading environment, the latter is used to represent multipath fading superimposed with shadowing over the channel. Also, channel path loss models, both LOS and NLOS, for 28 and 73 GHz mmWave bands are given.

Chapter 4 focuses on SE and EE metrics of an $M$-QAM communication system. Firstly, bounds on these metrics of the system for Nakagami-$m$ and GK channels are

derived. An investigation of trade-off between SE and EE metrics for efficient system design is also provided. An adaptive $M$-QAM technique is proposed to improve performance metrics, for a wide range of SNRs of practical interest and channel statistical parameters.

In Chapter 5, a closed-form expressions for BER metric of $M$-QAM system for Nakagami-$m$ and GK channels are derived using MGF approach. An adaptive $M$-QAM system is proposed to improve this metric of the system and expression for BER and outage probability of the system are derived and illustrated as a function of system and channel parameters.

In Chapter 6, efficiency metrics of an $M$-CPFSK system are derived based on the concept of average system mutual information for Nakagami-$m$ and GK channels. These metrics are illustrated as a function of modulation index, receiver observation length, normalized bandwidth, SNR and channel statistical parameters. The BER of $M$-CPFSK system is also derived and illustrated. The trade-offs among SE, EE, BER metric and system complexity are explained and used to design efficient systems.

In Chapter 7, trade-offs among performance metrics SE, EE, SSE, SEE, and coverage probability, of single- and multi-cell hexagonal cellular system are addressed. Three antenna configurations at BS, omni, sectorized $120^o$ and $60^o$, are considered and closed-form expressions for efficiency metrics are derived for Nakagami-$m$ multipath fading channel in addition to path-loss and co-channel interference. The efficiency metrics are illustrated for worst case co-channel interference as a function of SNR, system and channel statistical parameters.

Chapter 8 is devoted to evaluation of metrics SE and EE for the uplink in a cellular system with MU-MIMO system at BS. In particular, efficiency metrics are derived in closed-form for MRC receiver at BS, for multipath fading and shadowing wireless channel. The effect of path-loss and co-channel interference are also considered. The system performance metrics are illustrated as a function of user's transmitted power, $p_u$, antenna array size in MU-MIMO system ay BS, $\mathcal{M}$, normalized reuse distance, $R_d$, number of active users in each cell, $K_i$, path-loss exponent, $\upsilon$, and channel statistical parameters.

In Chapter 9, a dense mmWave cellular system is presented and analyzed using its efficiency metrics. These metrics are illustrated, using Monte Carlo simulations, as a function of SNR, channel model parameters, user distance from BS, and BS power. A discussion of these metrics in the design of efficient cellular system is also provided.

In Chapter 10, contributions of this thesis and conclusions from the results obtained are summarized. Also, areas for further research in the light of needs of spectral- and energy-efficient communication and cellular systems are outlined.

## 1.6   Chapter Summary

In this Chapter, an introduction to the thesis is provided with emphasis on the literature survey and the motivations for problems addressed in thesis. The primary objectives of thesis are outlined. Also, organization of the thesis is given.

# Chapter 2

# Performance Metrics of Communication and Cellular Systems

## 2.1 Introduction

Energy and spectrum are two basic communication system resources and have to be used efficiently to guarantee a certain level of system performance. The performance metrics of a communication system are directly or indirectly related to these two resources and their efficient utilization has become imperative due to increasing demand for a variety of communication services, growing number of users, and government regulations for minimizing greenhouse gas emissions. This Chapter presents definitions of performance metrics of communication and cellular systems and a discussion of trade-offs among these metrics in the design of efficient systems is also provided. Firstly, SE metric of a system is introduced from the viewpoint of using available system spectrum resource efficiently. Then, EE metric of a system used to efficiently handle system energy needs is presented. The trade-off between SE and EE metrics of a communication system in AWGN channel is discussed. The definitions of SE and EE metrics are then presented for a cellular system. Also, these definitions are extended to include spatial efficiency metrics of the

system. The SSE and SEE metrics are defined and explained for cellular system. Finally, the BER metric of a communication system is presented and its relationship to SE and EE metrics is discussed.

## 2.2   SE Metric

The SE metric has been traditionally used for measuring ability with which spectral resource of a communication system is used and is defined as amount of information that can be reliably transmitted per unit time over a given bandwidth. If $R_I$ is the number of bits/s that can be reliably transmitted over a channel of bandwidth $B$ Hz, SE metric, $\eta_S$, can be written as:

$$\eta_S = \frac{R_I}{B}, \quad (bit/s/Hz) \tag{2.1}$$

Using well-known Shannon's capacity theorem [15], SE metric can be upper bounded by

$$\eta_S = \log_2 (1 + \gamma), \quad (bit/s/Hz) \tag{2.2}$$

where $\gamma$ is the average SNR over the channel. The SE metric of a DCS can also be determined by modelling it as a discrete-input $(X)$ discrete output $(Y)$ channel formed by including modulator as demodulator as a part of the channel [73]. Such a channel is referred to as the Discrete Memoryless Channel (DMC). The input $X$ and the output $Y$, that is a noisy version of $X$, are both random variables, with $X = [x_1, x_2, ..., x_K]$ and $Y = [y_1, y_2, ..., y_J]$. The SE metric of such a channel is defined as the number of bits that

can be conveyed per channel use per unit Hz of channel bandwidth and is given by [74]

$$\eta_S = \frac{1}{BT_s} \max I\,(X;Y)\,, \qquad [bits/s/Hz] \tag{2.3}$$

where $B$ is the channel bandwidth and $T_s$ is the symbol of duration. The quantity $I\,(X;Y)$ (bits/ch use) is the average mutual information of the channel, between its input $X$ and output $Y$ and is given by [73]:

$$I(X;Y) = \sum_{k=1}^{K} \sum_{j=1}^{J} p(y_j|x_k)p(x_k) \log_2 \left[ \frac{p(y_j|x_k)}{p(y_j)} \right] \tag{2.4}$$

where $p(y_j|x_k)$ are the transition probabilities, $p(x_k)$ are the peior probabilities. The average mutual information of Discrete-input Continuous-output Memoryless Channel (DCMC) for $M$-ary symbols $(m = 1, ..., M)$ is given by [21]:

$$I(X;Y) = \sum_{m=1}^{M} \int_{-\infty}^{\infty} \cdots \int_{-\infty}^{\infty} p(\boldsymbol{y}|\boldsymbol{x})p(\boldsymbol{x}) \log_2 \left[ \frac{p(\boldsymbol{y}|\boldsymbol{x})}{p(\boldsymbol{y})} \right] d\boldsymbol{y} \tag{2.5}$$

where $\boldsymbol{x} = [x_1, x_2, ..., x_K]$ and $\boldsymbol{y} = [y_1, y_2, ..., y_J]$.

## 2.3   EE Metric

The SE metric is not explicit about how efficiently energy is utilized in a communication system. The generic definition of EE metric of a DCS is given by [75]:

$$\eta_E\,(x) = \frac{f(x)}{x} \tag{2.6}$$

where $f(x)$ represents maximum number of bits that can be reliably delivered and $x$ is the power consumption. Using $x = g(P)$ where $P$ is the power consumed in a system, (2.6) can be written as:

$$\eta_E\left(g(P)\right) = \frac{\eta_S\left(g(P)\right)}{g(P)}, \tag{2.7}$$

When $g(P)$ is the transmission power of a system, metric EE is measured in terms of bits/Joule [24], which is the maximum amount of bits that can be reliably delivered by the system per Joule of energy. Since SNR is directly related to transmitted power, EE metric can be related to SNR, $\gamma$, over an AWGN channel and is given by [37]

$$\eta_E(\gamma) = \frac{\eta_S(\gamma)}{\gamma} \tag{2.8}$$

Thus, EE metric quantifies number of bits per unit thermal noise energy, which corresponds to the number of bits communicated over a given channel bandwidth with noise Power Spectral Density (PSD) equal to that of thermal noise.

## 2.3.1 Power Consumption Models

Since EE metric of a communication system is a function of power consumption in the system, it should include all elements of the system that consume power. A communication system comprises of multiple components such as Power Amplifiers (PAs), filters, mixers, signal processing units, A/D and D/A converters etc. The sum total of power consumed by all these components is the circuit power, $P_c$, and is independent of transmission power, $P$, and data rate. Hence, a more general expression for total power

27

consumption of the system is:

$$P_t = P + P_c, \qquad Watts \tag{2.9}$$

In most theoretical works, while computing system metrics, EE and SE, transmission power, $P$, is used whereas ideally total power, $P_t$, consumed in communication system should be used.

## 2.4   Trade-off between SE and EE Metrics

Minimizing energy consumption of a communication system and at the same time maximizing its spectral efficiency is a conflicting goal and therefore a trade-off between SE and EE metrics must be considered in the design of the system. The trade-off between these metrics is introduced in [26] for an AWGN channel. The relationship between SE and EE is given by:

$$\eta_E = \frac{B\eta_S}{(2^{\eta_S} - 1) BN_o + P_c} \tag{2.10}$$

where $B$ is the channel bandwidth and $\frac{N_o}{2}$ is the two sided PSD of AWGN. The metric SE given by (2.2) and the metric EE given by (2.8) are plotted as functions of SNR for $B = 1$ Hz in Figure 2.1 to understand trade-off between the two metrics. It is obvious that SE metric improves as SNR increases; however, EE metric deteriorates as SNR increases. For low transmitted power, SNR over the channel is small, and hence system is energy efficient but system is poorer in terms of spectral utilization. The trade-off between SE and EE metrics as a function of circuit power $P_c$ of the system is given by (2.10) and is
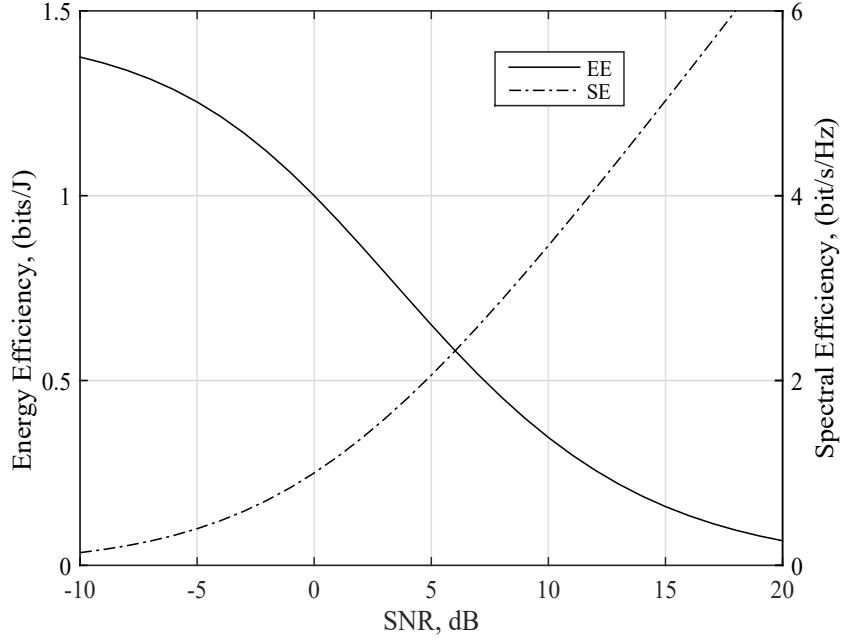
**Figure 2.1:** EE-SE trade-off as a function of SNR

plotted for for $B = 1$ Hz in Figure 2.2. It is observed that there always exists trade-off between SE and EE metrics of the system. For the ideal case, with $P_c = 0$, maximum value achieved for EE metric is given by $1/(N_o \log 2)$, for very low value of SE metric. It is noted that circuit power plays an important role in the design of a communication system and hence SE and EE metrics must be carefully considered. It is apparent that when circuit power is considered, between EE and SE metrics, the monotonicity of relationship is no longer valid and, in fact, system with better EE metric can be designed, for low circuit power.
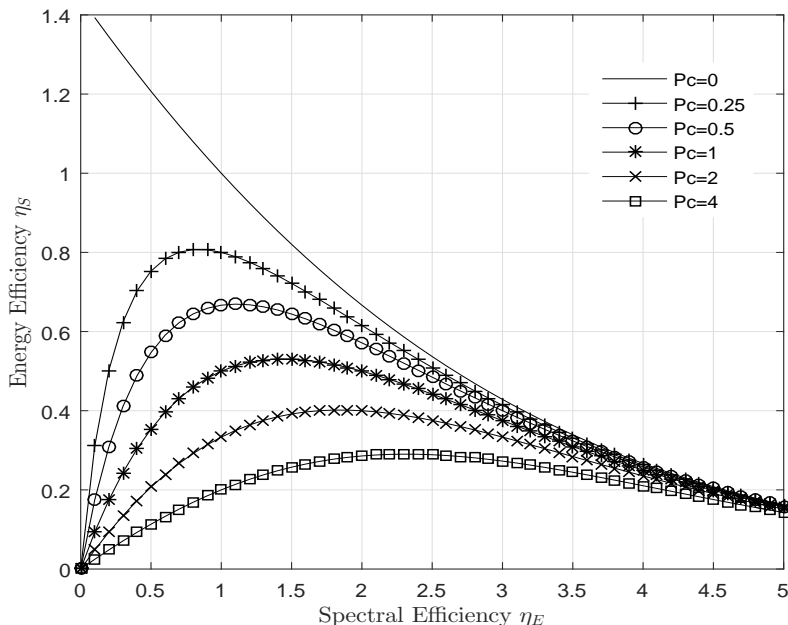
**Figure 2.2:** EE vs. SE metric as a function $P_c$

## 2.5 Performance Metrics of Cellular Systems

The SE metric for a cellular system quantifies delivered data tare to a user over a given bandwidth. The SE metric of a cell in the system is bounded by

$$\eta_S = \sum_{i=1}^{K} \log_2 \left(1 + \gamma_i\right) \tag{2.11}$$

where $K$ is the number of users in the cell. Using (2.8), EE metric of a cell in the system can be expressed as:

$$\eta_E = \sum_{i=1}^{K} \frac{\log_2 \left(1 + \gamma_i\right)}{\gamma_i} \tag{2.12}$$

For single cell system, $\gamma_i$ is SNR and for multicell system when cochannel interference is considered, $\gamma_i$ is SINR. The uplink and downlink SE and EE can be evaluated using (2.11) and (2.12) in which $\gamma_i$ has to be estimated at user for downlink and at BS for uplink.

In a cellular system, cell coverage is an important concern in its design. Expansion of coverage area of a cellular system can be accomplished either by increasing the reuse distance $D$ or by increasing number of cells in the system. However, BS transmit power can affect quality of transmission in the system for large values of $D$. Therefore, to improve SE, EE and quality of transmission, spatial reuse of spectrum can be used by shrinking cell size and increasing number of BSs in the system. Thus, SE and EE metrics are required to be examined as a function of spatial characteristics of the system. The spatial SE metric introduced in [43] captures relationships among SE, coverage area, and communication link quality. The concept of spatial efficiency can also be applied to EE metric [45] for a cellular system. These spatial metrics can be used to optimize deployment of BS for efficient operation of a cellular system. The SSE metric quantifies number of bits/s/Hz/unit of area of a cellular system that can be delivered reliably and characterizes spectral utilization of cellular system for a given coverage area. For a multi-cell cellular system, the SSE metric can be expressed as

$$\eta_{SS_{MC}} = \frac{\eta_S}{\pi \left(D/2\right)^2}, \tag{2.13}$$

For a single-cell system, SSE metric is given by [76]

$$\eta_{SS_{SC}} = \frac{\eta_S}{\mathcal{A}_{aff}}, \tag{2.14}$$

where $\mathcal{A}_{aff}$ is affected area in which considerable amount of transmission power is received. Similarly, SEE metric defines maximum energy efficiency of a cellular system

divided by coverage area. The SEE metric for a multi-cell system is given by:

$$\eta_{SE_{MC}} = \frac{\eta_E}{\pi \left(D/2\right)^2},$$ (2.15)

and for a single cell system, it is given by

$$\eta_{SE_{SC}} = \frac{\eta_E}{\mathcal{A}_{aff}},$$ (2.16)

The coverage probability for cellular system is defined as the probability that a typical user in the system is able to achieve a certain SINR threshold $\gamma_t$. For a reference user in a cellular system, coverage probability is defined as

$$P_{cov} = Prob. \left[SINR \geq \gamma_t\right]$$ (2.17)

Latency is an important metric for evaluating performance of real-time applications in cellular system. Transmission delay between users and BS in cellular system is significant part of overall system latency and it is defined as a ratio of information quantity delivered to users in a cell to information tare [77] and can be expressed as:

$$D = Q/R_I$$ (2.18)

where $Q$ is quantity of delivered information to users in the system.

## 2.6 BER vs. Efficiency Metrics

Bit Error Rate (BER) metric specifies quality of transmission in a communication system, which includes transmitter, receiver and propagation channel. For any communication system, this metric and SE metric are functions of transmitted power and both metrics become better as power is increased; however, EE metric of the system deteriorates as power is increased. Although SE and EE metrics play an important role in the design of an efficient communication system, BER metric determines quality of transmission and must be considered in its design. For example, for an $M$-QAM communication system, BER metric is analyzed as a function of transmitted power in [78] and for an $M$-CPFSK system in [79]. Designing a communication system based on EE and SE metrics subject to the constraint of BER metric is proposed in [80]. It is essential to associate BER metric with those of efficiency metrics for efficient design of a communication system.

## 2.7 Chapter Summary

In this Chapter, fundamental definitions of performance metrics used for designing communication and cellular systems are provided. The SE and EE metrics are presented, for a channel limited by thermal noise. The effect of total power consumption in a communication system on its performance metrics is described using a simple power consumption model. The trade-off between SE and EE metrics of a communication system is presented and illustrated. Also spatial efficiency metrics, SSE and SEE, have been defined for single- and multi-cell cellular systems. Finally, BER metric and its relation to SE and EE metrics is highlighted.

# Chapter 3

# Propagation Environment and Statistical

# Models

## 3.1    Introduction

The channel used in a communication system introduces a variety of effects on transmit-
ted signal. Besides additive noise and interference, signals over a wireless channel are
susceptible to distortion, multipath fading, shadowing, path-loss etc. These effects over
channel cause serious degradations to power of received signal at receiver leading to inef-
ficient performance in terms of energy and spectral resources of the system. The primary
purpose of this Chapter is to briefly review statistical models used in thesis to represent
real-world propagation environment with fading, shadowing, path loss etc. Statistical
descriptions of models are given and illustrated, as a function of its parameters.

## 3.2    Radio Channel Behavior

Radio signals propagate in free-space according to three mechanisms: $i$) reflection; $ii$)
diffraction and $iii$) scattering. Reflection occurs when radio signals hit an object surface
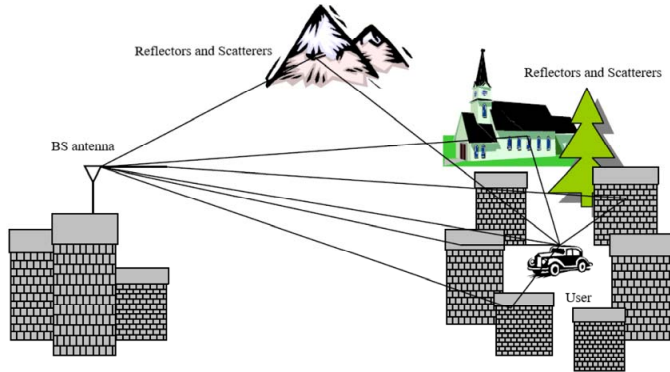
**Figure 3.1:** Illustration of reflection, diffraction and scattering phenomena over wireless channel

that is large compared to signal wavelength. However, when object dimensions are equal to or less than the wavelength of signal, it is redirected in different directions resulting in a phenomenon known as scattering. When there is an obstruction between transmitter and receiver antennas, secondary radio waves are generated due to a phenomenon known as diffraction of signal as shown in Figure 3.1. These three phenomena make signal at receiver consist of several replica of transmitted signal with random amplitudes and phases, resulting in random fluctuation of received signal due to multipath fading, shadowing and pathloss. Multipath fading is caused when transmitted signal arrives at receiver from many different directions with random amplitudes and phases. The envelope of sum of all these signals exhibits rapid variation as a function of time as shown in Figure 3.2. Flat-fading refers to condition of the channel with a constant but random gain over a given observation interval with linear phase response over a bandwidth greater than or equal to that of signal bandwidth. The existence of large scatterers in propaga-

tion environment such as trees, buildings, mountains, etc. results in random variations of mean of received signal and is referred to as shadowing as shown in Figure 3.2. Moreover, received signal level always decreases with distance form transmitter resulting in pathloss over the channel. A model of a typical wireless channel is shown in Figure 3.3, in which
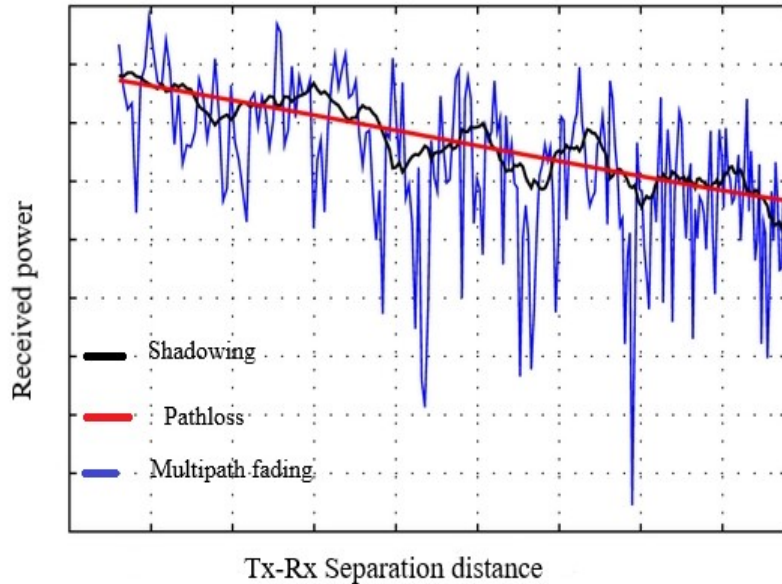


**Figure 3.2:** Received signal power over a typical channel with fading, path loss and shadowing effects [81]

the received signal is given by:

$$r(t) = \alpha S(t) + n(t), \tag{3.1}$$

where $\alpha$, the fading coefficient, is a random variable, $n(t)$ is AWGN, assumed zero-mean with two-sided PSD of $N_o/2$ Watts/Hz and $S(t)$ is the transmitted signal. The SNR over the flat-fading channel is $\gamma = \alpha^2 P/BN_o$ and its average value $\bar{\gamma} = \Omega P/BN_o$, where $B$ is channel bandwidth, $\Omega = \mathbb{E}\{\alpha^2\}$ and $P = \int_0^{T_s} S^2(t)dt$ with $T_s$, the symbol or observation interval. Several types of fading and shadowing statistical models are used to represent

36
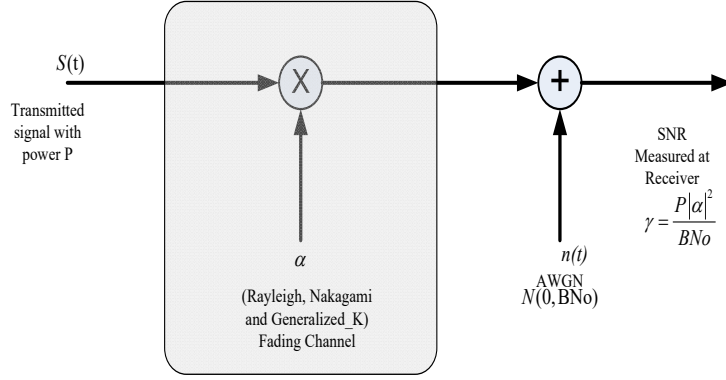
**Figure 3.3:** Model of a wireless channel with AWGN

**Table 3.1:** Propagation environment and corresponding statistical model of $\alpha$

| Propagation Environment | Model |
|---|---|
| Multipath with NLOS link, Urban environment | Rayleigh |
| Multipath with LOS and NLOS links, Urban and Suburban environment | Nakagami-$m$ |
| Multipath with shadowing, Dense downtown areas with slow-moving users | Generalized-$K$ |

the random variable $\alpha$ over real-world propagation environment. These are listed in Table 3.1 and are described next.

## 3.2.1 Nakagami-$m$ Fading Channel

Nakagami-$m$ distribution of random variable $\alpha$ in (3.1), is commonly used to represent a variety of multipath environment using parameter $m$, called the fading figure of distribution. Nakagami-$m$ probability density function (pdf) of random variable $\alpha$ is given by [82].

$$p_{\alpha,N}(\alpha) = \frac{2m^m \alpha^{2m-1}}{\Omega^m \Gamma(m)} \exp\left(-\frac{m\alpha^2}{\Omega}\right), \quad \alpha \geq 0 \qquad (3.2)$$

where $0.5 \leq m < \infty$ and $\Omega = \mathbb{E}[\alpha^2]$. This density can be used to fit a variety of propagation environments by choosing $m$ appropriately. In particular, when there is no

LOS path between transmitter and receiver, Rayleigh distribution is used to represent the channel, which is a special case of Nakagami-$m$ distribution with $m = 1$. For $m > 1$, Rician distribution is obtained and is used to model the environment when there exists a LOS path between transmitter and receiver. As $m \to \infty$, the density function $p_{\alpha,N}(\alpha)$ given by (3.2) approaches $\delta(\alpha - 1)$ and hence received signal in (3.1) becomes $r(t) = S(t) + n(t)$. Such a situation is refereed to as AWGN channel. It is noted that the pdf of $\gamma$ is given by $p_{\gamma,N}(\gamma) = p_{\alpha,N}\left(\sqrt{\frac{\Omega\gamma}{\bar{\gamma}}}\right) \Big/ 2\sqrt{\frac{\gamma\bar{\gamma}}{\Omega}}$. That is

$$p_{\gamma,N}(\gamma) = \left(\frac{m}{\bar{\gamma}}\right)^m \frac{\gamma^{m-1}}{\Gamma(m)} e^{-m\frac{\gamma}{\bar{\gamma}}}, \quad \gamma \geqslant 0 \qquad (3.3)$$

where $\bar{\gamma} = \frac{\Omega P}{BN_o}$ is the average value of SNR over the channel. The pdf of $\gamma$ is plotted as a function of $m$ in Figure 3.4 for $\bar{\gamma} = 5$ dB. It is noted that $\gamma$ represents SNR over flat-
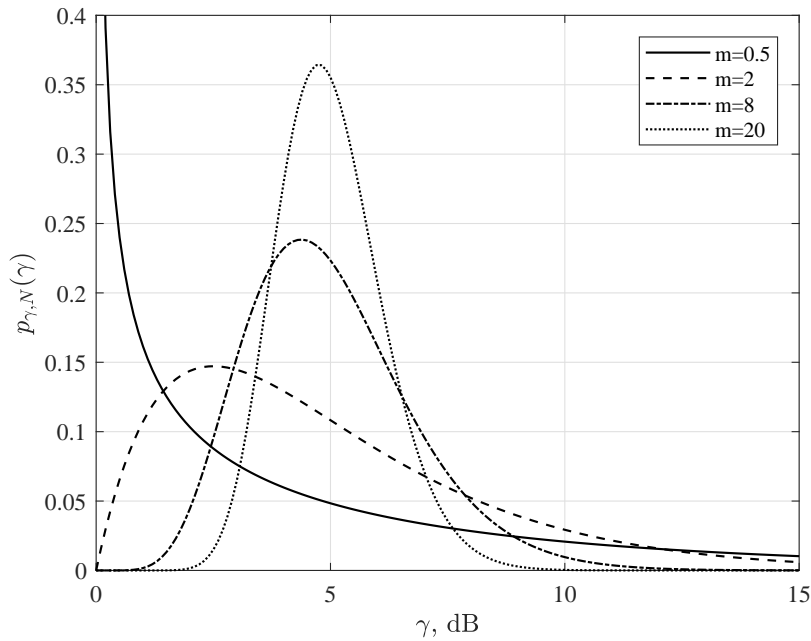


**Figure 3.4:** Probability density function of $\gamma$ given by (3.3)

fading channel. Nakagami-$m$ random variable can be generated in MATLAB by using transformation of *gamma* random variable $\mathscr{G} \sim Gamma(k, \varkappa)$ with $\alpha = \sqrt{\mathscr{G}}$ and letting $k = m$ and $\varkappa = \Omega/m$ [83].

## 3.2.2 Composite Fading and Shadowing Channel

When received signal at receiver encounters both mutlipath fading and shadowing effects over the channel, random variable $\alpha$ can be modelled using GK distribution [82]. This is a composite model that account for both multipath fading and shadowing over the channel. The pdf of a GK random variable is given by [81]:

$$p_{\alpha,GK}(\alpha) = 2 \left(\frac{cm}{\Omega}\right)^{\frac{c+m}{2}} \frac{\alpha^{\frac{c+m-2}{2}}}{\Gamma(c)\Gamma(m)} K_{c-m}\left(2\sqrt{\frac{cm}{\Omega}\alpha}\right), \alpha \geqslant 0 \qquad (3.4)$$

where $K_{c-m}(.)$ is the modified Bessel function of order $c - m$, and $\Gamma(.)$ is the Gamma function [84]. The parameters $c$ and $m$ are shadowing and fading figure, respectively. For $m = 1$, pdf in (3.4) reduces to the well-known Rayleigh-Gamma density and is used to model dense urban wireless propagation environment [81]. As $m$ and $c$ increase in value, fading and shadowing effects over channel become less severe. For $m, c \to \infty$, density of $\alpha$ in (3.4) becomes deterministic and is given by $\delta(\alpha - 1)$. The pdf of $\gamma = \frac{P\alpha^2}{BN_o}$ is given by:

$$p_{\gamma,GK}(\gamma) = 2 \left(\frac{cm}{\overline{\gamma}}\right)^{\frac{c+m}{2}} \frac{\gamma^{\frac{c+m-2}{2}}}{\Gamma(c)\Gamma(m)} K_{c-m}\left(2\sqrt{\frac{cm}{\overline{\gamma}}\gamma}\right), \quad \gamma \geqslant 0 \qquad (3.5)$$

The pdf of $\gamma$ is plotted as a function of $m$ and $c$ in Figure 3.5 for $\overline{\gamma} = 5$ dB. The GK
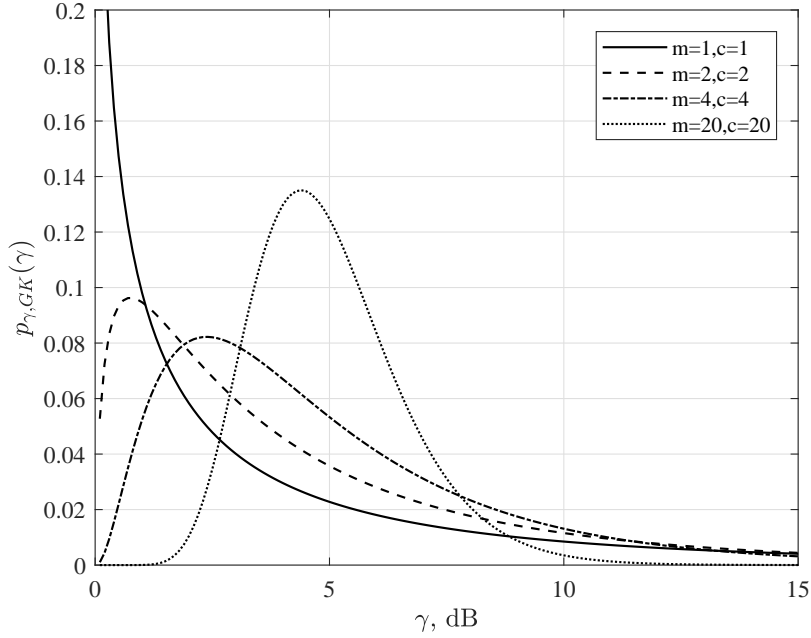
**Figure 3.5:** Probability density function of $\gamma$ given by (3.5)

random variable $\alpha$ can be generated, in MATLAB, using the transformation given by:

$$\alpha = \frac{2\sqrt{(\xi_m \times \xi_c)}}{\sqrt{|c - m| + 1}} \tag{3.6}$$

where $\xi_m$ and $\xi_c$ are independent *Gamma* random variables.

### 3.2.3   Path Loss Models

Path loss is a measure of average radio wave energy decay as a function of distance from transmitter. It is caused by dissipation of transmitted power over wireless channel. It is defined as the difference between transmitted and received powers, typically expressed in dB. A simple model is used to capture path loss over a wireless channel as a function

of distance from the transmitter and is given by [85]:

$$L = K(dB) - 10\log_{10}\left[\frac{d}{d_o}\right]^{\upsilon} \tag{3.7}$$

where $d$ is the distance between transmitter and receiver, $d_o$ is the reference distance form transmitter and $2 \leq \upsilon \leq 6$ is the path loss exponent and depends on propagation environment. For example, $\upsilon = 2$ for free space and $\upsilon = 3$, for shadowing urban environment. The quantity $K$ is a constant related to wavelength, $\lambda$, of radio signal and reference distance, $d_o$, from antenna at transmitter and is given by

$$K(dB) = -20\log_{10}\left(\frac{4\pi d_o}{\lambda}\right) \tag{3.8}$$

For example, $K = -31.5$ dB for free space at $f = 2$ GHz and $d_o = 1\ m$.

## 3.3 mmWave Wireless Channel Models

The propagation environment in mmWave band has been examined for various subbands and statistical models have been developed to fit their characteristics. It is shown that propagation loss due to radiated signal power at transmitter is dependent on distance from transmitter and frequency of operation. For 28 and 73 GHz frequency bands, models have been developed for LOS and NLOS transmission links. These bands are most likely to be deployed in mmWave cellular systems. According to these path loss models [60], the multipath fading has less impact on signals over these links compared to that of shadowing, and hence latter effect is considered in modelling behavior of these links. In

[61], a statistical path loss model based on real-world measurements is presented for an urban environment, for LOS and NLOS links, and is given by:

$$L[dB] = \kappa + \mu 10 \log_{10}(r) + \xi[dB], \quad \xi \sim \mathcal{N}(0, \sigma_s^2) \tag{3.9}$$

where $L$ is path loss in dB, $r$ is distance between transmitter and receiver in meters, $\kappa$ and $\mu$ are least square fits of floating intercept and slope over measured distances up to 200 m, and $\sigma_s^2$ is variance of lognormal shadowing random variable, $\xi$. The values of $\kappa$, $\mu$ and $\sigma_s^2$ are given in Table 3.2 for LOS and NLOS links, for 28 and 73 GHz bands.

**Table 3.2:** Values of parameters of path loss model given by (3.9) based on filed measurements [61]

| Path loss parameters | | $\kappa$ | $\mu$ | $\sigma_s^s$ |
|---|---|---|---|---|
| 28 GHz | NLOS | 72 | 2.92 | 8.7 |
| | LOS | 61.4 | 2 | 5.8 |
| 73 GHz | NLOS | 86.6 | 2.45 | 8.0 |
| | LOS | 69.8 | 2 | 5.8 |

## 3.4   Chapter Summary

In this Chapter, radio signal propagation environment is briefly described and statistical models used to represent fading and shadowing over radio channel are presented. The pdfs of Nakagami-$m$ and GK random variables and pdf of SNR over these channels are given and illustrated. A simple path loss model for power decay as a function of distance from transmitter for a wireless channel is given. Finally, statistical path loss models for 28 and 73 GHz frequency bands are provided, for LOS and NLOS transmission

links. The models described in this Chapter would be used in the design and analysis of communication and cellular systems in Chapters 4 to 9.

# Chapter 4

# Design and Analysis of $M$-QAM System using SE and EE Metrics over Fading and Shadowing Channels [1,2,3]

## 4.1  Introduction

The objective of this Chapter is to examine SE and EE metrics of an $M$-QAM communication system over fading and shadowing channels. Upper bounds of an arbitrary communication system on SE and EE metrics are first derived using statistical averaging and MGF methods, for Nakagami-$m$ and GK channels. Next, these metrics for an

1. Hamed, A., Alsharef, M. and Rao, R.K., "Analysis of Energy and Spectral Efficiency of $M$-QAM System in Urban Shadowing Environment," IAENG International Journal of Computer Science, vol. 43, no.2, pp. 237-244, June 2016.

2. Hamed, A.M.,; Rao, R.K., "Bandwidth and Power Efficiency Analysis of $M$-QAM System over Fading Communication Link," Proc. of Summer Simulation Multi-Conference (SummerSim'16) Montreal, QC, Canada, pp. 1-7 July, 2016

3. Hamed, A.M., Noorwali, A., and Rao, R.K., "Energy Efficient Adaptive Transmission in Generalized-K Fading Channel." Proc. of IEEE Canadian Conference on Electrical and Computer Engineering (CCECE), 2016 IEEE Canadian Conference on, pp. 1329-1334, Vancouver, BC, Canada, May 2016.

$M$-QAM system are derived and investigated over these channels. An adaptive $M$-QAM system is proposed to improve its efficiency metrics, subject to a the constraint of BER metric of the system. Finally, suggestions are offered for designing an efficient $M$-QAM communication system, as a function of statistical distributions representing parameters of fading and shadowing channels.

## 4.2 Description of $M$-QAM Communication System

An $M$-QAM technique is a two-dimensional modulation in which information is simultaneously mapped on phase and amplitude of carrier signal. It employs quadrature orthonormal carriers $\phi_1 = \sqrt{\frac{2}{T_s}} \cos(2\pi f_c t)$ and $\phi_2 = \sqrt{\frac{2}{T_s}} \sin(2\pi f_c t)$ and each of these is modulated by an independent information data sequence. The transmitted $M$-QAM signal can be written as

$$s_m(t) = A_{mc} g_T(t)\phi_1 + A_{ms} g_T(t)\phi_2, \ m = 1, 2, ..., M \tag{4.1}$$

where $g_T(t)$ is the symbol shaping function over symbol duration $T_s$ sec, $A_{m1}$ and $A_{m2}$ are in-phase and quadrature amplitude levels obtained by mapping $n$-bits to one of $M$ amplitude levels, and $E_{sm}, \ m = 1, 2, ..., M$ represents energies of signals $s_m(t)$. A functional block diagram of an $M$-QAM system is given in Figure 4.1. The geometric representation of $M$-QAM signal given by (4.1) can be represented using coordinates $\boldsymbol{s}_m = (s_{m1} = \sqrt{E_s} A_{m1}, s_{m2} = \sqrt{E_s} A_{m2}), \ m = 1, 2, ..., M$ in a two-dimensional signal-space. An example of a rectangular constellation of 16-QAM signal in signal-space is
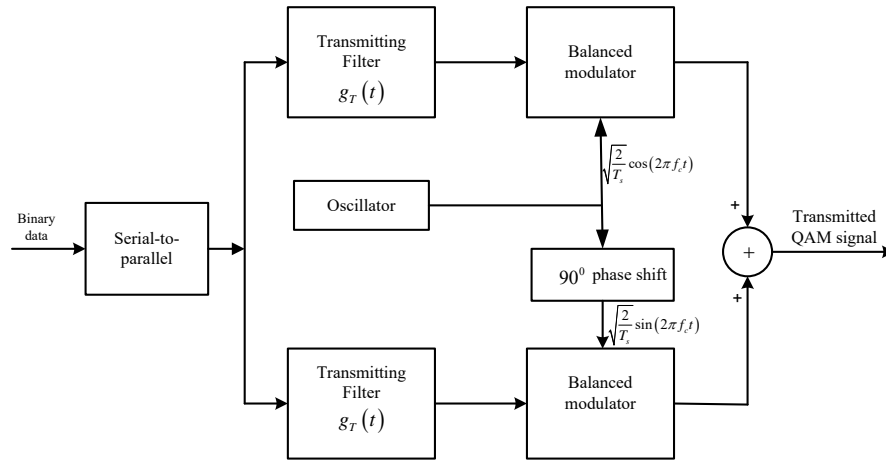
**Figure 4.1:** Block diagram of an $M$-QAM system

shown in Figure 4.2.
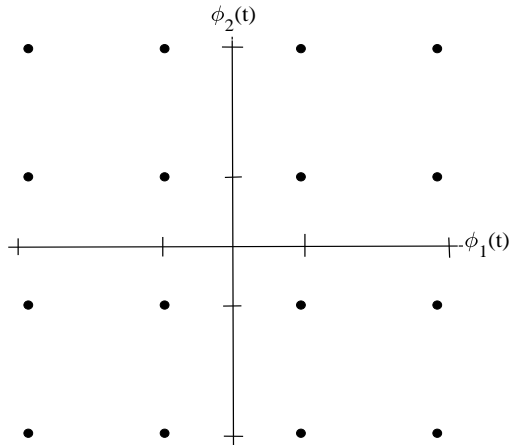


**Figure 4.2:** Rectangular signal constellation diagram of an 16-QAM system with $\phi_1 = \sqrt{\frac{2}{T_s}}\cos(2\pi f_c t)$ and $\phi_2 = \sqrt{\frac{2}{T_s}}\sin(2\pi f_c t)$

## 4.3 Bounds on SE and EE Metrics over Fading and Shadowing Channels

The metrics SE and EE are two important quantities used in the design of a communication system. For realistic system design, channel effects on these metrics have to be considered. Several methods can be exploited to determine these metrics for fading and shadowing channels. In this Chapter, statistical averaging, MGF approach and Monte Carlo simulation are used to obtain these metrics.

### 4.3.1 SE and EE Metrics over Nakagmai-$m$ Fading Channel

When LOS component is predominant between transmitter and receiver, Nakagami-$m$ distribution is used to represent multipath fading effect over the propagation environment. The metric SE is upper bounded by the Shannon's limit for an AWGN channel, and is a function of SNR, $\gamma$, over AWGN channel. However, for a fading channel, the metric SE needs to be averaged over density of $\gamma$, $p(\gamma)$, where random variable $\gamma$ is the SNR of received faded signal in AWGN channel and is given by:

$$\eta_S = \int_0^\infty \log_2 (1 + \gamma) \, p(\gamma) \, d\gamma \qquad (4.2)$$

47

For Nakagami-$m$ fading channel, the metric SE given by (4.2) needs to be averaged using $p_{\gamma,N}(\gamma)$ given by (3.3). Thus, using (3.3) in (4.2) we get:

$$\eta_{S_N} = \frac{\left(\frac{m}{\overline{\gamma}}\right)^m}{\Gamma(m)\log 2} \int\limits_0^\infty \gamma^{m-1} \log\left(1+\gamma\right) e^{-m\frac{\gamma}{\overline{\gamma}}} \, d\gamma \tag{4.3}$$

where $\eta_{S_N}$ represents an upper bound on SE metric for Nakagami-$m$ channel. By using $\log_2(1+\gamma) = \frac{1}{\log 2} G_{2,2}^{1,2}\left(\gamma \,\middle|\, \begin{matrix} 1,1 \\ 1,0 \end{matrix}\right)$ and $e^{-m\frac{\gamma}{\overline{\gamma}}} = G_{0,1}^{1,0}\left(m\frac{\gamma}{\overline{\gamma}} \,\middle|\, 0\right)$ [86, eq. (8.4.6/5),(8.4.3/1)], integral in (4.3) can be simplified using [87, eq.(07.34.21.0011.01)] and can be written in closed-form as:

$$\eta_{S_N} = \frac{1}{\Gamma(m)\log 2} G_{3,2}^{1,3}\left(\frac{\overline{\gamma}}{m} \,\middle|\, \begin{matrix} 1,1,1-m \\ 1,0 \end{matrix}\right) \tag{4.4}$$

where $G[.]$ is Meijer's G-function [86] and $\overline{\gamma} = \mathbb{E}[\gamma]$ represents average SNR over the channel. Below these bounds, design a spectral efficient communication system is possible with low BER. The EE metric of a communication system for an arbitrary fading channel is given by [27],

$$\eta_E = \frac{\int_0^\infty \log_2\left(1+\gamma\right) p_\gamma(\gamma) \, d\gamma}{\int_0^\infty \gamma p_\gamma(\gamma) \, d\gamma} \tag{4.5}$$

Using similar approach used for finding SE, metric EE for Nakagami-$m$ fading channel can be derived. Using $p_{\gamma,N}(\gamma)$ given by (3.3) in (4.5) and using [84, eq(3.383.10), eq(3.326.2)], metric EE in closed-form can be shown to be given by:

$$\eta_{E_N} = \frac{e^{\frac{m}{\overline{\gamma}}}}{\log 2} \sum_{k=1}^m \frac{\Gamma\left(-m+k, \frac{m}{\overline{\gamma}}\right) (\overline{\gamma})^{k-m-1}}{(m)^{k-m}} \tag{4.6}$$

where $\eta_{E_N}$ is the EE metric for Nakagami-$m$ channel and $\Gamma(\beta, x)$ is *complementary incomplete gamma function* and $m$ is a positive integer, which controls multipath fading over propagation environment. It is noted that $\eta_{S_N}$ and $\eta_{E_N}$ are functions of SNR over fading channel and fading figure, $m$, of Nakagami-$m$ density function. Figure 4.3 illustrates the bounds on SE and EE metrics as a function of SNR and $m$ for Nakagami-$m$ channel. It is observed form Figure 4.3 that both metrics cannot be optimized for
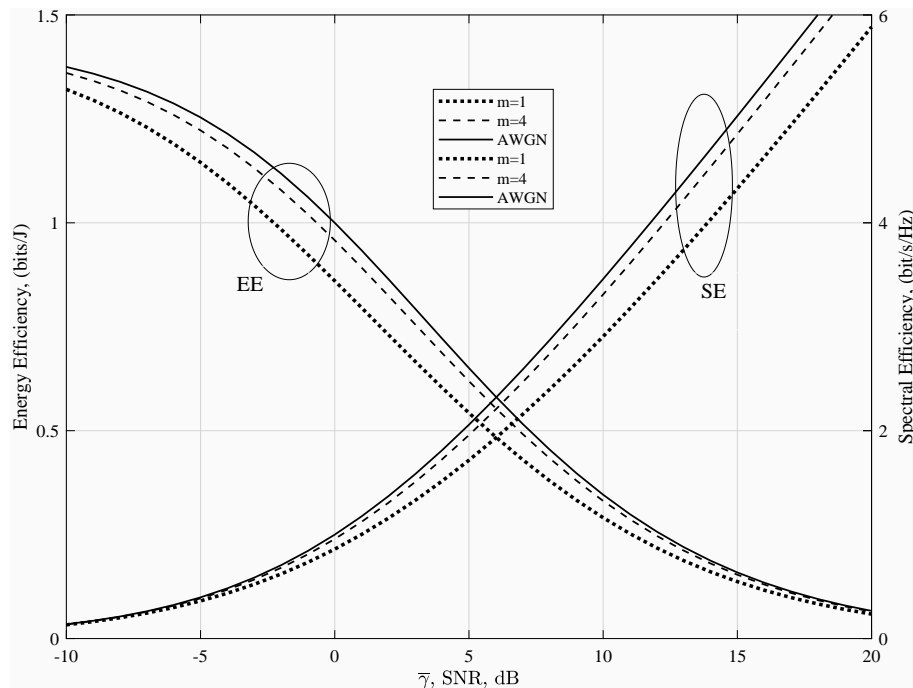


**Figure 4.3:** SE and EE metrics for Nakagami-$m$ channel

arbitrary SNR, $\gamma$, for all values of $m$ and a trade-off between the two in inevitable. This implies that if a communication system is designed for energy efficiency one is required to pay a price in terms of its spectral efficiency. In Figure 4.3, metrics for a purely AWGN channel (with no fading) are also shown. It is observed that regardless of whether fading exist or not over the channel a trade-off between SE and EE metrics must be made. For low values of SNR over the channel, energy-efficient systems can be designed and for

higher values of SNR spectrally efficient systems can be designed. Also, as value of fading figure $m$ of Nakagami-$m$ distribution increases, for low values of SNR, EE metric of the system improves. Similarly, for large values of SNR, system becomes more spectrally efficient as value of $m$ increases. As $m \rightarrow \infty$ in Nakagami-$m$ distribution, fading over the channel vanishes and channel becomes a purely AWGN channel. When $m = 1$, the EE bound is reduced by 15% compared to the case of purely AWGN channel, at low values of SNR. Similarly, the SE bound is decreased by nearly 1 bits/s/Hz for high values of SNR. Also, when $m = 1$, sacrificing 1.2 bits/s/Hz of SE (reducing SE metric from 2.9 to 1.7 bits/s/Hz) can save nearly 5 dB (decreasing SNR from 10 dB to 5 dB) which implies that energy efficiency of the system can be improved by 0.252 bits/J which is equivalent to making the system nearly 100% more energy-efficient.

## 4.3.2 SE and EE Metrics over GK fading and Shadowing Channel

Wireless signal strength often varies randomly from location to location within a given geographical region between transmitter and receiver. In an urban propagation environment, this type of behavior is observed and thus contributes to shadowing; due to terrain, buildings and other obstacles in the environment. When a communication system is employed in such an environment, it is necessary to consider both fading and shadowing effects over the channel for computation SE and EE metrics of the system. Composite GK distribution is often used to represent both fading and shadowing effects over the propagation environment. The parameters of this distribution can be adjusted to fit a

wide variety of fading and shadowing channels. An alternate approach to evaluate SE metric of a communication system is given by (4.3) has been developed in [88] using MGF approach and is given by:

$$\eta_S = \frac{1}{\log 2} \int\limits_0^\infty E_i\left(-z\right) \mathbb{M}_\gamma^{(1)}\left(z\right) \, dz \tag{4.7}$$

where $E_i(-z) = -z \int_1^\infty e^{-tz} \ln(z) dz$ is the exponential integral function [84]. The quantity $\mathbb{M}_\gamma^{(1)}\left(z\right)$ in (4.7) can be obtained by first finding $\mathbb{M}_\gamma\left(z\right)$ and is given by [82]:

$$\mathbb{M}_\gamma(z) \triangleq \int\limits_0^\infty \exp(-z\gamma) \, p_\gamma(\gamma) \, d\gamma \tag{4.8}$$

By substituting $p_{\gamma,GK}(\gamma)$ given by (3.5), for GK distribution when $m = 1$, for $p_\gamma(\gamma)$, in (4.8) and using [87, eq.(07.34.21.0011.01)], the MGF for GK channel can be written as:

$$\mathbb{M}_\gamma(z) = \frac{1}{\Gamma(c)} G_{2,1}^{1,2}\left(\frac{z\overline{\gamma}}{c} \, \middle| \, \begin{matrix} 1-c, \ 0 \\ 0 \end{matrix}\right) \tag{4.9}$$

The first derivative of $\mathbb{M}_\gamma(z)$ in (4.9) w.r.t $z$, using[87, eq.(07.34.20.0001.01)], is given by

$$\mathbb{M}_\gamma^{(1)}\left(z\right) = \frac{d}{dz}\mathbb{M}(z) = \frac{z}{\Gamma(c+1)} G_{3,2}^{1,3}\left(\frac{z\overline{\gamma}}{c} \, \middle| \, \begin{matrix} -1,-c,-1 \\ -1,0 \end{matrix}\right) \tag{4.10}$$

Using [86, eq.(8.4.11/1)] and (4.10) in (4.7) and using [87, eq.(07.34.21.0011.01)], a closed-form expression for an upper bound on SE metric for GK channel given $m = 1$ can be

obtained and is given by

$$\eta_{S_{GK}} = \frac{1}{\log 2\Gamma(c)} G_{4,2}^{1,4} \left( \frac{\overline{\gamma}}{c} \left|\begin{array}{c} 1,1,1-c,0 \\ 1,0 \end{array}\right.\right) \tag{4.11}$$

An expression for EE upper bound of communication system can be obtained using an equivalent expression for EE, eqn.(2.8), and is given by [88]:

$$\eta_E = \frac{\int\limits_0^\infty E_i\left(-z\right) \mathbb{M}_\gamma^{(1)}\left(z\right)\ ds}{\log 2 \lim\limits_{z\to 0} \mathbb{M}_\gamma^{(1)}\left(z\right)} \tag{4.12}$$

Using (4.10), $E_i(-z) = -G_{1,2}^{2,0}\left(z|\begin{array}{c}1\\0,0\end{array}\right)$ and using [87, 07.34.21.0011.01], (4.12) can be shown to be given by:

$$\eta_{E_{GK}} = \frac{(c)^{\frac{c+1}{2}}\left(\frac{1}{\overline{\gamma}}\right)^{\frac{c+3}{2}}}{\Gamma(c)\log 2} G_{2,4}^{4,1}\left(\frac{c}{\overline{\gamma}} \left|\begin{array}{c} -\left(\frac{c+1}{2}\right), \left(\frac{1-c}{2}\right) \\ \left(\frac{c-1}{2}\right), -\left(\frac{c-1}{2}\right), -\left(\frac{c+1}{2}\right), -\left(\frac{c+1}{2}\right) \end{array}\right.\right) \tag{4.13}$$

The SE and EE bounds given by, (4.11) and (4.13), respectively, are plotted as a function of SNR, $\overline{\gamma}$, and GK distribution parameters, $m$ and $c$ in Figure 4.4. The plots in this figure are similar to plots in Figure 4.3 except that they are function of $c$ and $m$. It is observed that for the case of $c = 1$ and $m = 1$, the EE metric is nearly reduced by 26% compared to EE metric of a purely AWGN channel for $-10 \leq$SNR$\leq 0$. Also, it is observed that SE metric is decreased by nearly 1.5 bits/s/Hz for $10 \leq$SNR$\leq 20$. Figure 4.4 shows that trade-off between SE and EE metrics cannot be avoided in the design of a communication system. For an energy-efficient communication system, a sacrifice in terms of SE is inevitable. For $0 \leq SNR \leq 10$ dB, and $c = 1$, $m = 1$,

52
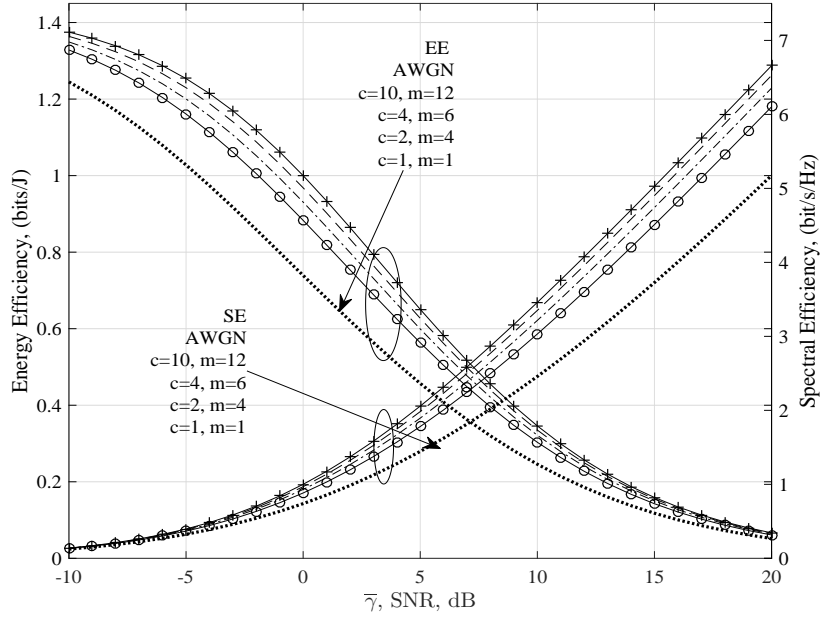
**Figure 4.4:** SE and EE metrics for GK channel as a function of $m$ and $c$

sacrificing a small amount of SE of the system, say, 0.18 bits/s/Hz, can make the system nearly 12% more energy efficient.

## 4.4 SE and EE Metrics of $M$-QAM System

In this section, SE and EE metrics of an $M$-QAM system are derived and investigated for Nakagami-$m$ and GK channels. The DCMC model of an $M$-QAM system is shown in Figure 4.5, where $\phi_1$ and $\phi_2$ are basis functions and $d_m$ is input data sequence. The received signal $r(t)$ can be written as:

$$r(t) = \alpha s_m(t) + n(t), \ 0 \leq t \leq T_s \tag{4.14}$$

where $n(t)$ is AWGN, $\alpha$ is the random attenuation factor introduced by the fading channel, $s_m(t)$ is the transmitted $M$-QAM signal and $T_s$ is the symbol duration. The received signal is processed by $M$-QAM demodulator in the system to recover the transmitted data. The transmitted signals, $s_m(t)$, $m = 1, 2, ..., M$, are assumed to be of finite-energy. Detailed description of $M$-AQM system can be found in [89], and here, SE and EE metrics of the system are evaluated. The metrics can be derived by finding average mutual information of DCMC that represents $M$-QAM system with input $\boldsymbol{s_m} = [s_{m1} \ s_{m2}]$ and output $\boldsymbol{y_m} = [y_1 \ y_2]$ as shown in Figure 4.5, where $s_{m1}$ and $s_{m2}$ are $M$-QAM symbols and $y_1$ and $y_2$ are noisy outputs of the channel. The input symbols $\boldsymbol{s_m}$ are equiprobable with *a prior* probabilities given by:

$$P(\boldsymbol{s_m}) = \frac{1}{M}, \quad m = 1, ...., M. \tag{4.15}$$

The mapping of source binary digits to $M$-QAM symbols $\boldsymbol{s_m}$ is explained in [90] as a function of $M$. Since $y_1$ and $y_2$ are independent, transition probabilities of DCMC are given by:

$$p(\mathbf{y}|\mathbf{s}_m, \alpha) = \prod_{n=1}^{2} \frac{1}{\sqrt{\pi N_o}} \exp\left(\frac{-(y_n - \alpha s_{mn})^2}{N_o}\right), \tag{4.16}$$

The metric SE (bits/s/Hz) of $M$-QAM system can be derived using (2.5), (2.3), (4.15) and (4.16) and is given by:

$$\eta_{S_M} = \frac{\log_2(M)}{1 + \varepsilon} - \frac{1}{M(1 + \varepsilon)} \sum_{k=1}^{M} \mathbb{E}\left\{\log_2\left[\sum_{i=1}^{M} \exp(\Phi_i)\right]\right\} \tag{4.17}$$

54
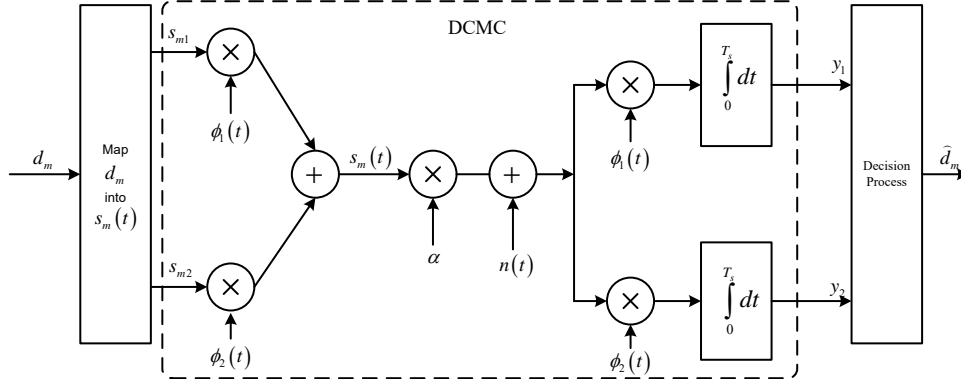
**Figure 4.5:** DCMC of $M$-QAM system [20]

with

$$\Phi_i = \frac{-|\alpha(\boldsymbol{s}_k - \boldsymbol{s}_i) + \boldsymbol{n}|^2 + |\boldsymbol{n}|^2}{N_o}$$

where complex notations are used to represent $\boldsymbol{s}_m = s_{m1} + js_m$ and $\boldsymbol{n} = n_c + jn_s$ (complex Gaussian random variable with power spectral density $N_o/2$). In (4.17), $(1 + \varepsilon)$ is normalized bandwidth of DCMC with $\varepsilon$ denoting roll-off factor of pulse shaping function and $\alpha$ is the fading coefficient given in (4.14). The expectation $\mathbb{E}[.]$ in (4.17) is taken over $\boldsymbol{n}$ and $\alpha$. The metric SE given by (4.17) can be evaluated, for a given distribution of $\alpha$, using Monte Carlo simulation. Similarly, the EE metric of an $M$-QAM system can be derived using (2.8) and (4.17) and can be shown to be given by:

$$\eta_{E_M} = \frac{1}{1+\varepsilon}\mathbb{E}\left[\frac{\log_2 M}{\alpha^2 E_{avg}} - \frac{1}{M\alpha^2 E_{avg}}\sum_{k=1}^{M}\left\{\log_2\left[\sum_{i=1}^{M}\exp\left(\Phi_i^m\right)\right]\right\}\right] \qquad (4.18)$$

where $E_{avg}$ is average energy of $M$-QAM signals. It is noted that in (4.17) and (4.18) suffix $M$ is used to represent the size of modulation used in $M$-QAM system. The SE and EE metrics are obtained using simulations in MATLAB for Nakagami-$m$ and GK channels as a function of SNR given by $\overline{\gamma} = \mathbb{E}\{\alpha^2\}E_{avg}/N_o$, roll-off factor, $\varepsilon$ and

55

parameters of functions distribution of $\alpha$. For Nakagami-$m$ fading channel, SE metrics
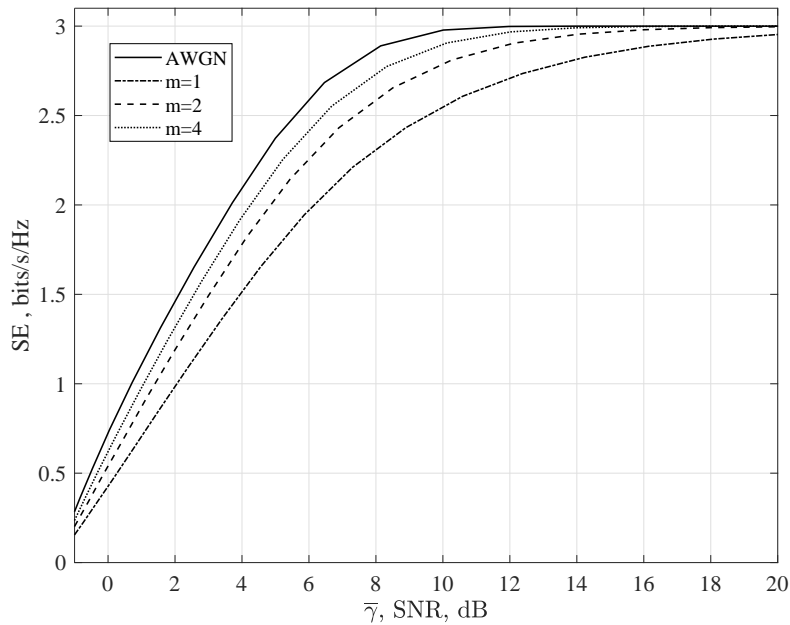


**Figure 4.6:** SE metric for 16-QAM system for Nakagami-$m$ channel as a function of SNR
and $m$ ($\varepsilon = 1/3$)

of 16-QAM are plotted in Figure 4.6 as a function of SNR and distribution parameters,

for $\varepsilon = 1/3$ as an illustration example. In the figure, plots of SE metrics are shown

for purely Gaussian channel ($m \to \infty$), Rayleigh channel (Nakagami-$m$ with $m = 1$)

and Nakagami-$m$ channels with $m = 2$ and 4. It is observed that spectral efficiency of

16-QAM system in AWGN channel improves as SNR over the channel increases form 0

dB to nearly 10 dB, beyond which, spectral efficiency of the system saturates, reaching

a value of $\frac{\log_2(M)}{1+\varepsilon}$ as SNR becomes large; due to the fact that the second term of (4.17)

diminishes as SNR increases. Similar trend is observed for Nakagami-$m$ channels with

$m = 1, 2$ and 4; however, saturation levels and corresponding values of SNR at which

they saturate varies slightly. The worst case SE is observed for Rayleigh channel ($m = 1$)

at all values of SNR. It can be said that SE metric of 16-QAM system becomes worse as

fading over the channel increases. The spectral efficiency of 16-QAM system improves by 0.75 bits/s/Hz when SNR increases from 5 dB to 7 dB. However, SE metric of the system is deteriorated by channel fading. For instance, it reduces by 0.6 bits/s/Hz for $m = 1$, at SNR = 8 dB relative to that of SE metric for AWGN at the same value of SNR. In Figure 4.7, SE metric of 4- and 16-QAM systems are plotted as a function of
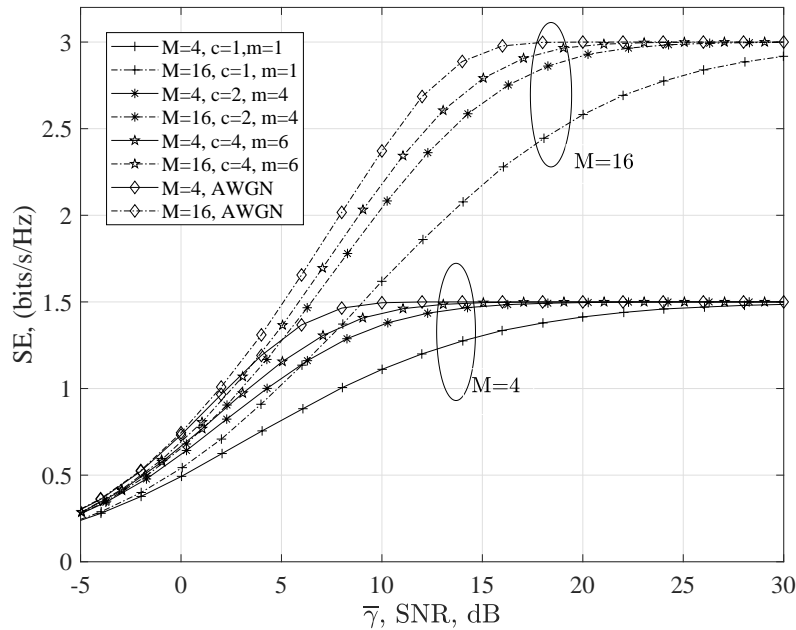


**Figure 4.7:** SE metric 4- and 16-QAM systems GK channel as a function of SNR, $m$ and $c$, and $(\varepsilon = 1/3)$

average SNR over the channel for several values of parameters of GK distribution, $c$ and $m$, and $\varepsilon = 1/3$. It is observed that SE metrics of 4- and 16-QAM systems improve as SNR increases. These metrics approach their maximum values 3 bits/s/Hz at SNR= 18 dB for 16-QAM system and 1.5 bits/s/Hz at SNR= 10 for 4-QAM system, for AWGN channel. However, SE metrics deteriorate as parameters $c$ and $m$ of GK distribution increase; that is, as the effects of fading and shadowing over the channel increase. For example, for $c = 2$ and $m = 4$, 4- and 16-QAM systems require 15 and 23 dB of SNR,

respectively, to achieve their maximum values, which is equivalent to nearly three times

the signal power, compared to that required for purely AWGN channel. The figure also

shows that worst cases SE are observed for $c = 1$ and $m = 1$; SE metric of 16-QAM

system is reduced by 30%, at SNR=12 dB, and it is reduced by 35% for 4-QAM system

at SNR=6 dB, respectively, compared to that for AWGN channel. The EE metrics of

16-QAM are plotted in Figure 4.8 and Figure 4.9 for Nakagami-$m$ and GK channels,

respectively, as a function of SNR and distributions parameters. For comparison, EE

metric for AWGN channel are also plotted in these figures. It is noted that EE metric
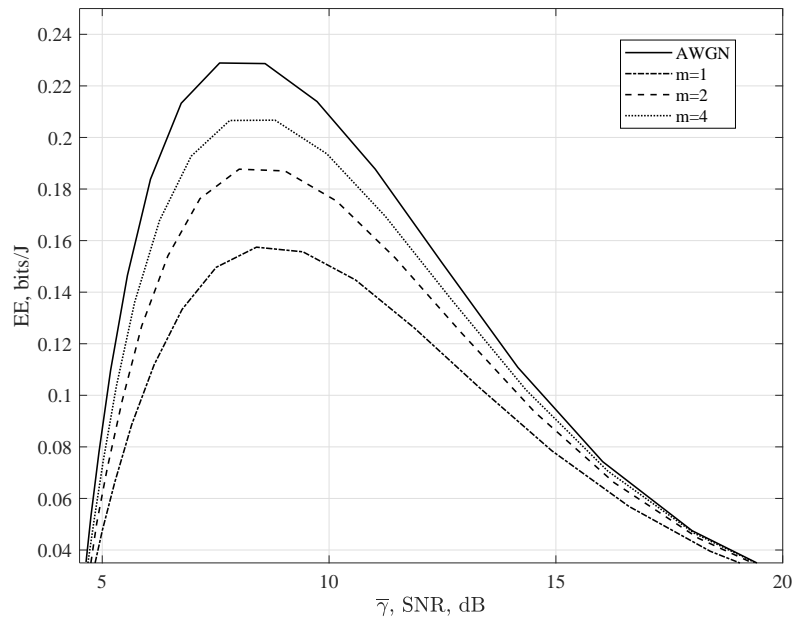


**Figure 4.8:** EE metric of 16-QAM system for Nakagami-$m$ channel as a function of SNR and $m$, $(\varepsilon = 1/3)$

of $M$-QAM system is a concave function of SNR with steep inclines for SNR $\leq 6$ dB

and maximum value in $8 \leq$ SNR $\leq 9.5$. For SNR $\geq 9.5$ dB, EE metric declines as SNR

increases. It is observed that EE metric decreases as fading over the channel becomes

severe. Figure Figure 4.8 demonstrates the effect of Nakagami-$m$ fading on EE metric
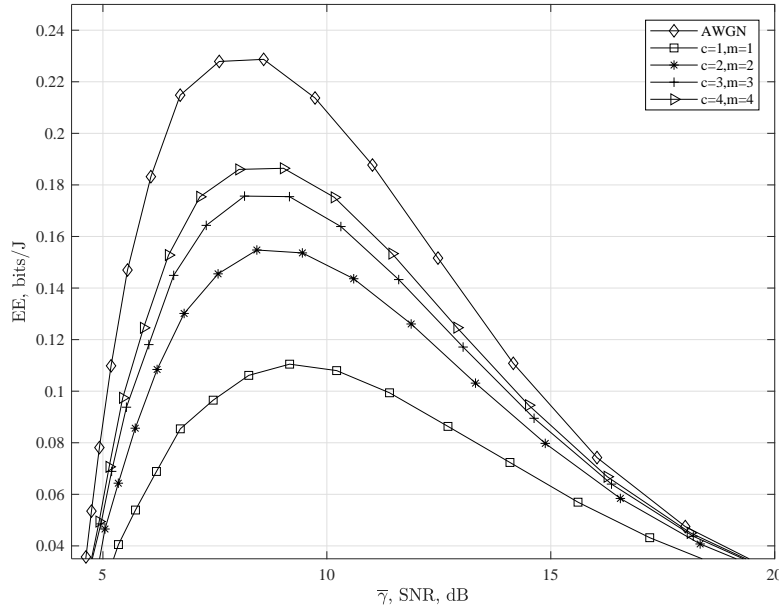
**Figure 4.9:** EE metric of 16-QAM system for GK channel as a function of SNR, $m$ and $c$, $(\varepsilon = 1/3)$

of 16-QAM system in which maximum values of the metric are deteriorated by 31%, 18% and 10% for $m = 1, 2$ and 4, respectively, compared to EE metric of purely AWGN channel. Figure 4.9 illustrates effect of fading and shadowing on EE metric of 16-QAM system. The maximum values of EE metric are reduced by nearly 51%, 32% and 18% for $(c = 1,\ m = 1)$, $(c = 2,\ m = 2)$, and $(c = 4,\ m = 4)$, respectively, compared to EE of AWGN channel for $8 \leq \text{SNR} \leq 9.5$. For an AWGN channel, $(\alpha = 1)$, EE metrics for 4- to 64-QAM systems are plotted as a function of SNR in Figure 4.10. It is evident that regardless of value of $M$ used in $M$-QAM system, EE metrics attain peak values; however, for different ranges of SNR. These ranges of SNR are shown in Table 4.1. For example, for 16-QAM system maximum value of EE of occurs over $10.00 \leq \text{SNR} \leq 13.2$. Roll-off factor, $\varepsilon$, is an important parameter that must be considered in the analysis of SE and EE metrics of a communication system. The effect of $\varepsilon$ on SE and EE metrics
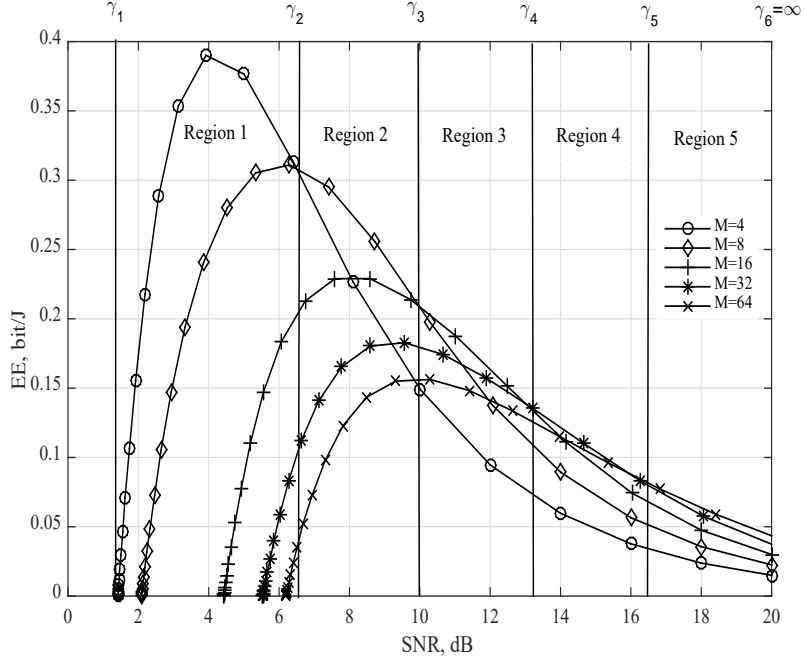
**Figure 4.10:** EE metric of 4- to 64-QAM systems for purely AWGN channel, ($\varepsilon = 1/3$)

is illustrated in Figure 4.11 and Figure 4.12 for a 4-QAM system as a function of SNR for GK channel with $c = 1$ and $m = 1$, and $c = 4$ and $m = 1$. It is evident that as $\varepsilon$ increases the system bandwidth is increased and hence SE and EE metrics of the system become poorer. It is noted that efficiency metrics are function of channel conditions and hence are dependent on parameters $c$ and $m$ of GK distribution. Consequently, one can find a technique a for enhancing efficiency metrics of the system as a function of channel condition. Thus, an adaptive transmission technique based on adjusting the modulation level, $M$, of an $M$-QAM system according to channel condition is proposed and is described in the next section.
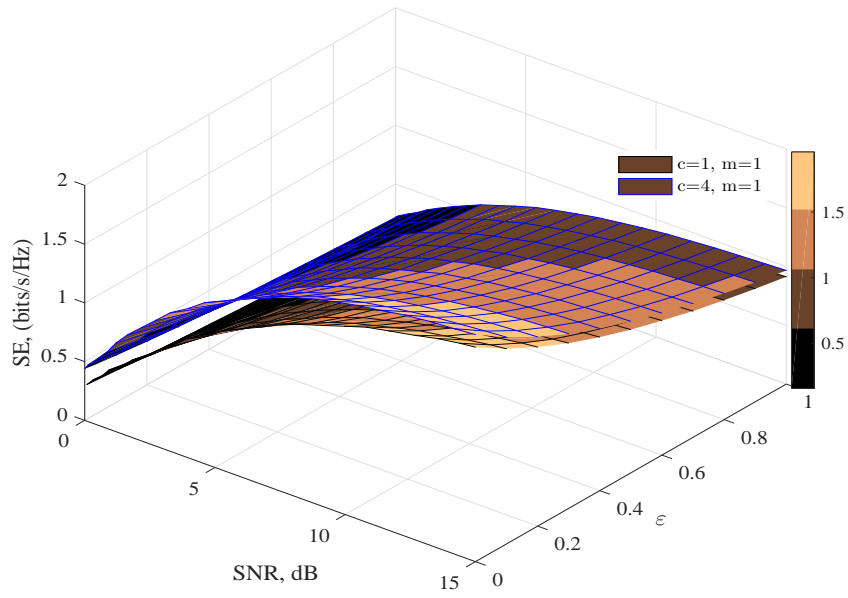
**Figure 4.11:** SE metric of 4-QAM system for GK channel as a function of SNR and roll-off factor $0 \leq \varepsilon \leq 1$
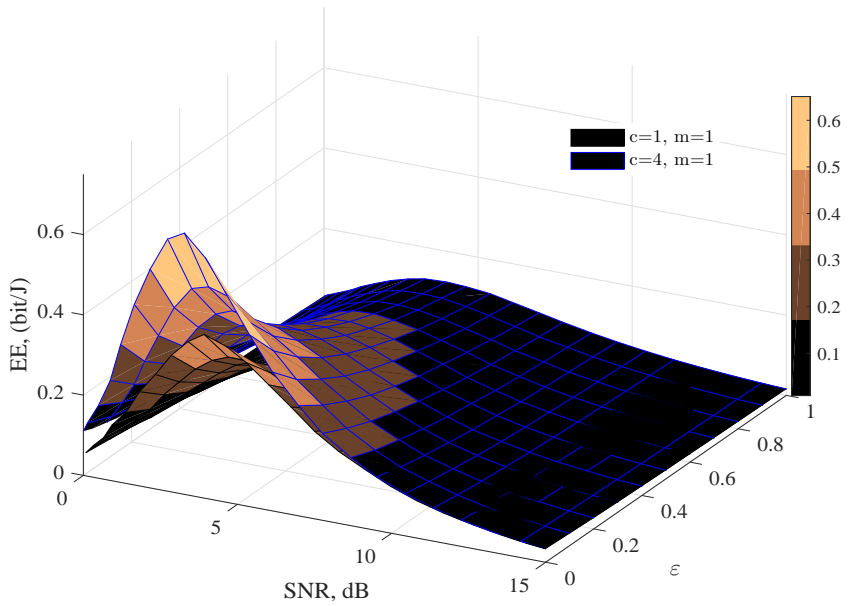


**Figure 4.12:** EE metric of 4-QAM system for GK channel as a function of SNR and roll-off factor $0 \leq \varepsilon \leq 1$

## 4.5 Design and Analysis of Adaptive $M$-QAM System

In this section, an adaptive $M$-AQM system is presented that adapts to changing SNR over fading and shadowing channel to maximize EE metric of the system thereby making it energy-efficient. The objective of the proposed adaptive system is to adjust the level of modulation, $M$, in an $M$-QAM system based on estimated SNR over channel so as to maximize its EE metric. In this system both modulator and demodulator are simultaneously configured with the same value of $M$ based on estimated value of SNR over the channel. The CSI of the link is assumed known both at transmitter and receiver. The feedback link between transmitter and receiver is assumed errors-free with zero delay. The entire range of estimated SNR over the channel is divided into $N$ disjoint regions $R_1$ to $R_N$ as shown Figure 4.13. Table 4.1 shows an example of dividing the range
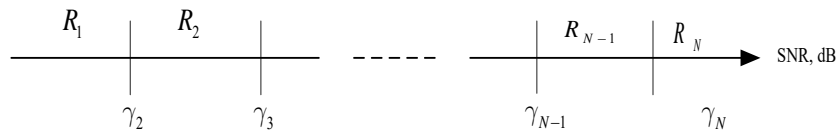


**Figure 4.13:** Regions of SNR for adaptive $M$-QAM system

of estimated SNR (dB) into 5 disjoint regions ($N = 5$) with corresponding value of $M$ $(4, 8, 16, 32$ and $64)$ assigned to each region. The table also shows boundaries of SNR $(\gamma_n, \ \gamma_{n+1})$, $n = 1, 2, ..., N = 5$, for these regions. The example shown in Table 4.1 is for purely AWGN channel and the method used to determine the number of regions and their boundaries is shown in Figure 4.10. In the proposed adaptive $M$-QAM system, once the SNR over channel is estimated, the system determines in which region the SNR lies and

hence chooses the value of $M$ to be used, for maximum EE, at transmitter and receiver and are configured to operate with this value of $M$. The steps used in this adaptive system is shown in Figure 4.14 and can be used for arbitrarily fading and shadowing channel. The energy-efficient adaptive system is next examined by evaluating SE and
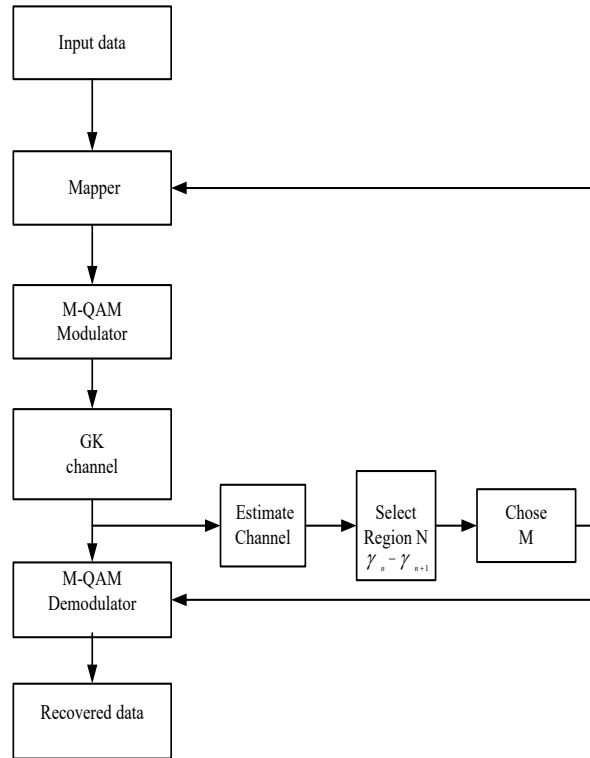


**Figure 4.14:** Block diagram of adaptive energy-efficient $M$-QAM system

EE metrics for GK channel. In order to determine an expression for EE metric of an

**Table 4.1:** SNR boundaries for energy-efficient adaptive $M$-QAM system

| Region $n$ | $M$ | $\gamma_n - \gamma_{n+1}$ [dB] |
| --- | --- | --- |
| 1 | 4 | $-\infty$-6.3 |
| 2 | 8 | 6.3-10.0 |
| 3 | 16 | 10.0-13.2 |
| 4 | 32 | 13.2-16.5 |
| 5 | 64 | 16.5-$\infty$ |

adaptive $M$-QAM system first probability that the estimated SNR falls in the $n^{th}$ region, $P(n) = \text{Prob.}[\gamma_n \leq \gamma \leq \gamma_{n+1}]$, is evaluated and is given by

$$P(n) = \int\limits_{\gamma_n}^{\gamma_{n+1}} p_\gamma(\gamma)\, d\gamma = \int\limits_{0}^{\gamma_{n+1}} p_\gamma(\gamma)\, d\gamma - \int\limits_{0}^{\gamma_n} p_\gamma(\gamma)\, d\gamma \qquad (4.19)$$

where $p_\gamma(\gamma)$ is the density function of SNR corresponding to the distribution of $\alpha$, fading coefficient. For GK channel using $p_{\gamma,GK}(\gamma)$ is place of $p_\gamma(\gamma)$ in (4.19), we get

$$P(n) = \frac{2}{\Gamma(c)} \sum_{k=0}^{m-1} \frac{1}{k!} \Bigg\{ \left( \sqrt{\frac{cm\gamma_{n+1}}{\overline{\gamma}}} \right)^{c+k} \times$$
$$K_{c-k}\left(2\sqrt{\frac{cm\gamma_{n+1}}{\overline{\gamma}}}\right) - \left(\sqrt{\frac{cm\gamma_n}{\overline{\gamma}}}\right)^{c+k} K_{c-k}\left(2\sqrt{\frac{cm\gamma_n}{\overline{\gamma}}}\right) \Bigg\} \quad (4.20)$$

It is noted that (4.20) is a function of average SNR, $\overline{\gamma}$, boundary values of estimated SNR, $(\gamma_n, \gamma_{n+1})$, and parameters $m$ and $c$ of GK distribution.

## 4.5.1  SE and EE Metrics of Adaptive $M$-QAM System

An expression for SE metric of an adaptive $M$-QAM system can be obtained by using statistical averaging of SE over each of the $N$ regions of SNR. That is,

$$\eta_{S_{AM,GK}} = \sum_{n=1}^{N} \eta_{S_{M,GK}} P(n) \qquad (4.21)$$

where for GK channel, $\eta_{S_{M,GK}}$ is determined by using (4.17) and $P(n)$ is given by (4.20).

Similarly, EE metric of adaptive system is given by:

$$\eta_{E_{AM,GK}} = \sum_{n=1}^{N} \eta_{E_{M,GK}} P(n) \qquad (4.22)$$

where $\eta_{E_{M,GK}}$ is given by (4.18). The SE and EE metrics given by (4.21) and (4.22) are plotted in Figure 4.15 and Figure 4.16, respectively, for GK channel. The entire region of estimated SNR is divided into 5 regions and $\varepsilon$ is fixed at $= 1/3$. From
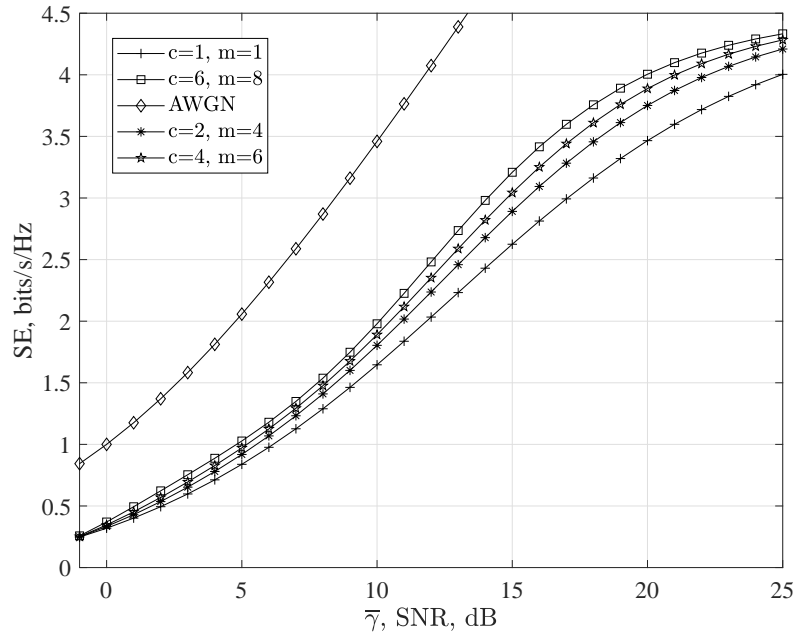


**Figure 4.15:** SE metric of adaptive $M$-QAM system for GK channel as a function $m$ and $c$ $(\varepsilon = 1/3)$

Figure 4.15, it is observed that the adaptive system shows enhanced SE metric even for severe channel condition (GK channel with $c = 1$ and $m = 1$). The GK distribution with these parameters represents the worst case fading and shadowing effects over the channel. For example, SE metrics of the adaptive system are increased by 1.4 and 0.53 bits/s/Hz
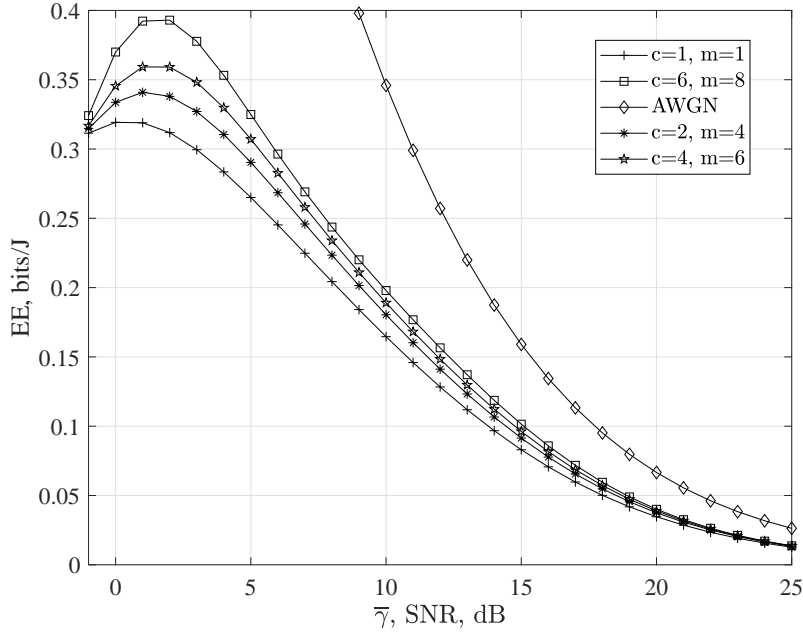
**Figure 4.16:** EE metric of adaptive $M$-QAM system for GK channel as a function $m$ and $c$ $(\varepsilon = 1/3)$

compared to SE metrics of conventional 4- and 16-QAM systems, respectively, at SNR= 16 dB. Figure 4.16 illustrates that EE metric of adaptive system shows improvement for a wide range of SNR. It is observed that for the severe case of fading and shadowing, (GK distribution with $c = 1$ and $m = 1$), EE metric of the adaptive system is nearly 8 times that of EE metric of conventional 16-QAM system for $0 \leq$ SNR $\leq 5$ dB. Also, it is noted that EE metric is increased by 52% and 28% at SNR= 10 and 15 dB, respectively, compared to EE metrics of conventional 16-QAM system at these SNRs. It is noted that SE and EE metrics of adaptive system are below their corresponding bounds on SE and EE for an AWGN channel, which implies that the adaptive system can offer low BER performance as well. However, adaptive system is complex due to SNR estimation and simultaneous switching of level of modulation required at transmitter and receiver. Also, complexity of the system is further increased if error-free feedback link with zero delay

is not available.

## 4.6   Chapter Summary

This chapter investigated SE and EE metrics of an arbitrary DCS in multipath and multipath superimposed by shadowing channels. Closed-form expressions have been derived for bounds on SE and EE metrics of the system for Nakagami-$m$ and GK channels using statistical averaging and MGF approach. The SE and EE metrics for an $M$-QAM system have been obtained and are illustrated as a of channel distribution parameters, roll-off factor and SNR over channel using Monte Carlo simulations. It is observed that these efficiency metrics are deteriorated as the fading and shadowing effects over the channel increases. In other words, it is sensitive to parameters of distribution function representing the channels. In the case of GK channel with $c = 1$ and $m = 1$, the results show that SE metric of 16-QAM system is reduced by 30%, at SNR=12 dB, and maximum value of EE metric is decreased by 51% compared to the metric for AWGN channel. Hence, an adaptive $M$-QAM system is proposed to enhance efficiency metric of the system. The efficiency metrics of adaptive system have been derived and illustrated for GK channel. The proposed adaptive system provides considerable improvement in SE and EE metrics; however, at the cost of increased system complexity. For example, SE metric of adaptive system is enhanced by 1.4 bits/s/Hz compared to SE metrics of conventional 4-QAM system at SNR= 16 dB. Also, EE metric of the adaptive system is increased by 52% at SNR= 10 dB compared to EE metric of conventional 16-QAM system.

# Chapter 5

# Adaptive $M$-QAM System for Target BER

# Metric over GK Channel [4,5]

## 5.1   Introduction

The BER metric plays an important role in the design of an arbitrary communication system. In this Chapter, BER metric of an $M$-QAM system is first investigated for GK fading and shadowing wireless channel. Then, an adaptive $M$-QAM system is proposed that adapts to changing SNR over the channel and assures a BER metric that is less than or equal to *a priori* target BER. Firstly, a closed-form expression for BER metric is derived for a GK channel using MGF approach. The parameters that affect this metric are identified and illustrated. Next, BER metric of the proposed adaptive $M$-QAM system

---

4. Hamed, A.M., Alsharef, M.A, and Rao, R.K., "MGF Based Performance Analysis of Digital Wireless System in Urban Shadowing Environment," Lecture Notes in Engineering and Computer Science: Proceedings of TheWorld Congress on Engineering and Computer Science, pp. 679-684, 2015

5. Hamed, A., Rao, R.K. and Primak, S.L., "Adaptive multidimensional modulation over faded shadowing channels," Electrical and Computer Engineering (CCECE), 2014 IEEE 27th Canadian Conference on , vol., no., pp. 1-4, 4-7 May 2014.

for GK channel is derived and illustrated as a function of its system and GK distribution parameters. A comparison of BER metrics of both conventional and adaptive $M$-QAM systems is provided.

## 5.2   BER Metric of $M$-QAM System

The BER metric of coherent $M$-QAM system shown in Figure 4.5 for an AWGN channel can be upper bounded by [91]:

$$P_M(\epsilon|\gamma) \cong 0.2 \ \exp\left(-\frac{1.5\gamma}{M-1}\right), \ \gamma \geq 0 \tag{5.1}$$

where $\gamma$ is SNR and $M$ is size of modulation in $M$-QAM system. The bound in (5.1) is valid for $M \geq 4$ and is tight for BER $\leq 10^{-2}$. The BER metric over an arbitrary fading and shadowing channel can be written as:

$$P_M(\epsilon) = \int\limits_0^\infty P_M(\epsilon|\gamma) \ p_\gamma(\gamma) \ d\gamma \tag{5.2}$$

where $P_M(\epsilon|\gamma)$ given in (5.2) is BER metric given the value of SNR, $\gamma$, over channel and $p_\gamma(\gamma)$ is density function of $\gamma$. For a GK channel, $p_\gamma(\gamma)$ is $p_{\gamma,GK}(\gamma)$ given by (3.5). Thus, (5.2) can be written as:

$$P_{M,GK}(\epsilon) = 0.2 \int\limits_0^\infty \exp\left(-\frac{1.5}{M-1}\gamma\right) p_{\gamma,GK}(\gamma)d\gamma \tag{5.3}$$

Using definition of MGF given by (4.8) in (5.3) and using (4.9), BER metric of $M$-QAM system for GK channel, $P_{M,GK}(\epsilon)$, can be shown to be given by

$$P_{M,GK}(\epsilon) = 0.2\mathbb{M}_\gamma(z)\big|_{z=\frac{1.5}{M-1}} = \frac{0.2}{\Gamma(m)\Gamma(m)}G_{2,1}^{1,2}\left(\frac{1.5\,\overline{\gamma}}{mc(M-1)}\;\middle|\;\begin{array}{c}(m-c),0\\0\end{array}\right) \quad (5.4)$$

where $M$ denotes level of modulation and $c$ and $m$ are parameters of GK distribution. Also, the quantity $\overline{\gamma}$ represents average SNR over the channel. The BER metric of 4- and 64-QAM systems are plotted as a function of SNR, $c$ and $m$, in Figure 5.1 and Figure 5.2, respectively. The performances of $M$-QAM system for AWGN and Rayleigh channels are also plotted in these figures. In order to understand influence of shadowing on BER metric of $M$-QAM system, for a fixed a value of $m$ ($m = 1$), shadowing parameter $c$ is varied ($c = 1, 1.5, 2, 5$) in these figures. It is observed that as $c$ increases BER metric approaches that for the Rayleigh channel. For example, it is observed that for ($m = 1$, $c = 1$) and ($m = 1$, $c = 5$), 4-QAM system is poorer by 8 and 1 dB, respectively, compared to the same system operating in Rayleigh channel.

The difference between SNR required for a communication system to operate over an AWGN channel to achieve a specific BER metric and SNR required for the same system to operate over a fading and shadowing channel to achieve same BER metric is referred to as the Power penalty (PP). The PP is an indication of additional signal power needed for the system to achieve same performance over fading or shadowing channel [81]. The PP of a 64-QAM system for GK channel is plotted in Figure 5.3 as a function of BER metric of the system, for several values of parameters of GK distribution. The figure shows that PP required decreases as shadowing effect over channel decreases. Moreover, from the
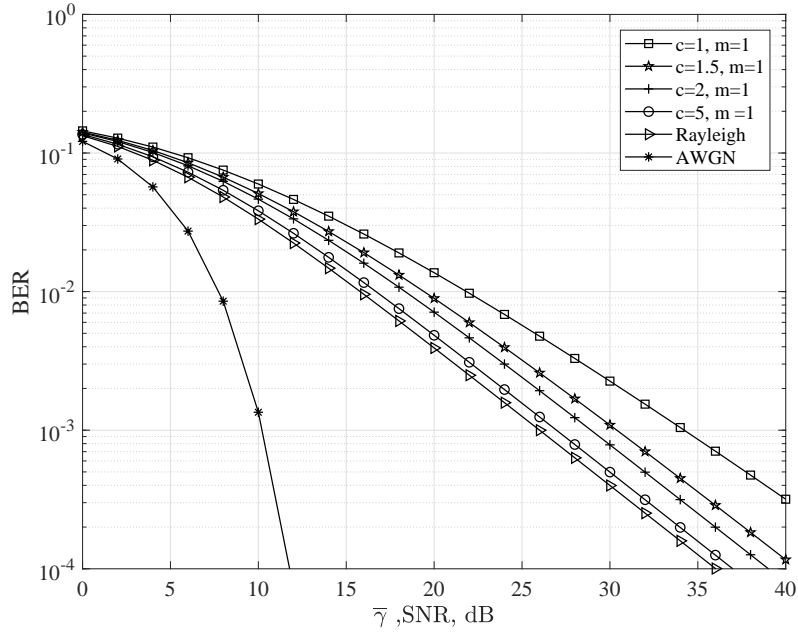
**Figure 5.1:** BER metrics of 4-QAM system, $P_4(\epsilon)$, as a function of GK distribution parameters
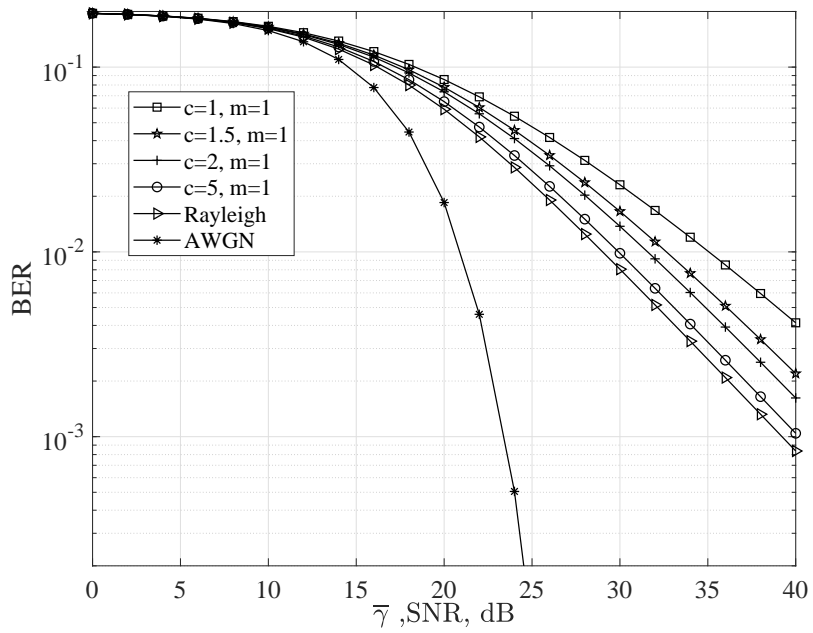


**Figure 5.2:** BER metrics of 64-QAM system, $P_{64}(\epsilon)$, as a function of GK distribution parameters
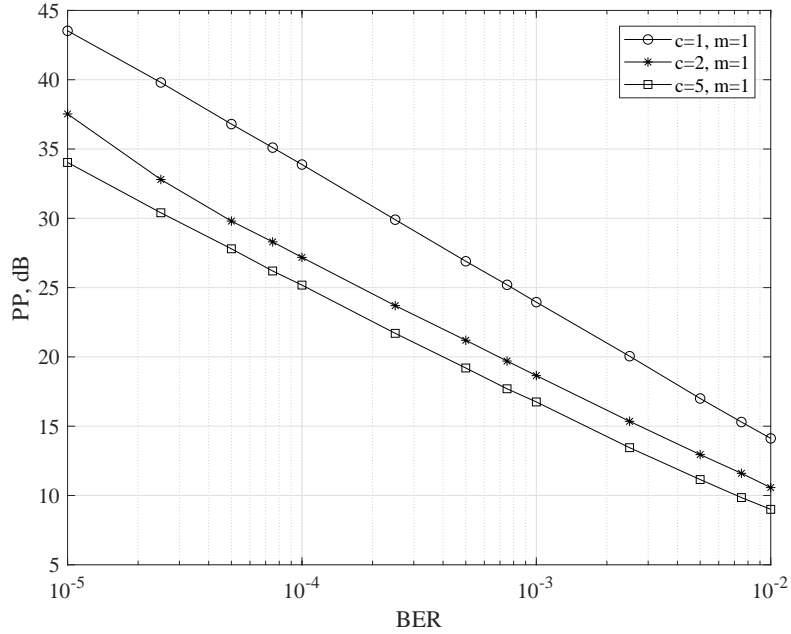
**Figure 5.3:** Power Penalty required for 64-QAM system operating in GK channel as a function of BER

figure, it is observed that PP required decreases as system BER increases. Once channel is estimated and link quality is specified, required transmitted power can be determined using Figure 5.3 for a 64-QAM system. Hence, PP metric is a useful parameter for designing reliable communication system.

## 5.3 Design and Analysis of Adaptive $M$-QAM System for Target BER

In the proposed adaptive $M$-QAM system, estimated SNR over the channel is used to adjust value of $M$ to be configured at both transmitter and receiver so that BER metric of the system is at least equal or less than set target BER metric. Again, it is assumed that in the system error-free feedback link with zero-delay is available. Suppose that $M$-

QAM system can be configured using $M = 4, 8, 16, 32$ and 64 levels, both at transmitter and receiver. Using (5.1), for a target BER, say $10^{-3}$, SNRs $\gamma_1$ to $\gamma_5$ are determined corresponding to $M = 4$ to 64 using inverse relationship between SNR and BER given by:

$$\gamma_i = \left(\frac{M-1}{1.5}\right) \ln \left(\frac{0.2}{P_M(\epsilon)}\right) \tag{5.5}$$

where $i = 1, 2, 3, 4, 5$ correspond to $M = 4, 8, 16, 32, 64$, respectively. Using $\gamma_i$, $i = 1, 2, ..., 5$, SNR boundaries can be arrived at as shown in Table 5.1. In the table SNR boundaries are shown for an AWGN channel. The table also shows value of $M$ to be

**Table 5.1:** SNR boundaries of adaptive system for target BER

| $n$ | $M$ | SNR range, dB |
|-----|-----|---------------|
| 1 | 4 | $10.2 < \gamma < 13.9$ |
| 2 | 8 | $13.9 \leq \gamma < 17.2$ |
| 3 | 16 | $17.2 \leq \gamma < 20.4$ |
| 4 | 32 | $20.4 \leq \gamma < 23.5$ |
| 5 | 64 | $23.5 \leq \gamma < +\infty$ |

used at transmitter and receiver, once range in which the estimated SNR lies. It is noted that number of regions of SNR is simply equal to number of $M$ values used in $M$-QAM system. The block diagram of adaptive $M$-QAM system for set target BER is shown in Figure 5.4. The block diagram is generic and can be used for an arbitrary fading and shadowing channel. For GK channel, Table 5.1 needs to be determined using $P_{M,GK}(\epsilon)$ given by (5.4).
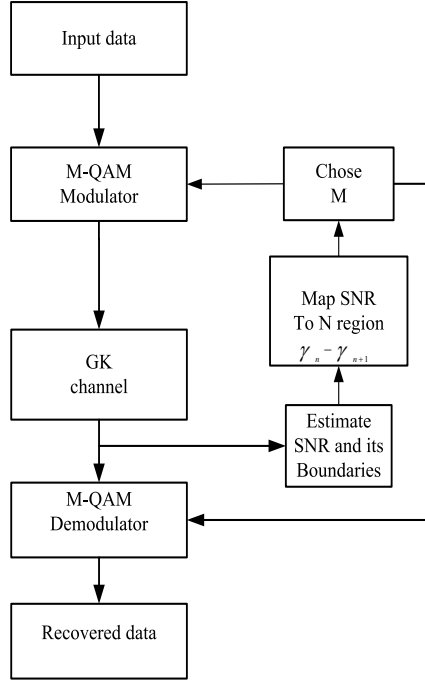
**Figure 5.4:** Block diagram of adaptive $M$-QAM system for set target BER

## 5.3.1   BER Analysis of Adaptive $M$-QAM system

Since adaptive $M-QAM$ system operates based on disjoint SNR regions, its BER metric can be obtained using statistical averaging over disjoint SNR regions. The BER metric is the ratio of average number of bits in error to that of average number of transmitted bits [18] and is given by:

$$P_{M,A}(\epsilon) = \frac{\sum\limits_{n=1}^{N} \eta_{S_M} P_n(\epsilon)}{\sum_{n=1}^{N} \eta_{S_M} P(n)} \tag{5.6}$$

where $\eta_{S_M}$ is spectral efficiency given in (4.17) and $P(n)$ is the probability that estimated SNR lies in region $n$ given by (4.20) and $P_n(\epsilon)$ is given by:

$$P_n(\epsilon) = Prob.[\gamma_n \leq \gamma \leq \gamma_{n+1}] = \int\limits_{\gamma_n}^{\gamma_{n+1}} P_M(\epsilon|\gamma) \ p_\gamma(\gamma) \, d\gamma \tag{5.7}$$

Using (5.1) in (5.7), we get

$$P_n(\epsilon) \;=\; 0.2 \int\limits_{0}^{\gamma_{n+1}} \exp\left(-\frac{1.5\gamma}{M-1}\right) p_\gamma(\gamma)\, d\gamma - 0.2 \int\limits_{0}^{\gamma_n} \exp\left(-\frac{1.5\gamma}{M-1}\right) p_\gamma(\gamma)\, d\gamma \quad (5.8)$$

Using truncated MGF [88] given by

$$\widehat{\mathbb{M}}_\gamma(z, \gamma_k) \triangleq \int\limits_{0}^{\gamma_k} \exp(-z\gamma)\, p(\gamma)\, d\gamma, \tag{5.9}$$

in (5.7), we get

$$P_n(\epsilon) = 0.2\widehat{\mathbb{M}}_\gamma(z, \gamma_{n+1})\big|_{z=\frac{1.5}{M-1}} - 0.2\widehat{\mathbb{M}}_\gamma(z, \gamma_n)\big|_{z=\frac{1.5}{M-1}} \tag{5.10}$$

The truncated MGF given by (5.9) for GK channels can be obtained in closed-from using [87, eq.(03.04.21.0021.01), eq.(07.34.03.0727.01) ] as

$$
\begin{aligned}
\widehat{\mathbb{M}}_\gamma(z, \gamma_k) = \frac{\left(\frac{mc\gamma_k}{\overline{\gamma}}\right)^{\frac{c+m}{2}}}{\Gamma(m)\Gamma(c)} \sum_{i=0}^{\infty} \frac{(-z\gamma_k)^i}{i!} \pi\csc\left(2\pi\left(\frac{m-c}{2}\right)\right) \\
\times \Bigg\{ \Gamma(c+i)\left(\frac{mc\gamma_k}{\overline{\gamma}}\right)^{\frac{c-m}{2}} {}_1F_2\left(c+i, c; c+i+m; \frac{c\gamma_k}{\overline{\gamma}}\right) - \\
\Gamma(m+1)\left(\frac{mc\gamma_k}{\overline{\gamma}}\right)^{-\frac{c-m}{2}} {}_1F_2\left(i+m, -c; i+2; \frac{mc\gamma_k}{\overline{\gamma}}\right) \Bigg\} \quad (5.11)
\end{aligned}
$$

where ${}_1F_2\left(.,.;.\right)$ is the generalized hypergeometric function [84]. Since the value of ${}_1F_2$ decreases rapidly as $i$ increases, it is sufficient to consider finite number of terms in the summation in (5.11). Thus, BER metric of adaptive $M$-QAM system can be easily calculated using (5.6). In Figure 5.5, $P_{M,A}(\epsilon)$ of adaptive $M$-QAM system as a

75

function of SNR, $\bar{\gamma}$, and GK distribution parameters, $c$ and $m$ is plotted. The figure
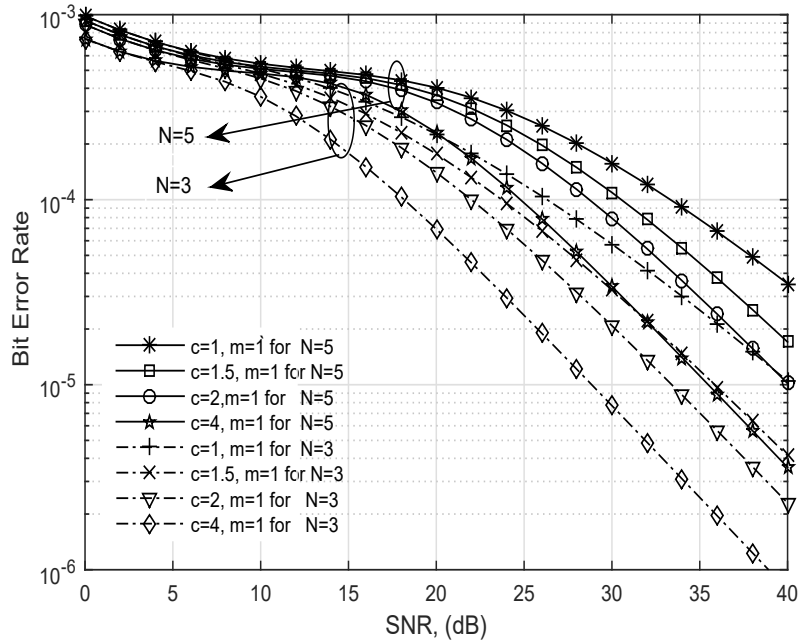


**Figure 5.5:** BER of adaptive $M$-QAM system for GK channel for target BER=$10^{-3}$

shows that adaptive system always maintains set target BER= $10^{-3}$. This is due to the fact that SNR regions are so determined the system always operates at or below set target BER. It is observed that the adaptive $M$-QAM system with 5 regions of SNR achieves BER=$3.5 \times 10^{-5}$ compared to BER=$4 \times 10^{-3}$ for conventional 64-QAM system, at SNR=40 dB for GK distribution parameters $c = 1$ and $m = 1$. The BER metric of adaptive $M$-QAM system improves as fading and shadowing effects over channel decrease (i.e. as $c$ and $m$ increase in value). Adaptive $M$-QAM system, in fact, employs highest available level of modulation, $M$, when estimated SNR is high and hence its BER performance is superior compared to conventional system.

### 5.3.2  Outage Probability of Adaptive $M$-QAM System

When estimated SNR over the channel falls below a certain value, $\gamma_1$, the adaptive $M$-QAM system operating in GK channel will suffer from outage. This probability of outage is given by:

$$P_o = Prob.[\gamma \leq \gamma_1]. \qquad (5.12)$$

When outage occurs, it is assumed that no transmission exists between transmitter and receiver. This occurs when estimated SNR is less than, say $\gamma_1$. The probability of outage is given by $P_o(\gamma_1) = \int_0^{\gamma_1} p_{\gamma,GK}(\gamma) \, d\gamma$. The threshold $\gamma_1$ is that SNR of 4-QAM system for target BER. Thus, outage probability, $P_o(\gamma_1)$, using (3.5), can be shown to be given by

$$P_o(\gamma_1) = 1 - \frac{2}{\Gamma(c)} \sum_{k=0}^{m-1} \frac{1}{k!} \left( \sqrt{\frac{cm}{\overline{\gamma}}\gamma_1} \right)^{c+k} K_{c-k} \left( 2\sqrt{\frac{cm}{\overline{\gamma}}\gamma_1} \right) \qquad (5.13)$$

$P_o(\gamma_1)$ is plotted in Figure 5.6 as a function of GK distribution parameters $c$ and $m$ for $\gamma_1 = 10.2$ dB. The figure shows that outage is more likely when fading and shadowing over the channel is severe (large values of $c$ and $m$).

## 5.4  Chapter Summary

In this Chapter, BER metric of an $M$-QAM system is derived in closed-form for GK channel using MGF approach. The PP required for $M$-QAM system operating over GK channel are evaluated and illustrated as a function of BER metric. It is observed that BER metric of $M$-QAM system rapidly deteriorates as fading and shadowing over the channel becomes severe. An adaptive $M$-QAM system is proposed and investigated that
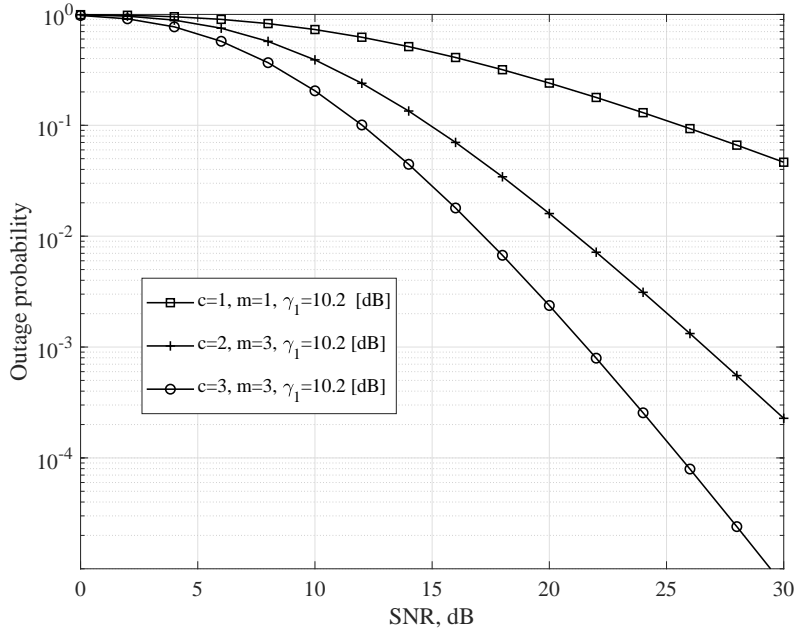
**Figure 5.6:** Outage probability of adaptive $M$-QAM system as a function of $c$ and $m$
($\gamma_1 = 10.2$ dB)

assures a specific set target BER metric for varying fading and shadowing conditions over the channel. Closed-form expression for BER metric of this adaptive system and its outage probability have been derived and illustrated as a function of SNR, GK distribution parameters and target BER metric. It is shown that adaptive $M$-QAM system can be designed that is robust to channel conditions and provides a performance that is superior to that of corresponding non-adaptive $M$-QAM system over GK channel. It is noted that proposed adaptive $M$-QAM system can be designed for efficient operation for any arbitrary fading and shadowing channel, although in this Chapter the system is demonstrated for GK channel

# Chapter 6

# Design and Analysis of $M$-CPFSK System over Fading and Shadowing Channels using SE, EE and BER Metrics [6,7]

## 6.1 Introduction

$M$-QAM is a linear memoryless digital modulation in which $M$-ary symbols are transmitted by varying amplitudes of two carriers in quadrature or equivalently by varying both amplitude and phase of a single carrier. The design and analysis of $M$-QAM system over fading and shadowing channels using SE, EE and BER metrics was presented in Chapters 4 and 5. It is well-known that nonlinear modulation with memory can offer

6. Hamed, A., and Rao, R.K., "Energy and Spectral Efficiencies of $M$-CPFSK in Fading and Shadowing Wireless Channels," Physical Communication Journal, Elsevier, pp. 1-9, July 2018.

7. Hamed, A., Alsharef, M.,; Rao, R.K., "Bit Error Probability Performance Bounds of CPFSK over Fading Channels," Electrical and Computer Engineering (CCECE), 2015 IEEE 28th Canadian Conference, pp. 1329-1334, IEEE, May 2015.

compact spectral characteristics and permits multiple-symbol-observation detection techniques thereby making it energy-efficient as well. One such modulation is $M$-CPFSK. In this Chapter, a DCS that uses $M$-CPFSK is presented and its spectral properties, as a function of modulation parameters, are presented. The SE and EE metrics of such a system are obtained based on mutual information between output and input of a discrete-input continuous-output channel that represents the system. The efficiency metrics of the system are derived and illustrated as a function of modulation parameter, observation length of receiver in the system, and normalized system bandwidth, for AWGN, Nakagami-$m$ and GK channels. The effect of system parameters on efficiency metrics is demonstrated and hence their role in efficient design of $M$-CPFSK system. The BER metric of the system is also analyzed and trade-offs among SE, EE and BER metrics for efficient design of $M$-CPFSK communication system are discussed. The contribution of this Chapter also includes derivation of closed-form expressions for SE, EE, and BER metrics of the system.

## 6.2 $M$-CPFSK System Model

$M$-CPFSK is a modulation in which phase is constrained to be continuous at symbol transitions. This phase continuity makes the signal bandwidth compact and also permits multi-symbol detection methods at receiver. These two attributes of $M$-CPFSK can be used to design communication system that is efficient in both energy and spectrum. In this section, signaling format and detection of $M$-CPFSK signals are presented.

## 6.2.1  $M$-CPFSK Signaling

The low pass $M$-CPFSK waveform during $i^{th}$ symbol interval is given by [79]:

$$s(t, \boldsymbol{a}) = \sqrt{\tfrac{2}{T_s}} \, \exp\left[ j(\phi(t, \boldsymbol{a}) + \phi_o) \right], \quad (i-1)T_s \leq t \leq iT_s \tag{6.1}$$

and the transmitted signal is $Re\{s(t, \boldsymbol{a})\sqrt{E_s}\exp(j2\pi f_c)\}$ where $E_s$ is symbol energy, $T_s$ is symbol duration, $f_c$ is carrier frequency, $\phi(t, \boldsymbol{a})$ is the information carrying phase, and $\phi_o$ is starting phase of signal. The phase $\phi(t, \boldsymbol{a})$ during $i^{th}$ $(i = 1, 2, ...)$ symbol interval is given by:

$$\phi_i(t, \boldsymbol{a}) = a_i g(t - (i-1)T_s) + \pi h \sum_{j=1}^{i-1} a_j, \quad (i-1)T_s \leq t \leq iT_s \tag{6.2}$$

where $\boldsymbol{a} = (a_1, a_2, ..., a_n, ...)$, $a_i \in \{\pm 1, \pm 3, ..., \pm(M-1)\}$ represents the sequence of data symbols and the phase function is given by:

$$g(t) = 2\pi \int_0^t f_d(\tau)d\tau = \begin{cases} 0, & t < 0, \\ \pi\frac{ht}{T_s}, & 0 \leqslant t \leqslant T_s, \\ \pi h, & t > T_s. \end{cases} \tag{6.3}$$

where $f_d(\tau)$ is the instantaneous frequency deviation and is given by:

$$f_d(t) = \begin{cases} \frac{h}{2T_s}, & 0 \leq t \leq T_s \\ 0, & otherwise \end{cases}$$

The quantity $h$ is the modulation index. From (6.2), it is noted that phase is piecewise continuous and the accumulated phase at the end of $i^{th}$ symbol interval is a function of all past $i$ symbols that have entered the modulator [92].

## 6.2.2   Multi-Symbol Detection of $M$-CPFSK Signals

The detection of $M$-CPFSK signal can be based on two approaches: $i$) coherent and $ii$) non-coherent. For coherent detection, $\phi_o$ in (6.1), is assumed known and set to zero with no loss of generality, whereas for non-coherent detection, $\phi_o$ is assumed to be uniform in $(0, 2\pi)$. Both coherent and non-coherent detection of $M$-CPFSK signal in AWGN channel are discussed in [79] and [93]. The detection strategy consists of observing the received signal over $nT_s$ and arriving at an optimum decision on transmitted sequence $(a_1, a_2, ..., a_n)$. The $M$-CPFSK system is shown in Figure 6.1 [94]. The receiver in the system consists of a bank of correlator receivers followed by a decision device. The receiver correlates received $M$-QAM signal in AWGN with each of $M^n$ possible transmitted signals over $nT_s$ observation interval. The decision device then decides the most likely sequence transmitted based on maximum value of correlations. The received signal, $r(t)$, over fading and shadowing channels can be written as

$$r(t) = \alpha e^{j\theta} \sqrt{E_s} \, s(t, \boldsymbol{a}) + n(t), \ 0 \leq t \leq nT_s \tag{6.4}$$

where $\alpha$ and $\theta$ are random amplitude and phase introduced over channel. Both are assumed constant but random over observation interval $0 \leq t \leq nT_s$. In (6.4), $n(t)$ represents a zero mean AWGN with two-sided PSD of $N_o/2$ Watts/Hz. The output of
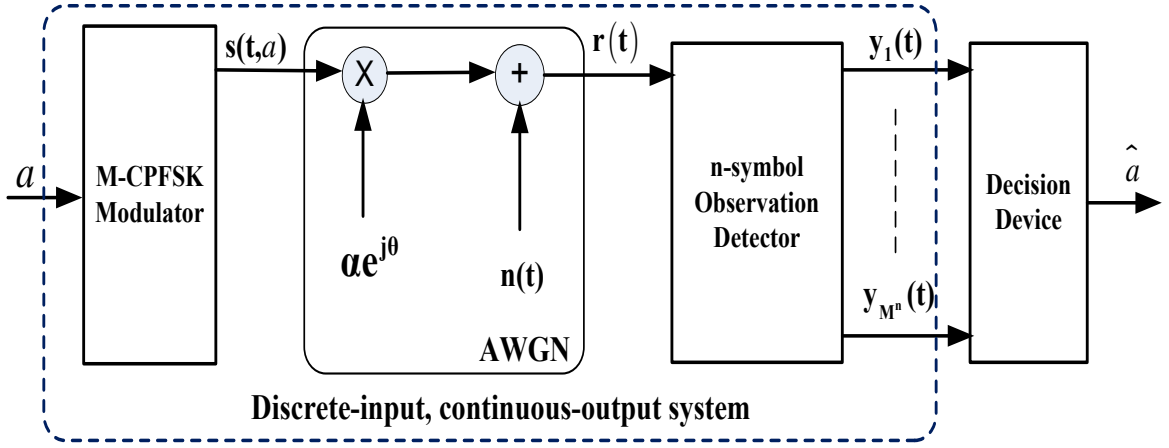
**Figure 6.1:** Block diagram of $M$-CPFSK system

correlator receiver is a vector consisting of $M^n$ complex elements with $n$ the number of observed symbols over $nT_s$ sec. That is,

$$\boldsymbol{y} = \alpha e^{j\psi} \sqrt{E_s}\, \boldsymbol{x} + \boldsymbol{w} \tag{6.5}$$

where $\psi = \theta + \phi_o$ is the received phase, $\boldsymbol{x}$ is a signal vector and $\boldsymbol{w}$ is a Gaussian noise vector. The elements of $\boldsymbol{x}$ and $\boldsymbol{w}$ are given by [95];

$$x_k = \int_0^{nT_s} s\,(t, \boldsymbol{a})\, s^*\,(t, \boldsymbol{b})\, dt$$

$$w_k = \int_0^{nT_s} n\,(t)\, s^*\,(t, \boldsymbol{b})\, dt \tag{6.6}$$

where $\boldsymbol{b}$ denotes all possible $n$-symbol sequences. These elements of $M^n \times M^n$ $\boldsymbol{Z}$ are given by

$$x_{l,j} = \sum_{k=1}^{n} \int_{(k-1)t_s}^{kT_s} s\,(t, \boldsymbol{a})\, s^*\,(t, \boldsymbol{b})\, dt$$

83

$$x_{l,j} = \sum_{k=1}^{n} Sinc\left(\frac{h}{2}(a_k - b_k)\right) e^{j\left(\frac{\pi h}{2}(a_k - b_k) + \pi h \sum_{i=1}^{k-1}(a_i - b_i)\right)} \qquad (6.7)$$

where $b's$ are the data symbols. The elements of $\boldsymbol{w}$, $w_k$, are zero mean Gaussian random variables and variance, $\sigma_k^2$. The elements of $\boldsymbol{V}$, $M^n \times M^n$ matrix, are given by:

$$\sigma_{l,j}^2 = E\left[w_l(t)w_j^*(t)\right]$$

$$\sigma_{l,j}^2 = E\left[\int_0^{T_s} n(t)s(t, \boldsymbol{a})\, dt \int_0^{T_s} n^*(\zeta)s^*(\zeta, \boldsymbol{b})\, d\zeta\right] \qquad (6.8)$$

where $*$ denotes complex conjugate. The elements of $\boldsymbol{V}$ matrix can be shown to be given by:

$$\sigma_{l,j}^2 = N_o x_{l,j} \qquad (6.9)$$

Note that for a specific input sequence $\boldsymbol{a}_v$, the signal vector $\boldsymbol{x}$ is represented by the column $\boldsymbol{Z}_{l=v,j}$ and the variance is going to be the column $\boldsymbol{V}_{l=v,j}$. From (6.5), $\boldsymbol{y}$ is a Gaussian distributed vector with mean $\alpha e^{j\psi}\sqrt{E_s}\boldsymbol{x}$ and variance $\boldsymbol{V}$. For single observation interval, $n = 1$, the probability density function of $\boldsymbol{y}$ for given $\alpha$, $\boldsymbol{a}$ and $\psi$ is a Gaussian and given as

$$p(\boldsymbol{y}|\boldsymbol{a}, \alpha, \psi) = \frac{1}{\pi^M |\boldsymbol{V}|} \exp^{\frac{-\left(\boldsymbol{y} - \alpha e^{j\psi}\sqrt{E_s}\boldsymbol{x}\right)^2}{\boldsymbol{V}}} \qquad (6.10)$$

84

For a given a $\boldsymbol{a}_v$ and from (6.9) $\boldsymbol{x}^H \boldsymbol{V}^{-1}\boldsymbol{x} = 1/N_o$ and $\boldsymbol{y}^H \boldsymbol{V}^{-1}\boldsymbol{y} = \|\boldsymbol{y}\|^2/N_o$ [87], the exponent can be simplified as

$$\left(\boldsymbol{y} - \alpha e^{j\psi}\sqrt{E_s}\boldsymbol{x}\right)^H \boldsymbol{V}^{-1}\left(\boldsymbol{y} - \alpha e^{j\psi}\sqrt{E_s}\boldsymbol{x}\right) = -\frac{\alpha^2 E_s + \|\boldsymbol{y}\|^2}{N_o} + \frac{2\alpha\sqrt{E_s}}{N_o}Re\{e^{j\psi}y_v\}$$

Thus, the conditional pdf of $\boldsymbol{y}$ is given by:

$$p\left(\boldsymbol{y}|\boldsymbol{a},\alpha,\psi\right) = Ke^{\frac{2\alpha\sqrt{E_s}}{N_o}Re\{e^{j\psi}y_v\}} \tag{6.11}$$

where $K$ is given by

$$K = \frac{1}{\left(\pi\sigma^2\right)^M}e^{-\frac{1}{N_o}\left(\alpha^2 E_s + \|\boldsymbol{y}\|^2\right)}$$

In detection process, phase $\psi$ is assumed uniformly distributed in $(0, 2\pi)$. By averaging (6.11) over $\psi$, the conditional pdf of $\boldsymbol{y}$ is given by:

$$p\left(\boldsymbol{y}|a_j,\alpha\right) = \frac{1}{2\pi}\int_0^{2\pi} p\left(\boldsymbol{y}|a_j,\alpha,\psi\right) d\psi \tag{6.12}$$

Thus, (6.11) can be written as

$$p\left(\boldsymbol{y}|a_j,\alpha\right) = KI_0\left(2\alpha\frac{\sqrt{E_s}}{N_o}|y_v|\right) \tag{6.13}$$

where $I_0(x)$ is the *modified zero order Bessel function* of the first kind with argument $x$. In the analysis, the fading is assumed to be flat over the observation length of the detection process. Let $\boldsymbol{a}^n = [\boldsymbol{a}_1, \boldsymbol{a}_2, ..., \boldsymbol{a}_n]$ be the transmitted symbol vectors. The

output of $M^n$ correlators are $\boldsymbol{x}^n = [\boldsymbol{x}_1,\ \boldsymbol{x}_2, ...,\ \boldsymbol{x}_n]$ and the $n$-received block symbols $\boldsymbol{y}^n = [\boldsymbol{y}_1,\ \boldsymbol{y}_2, ...,\ \boldsymbol{y}_n]$. The conditional pdf of the received block for given input sequence, fading coefficient, and phase, $\psi$, can be written as:

$$p\left(\boldsymbol{y}^n|\boldsymbol{a}^n, \alpha, \psi\right) = \prod_{k=1}^{n} p\left(\boldsymbol{y}_k|\boldsymbol{a}_k, \alpha, \psi_k\right) \tag{6.14}$$

which can be written as:

$$p\left(\boldsymbol{y}^n|\boldsymbol{a}^n, \alpha, \psi\right) = K' \exp\left(2\alpha \frac{\sqrt{E_s}}{N_o}\ Re\{e^{-j\psi}\beta(\boldsymbol{a}^n)\}\right) \tag{6.15}$$

where $\beta(\boldsymbol{a}^n)$ is

$$\beta(\boldsymbol{a}^n) = \sum_{i=1}^{n} y_{a_j} \exp\left(-j2\pi h \sum_{k=0}^{i-1} a_k\right) \tag{6.16}$$

Averaging (6.15) over $\psi$, which is uniformly distributed in $(0, 2\pi)$, and using (6.12), we get

$$p\left(\boldsymbol{y}^n|\boldsymbol{a}^n, \alpha\right) = K' I_0\left(2\alpha \frac{\sqrt{E_s}}{N_o}\ |\beta(\boldsymbol{a}^n)|\right) \tag{6.17}$$

The joint pdf of output of correlators obtained in (6.17) is a function of fading and shadowing coefficient over the channel, input sequence, symbol energy, and power spectral density of AWGN.

## 6.2.3 Spectral Properties of $M$-CPFSK

The bandwidth of $M$-CPFSK can be used to evaluate overall system spectral efficiency. The power spectral density (PSD) of $M$-CPFSK signal can be obtained by taking Fourier

transform of autocorrelation function of (6.7). The PSD of 2-CPFSK is plotted in Figure 6.2 as a function of normalized frequency $(BT_s)$ for several values of modulation index, $h$. It is noted that most of signal power is concentrated in the main lobe. In this
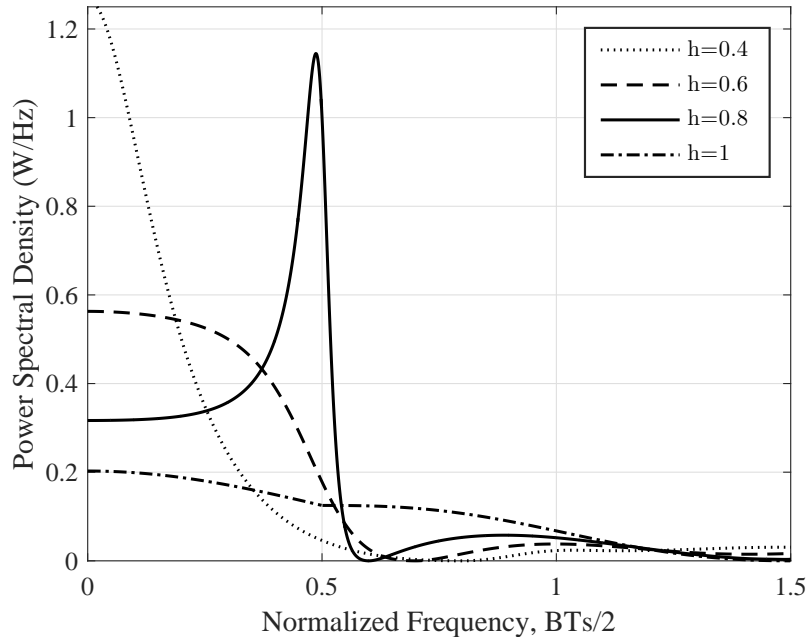


**Figure 6.2:** Power spectral density of 2-CPFSK system as a function of normalized bandwidth for $h = 0.2, 0.5, 0.6$ and $1.0$

thesis, 99% bandwidth is considered and it is obtained by

$$\int\limits_{-B/2}^{+B/2} |S(f)|^2 df = 0.99 \int\limits_{-\infty}^{+\infty} |S(f)|^2 df \qquad (6.18)$$

The bandwidth is dependent on modulation index, $h$, of $M$-CPFSK signal, and its relationship to bandwidth is discussed in [96]. The 99% bandwidth of binary CPFSK as a function of $h$ is tabulated in Table 6.1.

The normalized bandwidth plays an important role in obtaining spectral efficiency of $M$-CPFSK system and is used to accurately determine SE and EE metrics of the system.

87

**Table 6.1:** 99% bandwidth of binary 2-CPFSK as a function of modulation index, $h$

| $h$ | 0.1 | 0.2 | 0.3 | 0.4 | 0.5 | 0.6 | 0.7 | 0.8 | 0.9 | 1.0 |
|---|---|---|---|---|---|---|---|---|---|---|
| $BT_s$ | 0.45 | 0.78 | 0.98 | 1.1 | 1.18 | 1.35 | 1.7 | 1.92 | 2.0 | 2.13 |

## 6.3  SE and EE Metrics of $M$-CPFSK System

The SE metric can be evaluated using the concept of average mutual information rate and normalized bandwidth of the system using (2.3). For $M$-CPFSK system, SE metric can be determined by modelling $M$-CPFSK system as a discrete-input, continuous-output channel as shown in Figure 6.1 with $\boldsymbol{a}$ a vector of input data sequence and $\boldsymbol{y}$ a vector of outputs of correlators receiver. The average mutual information of this channel is given by:

$$I\left(\boldsymbol{a};\boldsymbol{y}\right) = \mathbb{E}\left[\log_2 \frac{p\left(\boldsymbol{y}^n|\boldsymbol{a}^n\right)}{p\left(\boldsymbol{y}^n\right)}\right] , bits/symbol \tag{6.19}$$

where all input data sequences are equally likely, $P(\boldsymbol{a}) = 1/M$, and $p\left(\boldsymbol{y}^n\right) = \sum_{\boldsymbol{a}^n} p\left(\boldsymbol{y}^n|\boldsymbol{a}^n\right) p\left(\boldsymbol{a}\right) = \frac{1}{M}\sum_{\boldsymbol{a}^n} p\left(\boldsymbol{y}^n|\boldsymbol{a}^n\right)$. The average mutual information can thus be written as

$$I\left(\boldsymbol{a};\boldsymbol{y}\right) = \log_2 M - \mathbb{E}\left[\log_2 \frac{\sum_{\boldsymbol{a}} p\left(\boldsymbol{y}^n|\boldsymbol{a}^n, \alpha\right)}{p\left(\boldsymbol{y}|\boldsymbol{a}, \alpha\right)}\right] \tag{6.20}$$

For a given fading coefficient $\alpha$, $p(\boldsymbol{y}|\boldsymbol{a}, \alpha)$ and $p(\boldsymbol{y}^n|\boldsymbol{a}^n, \alpha)$ are given by (6.13) and (6.17), respectively. Thus, SE metric of $M$-CPFSK system is given by

$$\eta_{S_M} = \frac{1}{BT_s} \left\{ \log_2 M - \mathbb{E} \left[ \log_2 \frac{\sum\limits_{\boldsymbol{a}^n \in M^n} I_0 \left( 2\alpha \frac{\sqrt{E_s}}{N_o} |\beta(\boldsymbol{a}^n)| \right)}{I_0 \left( 2\alpha \frac{\sqrt{E_s}}{N_o} |y_k| \right)} \right] \right\} \tag{6.21}$$

The EE metric of $M$-CPFSK system can be obtained using (2.8), where $\gamma = \alpha^2 E_s/N_o$, and is given by

$$\eta_{E_M} = \frac{1}{BT_s} \mathbb{E} \left[ \frac{1}{\alpha^2 E_s/N_o} \log_2 \left( M \frac{I_0 \left( 2\alpha \frac{\sqrt{E_s}}{N_o} |y_k| \right)}{\sum\limits_{\boldsymbol{a}^n \in M^n} I_0 \left( 2\alpha \frac{\sqrt{E_s}}{N_o} |\beta(\boldsymbol{a}^n)| \right)} \right) \right] \tag{6.22}$$

where expectation $\mathbb{E}[.]$ is with respect to $\alpha$. The SE and EE metrics of $M$-CPFSK system given by (6.21) and (6.22), respectively, can be numerically computed for arbitrary number of frequency tones, $M$, modulation index, $h$, number of observation symbols, $n$ and $\alpha$.

### 6.3.1 SE and EE Metrics of $M$-CPFSK system over Nakagami-$m$ Channel

In the previous section, canonical expressions for SE and EE metrics of $M$-CPFSK system were derived. In this section, these metrics are derived for Nakagami-$m$ channel. The fading coefficient, $\alpha$, in (6.13) and (6.17) can be averaged using $\int_0^\infty p(\boldsymbol{y^n}|\boldsymbol{a}^n, \alpha) \, p(\alpha) d\alpha$.

For Nakagami-$m$ channel, using (3.2), this integral is given by

$$p_N\left(\boldsymbol{y}^n|\boldsymbol{a}^n\right) = \frac{K^{'}2m^m}{\Omega^m\Gamma(m)} \int\limits_0^\infty \alpha^{2m-1} \exp^{-\frac{m\alpha^2}{\Omega}} I_o\left(2\alpha\frac{\sqrt{E_s}}{N_o}\beta(\boldsymbol{a^n})\right) d\alpha. \tag{6.23}$$

where suffix $N$ is used to represent Nakagami-$m$ channel. Using [87, eq. (03.02.26.0006.01)], [86, eq. (8.4.3/1)] and [87, eq. (07.34.21.0011.01)] in (6.23), we get

$$p_N\left(\boldsymbol{y}^n|\boldsymbol{a}^n\right) = K^{'}\frac{\pi}{\Gamma(m)}G_{2,3}^{1,1}\left(\frac{\Omega E_s}{mN_o^2}\beta(\boldsymbol{a^n})^2 \ \middle| \ \begin{matrix} 1/2, 1-m \\ 0, 0, 1/2 \end{matrix}\right) \tag{6.24}$$

Using similar averaging over $\alpha$ in (6.17) and (6.13) and using them (6.21), a closed-form expression of SE metric of $M$-CPFSK system in Nakagami-$m$ channel can be written as:

$$\eta_{S_{MN}} = \frac{1}{BT_s}\left\{\log_2 M - \left[\log_2 \frac{\sum\limits_{\boldsymbol{a}^n\in M^n} G_{2,3}^{1,1}\left(\frac{\Omega E_s}{mN_o^2}\beta(\boldsymbol{a}^n)^2 \ \middle| \ \begin{matrix} 1/2,1-m \\ 0,0,1/2 \end{matrix}\right)}{G_{2,3}^{1,1}\left(\frac{\Omega E_s}{mN_o^2}|y_k|^2 \ \middle| \ \begin{matrix} 1/2,1-m \\ 0,0,1/2 \end{matrix}\right)}\right]\right\} \tag{6.25}$$

The EE metric given (6.22) for $M$-CPFSK system, after averaging over $\alpha$ using density given by (3.2), we get

$$\eta_{E_{MN}} = \frac{1}{BT_s\Omega E_s/N_o}\log_2\left[\frac{MG_{2,3}^{1,1}\left(\frac{\Omega E_s}{mN_o^2}|y_k|^2 \ \middle| \ \begin{matrix} 1/2,1-m \\ 0,0,1/2 \end{matrix}\right)}{\sum\limits_{\boldsymbol{a}^n\in M^n} G_{2,3}^{1,1}\left(\frac{\Omega E_s}{mN_o^2}\beta(\boldsymbol{a}^n)^2 \ \middle| \ \begin{matrix} 1/2,1-m \\ 0,0,1/2 \end{matrix}\right)}\right] \tag{6.26}$$

For 2-CPFSK system, theoretical SE metrics, given (6.25), are plotted in Figure 6.3 as a function of modulation index ($h = 0.5, 1$) and parameter of Nakagami-$m$ density ($m = 1, 4$). Also, shown in the figure are SE metrics using Monte Carlo simulation. For

90

comparison, SE metrics for AWGN channel are also shown in the figure. The EE metrics of 2-CPFSK system are plotted in Figure 6.4, for observation length $n = 3$, $h = 0.5, 1$ and normalized bandwidth $BT_s$ [96]. It is observed from Figure 6.3 that 2-CPFSK
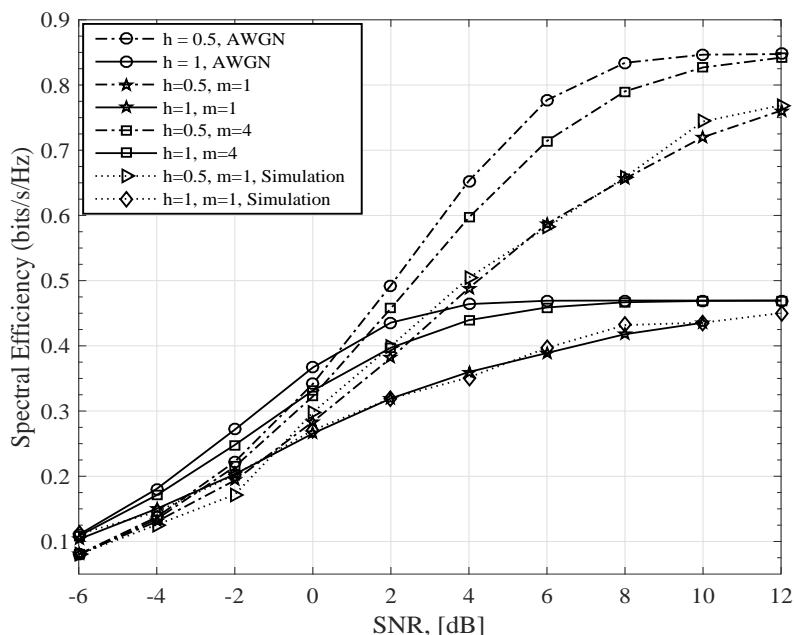


**Figure 6.3:** SE metric of 2-CPFSK system for Nakagami-$m$ channel, $h = 0.5, 1$

system with $h = 1$ achieves slightly higher SE metric for, $-6 \leq$ SNR $\leq 0$ dB. On the other hand, same system with $h = 0.5$, i.e. minimum-shift keying (MSK), is superior for SNR$\geq 2$ dB. Also, it is noted that SE converges to $\frac{1}{BT_s}$ for SNR $\geq$ 10 dB. Figure 6.3 and Figure 6.4 show that SE and EE metrics of 2-CPFSK system are adversely affected over Nakagami-$m$ channel for $m = 1$, which represents the case of severe fading with no direct signal path between transmitter and receiver. Both SE and EE metrics are degraded by nearly 25% for $-5$ dB $\leq$ SNR $\leq 8$ dB. These metrics improve as value of $m$ increases and approaches metrics for AWGN channel $m \rightarrow \infty$. It is noted that both simulation and theoretical results are nearly the same. Form Figure 6.3 and Figure 6.4, it is observed
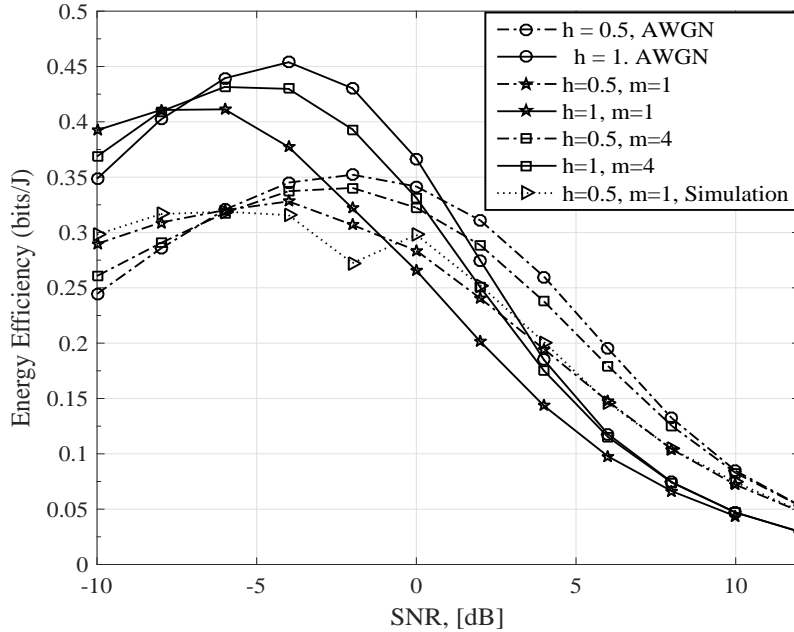
**Figure 6.4:** EE metric of 2-CPFSK system ($h = 1$ and $= 0.5$) for Nakagami-$m =$ channel

that energy-efficient 2-CPFSK systems can be designed for lower values of SNR; however, these systems will be spectrally inefficient. On the other hand, spectrally-efficient systems can be designed for larger values of SNR and these systems will be energy-inefficient.

## 6.3.2 SE and EE Metrics of $M$-CPFSK System over GK Channel

When fading and shadowing effects exist over the channel, it is best modelled using GK distribution, as discussed in Chapter 3. Using statistical averaging approach used in Section 6.3.1, SE and EE metrics of $M$-CPFSK system for GK channel can be derived

and are given by:

$$\eta S_{MGK} = \frac{1}{BT_s} \left\{ \log_2 M - \left[ \log_2 \frac{\sum\limits_{\boldsymbol{a}^n \in M^n} G_{3,3}^{1,2} \left( \frac{\Omega E_s}{cmN_o^2} \beta(\boldsymbol{a}^n)^2 \left| \begin{matrix} 1/2,1-c,1-m \\ 0,0,1/2 \end{matrix} \right. \right)}{G_{3,3}^{1,2} \left( \frac{\Omega E_s}{cmN_o^2} |y_k|^2 \left| \begin{matrix} 1/2,1-c,1-m \\ 0,0,1/2 \end{matrix} \right. \right)} \right] \right\}$$

(6.27)

and

$$\eta E_{MGK} = \frac{1}{BT_s \Omega E_s/N_o} \log_2 \left[ \frac{MG_{3,3}^{1,2} \left( \frac{\Omega E_s}{cmN_o^2} |y_k|^2 \left| \begin{matrix} 1/2,1-c,1-m \\ 0,0,1/2 \end{matrix} \right. \right)}{\sum\limits_{\boldsymbol{a}^n \in M^n} G_{3,3}^{1,2} \left( \frac{\Omega E_s}{cmN_o^2} \beta(\boldsymbol{a}^n)^2 \left| \begin{matrix} 1/2,1-c,1-m \\ 0,0,1/2 \end{matrix} \right. \right)} \right]$$

(6.28)

It is noted that SE and EE metrics given by (6.27) and (6.28) are in closed-form and can

be numerically computed. These metrics represent theoretical estimates of SE and EE

metrics. For 2-CPFSK system, both simulation and theoretical SE metrics are plotted

in Figure 6.5 as a function of modulation index ($h = 0.5, 1$), and parameters of GK

distribution. Similar plots for EE metric are shown in Figure 6.6. The plots in these

figures are for $n = 3$ (observation length of receiver is $3T_s$) and for normalized bandwidth

$BT_s$. For comparison, SE and EE metrics for AWGN channel are also plotted in

Figure 6.5 and Figure 6.6. These figures show that both SE and EE metrics deteriorate

sharply when fading and shadowing effects are severe over the channel. For example, SE

metric of 2-CPFSK system with $h = 0.5$, when GK distribution parameters are $c = 2$

and $m = 2$, decreases by 0.35 bits/s/Hz on average for $2 \leq \text{SNR} \leq 8$ dB compared

to SE metric of AWGN channel over the same range of SNR. For the GK distribution

parameters, EE metric of the system becomes poorer by at least 55%, for $-8 \leq \text{SNR}$
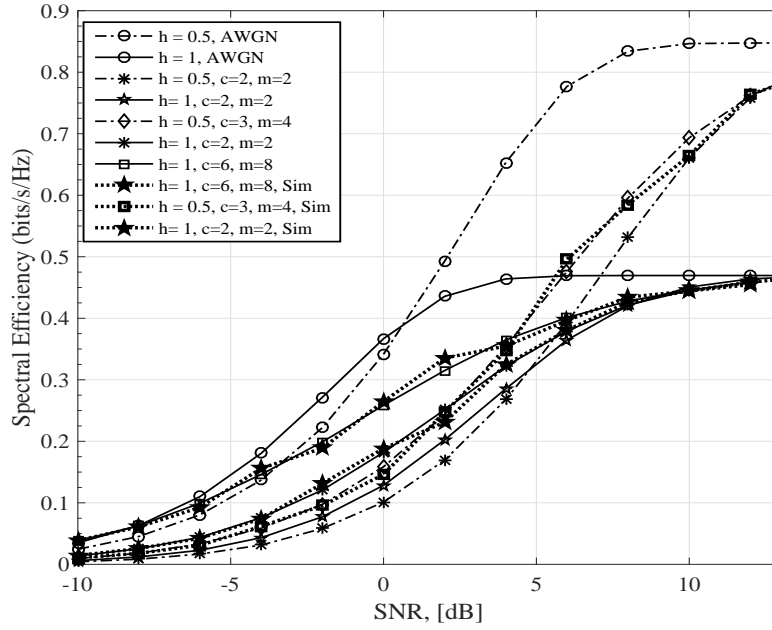
**Figure 6.5:** SE metrics of 2-CPFSK ($h = 1, 0.5$) system for GK channel
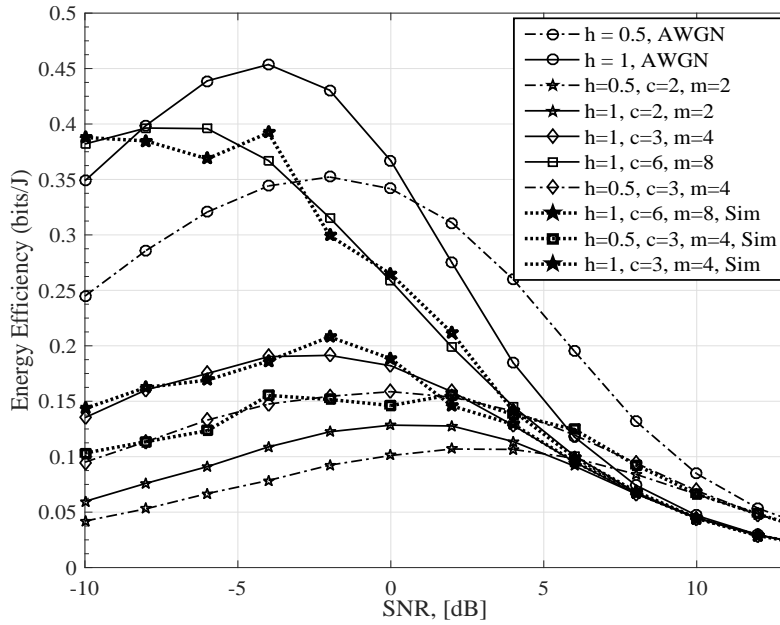


**Figure 6.6:** EE metrics of 2-CPFSK ($h = 1, 0.5$) system for GK channels

$\leq 2$ dB compared to EE metric of AWGN channel for same range of SNR. The results

show that SE and EE metrics of 2-CPFSK system are much lower compared to metrics of

same system in AWGN channel, indicating severe effect of fading and shadowing over the channel on system efficiency metrics. From Figure 6.6, it is observed that EE metric is a convex function of SNR over the channel. Hence, in order to design an energy-efficient 2-CPFSK system, the operating SNR should be between $-5$ dB and 5 dB. Spectrally efficient 2-CPFSK system can be designed for SNR between 5 dB and 12 dB. Thus, trade-off between EE and SE metrics is inevitable in the design of efficient $M$-CPFSK systems.

### 6.3.3 Multi-Symbol Detection in $M$-CPFSK System to Improve SE and EE Metrics

The numerical results of SE and EE metrics of 2-CPFSK system in Sections 6.3.1 and 6.3.2 reveal that fading and shadowing effects over channel can severely impact its efficiency metrics. Therefore, it is important to find methods to make SE and EE metrics less sensitive to effects of fading and shadowing over the channel and also improve SE and EE metrics of the system. It is well-known that in $M$-CPFSK system multiple-symbol-observation receiver can employed which makes the system energy-efficient. Thus, in this Section an $M$-CPFSK system is proposed in which observation length of receiver can be adjusted depending on channel conditions to improve efficiency metrics of the system. The multiple-symbol-observation technique is based on observing received $M$-CPFSK signal over fading and shadowing channel over $n$ symbol intervals and then deciding on most likely symbol transmitted using maximum likelihood detection and is discussed at length in [94]. An important observation of such a technique in $M$-CPFSK system is

that its performance improves as a function of observation length, $n$, of receiver, before a decision is made on most likely symbol transmitted. Thus, the SE and EE metrics are examined as a function of $n$ for 2-CPFSK system. These metrics are plotted for 2-CPFSK system for $h = 0.715$ in Figure 6.7 and Figure 6.8, respectively, as a function of $n$ ($= 1, 3$ and $5$) for GK channel ($m = 3, c = 2$). The value of $h = 0.715$ is optimum and maximizing BER metric of 2-CPFSK system. It is observed that spectral and energy efficiencies increase as $n$ increases, particularly for $-10$ dB $\leq$ SNR $\leq 0$ dB. For instance, SE metric is increased by 50% and EE metric by 90% when 5-symbol detection receiver is used relative to a corresponding system with one-symbol-observation receiver. However, this improvement is possible at the cost of increased the complexity of the system and complexity increases exponentially as the observation length of receiver.
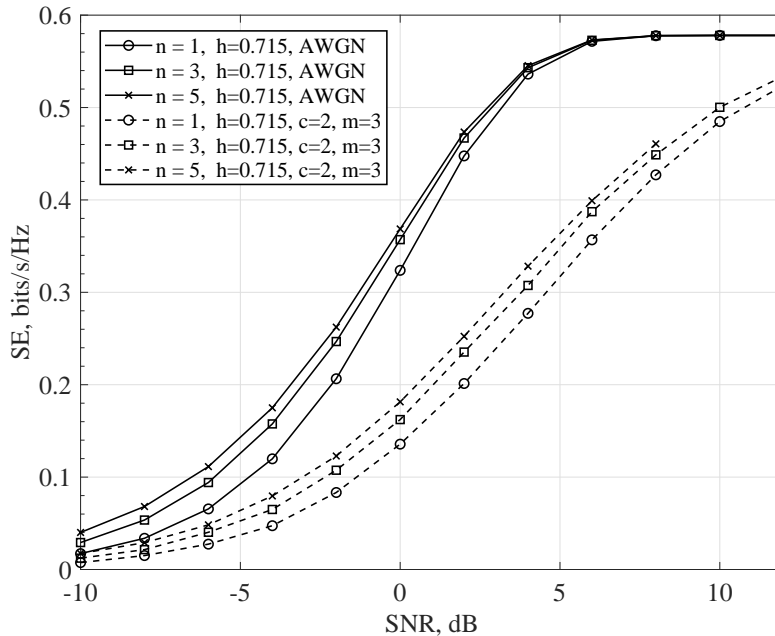


**Figure 6.7:** SE metrics of 2-CPFSK ($h = 0.715$) system as function of $n$ for GK channel ($m = 3, c = 2$)
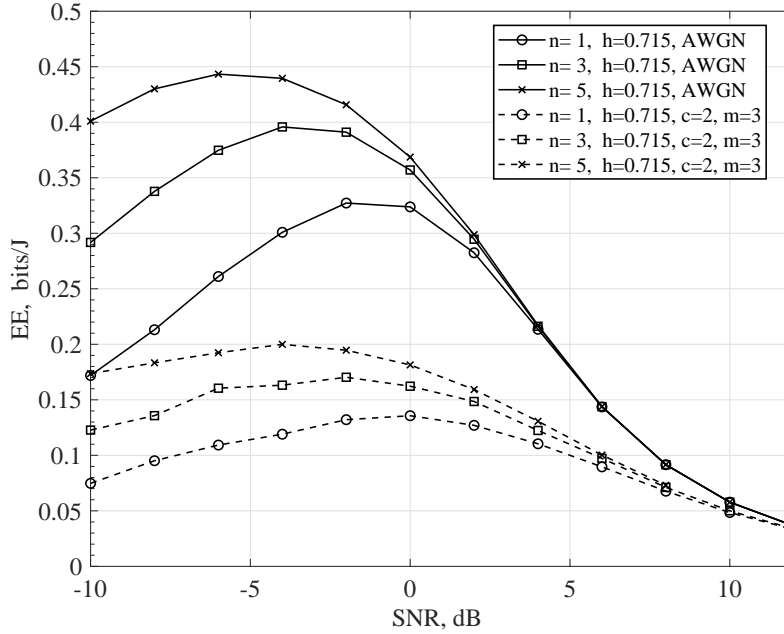
**Figure 6.8:** EE metrics of 2-CPFSK ($h = 0.715$) system as a function of $n$ for GK channel

## 6.3.4 Effect of $M$-CPFSK System Parameters on SE and EE Metrics

The efficiency metrics of $M$-CPFSK system are dependent on its parameters, $M$, $h$, and $n$. The normalized bandwidth, $BT_s$ is a function of $M$ and $h$. To illustrate the role of these parameters on efficiency metrics of $M$-CPFSK system, SE and EE metrics are plotted for AWGN channel as a function of $BT_s$ and SNR in Figure 6.9 and Figure 6.10, respectively, with observation length of receiver fixed at 3 symbol intervals. It is noted that SE metric attains its maximum value for $0.78 \leq BT_s \leq 1.18$ and $10 \leq \text{SNR} \leq 15$ dB; the metric reaches a value of 0.877 bits/s/Hz implying that bandwidth is efficiently utilized in the system. From Figure 6.10, it is observed that $M$-CPFSK system achieves maximum values of EE metric for $-2 \leq \text{SNR} \leq 2$ dB and $1.35 \leq BT_s \leq 2.13$. However, these ranges of SNR and $BT_s$ do not provide high values of SE metric implying that trade-

off between SE amd EE metrics is important in designing an efficient $M$-CPFSK system.
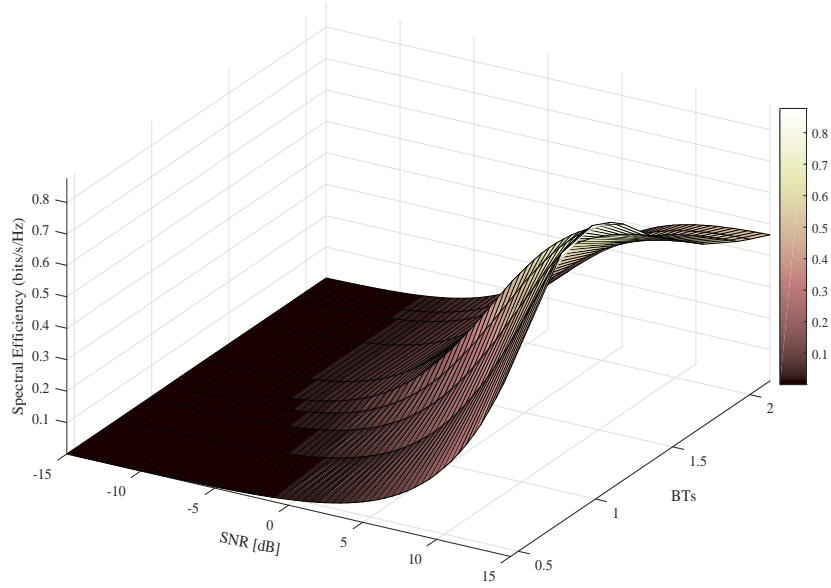


**Figure 6.9:** SE metric of 2-CPFSK system as a function of SNR and $BT_s$ for $n = 3$
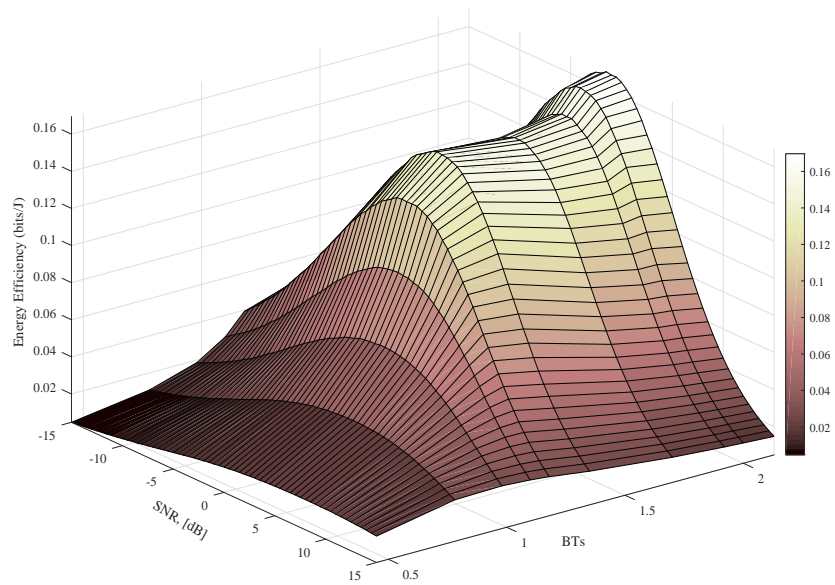


**Figure 6.10:** EE metric of 2-CPFSK system as a function of SNR and $BT_s$ for $n = 3$

Since modulation index, $h$, of $M$-CPFSK system is an important parameter, its influence

on SE and EE metrics is investigated in Figure 6.11 and Figure 6.12, respectively.    In
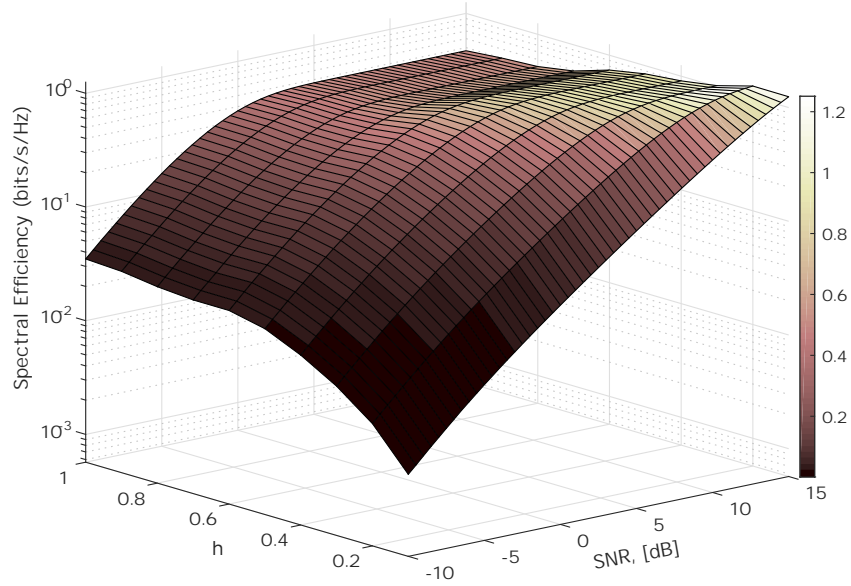


**Figure 6.11:** SE of 2-CPFSK system as a function of SNR and modulation index
$0.1 \leq h \leq 1$ for $n = 3$
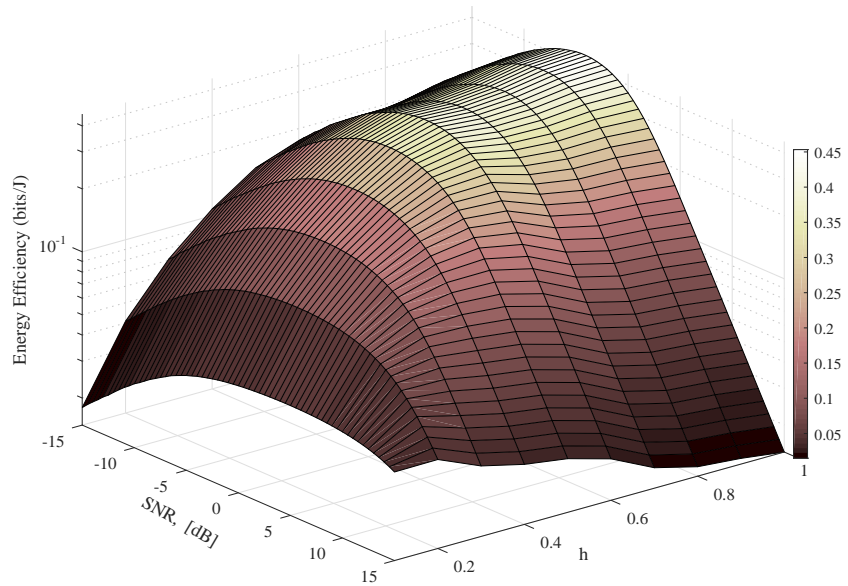


**Figure 6.12:** EE of 2-CPFSK system as a function of
SNR and $0.1 \leq h \leq 1$ for $n = 3$

Figure 6.11, it is observed that SE metric increases for $h \leq 0.4$ and starts to decline for $0.4 < h \leqslant 1$; it is noted that SE is an increasing function of average SNR over the channel. The EE metric, on the other hand, is an increasing function of $h$; and is a concave function of SNR and attains maximum value over $-5\ dB < \text{SNR} < 5\ dB$, as shown in Figure 6.12. Thus, $h$, $BT_s$ and SNR can be determined for designing efficient 2-CPFSK system using plots of SE and EE metrics given in Figure 6.11 and Figure 6.12.

## 6.4 Bounds on BER Metric of $2$-CPFSK System for Nakagami-$m$ and GK Channels

The BER metric plays an important role in the design of any communication system, and for a 2-CPFSK system, this metric is derived for Nakagami-$m$ and GK channels. The upper and lower bounds on maximum likelihood multi-symbol observation receiver are derived in [79] for 2-CPFSK system operating in AWGN channel. These bounds are given by:

$$P_u(\epsilon) = \frac{1}{2^{n-1}} \sum_{l=1}^{2^{n-1}} \sum_{j=1}^{2^{n-1}} Q\left( \sqrt{\frac{nE_b}{N_o}\left[1 - \rho(l,j)\right]} \right) \tag{6.29}$$

and

$$P_l(\epsilon) = \frac{1}{2^{n-1}} \sum_{l=1}^{2^{n-1}} Q\left( \sqrt{\frac{nE_b}{N_o}\left[1 - \rho^*(l)\right]} \right) \tag{6.30}$$

where $Q(x) = \frac{1}{\sqrt{2\pi}} \int_x^\infty e^{-t^2/2} dt$ and $\rho^*(l) = \max[\rho(l,j)]$ and $\rho(l,j)$ is the normalized correlation given by:

$$\rho(l,j) = \frac{1}{n} \sum_{k=1}^{n} sinc\left(\frac{h}{2}(a_k - b_k)\right) . \cos\left[\frac{\pi h}{2}(a_k - b_k) + \sum_{j=1}^{k-1}(a_j - b_j)\right] \quad (6.31)$$

where $a_k$ and $b_k$ are data corresponding to $\boldsymbol{a} = (a_1 = +1, a_2, ...., a_n)$ and $\boldsymbol{b} = (b_1 = -1, b_2, ..., b_n)$ with $a_k$ and $b_k$ taking values $\pm 1$ as defined in (6.2). It is noted that upper and lower bounds are the same for SNR$\geq 4$ dB. The 2-CPFSK signal received over fading channel can be modelled as

$$r(t) = \alpha s(t, \boldsymbol{a}) + n(t), \quad 0 \le t \le nT_s \quad (6.32)$$

where $\alpha$ is fading coefficient and $n(t)$ is AWGN with zero mean and two-sided PSD of $N_o/2$ watts/Hz. The SNR of signal in (6.32) is $\gamma = \frac{\alpha^2 nE_b}{N_o}$ and its average is given by $\overline{\gamma} = \mathbb{E}[\gamma] = \mathbb{E}[\alpha^2]nE_b/N_o$. The BER metric is thus given by

$$P_F(\epsilon) = \int_0^\infty P_l(\epsilon|\gamma)p_\gamma(\gamma)d\gamma \quad (6.33)$$

where $P_l(\epsilon|\gamma)$ is given by (6.30) with $nE_b/N_o$ replaced by $\gamma = \frac{\alpha^2 nE_b}{N_o}$ and $p_\gamma(\gamma)$ is the density of $\gamma$. For Nakagami-$m$ fading channel, a closed-form expression for BER metric can be derived and is given by:

$$P_N(\epsilon) = \frac{1}{2^n \sqrt{\pi}\Gamma(m)} \sum_{l=1}^{2^{n-1}} G_{2,2}^{2,1}\left(\frac{\beta(l)}{m}\frac{\Omega E_b}{N_o} \,\bigg|\, \begin{matrix} 1, \ 1-m \\ 0, \ 1/2 \end{matrix}\right) \quad (6.34)$$

101

where $\beta(l) = \frac{n}{2}[1 - \rho^*(l)]$. It is noted that $P_N(\epsilon)$ is a function of $\bar{\gamma} = \Omega n E_b/N_o$, modulation index, $h$, and the observation length, $n$, of receiver. In Figure 6.13, $P_N(\epsilon)$ vs. SNR are plotted for various values of fading figure $(m)$, for observation length, $n (= 3)$, and modulation index, $h (= 0.715)$. It is observed that as $m$ increases BER performance of the system improves. As $m \to \infty$, $P_N(\epsilon)$ approaches the BER performance of a 2-CPFSK system in AWGN channel. The PP metric for Nakagami-$m$ channel is shown in
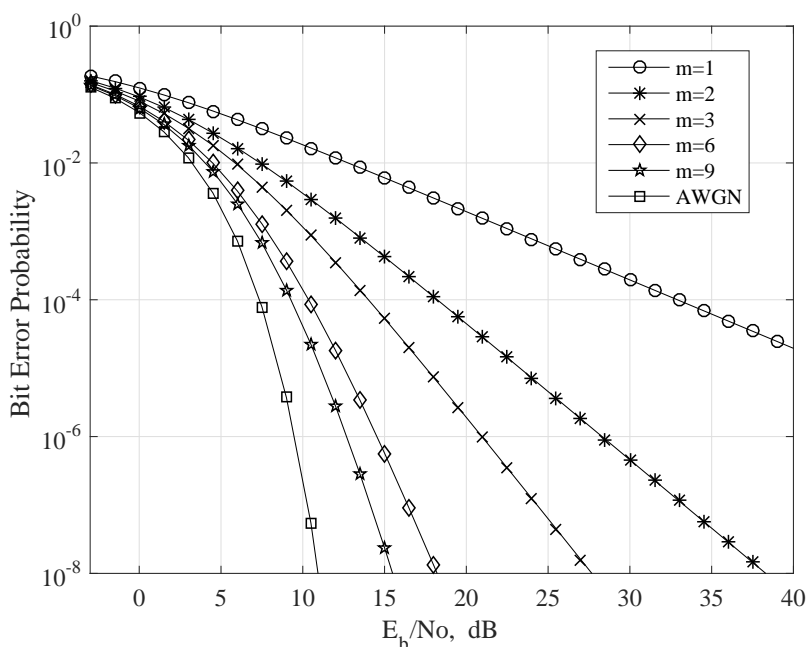


**Figure 6.13:** BER metric of 2-CPFSK system over Nakagami-$m$ channel for $n = 3$

Figure 6.14 for various BER metrics for $m = 2, 3, 6$, and $9$ and $n = 2, 4$ for a 2-CPFSK system with $h = 0.715$. It is noted that as fading effect over channel decreases (i.e. as m increases) the PP required decreases. For $n = 4$, the PP is reduced by about 1.2 dB relative to PP required when $n = 2$. From Figure 6.14 it is also observed that less PP is required as BER metric of the system increases. For $m = 3$ and $P_N(\epsilon) = 10^{-4}$, PP required for $n = 2$ and $n = 4$ are 6.5 dB and 5.3 dB, respectively.
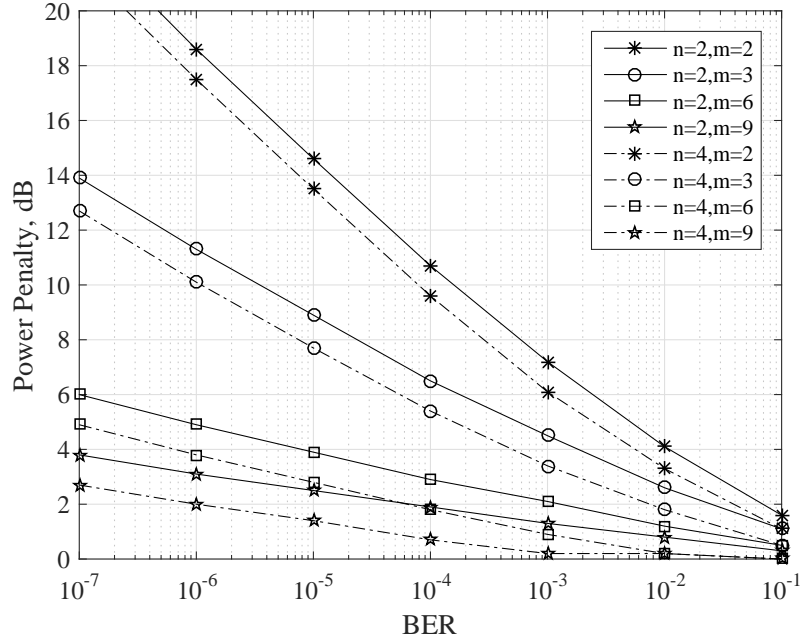
**Figure 6.14:** Power Penalty versus BER of 2-CPFSK for Nakagami-$m$ channel

The BER metric of 2-CPFSK system for GK channel has been derived in closed-form using similar technique used for Nakagami-$m$ channel and is given by:

$$P_{GK}(\epsilon) \quad = \quad \frac{1}{2^n\sqrt{\pi}\Gamma(c)\Gamma(m)} \sum_{l=1}^{2^{n-1}} G_{3,2}^{2,2}\left(\frac{\beta(l)}{c\,m}\Omega E_b/N_o \;\middle|\; \begin{matrix} 1,\, 1-c,\, 1-m \\ 0,\, 1/2 \end{matrix}\right) \quad (6.35)$$

In Figure 6.15, $P_{GK}(\epsilon)$ vs. SNR for a 2-CPFSK system is plotted as a function of GK distribution parameters $m$ and $c$. Also, plotted in the same figure are BER metrics for AWGN channel. From this figure, it is observed that the effect of fading coupled with shadowing over channel deteriorates BER metric of the system. The worst case performance is observed for $m = 1$ and $c = 2$, for which fading and shadowing effects over the channel are worst. It is noted that BER performance at $c = 1$ is poorer than the performance over Nakagami-$m$ channel with $m = 1$ which shows that shadowing

103
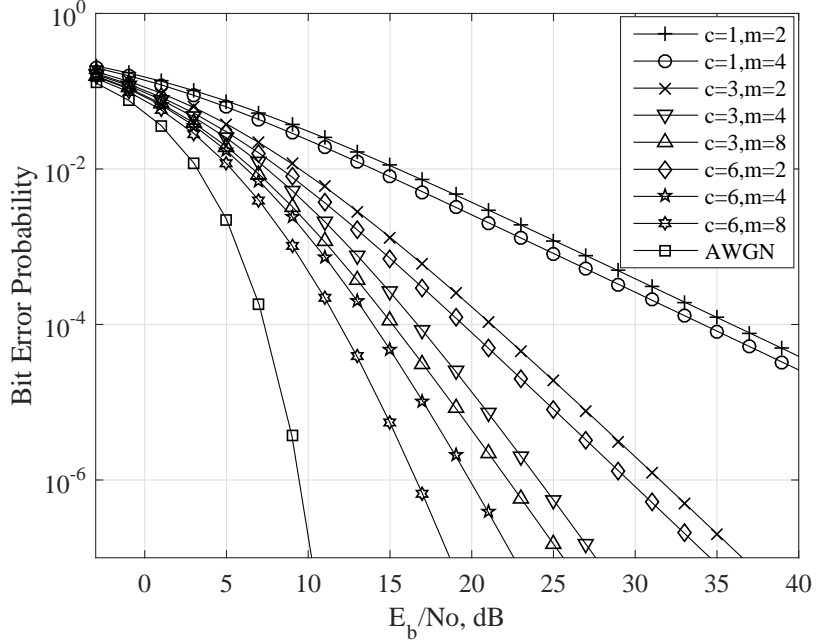
**Figure 6.15:** BER metric of 2-CPFSK system ($h = 0.715$) over $GK$-channel as function of $c$ and $m$, $n = 3$

effect over channel has more impact on BER metric of the system than just fading effect.

From Figure 6.15, it can also be observed that $P_{GK}(\epsilon)$ becomes better and better as $c$ and/or $m$ increase. In Table 6.2, PP for 2-CPFSK system for selected parameters of GK distribution are shown at two specific values of BER ($10^{-4}$ and $10^{-6}$). It is noted that

**Table 6.2:** PP for 2-CPFSK system as a function of observatio length, $n$, of the receiver for $GK$ channel

| $GK$ channel model parameters $(c, m)$ | | | $c = 1$ $m = 4$ | $c = 3$ $m = 4$ | $c = 6$ $m = 4$ | $c = 6$ $m = 8$ |
|---|---|---|---|---|---|---|
| Power Penalty (dB) | $10^{-4}$ | $n = 2$ | 26.75 | 9.25 | 6.55 | 4.5 |
| | | $n = 4$ | 25.5 | 8.15 | 5.45 | 3.35 |
| | $10^{-6}$ | $n = 2$ | 49.5 | 14.4 | 10.25 | 7 |
| | | $n = 4$ | 48.25 | 13.25 | 9.1 | 5.8 |

PP varies as a function $c$, $m$ and $P_{GK}(\epsilon)$. For severe fading and shadowing effects over channel (small values $c$ and $m$), 2-CPFSK system requires large PP and small PP are

required as fading and shadowing effects over channel decrease (large values of $c$ and/or $m$). It is noted that PP required can be reduced by increasing the observation length of the receiver for 2-CPFSK system; however, at the cost of increased complexity of the system.

## 6.5    Chapter Summary

In this Chapter, SE and EE metrics of $M$-CPFSK system are examined for AWGN, multi-path fading and multi-path fading with shadowing channels. To begin with, SE and EE metrics of $M$-CPFSK system are derived using average mutual information of DCMC that represents the system. The SE and EE metrics are functions of SNR, $M$, $h$, $n$ and channel distribution parameters. The effects of fading and shadowing over the channel significant impacts SE and EE metrics of the system. These metrics have been extensively illustrated for 2-CPFSK system, although the expressions for SE and EE metrics presented in this Chapter are valid for arbitrary $M$-CPFSK system. For example for a 2-CPFSK system with $h = 1$, both SE and EE metrics are degraded by nearly 25% for $-5$ dB $\leq$ SNR $\leq 8$ dB, for Nakagami-$m$ channel ($m = 1$). Also, SE metric of the system with $h = 0.5$, for GK channel ($c = 2$ and $m = 2$) decreases by 0.35 bits/s/Hz on average for $2 \leq$ SNR $\leq 8$ dB compared to SE metric of AWGN channel over same range of SNR. A multi-symbol observation receiver in an $M$-CPFSK system is presented. The efficiency metrics of the system can be enhanced by increasing observation length of receiver in the system; however, at the cost of increased system complexity. For instance, in a 2-CPFSK system with $h = 0.715$, SE metric is doubled and EE metric is tripled,

when 5-symbol detection receiver is used relative to a corresponding system with one-symbol-observation receiver for GK channel, $(m = 3, c = 2)$, for -10 dB $\leq$ SNR $\leq$ 0 dB. Closed-form expressions for BER metrics of 2-CPFSK system are derived for Nakagami-$m$ and GK channels. The effect of receiver observation length $n$ and channel distribution parameters, $c$ and $m$, on BER metric are illustrated. It is observed that BER metric of 2-CPFSK system with $h = 0.715$ and $n = 4$ is improved by 1.2 dB compared to BER metric of same system for $n = 2$. The impact of fading and shadowing on BER performance of 2-CPFSK system is illustrated using PP as a function of system BER. It is noted that for a 2-CPFSK system PP is reduced as observation length of receiver increases; however, at the cost of increased system complexity. It is noted that efficient $M$-CPFSK system can be designed by using observation length of receiver as an adaptive parameter accordingly as the estimated SNR over the channel. Although, numerical results are presented for a 2-CPFSK system all through the Chapter, analytical expressions derived for various metrics are valid for arbitrary values of $M$ and $h$ of $M$-CPFSK system.

# Chapter 7

# Design and Analysis of Cellular Systems

# Based on SE, EE, SSE and SEE Metrics [8,9]

## 7.1   Introduction

In this Chapter, a comprehensive framework for design of a hexagonal cellular system using SE, EE, SSE and SEE metrics is presented. The communication environment in the system is assumed to be Nakagami-$m$ fading coupled with path loss and co-channel interference. Three BS antenna configurations namely, omni, $120^o$ and $60^o$ are considered. Closed-form expressions for SE and EE metrics are first derived for single- and multi-cell systems using statistical averaging. Then, expressions for SSE and SEE metrics and coverage probability are derived and illustrated as a function of SNR, cell radius,

8. Hamed, A., and Rao, R.K., "Spatial Spectral and Energy Efficiencies of Cellular Networks Limited by Co-channel Interference and Path Loss in Nakagami-$m$ Fading Environment," EURASIP Journal on Wireless Communications and Networking, vol. 2018, no.1, pp. 118-134, 2018.

9. Hamed, A.M.,; Rao, R.K., "Energy and spectral efficiency in cellular networks considering fading, path loss, and interference." In Electrical and Computer Engineering (CCECE), pp. 1-5. IEEE, 2017.

reuse distance, path loss exponent factor and fading figure. A discussion of trade-offs among SE, EE, SSE, SEE and coverage probability as a function of cellular system parameters and propagation environment is also provided. A technique for improvement of efficiency metrics using sectorized antenna system at BS is suggested and investigated. The contributions of this Chapter among other results include: $i$) analysis of SE and EE metrics for single- and multi-cell cellular systems; $ii$) investigation of SSE and SEE metrics for these two systems; and $iii$) evaluation of coverage probability. Antenna sectorization at BS is discussed for efficient design of cellular systems using efficiency metrics.

## 7.2 Cellular System and Propagation Environment

A cellular system consisting of homogeneous macro-cells with hexagonal tessellation is shown in Figure 7.1. The BSs are located at the center of each cell and users are assumed to be served by their closest BS. The power and bandwidth resources are assumed to be equally assigned to all cells in the system. The downlink, BS to user, efficiency analysis is of interest in this work. Three different BS antenna configurations are considered: i) omni; ii) $120^o$; and iii) $60^o$. Figure 7.1 shows an omni hexagonal cellular system with $R$, the cell radius, $D$, the frequency reuse distance, and $D_{k,i}$, the distance between $i^{th}$ user and the $k^{th}$ interfering BS. The blue cells in Figure 7.1 use same frequency band and hence are co-channel cells.
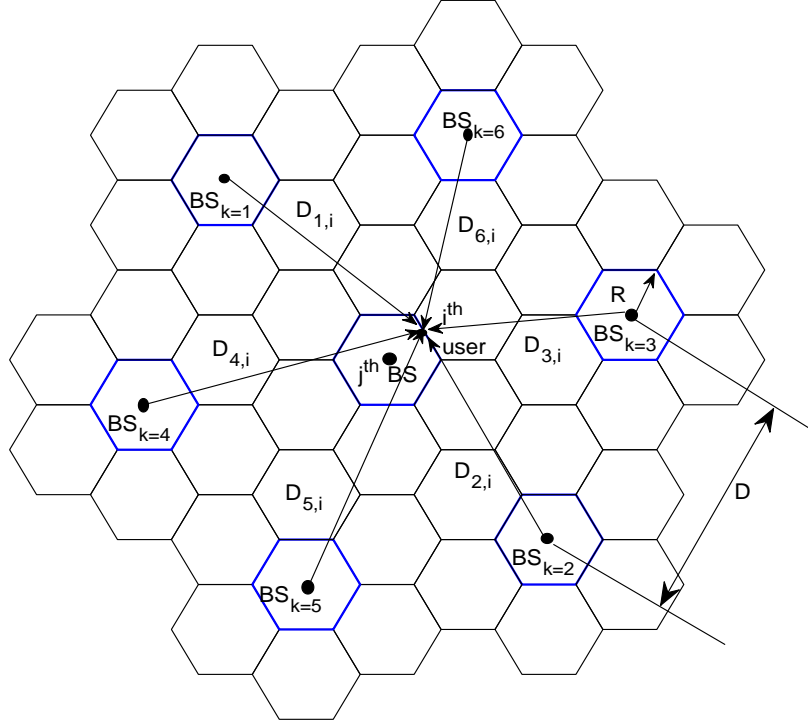
**Figure 7.1:** Hexagonal cellular system

## 7.2.1 Propagation and Interference Models

In the cellular system shown in Figure 7.1, let transmission power of $j^{th}$ BS be $P_j$ and mobile user $i$ be served by its closest BS. Thus, power received at $i^{th}$ mobile user at a distance of $r_{j,i}$ from $j^{th}$ BS can be written as

$$P_{j,i} = P_j r_{j,i}^{-\upsilon} \alpha_{j,i}^2, \tag{7.1}$$

where $\upsilon$ is path-loss exponent, and $\alpha_{j,i}$ is a random variable representing channel fading coefficient between $i^{th}$ user and $j^{th}$ BS. The aggregated interference power at $i^{th}$ user

due to $k^{th}$ co-channel BS can be expressed as

$$I_i = \sum_{j=1}^{N_I} P_k D_{k,i}^{-\upsilon} \alpha_{k,i}^2,$$

(7.2)

where $D_{k,i}$ is distance between $k^{th}$ interfering BS and $i^{th}$ user, and $N_I$ is number of co-channel interfering cells in the system. The generic expression for instantaneous signal-to-interference plus noise ratio (SINR) at $i^{th}$ user can be expressed as [38]:

$$\gamma_{j,i}^I = \frac{P_j r_{j,i}^{-\upsilon} \alpha_{j,i}^2}{B N_o + \sum_{\substack{k=1 \\ k \neq j}}^{N_I} P_k D_{k,i}^{-\upsilon} \alpha_{k,i}^2},$$

(7.3)

where $N_o$ is power spectral density of AWGN, and $B$ is bandwidth of user. The resulting SINR is a random variable in which $\alpha_{k,i}^2$ represents power associated with fading coefficient of channel.

## 7.2.2   User's Location Model

It is assumed that users are randomly distributed across a given cell; hence, it is important to model users' locations in the system. The BS coverage area can be approximated to that of a circle with radius $R$. The users' locations can be defined using polar coordinates as:

$$\mathcal{L}(r,\theta) = r e^{j\theta}$$

(7.4)

110

where $r$ is distance from BS and $\theta$ is the angle with respect to a certain reference. The pdf of $r$ and $\theta$ are given by [97]

$$p_r(r) = \frac{2r}{R^2}, \qquad 0 \leqslant r \leqslant R \tag{7.5}$$

$$p_\theta(\theta) = \begin{cases} \frac{1}{2\pi}, & 0 \leqslant \theta \leqslant 2\pi \\ \\ 0, & elsewhere \end{cases} \tag{7.6}$$

Using (7.5) and (7.6), user's location can be estimated and hence received power in (7.1) and (7.2).

### 7.2.3 Fading Channel Model: Nakagami-$m$

The powers in (7.1) and (7.2) are randomly scaled by factor $\alpha_{j,i}^2$. Many distributions have been used to model multi-path fading coefficient $\alpha_{j,i}^2$ in cellular systems. In this chapter, Nakagami-$m$ fading model is used to model $\alpha_{j,i}^2$ and its pdf $\alpha_{j,i}^2 \sim \mathcal{G}(m, \Omega)$ is given by (3.3). The density of $\gamma_{j,i}$ for $\alpha_{j,i}$ Nakagami-$m$ density are given by

$$p_{\gamma_{j,i}}(\gamma_{j,i}) = \frac{m^m \gamma_{j,i}^{m-1}}{\overline{\gamma}_{j,i}^m \Gamma(m)} \exp\left(-\frac{m\gamma_{j,i}}{\overline{\gamma}_{j,i}}\right), \qquad \gamma_{j,i} \geqslant 0 \tag{7.7}$$

where $m$ is fading figure, $\Omega = \overline{\alpha_{j,i}^2}/m$, $\gamma_{j,i} = \frac{P_{j,i}\alpha_{j,i}^2}{BN_o}$ is instantaneous SNR, $\overline{\gamma}_{j,i} = \frac{P_{j,i}\overline{\alpha^2}_{j,i}}{BN_o}$ is average SNR, and $P_{j,i} = P_j r_{j,i}^{-\upsilon}$ is $i^{th}$ user's received power at a distance $r_{j,i}$ from $j^{th}$ BS and hence average SNR is $\overline{\gamma}_{j,i} r^{-\upsilon}$.

## 7.3    SE and EE Metrics of Single- and Multi-Cell Systems

Bandwidth and power are two main resources of concern in the design of a cellular system. Since demand for high data rates is growing rapidly, SE-oriented cellular system design causes a large increase in energy consumption when quality of link performance required is high. The next generation of efficient cellular systems, therefore, must be designed not only for high SE metric but also for high EE metric. In this section, downlink energy and spectral efficiencies are studied considering multi-path fading, co-channel interference, and frequency reuse factor for single and multi-cell scenarios.

### 7.3.1    Analysis of SE and EE Metrics of a Single Cell System

In this section, SE and EE metrics of a single cell system with cell radius $R$ as shown in Figure 7.2 are examined. The BS serves a set of $K$ users with power and bandwidth resources equally shared among all users in the system. Thus, each user occupies $B$ Hz of bandwidth and receives power $P_i$. The users are randomly located as described by (7.4).

#### 7.3.1.1    Expression for SE Metric

The downlink spectral efficiency quantifies delivered data rate to a user over a given bandwidth. Assuming random fading coefficients are independent, aggregated downlink
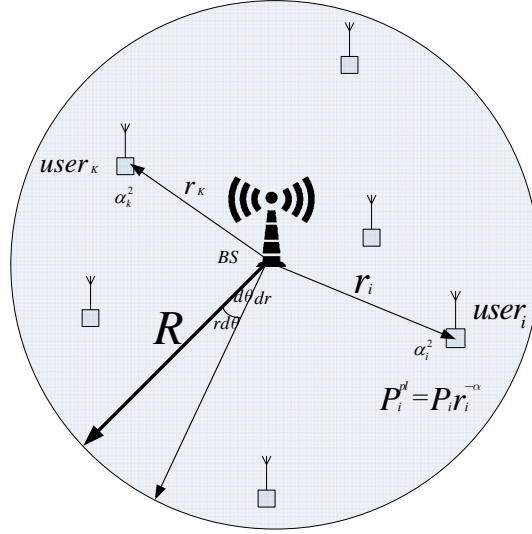
**Figure 7.2:** Single cell system with omni antenna at BS

conditional spectral efficiency can be expressed as

$$\eta_{S|\alpha_i} = \sum_{i=1}^{K} \mathbb{E}\left[\log_2\left(1 + \frac{P_i\alpha_i^2}{BN_o}r_i^{-\upsilon}\right)\right], \quad (bit/s/Hz) \tag{7.8}$$

where $K$ is total number of users in cell, superscript $d$ denotes downlink, and expectation, $\mathbb{E}$, is over $\alpha_i$ and $\gamma_i = \frac{P_i\alpha_i^2}{BN_o}r_i^{-\upsilon}$ represents instantaneous SNR at $i^{th}$ user located at a distance of $r_i$ form BS with $\upsilon$ the pathloss coefficient. Averaging over conditional random variable in (7.8), spectral efficiency of a single-cell system can be written as:

$$\eta_{S,sc} = \int_0^\infty \sum_{i=1}^{K} \left[\log_2\left(1 + \gamma_i r_i^{-\upsilon}\right)\right] p_{\gamma_i}(\gamma_i)d\gamma_i \tag{7.9}$$

Using pdf of $\gamma_i$ given by (7.7), where the subscript $j$ is dropped for the case of single BS in (7.9) and using [84, eq. (3.383.10), eq. (3.326.2)], we get

$$\eta_{S,sc}(r_i, \upsilon) = \frac{1}{\log 2}\sum_{i=1}^{K}\sum_{k=1}^{m} e^{\frac{m}{\overline{\gamma}_i}r_i^{\upsilon}} \times \Gamma\left(-m+k, \frac{m}{\overline{\gamma}_i}r_i^{\upsilon}\right)\left(\frac{\overline{\gamma}_i}{m}r_i^{-\upsilon}\right)^{k-m} \tag{7.10}$$

where $\bar{\gamma}_i$ is $\mathbb{E}[\gamma_i]$ and represents average SNR at $i^{th}$ user and $\eta_{S,sc}$ is a function of $r$ and $v$, and hence it is written as $\eta_{S,sc}(r,v)$. It is noted that spectral efficiency is also function of Nakagami-$m$ distribution parameter $m$. Since user's distance $r_i$ is random, (7.10) needs to be averaged over density of $r_i$ given by (7.5). By expressing incomplete gamma function $\Gamma\left(-m+k, \frac{m}{\bar{\gamma}_{j,i}} r_i^v\right)$ in (7.10) using [87, eq.(06.06.03.0009.01)] and using (7.5) in (7.10), downlink spectral efficiency can be obtained in closed-form as:

$$\eta_{S,sc}(R,v) = \frac{2}{v\log 2} \sum_{i=1}^{K} \sum_{k=1}^{m} \sum_{l=1}^{m-k} \frac{(m-k)!}{l!} \times \left(\frac{\bar{\gamma}_i}{m}\right)^{k-m-l} R^{v(m-k+l)} \tag{7.11}$$

It is apparent that downlink spectral efficiency is a function of cell radius $R$ and path loss exponent $v$ as well.

### 7.3.1.2 Expression for EE Metric

The energy efficiency is defined as $\eta(x)/x$ as discussed in Section 2.3. In the analysis of a cellular system, $\eta(x)$ represents downlink data rate and $x$ is SNR, which depends on transmitted power at BS, AWGN and channel effects. For a single cell system, downlink conditional EE metric is given by:

$$\eta_{E|\alpha_i} = \sum_{i=1}^{K} \mathbb{E}\left[\frac{\log_2\left(1 + \frac{P_i^{pl}\alpha_i^2}{BN_o}\right)}{\frac{P_i^{pl}\alpha_i^2}{BN_o}}\right], \; [bits/J] \tag{7.12}$$

114

Following steps similar to those used for finding SE metric in Section 7.3.1.1, an expression for EE metric can be derived and is given by

$$\eta_{E,sc}(r_i, \upsilon) = \frac{(m)^m}{\Gamma(m)\log 2} \sum_{i=1}^{K} \frac{r_i^{\upsilon(m+1)}}{\overline{\gamma}_i^{m+1}} \times G_{2,3}^{3,1}\left(\frac{mr_i^\upsilon}{\overline{\gamma}_i} \,\middle|\, \begin{matrix} -m, 1-m \\ 0, -m, -m \end{matrix}\right) \qquad (7.13)$$

Again averaging over $r_i$ using (7.5) and using [87, eq.(07.34.21.0003.01)], a closed-form expression can be obtained and is given by

$$\eta_{E,sc}(R, \upsilon) = \frac{(m)^m \, R^{\upsilon(m+1)-1}}{\upsilon\Gamma(m)\log 2} \sum_{i=1}^{K} \frac{1}{\overline{\gamma}_i^{m+1}} \times G_{3,4}^{3,2}\left(\frac{mR^\upsilon}{\overline{\gamma}_i} \,\middle|\, \begin{matrix} -(m+1/\upsilon), -m, -m \\ 0, -m, -m, -(m+1+1/\upsilon) \end{matrix}\right)$$
$$(7.14)$$

It is noted that EE metric given by (7.14) is a function of $R$, $\upsilon$, $\overline{\gamma}_i$, and $m$.

## 7.3.2 Analysis of SE and EE Metrics of a Multi-Cell System

Analysis presented for single-cell system in previous section is extended to the case of multi-cell system shown in Figure 7.1, in which co-channel interference is inevitable. The primary interest is to obtain expressions for downlink SE and EE metrics by taking into account both interference and channel effects.

### 7.3.2.1 Signal-to-Interference plus Noise Ratio Model

The instantaneous SINR given by (7.3) can be written as

$$\gamma_{j,i}^{I} = \frac{\frac{P_j \alpha_{j,i}^2}{BN_o} r_{j,i}^{-\upsilon}}{1 + \sum_{\substack{k=1 \\ k\neq j}}^{N_I} \frac{P_k \alpha_{k,i}^2}{BN_o} D_{k,i}^{-\upsilon}}, \qquad (7.15)$$

115

where $\frac{P_j \alpha_{j,i}^2}{BN_o}$ is instantaneous SNR. Assuming all BSs transmit same power and $\alpha_{j,i}^2 \sim$ $\mathcal{G}(m, \Omega)$, implies that $\overline{\gamma}_{j,i} = \frac{P_j \overline{\alpha^2}_{j,i}}{BN_o}$ and $\overline{\gamma}_{k,i} = \frac{P_k \overline{\alpha^2}_{k,i}}{BN_o}$, and (7.15) can be written as [37]

$$\overline{\gamma}_{j,i}^I = \frac{\overline{\gamma}_{j,i} r_{j,i}^{-\upsilon}}{1 + \mathbf{\Xi}(N_I, D_k, r_i, \upsilon, \overline{\gamma}_{k,i})} \tag{7.16}$$

where $\mathbf{\Xi}(N_I, D_k, r_i, \upsilon, \overline{\gamma}_{k,i}) = \sum_{\substack{k=1 \\ k \neq j}}^{N_I} \overline{\gamma}_{k,i} \left( \frac{D_{k,i}}{r_{j,i}} \right)^{-\upsilon}$ depends on system geometry. Since investigation is based on highest co-channel interference power, user is assumed to be located at cell boundary, i.e., $r_{j,i} = R$. The distance $D_{k,i}$ for each co-channel interferer is determined in terms of $R$ and $D$. For three BS antenna configurations, average SINR is expressed as a function of normalized reuse distance, $R_d = D/R$. For the case of omni antenna configuration at BS, $i$th user is located at cell boundary of $BS_{j=0}$. Thus, other co-channel cells $BSs_{j=1,..,6}$ are using same frequency band and contribute to co-channel interference at $i$th user. The aggregated interference power, $\mathbf{\Xi}$, is a function of normalized reuse distance and user location angle and path-loss exponent and is given by

$$\begin{aligned} \mathbf{\Xi}^o(\theta, R_d, \upsilon) = &\left( R_d - \sin(\theta - \frac{\pi}{3}) \right)^{-\upsilon} \overline{\gamma}_{1,i} + \left( R_d - \sin(\theta + \frac{\pi}{3}) \right)^{-\upsilon} \overline{\gamma}_{2,i} \\ &+ \left( R_d + \sin(\theta - \frac{\pi}{3}) \right)^{-\upsilon} \overline{\gamma}_{3,i} + \left( R_d + \sin(\theta + \frac{\pi}{3}) \right)^{-\upsilon} \overline{\gamma}_{4,i} \\ &+ (R_d + \sin(\theta))^{-\upsilon} \overline{\gamma}_{5,i} + (R_d - \sin(\theta))^{-\upsilon} \overline{\gamma}_{6,i} \end{aligned} \tag{7.17}$$

where $\theta$ is user's angle, $0 \leq \theta \leq 2\pi$. When sectorization is used in the system, frequency bands in each cell are divided into disjoint sets and used in different sectors. Consequently, co-channel interference is going to be less severe, which leads to better system efficiency. Cell sectorization can be used to improve cellular system capacity and has

116

been investigated in [97]. In this section, two cell sectorization techniques are considered: $i$) three sectors in each cell with $120^o$ directivity antennas; and $ii$) six sectors in each cell with $60^o$ directivity antennas as shown in Figure 7.3 and Figure 7.4. In the case of $120^o$ antenna configuration, $\mathrm{BS}_{j=1}$ and $\mathrm{BS}_{j=2}$ create co-channel interference on $i$th user in $\mathrm{BS}_{j=0}$ as shown in Figure 7.3. The interference term can be expressed as a function of $R_d$, $\upsilon$ and $\theta$ as:
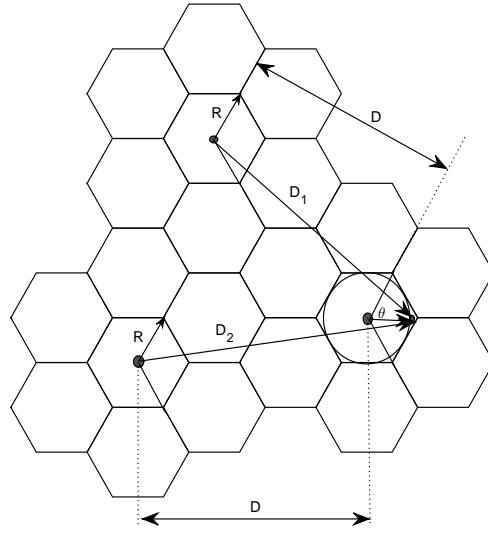


**Figure 7.3:** Hexagonal cellular system with $120^o$ sectorized antenna system at BS

$$\Xi^{120^o}(\theta, R_d, \upsilon) = \left(R_d + \sin(\theta + \frac{\pi}{6})\right)^{-\upsilon} \overline{\gamma}_{1,i} + (R_d + \sin\theta)^{-\upsilon} \overline{\gamma}_{2,i} \quad , 0 < \theta < \frac{2\pi}{3} \quad (7.18)$$

Similarly, for the case of $60^o$ antenna configuration, it is noted that $\mathrm{BS}_{j=1}$ creates co-channel interference at $i$th user as shown in Figure 7.4 and corresponding interference can be expressed as:

$$\Xi^{60^o}(\theta, R_d, \upsilon) = \left(R_d + \sin(\theta + \frac{\pi}{4})\right)^{-\upsilon} \overline{\gamma}_{1,i} \quad , 0 < \theta < \frac{\pi}{3} \quad (7.19)$$

117
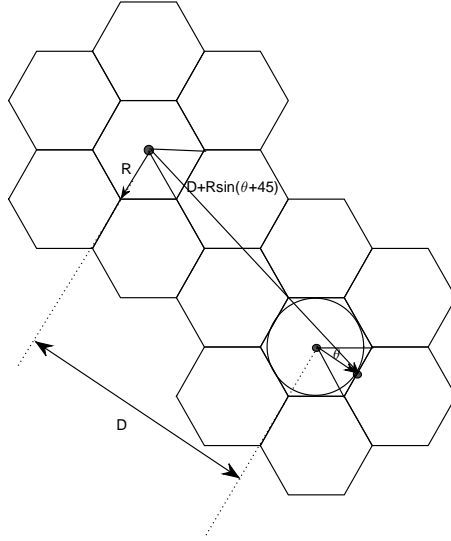
**Figure 7.4:** Hexagonal cellular system with $60^o$ sectorized antenna system at BS

Using knowledge of average SINR for each antenna configuration, SE and EE metrics can be obtained using (7.10) and (7.13) for a multi-cell system, assuming users are randomly located at cell boundaries.

## 7.3.3   Numerical Results of SE and EE Metrics

This section presents numerical results for SE and EE metrics for single- and multi-cell systems. For single-cell system, SE and EE metrics are evaluated using (7.11) and (7.14) and for multi-cell system. Monte Carlo simulations have been performed using (7.10) and (7.13). The steps used in simulation are given below. The system parameters used in simulations are given in Table 7.1.

1. The user's position is randomly selected using (7.5) and (7.6).

2. The distance of co-channel interference is obtained from Figure 7.1, Figure 7.3 and Figure 7.4 as a function of $R$ and $D$.

3. The interference $\Xi$ is calculated using (7.17), (7.18) and (7.19) for a given BS antenna configuration.

4. The SINR at user's location, $\overline{\gamma}_{j,i}^{I}$, is determined using (7.15) and (7.16).

5. The SE and EE metrics are calculated using (7.10) and (7.13).

**Table 7.1:** Cellular system parameters used for simulation of SE and EE metrics

| Symbol | Description | Value |
|---|---|---|
| $R$ | Cell radius | 1 Km |
| $\upsilon$ | Path loss exponent | 4 |
| $\overline{\gamma}$ | Signal to Noise ratio (SNR) | $0 - 20$ dB |
| $R_d$ | Normalized reuse distance | $2 - 6$ |
| $N_I$ | Number of interfering cells | $6, 2, 1$ |
| $\theta$ | User's angle | $0 - 2\pi, \frac{2\pi}{3}, \frac{\pi}{3}$ |
| $m$ | fading figure | $m \geq 1$ |

For single- and multi-cell systems, SE and EE metrics are plotted as a function of SNR for omni, $120^o$, and $60^o$ sectorized antenna systems for Nakagami-$m$ fading channel in Figure 7.5 and Figure 7.6, respectively. It is observed that SE metric is an increasing function of SNR whereas EE metric decreases monotonically as SNR increases. The single-cell system is superior in terms of SE and EE metrics compared to multi-cell system as former system is devoid of co-channel interference. However, for sectorized antenna systems, it is possible to obtain improved SE and EE metrics. For example, SE and EE metrics of a multi-cell system for $60^o$ sectorization approaches that of a single cell system and the same metrics for $120^o$ sectorization is far better than that for omni system at high SNR. In contrast, overall SE of multi-cell system is much higher than that of a single-cell system. As given by (7.17)-(7.19), the interference $\Xi$ is a function of $R_d$ and,

119
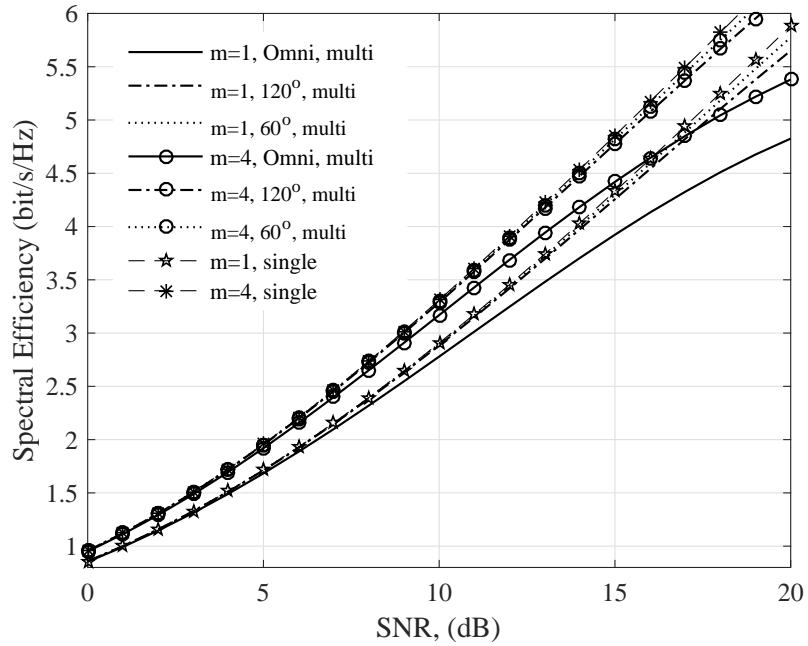
**Figure 7.5:** SE metric for single- and multi-cell cellular systems (omni, $120^o$ and $60^o$) as a function of SNR with $R_d = 3.5$ and $\upsilon = 4$
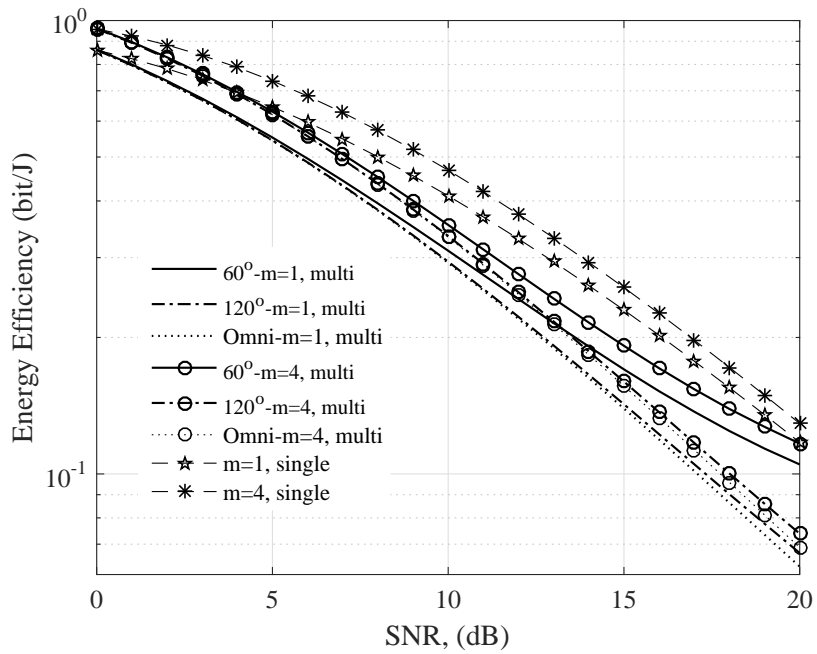


**Figure 7.6:** EE metric for single- and multi-cell cellular systems (for omni, $120^o$ and $60^o$) as a function of SNR with $R_d = 3.5$ and $\upsilon = 4$

therefore, SE and EE metrics are functions of $R_d$ for fixed SNR and antenna configuration used. Figure 7.7 illustrates SE metric for a multi-cell system for Nakagami-$m$ channel and omni, $120^o$ and $60^o$ antenna configurations as a function of $R_d$. It is observed that
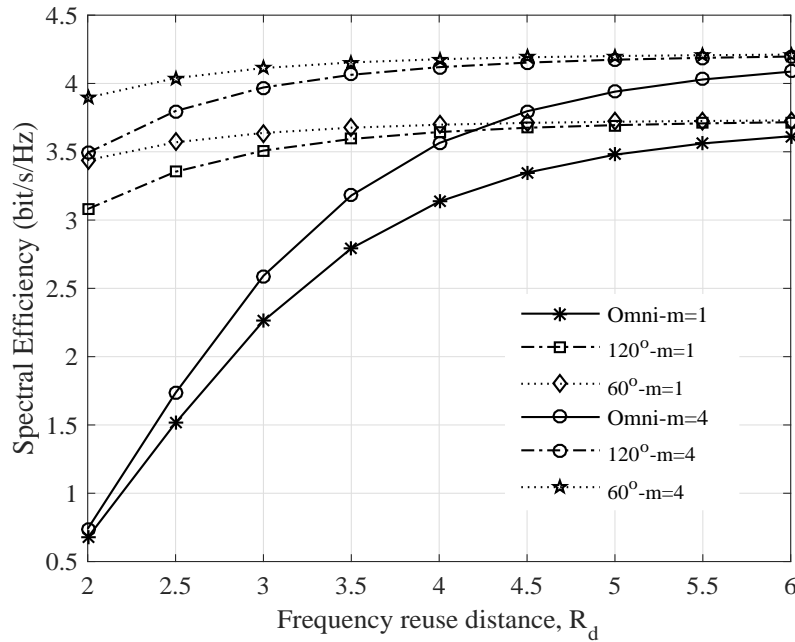


**Figure 7.7:** SE metric of cellular systems (for omni, $120^o$ and $60^o$) as a function of normalized reuse distance at (SNR= 10 dB, and $\upsilon = 4$)

SE metric improves as $R_d$ increases, which is due to low co-channel interference in the system. It is observed that $60^o$ system achieves better SE than $120^o$ and omni systems. Also, it is evident that fading over channel impacts SE metric, particularly at high $R_d$ for omni system. The EE metric is plotted as a function of $R_d$ in Figure 7.7. It is observed that EE metric, for all three antenna configurations, decreases as $R_d$ is increased, which implies more transmission power is required at BS to make the system energy efficient. It is also noted that EE metric for each antenna system considered approaches same value as $R_d$ is increased due to less co-channel interference at user. The results shown in these figures can be used for designing energy- and spectral-efficient cellular system.
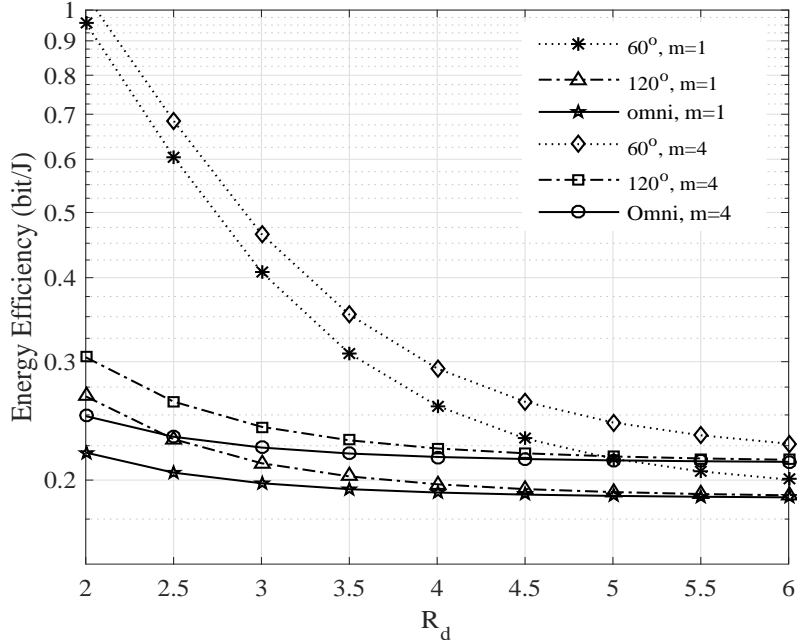
**Figure 7.8:** EE metric of cellular systems (for omni, $120^o$ and $60^o$) as a function of normalized reuse distance at (SNR$= 10$ dB, and $\upsilon = 4$)

For example, in terms of reuse distance, sectorization system significantly improves SE and EE metrics of cellular system, particularly, for $R_d \leq 4$. At $R_d = 2.5$, SE metric is improved by 1.8 and 2.1 bits/s/Hz for $120^o$ and $60^o$ sectorization systems, respectively, compared to omni antenna system for severe case of fading, $(m = 1)$. Also, it is observed that $120^o$ sectorization system slightly improves EE metric for the same value of $R_d$ and $m$; however, $60^o$ system achieves twice the energy efficiency compared to that of omni system.

## 7.4 Affected Area, SSE and SEE Metrics

In the previous section, cellular systems were analyzed using SE and EE metrics without considering their spatial characteristics. Expanding the coverage area is an important

issue in the design of cellular systems, as already noted an increase of reuse distance $D$ expands coverage area in a cellular system. The power transmitted by BS can affect quality of transmission in the system for large value $D$ and hence SE and EE metrics are required to be examined as a function of coverage area. The SSE and SEE metrics have been used in [43] and [98] to examine spatial characteristics of a cellular system. The SSE metric quantifies number of bits/s/Hz/unit area of cellular system that can be reliably delivered to a user. Also, it characterizes spectrum utilization of a cellular system for a certain coverage area. The SEE metric is defined energy efficiency of a cellular system divided by its coverage area. These definitions capture trade-off between SSE and SEE metrics and depend on SE and EE metric of system, and area covered due to power transmitted by BS.

### 7.4.1 Affected Area

For single-cell system shown in Figure 7.2, affected area is the area over which user is able to detect BS power, say, above a certain threshold [76]. This affected area is a function of BS power, propagation environment, and antenna configuration used at BS. The affected area is a useful metric and can be used to quantify spatial properties of a cellular system. Assuming BS coverage area to a circle as shown in Figure 7.2, the affected area can be written as

$$\mathcal{A}_a = \int\limits_0^{2\pi} \int\limits_0^{\infty} P_a\left(\gamma_t, r\right) r\, dr\, d\theta, \tag{7.20}$$

123

where $P_a\left(\gamma_t, r\right)$ is probability that SNR, $\gamma_i$, is a greater than a specified threshold SNR, $\gamma_t$, at user located at a distance $r$ from BS and is given by

$$P_a\left(\gamma_t, r\right) = Prob.\left[\gamma > \gamma_t\right] \tag{7.21}$$

where density of $\gamma$, $p_\gamma(\gamma)$, is given by (7.9) for Nakagami-$m$ channel. An expression for $P_a$ can thus be derived and is given by:

$$P_a\left(\gamma_t, r\right) = \frac{\Gamma\left(m, m\frac{\gamma_t}{\bar{\gamma}}r^\upsilon\right)}{\Gamma(m)} \tag{7.22}$$

By substituting (7.22) in (7.20) and using [86, eq. (8.4.16/2), eq. (2.24.2/1)], affected area for Nakagami-$m$ channel can be derived as

$$\mathcal{A}_a^N(\gamma_t, \upsilon) = \frac{2\pi}{\upsilon}\left(m\frac{\gamma_t}{\bar{\gamma}}\right)^{-2/\upsilon} \frac{\Gamma\left(\frac{2}{\upsilon}\right)\Gamma\left(\frac{2}{\upsilon}+m\right)}{\Gamma\left(\frac{2}{\upsilon}+1\right)\Gamma(m)} \tag{7.23}$$

The affected area is as a function of average SNR at user, threshold SNR, $\gamma_t$, fading figure $m$, and path loss exponent $\upsilon$ and is plotted for $\gamma_t = 10$ and 15 dB, $\upsilon = 4$, and $m = 1$, 4 in Figure 7.9. It is observed that affected area is reduced as fading becomes severe over the channel. For example, for $m = 1$ (which represents worst case of fading), affected area is decreased by nearly 9% compared to affected area when $m = 4$. Also, it is noted that low threshold SNR level provides large affected area which implies that receiver at user be capable of detecting weaker signals. For example, when average SNR=10 dB at user, affected area is increased by 87% for $\gamma_t = 10$ dB compared to when $\gamma_t = 15$ dB, for Nakagami-$m$ channel with $m = 1$.
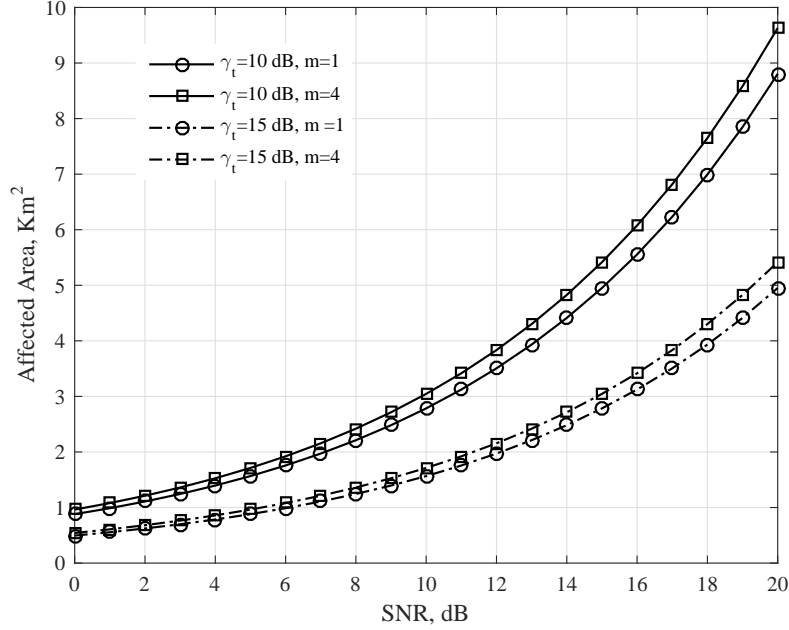
**Figure 7.9:** Affected area as a function of threshold SNR $\gamma_t (= 10, 15$ dB), for Nakagami-$m$ environment in a cellular system ($v = 4$)

## 7.4.2   SSE and SEE Metrics for a Single-Cell System

For a single cell system, SSE metric can be defined as ratio of SE metric of a single-cell system to that of affected area of BS. Using SE metric for a single-cell system given by (7.11) and affected area given by (7.23), for Nakagami-$m$ environment in the system, SSE metric can be written as:

$$\eta_{SS,sc}^{N} = \frac{\eta_{S,sc}(R,v)}{\mathcal{A}_a(\gamma_t,v)}, \tag{7.24}$$

Where $\eta_{SS,sc}^{N}$ denotes SSE metric for downlink for a single-cell system with Nakagami-$m$ environment. Using similar approach used for finding SSE metric, the SEE metric for single-cell system is given by:

$$\eta_{SE,sc}^{N} = \frac{\eta_{E,sc}(R,v)}{\mathcal{A}_a^{N}(\gamma_t,v)}, \tag{7.25}$$

where $\eta_{E,sc}(R,\upsilon)$ is given by (7.14). The SSE and SEE metrics for a single-cell system are plotted in Figure 7.10 and Figure 7.11, respectively, as a function of SNR for $m = 1, 4$, $\gamma_t = 10, 15$ dB and $\upsilon = 4$. Figure 7.10 demonstrates that SSE metric attains maximum
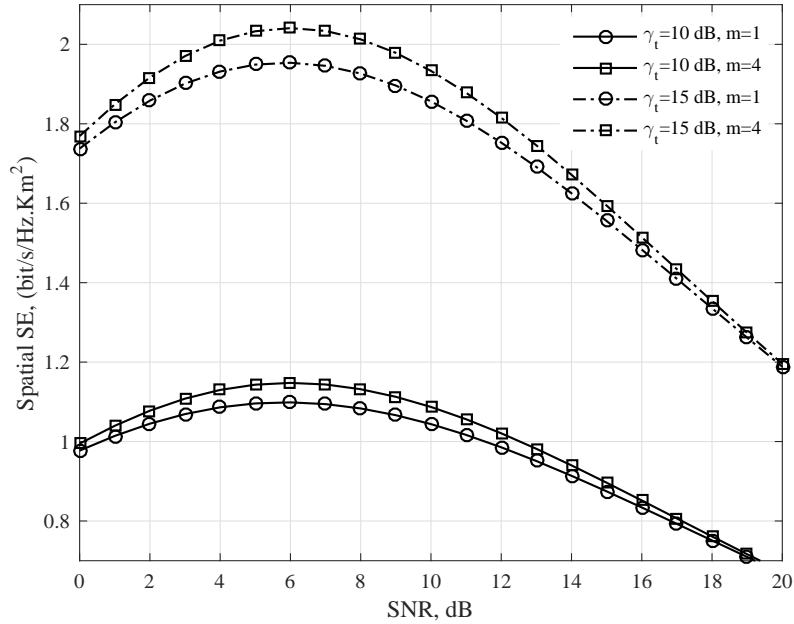


**Figure 7.10:** SSE metrics for single cell system as a function of average SNR for $\gamma_t = 10, 15$ dB, $m1, 4$ and $\upsilon = 4$

value over specific region of SNR, which defines optimum operating range of SNR. Also, it is evident that for large value of affected area, SSE metric is considerably affected. For example for $\gamma_t = 10$ dB and $m = 4$, SSE metric is below 1.2 bits/s/Hz/Km$^2$ as covered area is large. From Figure 7.11, it is observed that SEE metric is an exponentially decreasing function of average SNR, and high SNR threshold provides better SEE metric. It is observed from Figure 7.10 and Figure 7.11, optimum range of SNR, $2 \leq \bar{\gamma} \leq 10$ dB, provides most spectrally efficient systems with acceptable energy efficiency.
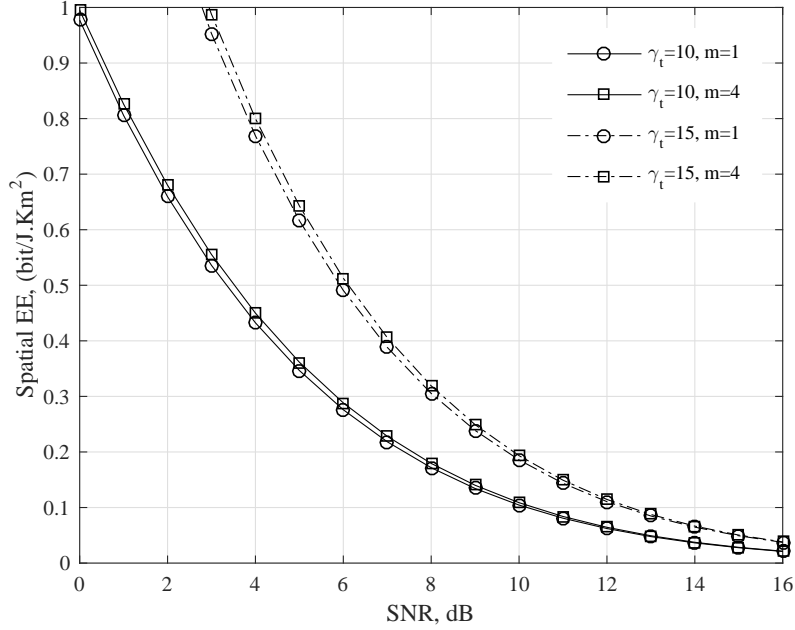
**Figure 7.11:** SEE metrics for single cell system as a function of average SNR for $\gamma_t = 10, 15$ dB, $m1, 4$ and $\upsilon = 4$

### 7.4.3 SSE and SEE Metrics for a Multi-Cell System

For multi-cell systems shown in Figure 7.1, Figure 7.3 and Figure 7.4, SSE and SEE metrics are defined as ratios of SE and EE metrics of multi-cell system to that of covered area. For given frequency reuse distance $D$, the covered area is given by $\pi D^2/4q$, where $q$ is the sectorization factor. The values of $q = 1$, 3 and 6 correspond to omni, $120^o$ and $60^o$ antenna systems at BS, respectively. The SSE and SEE metrics can thus be written as

$$\eta_{SS,mc}^N = 4q \frac{\eta_{S,mc}(r_i, \upsilon)}{\pi R_d^2 R^2}, \tag{7.26}$$

$$\eta_{SE,mc}^N = 4q \frac{\eta_{E,mc}(r_i, \upsilon)}{\pi R_d^2 R^2}, \tag{7.27}$$

127

Since SSE and SEE metrics in Figure 7.12 and Figure 7.13, respectively, are functions of $m$, SNR and $R_d$, they are plotted as functions of these quantities using Monti Carlo simulations for omni, $120^o$ and $60^o$ antenna configurations. The parameters used in simulations are given in Table 7.1. It is observed from Figure 7.12 that SSE metric of $60^o$ antenna system is superior compared to omni and $120^o$ antenna systems, as co-channel interference is minimum in the $60^o$ system. As can be observed from Figure 7.13, SEE metric of the system degrades as $R_d$ increases. It is noted that as $R_d$ increases, coverage area also increases and to maintain same SSE metric, BS is required to transmit more power. Furthermore, it is observed that while SSE metric is an increasing function of average SNR, SEE metric is a decreasing function of SNR. From Figure 7.12 and Fig-
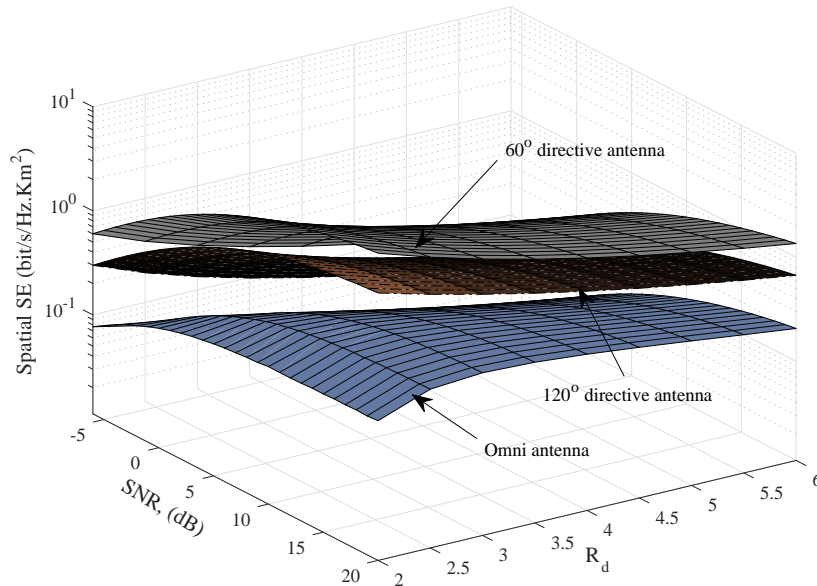


**Figure 7.12:** SSE metrics of multi-cell system (for omni, $120^o$ and $60^o$) as a function of average SNR and $R_d$ ($m = 4$, $\upsilon = 4$)

ure 7.13, it is observed that sectorized antenna system can be gainfully employed for designing an energy efficient multi-cell system; however, sectorization increases complex-

128
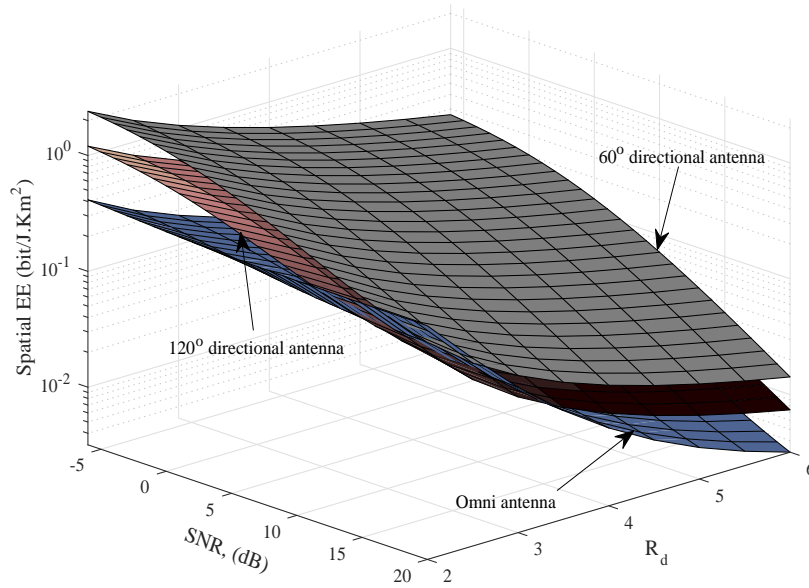
**Figure 7.13:** SEE metrics of multi-cell system (for omni, $120^o$ and $60^o$) as a function of average SNR and $R_d$ ($m = 4,\ v = 4$)

ity of the system. Shrinking reuse distance in the system reduces coverage area which in turn will increase SSE metric of the system. However, co-channel interference will increase and hence will decrease SSE metric. Thus, it is observed that a trade off between the two metrics is inevitable for designing an efficient system, for $R_d \geq 4$. Figure 7.13 shows that SEE metric decreases gracefully with reuse distance and SINR in the system. That is, for $R_d \geq 4$, SEE metric is deteriorated while SSE metric is not improved. By using antenna sectorization at BS, it is possible to design a multi-cell system with better SSE and SEE metrics than using simply an omni system at BS. This is due to: $i$) better power directed to specific regions of cell; $ii$) decreased co-channel interference and $iii$) better utilization of area within cell. However, as noted earlier system becomes more complex due to sectorization. The efficiency metrics are always in conflict for a given SNR and $R_d$, and hence, a trade off between the two metrics must be considered when

designing an efficient multi-cell system.

## 7.5 Coverage Probability in Nakagami-$m$ Fading with Co-channel Interference

A cellular system is energy efficient when transmitted power at BS is reduced. However, this will reduce coverage area of the system. Thus, to precisely address the issue of energy efficiency of a cellular system, its energy consumption and coverage performance must be jointly examined. Thus, for efficient deployment, a cellular system must minimize its energy consumption and maximize its coverage probability [36]. The coverage probability in $j$th cell is the probability that SINR at user is greater than or equal to a certain threshold $\gamma_t$. For a user in a cellular system, coverage probability is defined as

$$P_{cov} \triangleq Prob.\,[SINR \geq \gamma_t] \tag{7.28}$$

Using (7.15), (7.28) can be written as:

$$P_{cov} \triangleq Prob.\left[\gamma \geq \frac{\left(1/\overline{\gamma} + \mathbf{\Xi}\left(\upsilon, r, N_I\right)\right)\gamma_t}{r^{-\upsilon}}\right] \tag{7.29}$$

where density of $\gamma \quad \sim \mathcal{G}\left(m, \Omega\right)$ is given by (7.7). For a user operating in Nakagami-$m$ fading environment, conditional $P_{cov}$ is give by [99]:

$$P_{cov}|_{I,r} = \mathbb{E}\left[P_\gamma\left(\frac{\left(1/\overline{\gamma} + \mathbf{\Xi}\left(\upsilon, r, N_I\right)\right)\gamma_t}{r^{-\alpha}}\right)\right] \tag{7.30}$$

where $P_\gamma$ is distribution function of $\gamma$. Using distribution of $\gamma$, (7.30) can be written as

$$P_{cov}|_{I,r} = \frac{1}{\Gamma(m)}\mathbb{E}\left[\Gamma\left(m, \frac{m\left(1 + \Xi\left(v, r, N_I\right)\right)\gamma_t\overline{\gamma}}{\overline{\gamma}^2 r^{-v}}\right)\right] \qquad (7.31)$$

The expectation in (7.31) is over user's location, $r$, given in (7.4), and co-channel interference. Extensive Monte Carlo simulations were conducted to evaluate coverage probability for three antenna configurations (omni, $60^o$, and $120^o$) at BS using parameters shown in Table 7.1. Without loss of generality, mobile user was assumed to be at cell boundary, which is the worst case scenario. The coverage probability as a function of SNR threshold, $\gamma_t$, is plotted in Figure 7.14 for $m = 1, 4$. In Figure 7.15, coverage probability as a function of $R_d$ is plotted for $v = 3.8, 2.7$ and $\frac{\gamma_t}{\overline{\gamma}} = 1$. It is observed that coverage
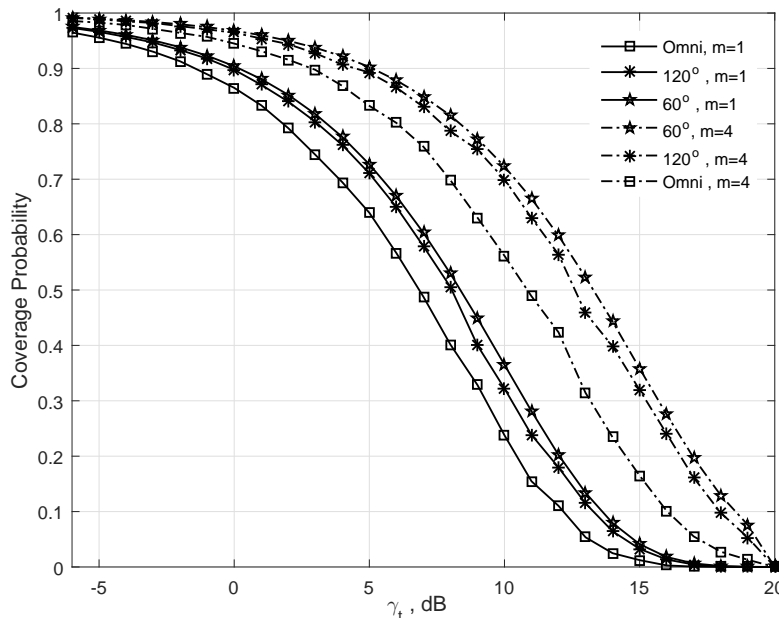


**Figure 7.14:** Coverage probability of cellular system (omni, $120^o$ and $60^o$ antenna configurations) as a function of threshold SNR $\gamma_t$ with $\overline{\gamma} = 10$ dB, $R_d = 4$ and $v = 4$

probability is significantly impacted for small values of $2 \leq R_d \leq 3.5$ for omni antenna at
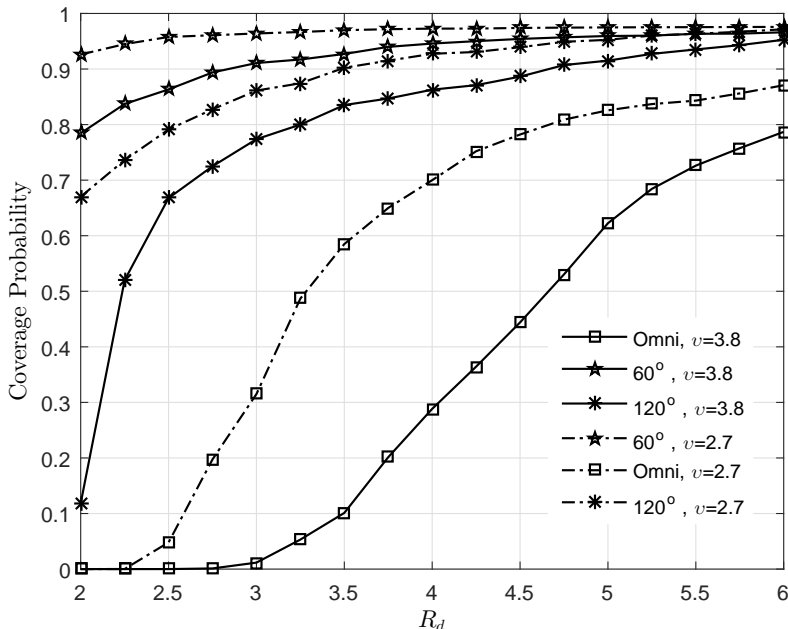
131

**Figure 7.15:** Coverage probability of cellular system (omni, $120^o$ and $60^o$ antenna configurations) as a function of $R_d$ for path loss exponent $\upsilon = 3.8,\ 2.7$, and $\frac{\gamma_t}{\bar{\gamma}} = 1$

BS. This is in contrast to coverage probabilities of $60^o$ and $120^o$ antenna systems at BS, because of less interferences at user due to directed signal power form antenna systems. For large values of $R_d \geq 4$, coverage probability improves for omni and approaches unity for $60^o$ antenna system, as path loss factor reduces in value. It is observed that path loss factor, $\upsilon$, affects coverage probability significantly, particularly, with omni antenna system at BS. From Figure 7.5, Figure 7.7 and Figure 7.15, it is observed that SE and SSE metrics and coverage probability are increasing functions of normalized reuse distance, $R_d$. The results in these figures can be used to design spectrally efficient cellular system design. From Figure 7.8, Figure 7.13 and Figure 7.15, it is observed that coverage probability increases as $R_d$ increases and EE and SEE metrics decrease as $R_d$ increases. This implies that designing an energy-efficient cellular system requires a price to be paid in terms of coverage area and spectrum efficiency of the system. Table 7.2 provides a

comparison of various metrics of a cellular system for three antenna systems at BS.

**Table 7.2:** Comparison of efficiency metrics and coverage probability of a cellular system ( omni, $60^o$ and $120^o$ antenna configurations) for SNR=10 dB, $R_d = 3$, $v = 4$ and $m = 4$.

| Metric | Omni | $120^o$ | $60^o$ |
|---|---|---|---|
| SE, bit/s/Hz | 2.6 | 3.63 | 4.11 |
| EE, bit/J | 0.22 | 0.24 | 0.46 |
| SSE, bit/s/Hz/Km$^2$ | 0.32 | 1.35 | 2.76 |
| SEE, bit/J/Km$^2$ | 0.074 | 0.15 | 0.29 |
| Coverage Probability ($\gamma_t = 10$ dB) | 0.420 | 0.862 | 0.945 |

The metrics in Table 7.2 show superiority of sectorized antenna system over omni system at BS. It is clear form the table that efficiency metrics and coverage probability are superior for sectorized systems at BS. For instance, $60^o$ configuration enhances SE and EE metrics by 58% and 107%, respectively, relative to metrics of omni system at BS. Also, spatial efficiencies have improved significantly for sectorized systems at BS relative to omni system with coverage probabilities close to unity.

## 7.6    Chapter Summary

This Chapter, a framework for designing an efficient cellular system is presented. A multi-cell system consisting of hexagonal cells with radius $R$ and reuse distance $D$ with BS equipped with omni, $120^o$, and $60^o$ antennas is considered. The design framework is based on analysis of SE, EE, SSE, SEE and coverage probability metrics of the cellular system. The analysis of metrics takes into account co-channel interference, signal path loss, and multi path fading in the system. The fading environment is modelled as Nakagami-$m$. A generic expression for Signal-to-Interference-Noise Ratio (SINR) at an arbitrary user in a cell in the system is first derived. Using this, expressions for the efficiency metrics of the system are derived and analyzed as a function of SINR, reuse distance, cell radius, path loss exponent, location of user, and fading figure. Statistical averaging and Monte Carlo simulations are used to evaluate these metrics (omni, $120^o$, and $60^o$)for each of three BS antenna configurations. The results show that in the design of an efficient cellular system, one must carefully deal with trade-offs among coverage probability, SEE, and SSE metrics. The BS antenna sectorization is an effective technique to improves overall energy efficiency of cellular system, but at the cost of increased complexity of the system. For example, for SNR=10 dB, $R_d = 3$, $v = 4$ and $m = 4$, EE metric of $60^o$ antenna system is enhanced by nearly 109% compared to that of omni antenna system. Also, SE metric of $120^o$ and $60^o$ systems is increased by nearly 1 and 1.5 bits/s/Hz, respectively, compared to omni antenna system.

# Chapter 8

# Design and Analysis of MU-MIMO Cellular System using SE and EE Metrics [10]

## 8.1   Introduction

In this Chapter, a MU-MIMO cellular system and its efficiency metrics are considered. The communication system between BS and users in a cell and SINR model at BS are presented. It is assumed that BS is equipped with MU-MIMO system with MRC diversity receiver. Expressions for SE and EE metrics of the systems are then developed. The environment in cellular system is assumed to be multipath fading and shadowing with path loss and interference from intracell and intercells. Both fading and shadowing over the channel are assumed independent and Gamma distributed. Closed-form expressions for SE and EE metrics for uplink (users to BS) are derived using MGF approach. The parameters that influence these metrics are identified as: $i$): number of BSs in the

---

10. Hamed, A. and Rao, R.K "Spectral and Energy Efficiencies of Multicell MU-MIMO Systems in Composite Propagation Environment," IEEE Wireless Communications and Networking Conference, $11 - 18$ April 2019, Marrackech, Morocco.

system, $(J)$; $ii$) number of users served by BS, $(K_i)$; $iii$) antenna array size, $(\mathcal{M})$ at BS; $iv$) parameters of fading and shadowing distributions; $v$) path loss exponent; and $vi$) interference power at BS. Assuming users transmit identical power, design considerations for efficient MU-MIMO cellular system are presented.

## 8.2   MU-MIMO System

MIMO technology is widely studied and is used in many communication standards by virtue of its superior capacity and reliability [46], [100]. In recent years, there have been wide spread application of MU-MIMO system in various wireless communication systems [52]-[56] including cellular systems. In a MIMO cellular system, each user is scheduled using disjoint time-frequency resource. In a Single User (SU) MIMO system, one user is served on a given time-frequency resource. However, multiple users can be simultaneously served over a given time-frequency resource using spatial multiplexing as shown in Figure 8.1. Such a system enables several independent users to access same channel by using spatial dimension in the system. This spatial sharing of radio channel is achieved by increasing the number of antennas in the system, with additional complexity required due to signal processing of beams from users. A MU-MIMO system offers advantages such as: $i$) higher spectral efficiency; $ii$) reduced effects of propagation environment; and $iii$) spatial multiplexing without need for multiple antennas at users. In a MU-MIMO cellular system, each BS is equipped with a large number of antennas so that many users can be accommodated using same time-frequency resource. In order to minimize cost, each user is assigned a single or a few antennas of BS equipped. Thus, expensive equip-
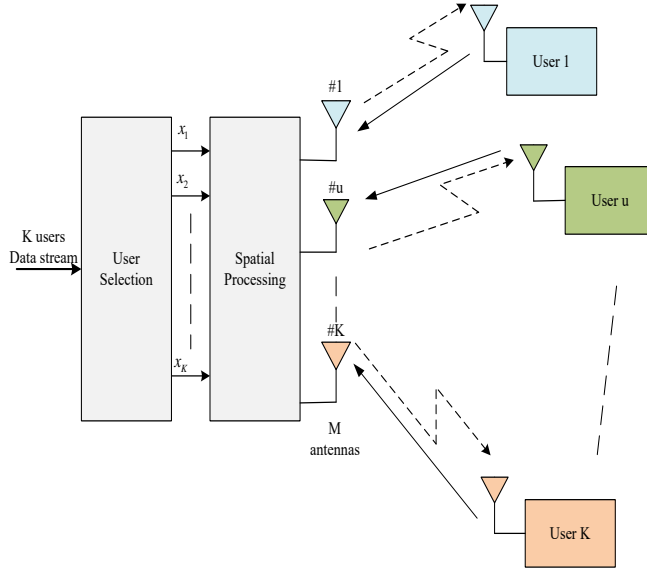
**Figure 8.1:** MU-MIMO system at BS communicating simultaneously with several users

ment is only needed at BS with users of system requiring only single or a few antennas. Such a MU-MIMO system has become an integral part of communications standards, such as 802.11ac (WiFi), 802.16 (WiMAX) and LTE [101], [102], [103]. The MU-MIMO cellular system is illustrated in Figure 8.2 with blue cells using identical frequency bands referred to as co-channel cells. Such a system offers high spectral efficiency as BS is capable of communicating simultaneously with multiple users in each cell. However, such a system is faced with several challenges such as multiuser interference, increased system complexity and requirement of increased energy by users.

## 8.2.1 Mathematical Model of MU-MIMO System and Assumptions

A multi-cell MU-MIMO cellular system is considered with $J$ number of cells as shown in Figure 8.2. Each cell is assumed to consist of one BS equipped with $\mathcal{M}$ antennas serving
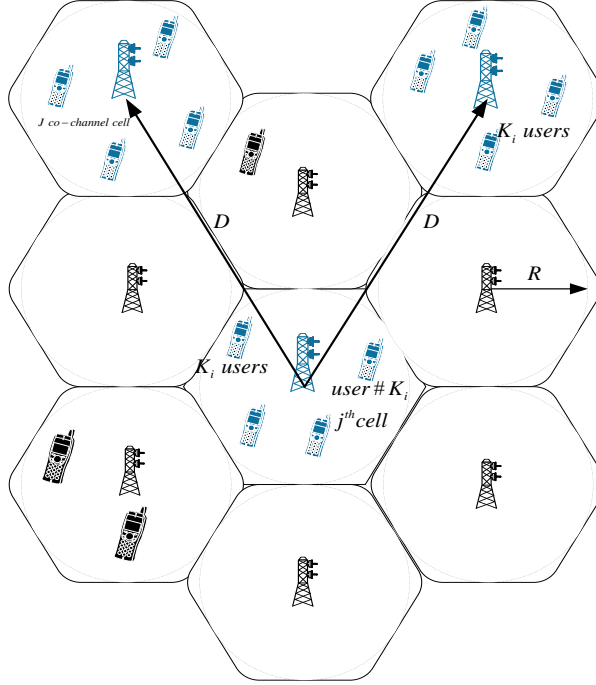
**Figure 8.2:** Diagram of MU-MIMO cellular system

$K_i$ single-antenna users. The communication between BS and users is over the same time-frequency resource. Since $K_i$ users simultaneously transmit data over the channel to their BS, cochannel interference is expected to be severe which impacts the efficiency metrics at the BS. Thus, the analysis is presented for uplink; with users transmitting same power to BS. The received $\mathcal{M} \times 1$ signal vector at $j^{th}$ BS can be expressed as

$$\boldsymbol{y}_j = \sqrt{P_u} \sum_{i=1}^{J} \boldsymbol{G}_{ji}\boldsymbol{x}_i + \boldsymbol{n}_j \qquad (8.1)$$

where $\boldsymbol{G}_{ji}$ represents $\mathcal{M} \times K_i$ channel matrix between $j^{th}$ BS and $K_i$ users in $i^{th}$ cell, i.e., $g_{jimk} \triangleq \left[\boldsymbol{G}_{ji}\right]_{mk}$ is the channel coefficient between $m^{th}$ antenna of the $j^{th}$ BS and $k^{th}$ user in $i^{th}$ cell, $\sqrt{P_u}\boldsymbol{x}_i$ represents $K_i \times 1$ vector of data transmitted simultaneously by $K_i$ users in $i^{th}$ cell ($P_u$ is transmitted power of each user), and $\boldsymbol{n}_j$ is $K_j \times 1$ vector of Gaussian random variables (each assumed to be zero-mean with unit variance). It is

138

assumed that BS is equipped with perfect CSI. The quantity $P_u$ in (8.1), thus, represents

normalized SNR. The elements of channel matrix $\boldsymbol{G}_{ji}$ are assumed independent and

represent multipath fading and shadowing channel effects and can be expressed as:

$$\boldsymbol{G}_{ji} = \boldsymbol{H}_{ji}\boldsymbol{D}_{ji}^{1/2} \tag{8.2}$$

where $\boldsymbol{H}_{ji}$ is $\mathcal{M} \times K_i$ matrix of multipath fading coefficients between $j^{th}$ BS and $K_i$ users

in $i^{th}$ cell, i.e., $h_{jimk} \triangleq \left[\boldsymbol{H}_{ji}\right]_{mk}$ represents fading coefficient between $m^{th}$ antenna of $j^{th}$

BS and $k^{th}$ user in $i^{th}$ cell and is complex Gaussian with zero mean and unit variance,

and $\boldsymbol{D}_{ji}$ is a $K_i \times K_i$ diagonal matrix, models shadow fading, i.e., $\xi_{jik} \triangleq \left[\boldsymbol{D}_{ji}\right]_{kk}$. Thus,

coefficient $g_{jimk}$ can be expressed as

$$g_{jimk} = h_{jimk}\sqrt{\xi_{jik}} \tag{8.3}$$

## 8.2.2 Detection Techniques

At BS, signals from $K_i$ users need to be reliably detected. To obtain optimal performance,

complex signal processing techniques are required. Several techniques have been proposed

and among them Zero-Forcing (ZF) receiver aims to reduce interference from various

users of the system. The implementation requires $\mathcal{M} \geq K_i$. The signal processing

in ZF receiver is simple and reliable for interference-limited scenarios. However, more

transmit power from users are required for a desired level of SINR at BS; otherwise,

receiver performs poorly for low values of SNR. Furthermore, ZF receiver is complex as

it requires for its operation inverse of channel gain matrix. Instead, a Minimum Mean-

Square Error (MMSE) receiver that maximizes SINR can be used to estimate signals from users. This receiver works well at all SNRs; however, it is complex and consumes high power due to computations involved. The MRC diversity receiver at BS is yet another solution that can be used to maximize SNR and consists of $\mathcal{M}$ receivers, followed by a linear combiner. The output from $\mathcal{M}$ receivers are suitably weighted and summed to
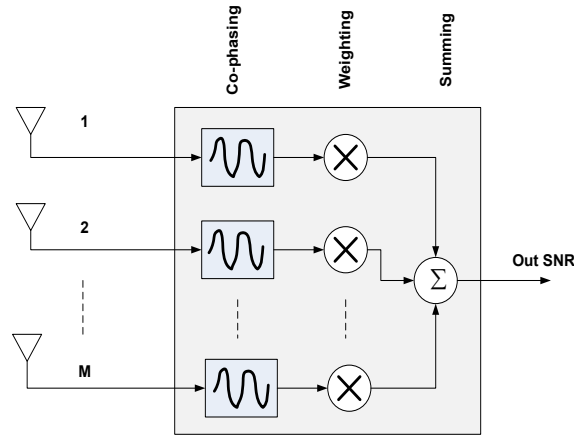


**Figure 8.3:** Block diagram of MRC receiver at BS with $\mathcal{M}$ antennas

maximize SNR at its output as shown in Figure 8.3. The signal processing involved is simple since at BS multiplication of received vector with conjugate-transpose of channel matrix is all that is needed to detect signals from users. More importantly, MRC receiver can be implemented in a distributed manner [104]. Furthermore, for small transmitted power from users, MRC receiver achieves a gain equivalent to that of a single-user system. The objective in this Chapter is to determine SE and EE metrics of a MU-MIMO cellular system in which BS is equopped with MU-MIMO system with MRC receive as it performs better than ZF receiver for low values of SNR and is easy to implement. A comparison of performances of MRC and ZF receivers is shown in Figure 8.4. It is clear that MRC achieves higher SE than ZF for low range of SNR which is our concern in designing energy

efficient MU-MIMO system. Also, it is noted that implementation of MRC receiver is less complex than ZF receiver, particularly, for large number of antennas at BS.
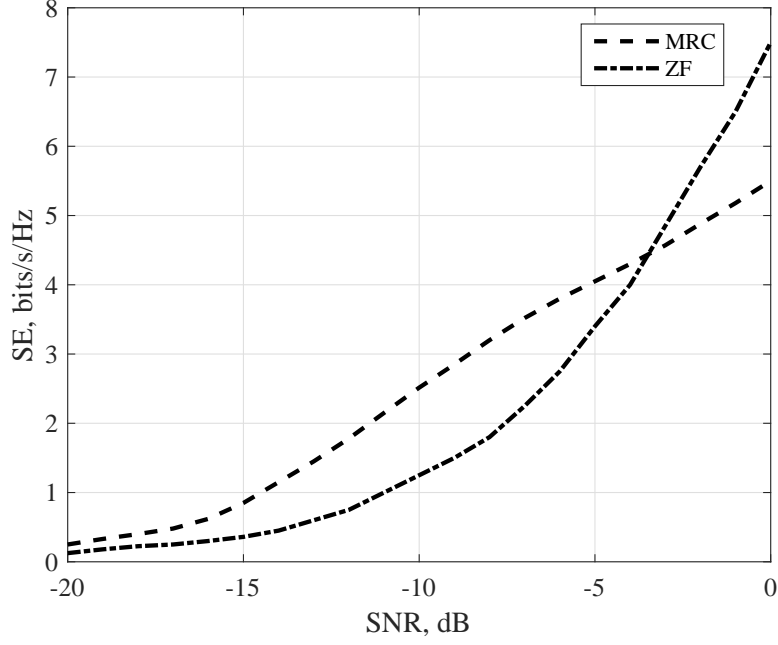


**Figure 8.4:** SE of MRC and ZF receivers for the uplink [105]

### 8.2.3 SINR Analysis at BS with MRC Receiver

For an MRC receiver at BS, assuming perfect CSI for all users in a cell, the vector $\boldsymbol{r}_j$ after multiplying received vector $\boldsymbol{y}_j$ by $\boldsymbol{G}_{jj}^H$ can be written as:

$$\boldsymbol{r}_j = \boldsymbol{G}_{jj}^H \boldsymbol{y}_j = \sqrt{P_u} \boldsymbol{G}_{jj}^H \boldsymbol{G}_{jj} \boldsymbol{x}_j + \sqrt{P_u} \sum_{i \neq j}^{J} \boldsymbol{G}_{jj}^H \boldsymbol{G}_{ji} \boldsymbol{x}_i + \boldsymbol{G}_{jj}^H \boldsymbol{n}_j \qquad (8.4)$$

141

Then, $u^{th}$ element of $\boldsymbol{r}_j$ can be expressed as

$$r_{j,u} = \sqrt{P_u}\boldsymbol{g}_{jj,u}^{H}\boldsymbol{g}_{jj,u}x_{j,u} + \sqrt{P_u}\boldsymbol{g}_{jj,u}^{H}\sum_{n\neq u}^{K_j}\boldsymbol{g}_{jj,n}x_{j,n}+$$

$$\sqrt{P_u}\boldsymbol{g}_{jj,u}^{H}\sum_{i\neq j}^{J}\sum_{n=1}^{K_i}\boldsymbol{g}_{ji,n}x_{i,n} + \boldsymbol{g}_{jj,u}^{H}\boldsymbol{n}_j \quad (8.5)$$

where $\boldsymbol{x}_{j,u}$ is $u$th element of vector $\boldsymbol{x}_j$ . In (8.4), there are four terms: $i$) desired signal, $ii$) intercell interference, $iii$) intracell interference, and $iv$) noise. The uplink instantaneous SINR, $\gamma_u$, from $u^{th}$ user in $j^{th}$ cell is equal to

$$\gamma_u = \frac{P_u\left\|\boldsymbol{g}_{jj,u}\right\|^4}{P_u\sum_{n\neq u}^{K_j}\left|\boldsymbol{g}_{jj,u}^{H}\boldsymbol{g}_{jj,n}\right|^2 + P_u\sum_{i\neq j}^{J}\sum_{n=1}^{K_i}\left|\boldsymbol{g}_{jj,u}^{H}\boldsymbol{g}_{ji,n}\right|^2 + \left\|\boldsymbol{g}_{jj,u}\right\|^2} \quad (8.6)$$

Using (8.3), $\left\|\boldsymbol{g}_{jj,u}\right\|^2$ can be written as

$$\left\|\boldsymbol{g}_{jj,u}\right\|^2 = \xi_{ju}\left\|\boldsymbol{h}_{jj,u}\right\|^2 \quad (8.7)$$

where $\xi_{j,u} = \beta_{j,u}r_u^{-\upsilon}$; the quantity $\beta_{j,u}$ represents shadowing and $r_u^{-\upsilon}$ is path-loss with $\upsilon$ path-loss exponent, $\upsilon \geq 2$. Thus, SINR can be expressed as

$$\gamma_u = \frac{P_u\beta_{j,u}r_u^{-\upsilon}\left\|\boldsymbol{h}_{jj,u}\right\|^2}{P_u\sum_{n\neq u}^{K_j}\beta_{j,n}r_n^{-\upsilon}\left|\frac{\boldsymbol{h}_{jj,u}^{H}\boldsymbol{h}_{jj,n}}{\left\|\boldsymbol{h}_{jj,u}\right\|}\right|^2 + P_u\sum_{i\neq j}^{J}\sum_{n=1}^{K_i}\beta_{j,n}D_i^{-\upsilon}\left|\frac{\boldsymbol{h}_{jj,u}^{H}\boldsymbol{h}_{ji,n}}{\left\|\boldsymbol{h}_{jj,u}\right\|}\right|^2 + 1} \quad (8.8)$$

where $r_u$ is distance of user to $j^{th}$ BS and $D_i$ is distance of $i^{th}$ interfering user using same frequency resource. It is noted from (8.8) that fading effects due to user ,$\boldsymbol{h}_{jj,u}$, is a vector

142

and $\|\cdot\|$ is Euclidean norm. Defining $X_u = \left\|\boldsymbol{h}_{jj,u}\right\|^2 = \sum_i^M e_i$ where $e_i, \ i = 1, 2, .., M,$ are statistically independent and identically distributed (i.i.d) exponential random variables. Thus, $X_u$ is Gamma distributed [106]. Let $I_n = \left|\dfrac{\boldsymbol{h}_{jj,u}^H \boldsymbol{h}_{jj,n}}{\left\|\boldsymbol{h}_{jj,u}\right\|}\right|^2$ in (8.8), where $\dfrac{\boldsymbol{h}_{jj,u}^H \boldsymbol{h}_{jj,n}}{\left\|\boldsymbol{h}_{jj,u}\right\|}$, conditioned on $\boldsymbol{h}_{jj,u}$, is Gaussian (mean zero and variance $\beta_{j,n}$) [105] and is independent of $X_u$. Since $I_n$ is present in inter- and intra-cell interference terms in (8.8), both can be combined. Also, assuming users of $j^{th}$ BS are located at cells boundaries, $r_n = R_j$, which represents the worst case, (8.8) can be written as:

$$\gamma_u = \frac{P_u \beta_u X_u}{P_u \sum\limits_{i=1}^{J} \sum\limits_{n \neq u \in K_1}^{K_i} \rho \beta_{jn} I_{n,i} + 1} \tag{8.9}$$

where $\rho = 1 + (R_d)^{-\upsilon}$ and $R_d = \frac{D_i}{R_j}$. Since $D_i$ and $R_j$ are fixed for a specific design of cellular system, $\rho$ will be a constant.

## 8.3  SE and EE Metrics of MU-MIMO Cellular System

The SE metric of a multi-cell MU-MIMO cellular system for $u^{th}$ user within $j^{th}$ BS can be written as

$$\eta_{S_{j,u}} = \mathbb{E}\left[\log_2\left(1 + \frac{P_u \beta_u X_u}{P_u \sum\limits_{i=1}^{J} \sum\limits_{n \neq u \in K_1}^{K_i} \rho \beta_{jn} I_{n,i} + 1}\right)\right] \tag{8.10}$$

where $\gamma_u$ is SINR given by (8.9). For the case of fading and shadowing channel in the system, using MGF approach and using the following observation [107]:

$$\ln\left(1 + \frac{\sum_{n=1}^{N} x_n}{\sum_{m=1}^{M} y_m + 1}\right) = \int_0^\infty \frac{e^{-z}}{z}\left(\mathbb{M}_y(z) - \mathbb{M}_{x,y}(z)\right) dz \tag{8.11}$$

where $x_1, ..., x_N, y_1, ..., y_M$ are arbitrary non-negative random variables, $\mathbb{M}_x(z) = \mathbb{E}\left[e^{-z\sum_{m=1}^{M} y_n}\right]$ and $\mathbb{M}_{x,y}(z) = \mathbb{E}\left[e^{-z\left(\sum_{n=1}^{N} x_n + \sum_{m=1}^{M} y_m\right)}\right]$, the SE metric given in (8.10) can be derived and is given by:

$$\begin{aligned} \eta_{S_{j,u}} &= \mathbb{E}\left[\log_2(e)\int_0^\infty \frac{e^{-z/p_u}}{z}(1 - e^{-zX_u\beta_u})e^{-z\sum_n \rho\beta_{jn}I_n} dz\right] \\ &= \log_2(e)\int_0^\infty \frac{e^{-z/p_u}}{z}\left(1 - \mathbb{E}\left[e^{-zX_u\beta_u}\right]\right)\mathbb{E}\left[e^{-z\sum_n \rho\beta_{jn}I_n}\right] dz \end{aligned} \tag{8.12}$$

where $\eta_{S_{j,u}}$ is SE metric in bits/s/Hz for $u^{th}$ user at $j^{th}$ BS with MRC receiver. The expectation $\mathbb{E}$ is with respect to fading random variable $X_u$, shadowing random variable $\beta_u$ and $I_n$ which are all independent. The two MGFs in (8.12) are given by:

$$\mathbb{M}_{X_u,\beta_u}(z) = \mathbb{E}\left[e^{-zX_u\beta_u}\right] \tag{8.13}$$

$$\mathbb{M}_{I_n}(z) = \mathbb{E}\left[e^{-z\sum_n \rho\beta_{jn}I_n}\right] \tag{8.14}$$

In (8.13), expectation is first taken over fading random variable $X_u$ and then over shadowing random variable $\beta_u$. The expectation in (8.13) can be written as [105]:

$$\mathbb{E}\left[e^{-zX_u\beta_u} \mid \beta_u\right] = \int_0^\infty e^{-zX_u\beta_u} dF_{X_u}(X_u) \qquad (8.15)$$

where $F_{X_u}(X_u)$ is distribution of $X_u$ [106, eq. (40)] and is given by:

$$F_{X_u}(X_u) = 1 - e^{-(X_u/\beta_u)} \sum_{n=0}^{\mathcal{M}-1} \frac{1}{n!} \left(\frac{X_u}{\beta_u}\right)^n, \quad X_u > 0 \qquad (8.16)$$

It is assumed that fading between $u^{th}$ user and $\mathcal{M}$ antennas at BS are statistical i.i.d random variables. Fading effect is less severe as number of antennas at BS increase, and hence, shaping parameter of used Gamma distribution is set as number of antennas, $\mathcal{M}$, at BS. Using (8.16) and [84, eq. (3.326)], (8.15) can be written as

$$\mathbb{E}\left[e^{-zX_u\beta_u} \mid \beta_u\right] = 1 - z\beta_u \sum_{n=0}^{\mathcal{M}-1} \left(\frac{1}{1+\beta_u z}\right)^{n+1} \qquad (8.17)$$

The quantity $\mathbb{M}_{X_u,\beta_u}(z)$ in (8.17) can be simplified by noting that $\beta_u$ is Gamma random variable with density given by:

$$f_{\beta_u}(\beta_u) = \frac{1}{\Gamma(c_u)\Omega_u^{c_u}} \beta_u^{c_u-1} e^{-\frac{\beta_u}{\Omega_u}}, \qquad (8.18)$$

where $\Omega_u = \mathbb{E}[\beta_u]/c_u$ and $\beta_u, C_u, \Omega_u > 0$. Thus,

$$\mathbb{M}_{X_u,\beta_u}(z) = 1 - z \sum_{n=0}^{\mathcal{M}-1} \int_0^\infty \beta_u \left(\frac{1}{1+\beta_u z}\right)^{n+1} f_{\beta_u}(\beta_u) d\beta_u$$

145

Using [86, eq. (8.4.2.5)] and [84, eq. (7.813)], MGF in (8.13) can be shown to be given by:

$$\mathbb{M}_{X_u,\beta_u}(z) = 1 - z \sum_{n=0}^{\mathcal{M}-1} \frac{\Omega_u}{\Gamma(n+1)\Gamma(c_u)} G_{2,1}^{1,2}\left(\Omega_u z \,\middle|\, \begin{matrix} -c_u, n \\ 0 \end{matrix}\right) \tag{8.19}$$

Using similar approach, MGF in (8.14) can be simplified and is given by:

$$\mathbb{M}_{I_u}(z) = \mathbb{E}_{\beta_n}\left[\mathbb{E}_{I_n}\left[e^{-z\sum^J\sum^{K_i}\rho\beta_{jn}I_{n,i}} \,\middle|\, \beta_{jn}\right]\right] \tag{8.20}$$

Using expectation operation with respect to $I_n$, we get [56]

$$\mathbb{E}_{I_u}\left[e^{-z\sum^J\sum^{K_i}\rho\beta_{jn}I_{n,i}} \,\middle|\, \beta_{jn}\right] = \prod^J\prod^{K_i}\left(\frac{1}{1+\rho\beta_{jn}z}\right) \tag{8.21}$$

By noting that $I_1,\ I_2,...,I_n$ and $\beta_1,\ \beta_2,....,\beta_M$ are i.i.d random variables and using [86, eq. (8.4.2.5)] and [84, eq. (7.813)], we get

$$\mathbb{M}_{I_u}(z) = \prod^J\prod^{K_i} \frac{1}{\Gamma(c_u)} G_{2,1}^{1,2}\left(\Omega_u z \,\middle|\, \begin{matrix} -c_u+1, 0 \\ 0 \end{matrix}\right) \tag{8.22}$$

Using the well-known Gauss-Laguerre quadrature rule [108, eq. (25.4.45)], SE metric of uplink for $u^{th}$ user to BS of $j^{th}$ cell is given by:

$$\eta_{S_{j,u}} = (\log_2 e)P_u \sum_{v=1}^{V} \omega_v \left\{\left[\sum_{n=0}^{\mathcal{M}-1} \frac{\Omega_u}{\Gamma(n+1)\Gamma(c_u)} G_{2,1}^{1,2}\left(\Xi_v \,\middle|\, \begin{matrix} -c_u, n \\ 0 \end{matrix}\right)\right] \times\right.$$

$$\left[ \prod_{}^{J} \prod_{}^{K_i} \frac{1}{\Gamma(c_u)} G_{2,1}^{1,2} \left( \Xi_v \ \middle| \ \begin{matrix} -c_u + 1, 0 \\ 0 \end{matrix} \right) \right] \right\} + R_v$$

$$(8.23)$$

where $\omega_v = \frac{\xi_v}{(q+1)^2 [L_{q+1}(\xi_v)]^2}$, $\Xi_v = \rho \Omega_u P_u \xi_v$ and $L_q$ is the Laguerre polynomial. The values of $\xi_v$ and $\omega_v$ can be easily determined [108, Table. (25.9)]. The SE metric of uplink of $j^{th}$ BS can be expressed as:

$$\eta_{S,j} = \sum_{u=1}^{K_j} \eta_{S_{j,u}} \tag{8.24}$$

where $K_j$ is number of users in $j^{th}$ BS.

The EE metric of MU-MIMO cellular system can be obtained using (2.7) where power transmitted is assumed to be $g(P) = P$ for the ideal case. Consequently, uplink EE metric of $u^{th}$ user in $j^{th}$ BS is given by:

$$\eta_{E_{j,u}} = \eta_{S_{j,u}} / P_u \tag{8.25}$$

where $\eta_{S_{j,u}}$ is given by (8.23). The uplink EE metric in $j^{th}$ BS is given by [104]

$$\eta_{E,j} = \frac{\sum_{u=1}^{K_j} \eta_{S_{j,u}}}{\sum_{u=1}^{K_j} P_u} \tag{8.26}$$

## 8.4 Numerical Results and Discussion

A MU-MIMO cellular system with seven cells, $J = 7$, as shown in Figure 8.2 is considered for evaluating SE and EE metrics. The numerical results are presented taking

into account fading and shadowing, path loss, and co-channel interference. The users are assumed to be uniformly distributed within the cells. The efficiency metrics are investigated assuming MU-MIMO system with MRC receiver at BS, user power $-20 \leq P_u \leq 10$ dBm and normalized reuse distance $1 \leq R_d \leq 6$. The numerical results of EE and SE metrics presented are for uplink of $u^{th}$ user in $j^{th}$ BS. These are representative metrics fo the entire MU-MIMO cellular system.

### 8.4.1  SE Metric of MU-MIMO Cellular System

Using (8.23), SE metric for $u^{th}$ user in $j^{th}$ BS is examined as a function of user's transmitted power $P_u$, normalized reuse distance $R_d$, number of users in co-channel cells $K_i$, and BS array size $\mathcal{M}$. The $\mathcal{M}$ fading coefficients as described in (8.16) correspond to shaping parameter of Gamma distribution and shadowing parameter is fixed at $c_u = 3$. Path loss exponent is assumed to be $\upsilon = 3.5$ for shadowed urban cellular environment. As given by (8.2), the dimension of channel matrix in a MU-MIMO system depends on number of users and antenna array size at BS. For $K_i = 4$ and $\mathcal{M} = 20$, the dimension of fading coefficient matrix, $\boldsymbol{H}_{ji}$, is $20 \times 4$ and that of shadowing diagonal matrix $\boldsymbol{D}_{ji}$ is $4 \times 4$. For $u^{th}$ user, first row of $\boldsymbol{H}_{ji}$ represents fading coefficient and shadowing coefficient is simply $\beta_u$. In Figure 8.5, SE metric is plotted as a function of $P_u$ and $\mathcal{M}$ for $R_d = 4$ and $K_i = 4$ users in co-channels. It is observed that SE metric is an increasing function of power transmitted by user. Also, it is noted that MRC receiver enhances SE metric particularly for low values of $P_u$ as BS array size increases. For example for $P_u = -10$ dBm, SE metric improves by 56%, 123%, 195% and 218% for $\mathcal{M} = 20, 40, 80$ and

**Figure 8.5:** SE metrics of MU-MIMO cellular system as a function of $P_u$ and $\mathcal{M}$ ( $R_d = 4$, $\upsilon = 3.5$, $c_u = 3$, $K_i = 4$)
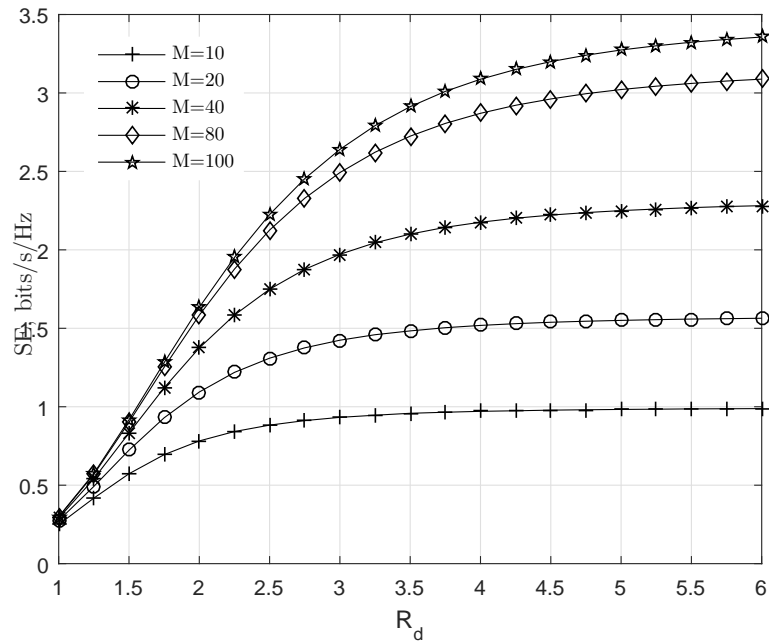


**Figure 8.6:** SE metrics of MU-MIMO cellular system as a function of $R_d$ and $\mathcal{M}$ ($P_u = -10$ dBm, $\upsilon = 3.5$, $c_u = 3$, $K_i = 4$)

100, respectively, compared to SE metric for $\mathcal{M} = 10$. The SE metric is also examined as a function of normalized reuse distance $R_d$ using (8.23) for several values of $\mathcal{M}$ and $P_u = 10$ dB in Figure 8.6. It is observed that SE metric increases due to decreased co-channel interference as $R_d$ increases. For example, for $\mathcal{M} = 80$ and $R_d = 4$, SE metric increases by 1.25 bits/s/Hz compared to that when $R_d = 2$ for the same value of $\mathcal{M}$. A significant improvement in SE metric can be achieved by increasing number of antennas at BS for $R_d \leq 4$. For example, for $R_d = 3.75$ and $\mathcal{M} = 100$, SE metric is enhanced by 1.5 bits/s/Hz compared to that for $\mathcal{M} = 10$. However, for $R_d \geq 4$, SE metric almost remains constant indicating the effect of path loss over channel on SE as dimension of cellular system increases. The antenna array size at BS is an important parameter in the design of a MU-MIMO cellular system and, thus, SE metric is also examined as a function of $\mathcal{M}$, for several values of $P_u$ and $R_d$ in Figure 8.7. It is noted that SE
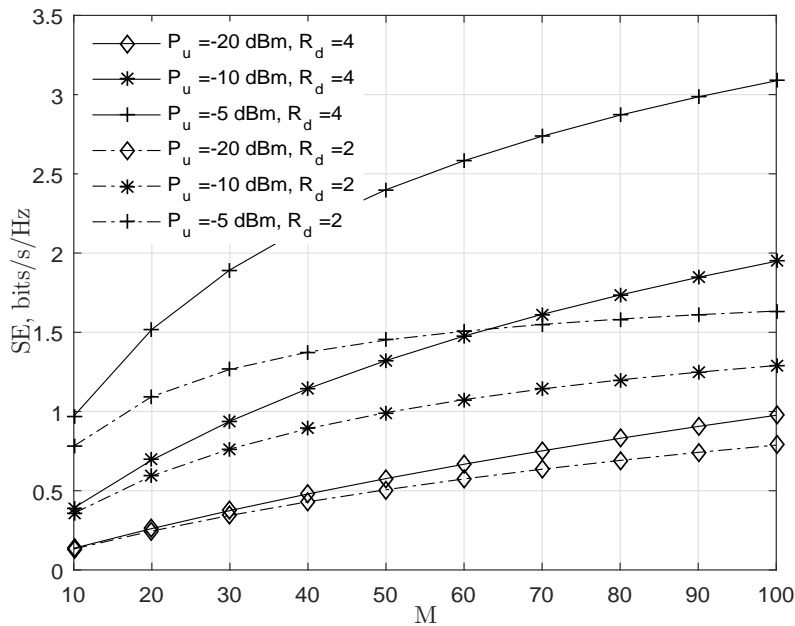


**Figure 8.7:** SE metrics of MU-MIMO cellular system as a function of $\mathcal{M}$, $P_u$ and $R_d$ $(K_i = 4)$
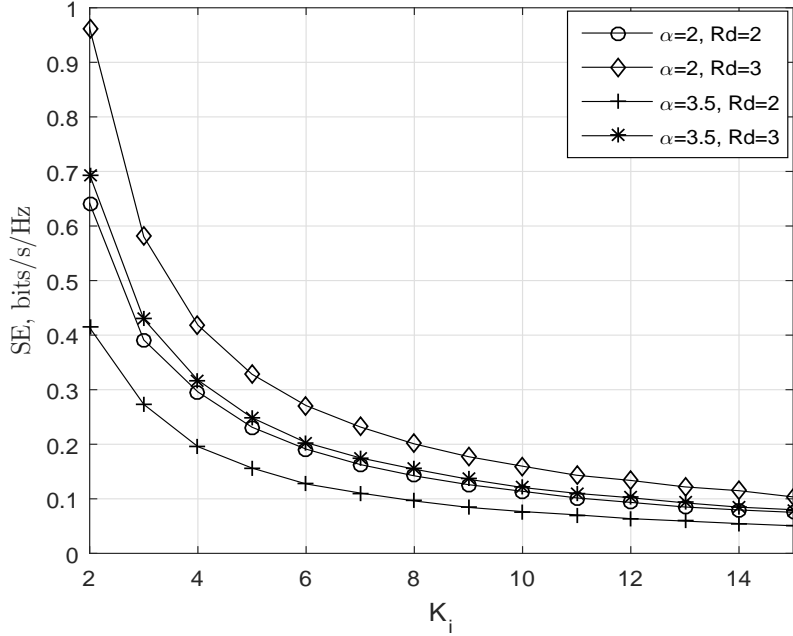
**Figure 8.8:** SE metrics of MU-MIMO cellular system as a function of $K_i$ and $R_d$ ($P_u = 0$ dBm and $M = 20$)

metric improves as number of antennas at BS increases. The relationship between SE metric and antenna array size at BS, $\mathcal{M}$, is nearly linear (for $R_d \leq 4$) with a slop of 0.02 bits/s/Hz/antenna. Since cochannel interference in the system depends on number of users in cochannel cells, the SE metrics are plotted in Figure 8.8 as a function of $K_i$ for $v = 2, 3.5$ and $R_d = 2, 3$. It is observed that SE metric decays exponentially as $K_i$, since cochannel interference at BS increases as number of users in cochannel, increases. For example, for $K_i = 4$ and $v = 3.5$ and $R_d = 3$, SE metric is reduced by 0.4 bits/s/Hz compared to that when $K_i = 2$.

## 8.4.2 EE Metric of MU-MIMO Cellular System

The EE metric is important for designing an energy-efficient MU-MIMO cellular systems. Using (8.25) and (8.23), EE metrics for uplink between $u^{th}$ user in $j^{th}$ BS of MU-MIMO

cellular system are plotted as a function of $P_u$ and $\mathcal{M}$ in Figure 8.9, for fixed values of $R_d = 4$, $v = 3.5$, $c_u = 3$ and $K_i = 4$. The EE metric is typically inversely proportional
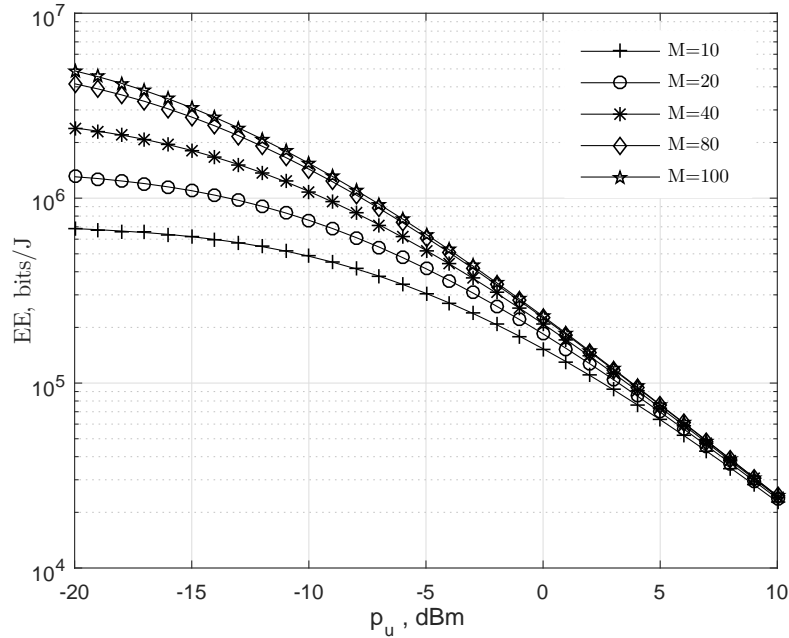


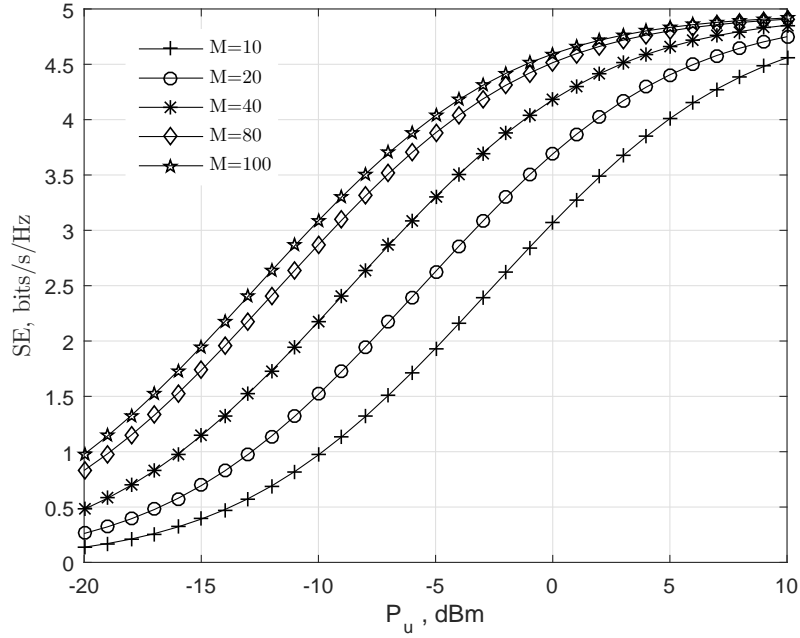**Figure 8.9:** EE metrics of MU-MIMO cellular system as a function of $P_u$ and $\mathcal{M}$ ($R_d = 4$, $v = 3.5$, $c_u = 3$, $K_i = 4$)

to $P_u$. However, with the use of MRC receiver in MU-MIMO system at BS, EE metric can be enhanced by increasing the array size at BS, even for low values of $P_u$. For example, EE metric at $P_u = -20$ dBm is doubled, tripled and quadrupled for $\mathcal{M} = 40, \ 80, \ 100$, respectively, compared to EE metric for $\mathcal{M} = 10$ with same value of $P_u$. EE metric of the system is plotted as a function of $R_d$ and $\mathcal{M}$ for $P_u = -10$ dBm, $v = 3.5$, $c_u = 3$ and $K_i = 4$ in Figure 8.10. It is observed that EE metric declines as $R_d$ is decreased, due to increased cochannle interference from cochannel cells. On the other hand, EE metric marginally improves for $R_d \geq 4$, due to path loss increases for larger values of $R_d$. The effect of number of antennas at BS on EE metric of the system is considered by plotting EE metric vs $\mathcal{M}$ in Figure 8.11, for several set of values of $P_u$ and $R_d$. It is observed
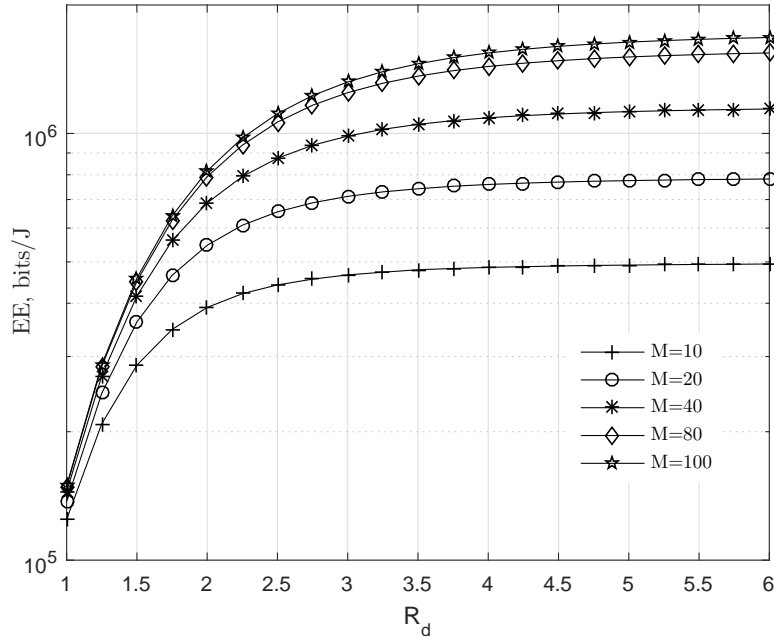
**Figure 8.10:** EE metrics of $u^{th}$ as a function of $R_d$ and $\mathcal{M}$ ($P_u = -10$ dBm, $v = 3.5$, $c_u = 3$, $K_i = 4$)
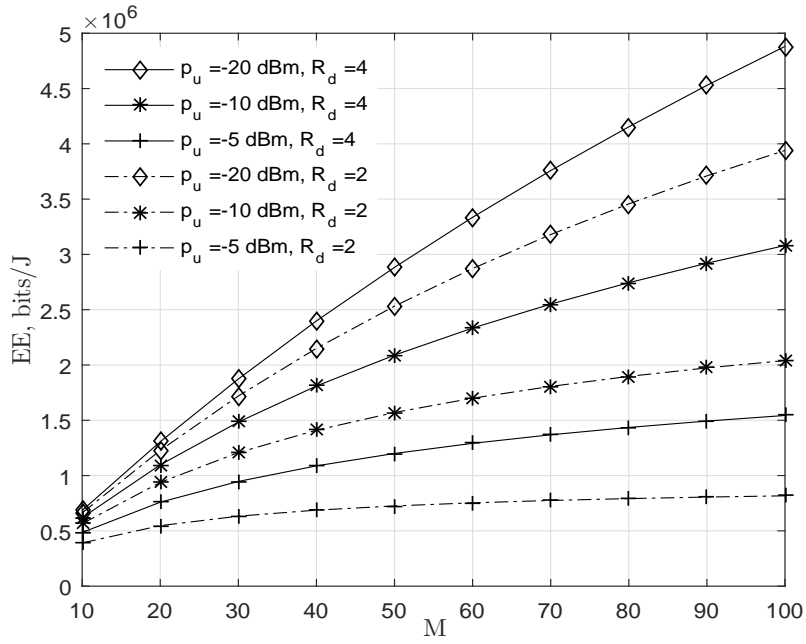


**Figure 8.11:** EE as a function of BS array size for given $K_i = 4$, $P_u$ and $R_d$

that EE metric is nearly a linear function of $\mathcal{M}$ with slope depending on values of $R_d$

and $P_u$. For example, EE metric is enhanced by $4.22 \times 10^4$ and $1 \times 10^4$ bits/J/antenna
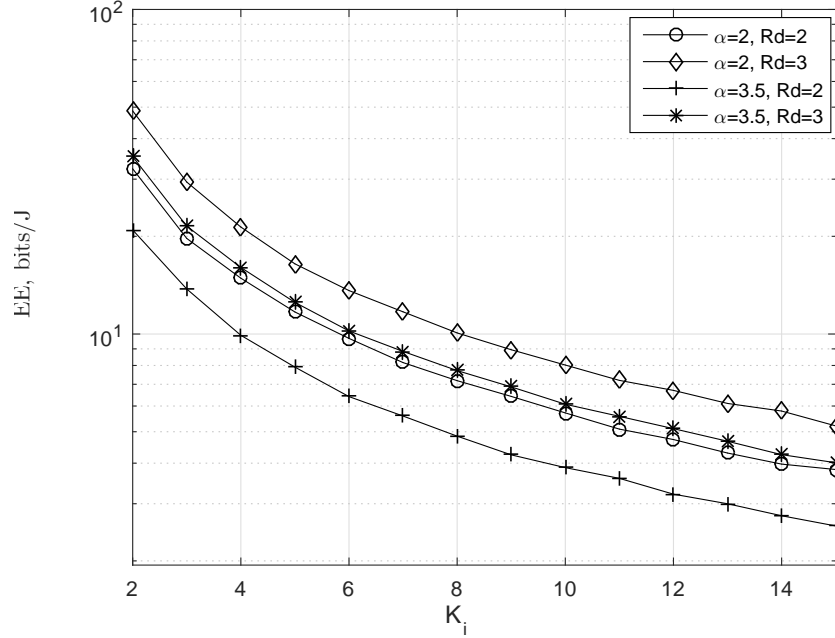
**Figure 8.12:** EE metrics of MU-MIMO system as a function of $K_i$ and $R_d$ ($P_u = 0$ dBm and $\mathcal{M} = 20$)

for ($R_d = 4$, $P_u = -20$ dBm) and ($R_d = 2$, $P_u = -10$ dBm), respectively. As number of users in cochannel cells increases, the intra- and inter-cell interferences become severe and impacts EE metric. Figure 8.12 shows the behavior of EE metric of the system as a function of users number in cochannel cells. It is observed that EE metric decreases exponentially as users in cochannel increases in number. For example with $K_i = 6$, the EE metric is reduced by 35 bits/J compared to EE metric when $K_i = 2$, assuming in both cases $\upsilon = 2$, $R_d = 3$ and $P_u = 0$ dBm.

## 8.5 Chapter Summary

In this Chapter, uplink SE and EE metrics have been investigated for a MU-MIMO system equipped with MRC diversity receiver at BS in a cellular system. The fading,

shadowing, path loss and cochannel interference are considered in the analysis and derivation of closed-form expressions of these metrics. In the derivation of expressions for SE and EE metrics, MGF approach is used and these metrics are illustrated as a function of user's transmitted power, normalized reuse distance, BS antenna array size, number of users in each cell and parameters of fading and shadowing distributions. Both fading and shadowing are assumed independent and Gamma distributed. The results show that MRC diversity receiver in MU-MIMO system at BS is attractive for low values of transmitted power of users in the system. Also, it is observed that range of normalized reuse distance $2 \leq R_d \leq 4$ is optimum in dimensioning MU-MIMO cellular system. Use of appropriate antenna array size at BS can significantly improve SE and EE metrics of the cellular system by 0.02 bits/s/Hz/antenna and $4.22 \times 10^4$ bits/J/antenna, respectively.

# Chapter 9

# Analysis and design of mmWave Cellular System using Efficiency Metrics [11,12]

## 9.1 Introduction

Millimeter wave (mmWave) spectrum has been proposed for use in commercial cellular systems to relieve already severely congested microwave spectrum. Thus, design of efficient mmWave cellular system has gained considerable importance in recent years. Also, it is important to take into account regulations imposed by government agencies with regard to global warming and sustainable development in its design. In this Chapter, a dense mmWave hexagonal cellular system with each cell consisting of number of smaller cells with their own Base Stations (BSs) is presented as a solution to meet increasing

11. Hamed, A., and Rao, R.K., "Spectral and Energy Efficiencies in mmWave Cellular Networks for Optimal Utilization," Wireless Communications and Mobile Computing, Hindawi, vol. 2018, pp. 1-11 April 2018.

12. Hamed, A.M.,; Rao, R.K., "Evaluation of Capacity and Power Efficiency in Millimeter-Wave Bands," The Society for Modeling and Simulation International, 2016 Summer Simulation Multi-Conference (SummerSim'16), pp. 1-6. IEEE, 2016.

demand for a variety of high data rate services and growing number of users of cellular systems. Since spectrum and power are two critical resources, a framework is presented for their efficient utilization in mmWave cellular system in 28 and 73 GHz bands. These bands are already an integral part of well-known standards such as IEEE 802.15.3c, IEEE 802.11ad, and IEEE 802.16.1. In the analysis and design of mmWave cellular system, well-known and accurate mmWave channel models for LOS and NLOS links are used [60], [61]. The system is analyzed using SE, EE, SSE, SEE, and network latency metrics. These metrics are illustrated, using extensive Monte Carlo simulations, as a function of SNR, channel model parameters, user distance from BS, and BS transmission power. The efficiency metrics for optimum deployment of mmWave cellular systems in 28 and 73 GHz bands are investigated.

## 9.2    mmWave Cellular System Model

Heterogeneous cellular systems are evolving toward small cell deployment using pico and femtocells. Deploying such small cells is used to provide high data rate and coverage in a cellular system. A BS in small cell is required to transmit low power, due to smaller distances to Mobile Users (MUs), and therefore can be energy- and spectral-efficient. Since cell radius in many dense urban areas is less than 200 $m$, transmission of signals in mmWave bands is gaining importance. However, deployment of small cells pose serious challenge in terms of co-channel interference in designing of efficient mmWave systems. In the mmWave cellular shown in Figure 9.1, macrocells are divided into smaller cells and blue cells are cochannel cells. The $J$ cochannel cells use same frequency resources
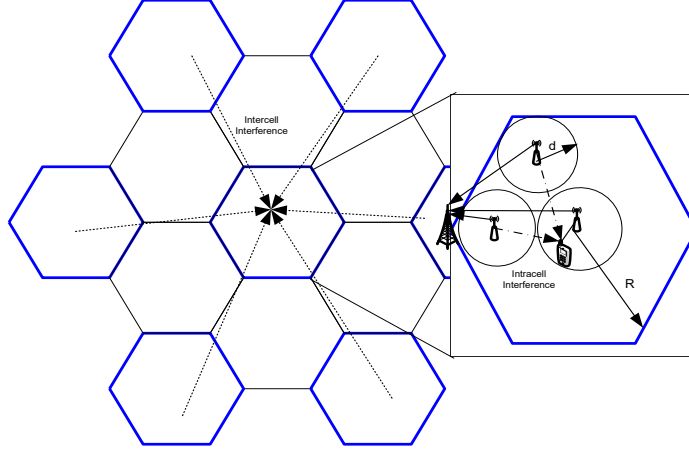
**Figure 9.1:** Model of a mmWave cellular system [links: .\_.\_, intracell interference; ..., intercell interference; and (—), BSs and macrocells]

and therefore create intercell interference. Each of $j$ $(j = 1, ..., J)$ cells is overlaid with $I$ smaller cells each with its own BS. Every small $i$ BS $(i = 1, ..., I)$ uses same frequency resource causing intracell interference. It is assumed that there are $K$ MUs in each small cell and each $k^{th}$ MU $(k = 1, ..., K)$ is served by its own BS. The BS is assumed to be located at the center of each small cell and connected to gateway of the macrocell. The MUs are spatially distributed and associated with BS of a single cell at any time.

### 9.2.1 SNR and SINR Models

The channel model given by (3.9) is used to obtain an estimate of SNR at $k^{th}$ MU in $i^{th}$ BS. That is

$$SNR_{i,k[dB]} = 10 \log_{10} |h_{i,k}|^2 + P_{i[dBm]} + G_{i[dBi]} + G_{k[dBi]} -$$

$$L_{i,k[dB]} \left( r_{i,k} \right) - \left( KT_{[dBm/Hz]} + 10 \log_{10}(B_k) + NF_{[dB]} \right) \quad (9.1)$$

158

where $P_i$ is power transmitted by BS$_i$, $KT$ is noise power density at MU, and NF is noise figure (NF). The transmitter and receiver antenna gains, $G_i$ and $G_k$, are calculated using $G = 20 \log_{10} \left( \frac{\pi l}{\lambda} \right)$ for 28 and 73 GHz frequency bands, where antenna length is $l$. Assuming independent Nakagami-$m$ fading for each link $|h_{i,k}|^2$ can be modeled as a normalized Gamma random variable, i.e., $|h_{i,k}|^2 \sim \mathcal{G}(v, 1/v)$ [69]. The fading is less severe in mmWave band [67], and fading figure $v$ is large for LOS link, and $v = 1$ for NLOS link. The path loss, $L_{i,k}$, can be easily calculated using (3.9).

With reference to system model shown in Figure 9.1, for $k^{th}$ MU in $i^{th}$ small cell in $j^{th}$ macro-cell, the interference consists of two components: $i$) intracell interference and $ii$) intercell interference. The first one is caused by active BSs located in the same $j^{th}$ macrocell and is more severe since it is close to the MU. The second component is generated due to BSs in the other macro-cells and is less severe. The co-channel interference due to first tier macrocells, the aggregate downlink interference in $s$ small cell BSs and $p$ macro-cell for $k^{th}$ MU can be expressed as

$$\Lambda_{j,i,k} = \sum_{\substack{i=1 \\ i \neq s}}^{I} P_{p,i} G_{p,i} G_{p,s,k} |h_{p,i,k}|^2 L_{p,i,k}(r_{i,k}) + \sum_{\substack{j=1 \\ j \neq p}}^{J} \sum_{i=1}^{I} P_{j,i} G_{j,i} G_{j,i,k} |h_{j,i,k}|^2 L_{j,i,k}(r_{j,i,k})$$

$$(9.2)$$

Therefore, SINR at MU$_k$ for BS$_i$ can be written as:

$$SINR_{j,i,k[dB]} = SNR_{i,k[dB]} - 10 \log_{10} \left( \frac{\Lambda_{i,k}}{\sigma_k^2} + 1 \right) \qquad (9.3)$$

where $\sigma_k^2$ is thermal noise power at $k^{th}$ MU. The distance $r_{i,k}$ between BS$_i$ and MU$_k$ is $< 200\ m$ and is a random variable with probability density function $f_d(r) = 2r/d^2$, $0 \leq$

$r \leq 200\ m$.

## 9.3  Analysis of Efficiency Metrics for mmWave Cellular System

Energy and spectrum are two resources that have to be carefully traded for efficient design of mmWave system. Minimal use of energy resource is an important issue; however, efficient use of mmWave spectrum requires more power due to high path loss. Therefore, a balance between the two resources of system deserves a careful study. This is examined in this section for a mmWave cellular system by obtaining expressions for of SE and EE metrics. Also, other important metrics such as outage probability, SSE, and SEE of the system are discussed.

### 9.3.1  Outage Probability

The SE and EE metrics of a mmWave system depend on outage probability of users in the system. When users experience outage, they cannot be served by any BS within their communication range. The outage probability within a communication range $R$, $P_{out,j}$, is given by [109]

$$P_{out,j}(R) = \exp\left(-\frac{2\pi\rho_j}{\varrho_j^2}\left(1 - \left(1 + \varrho_j R\right)e^{-\varrho_j R}\right)\right) \tag{9.4}$$

where $\varrho_j$ is a parameter that depends on density and size of obstacles in the path from BS to user. The larger the value of $\varrho_j$, higher is the probability of outage. The quantity $\rho_j$

denotes average number of BSs per unit area. For example, if there are 25 BSs uniformly deployed over an area of $500 \ m \times 500 \ m$ square, $\rho_j = 25/(500 \times 500) = 10^{-4} \ (BSs/m^2)$. The outage probability is plotted as a function of $\varrho_j$ and $R$ for $\rho_j = 10^{-4}$ in Figure 9.2. It is observed that $P_{out}$ is nearly constant for $R > 200 \ m$. Thus, the outage probability in (9.4) can be approximated by $P_{out,j} = e^{-\frac{2\pi\rho_j}{\varrho_j^2}}$ for $R \geq 200 \ m$
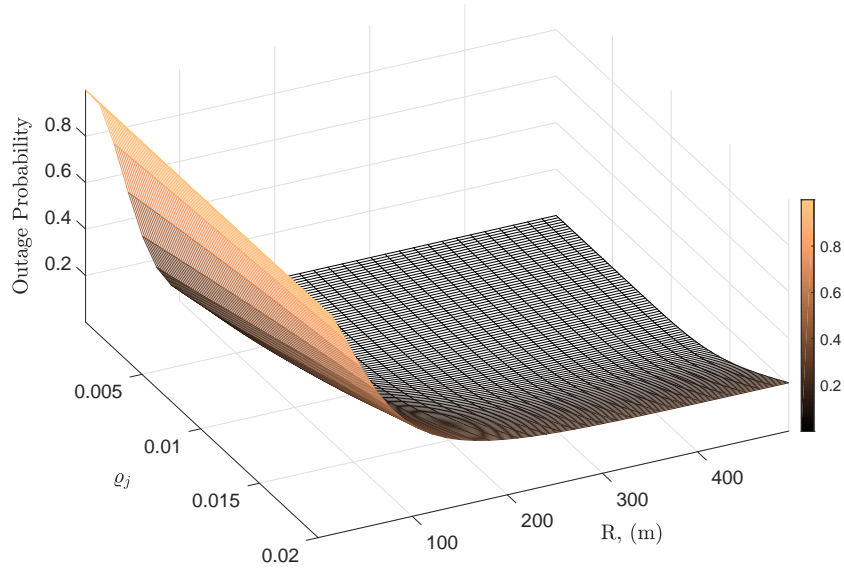


**Figure 9.2:** Outage probability as a function of $\varrho_j$ and $R$ for $\rho_j = 10^{-4}$

## 9.3.2 SE Metric of mmWave Cellular System

The downlink SE metric quantifies data rate delivered by BS to MUs over a certain bandwidth, $B_k$. This metric indicates how efficiently mmWave spectrum is utilized. The SE metric is bounded by Shannon's limit $B_k \log_2 (1 + SNR_k)$ [15], where $SNR_k$ is the SNR at $MU_k$. For a mmWave system, SNR is replaced by corresponding SINR. Thus,

161

SE metric of mmWave system, depicted in Figure 9.1, can be written as

$$\eta_{SE} = \sum_J \sum_I \sum_K B_k \mathbb{E}_r \left[ \mathbb{E}_h \left[ \log_2 \left( 1 + SINR_{j,i,k} \right) \right] \right] \left( 1 - P_{out,j}(R) \right), \quad (bit/s) \quad (9.5)$$

where $\text{SINR}_{j,i,k}$ can be obtained from (9.3), and $B_k$ is the allocated mmWave bandwidth for MUs. The $\mathbb{E}_r$ and $\mathbb{E}_h$ are expectations taken over random location of MUs and fading coefficients, respectively.

### 9.3.3 EE Metric of mmWave Cellular System

The EE metric is defined as ratio between what system delivers to what it consumes, and is $f(x)/x$ where $x \in [0, X]$ indicates the system's resource constrained by $X$ [75]. The function $f(x)$ represents downlink data rate reliably communicated by the system, and $x$ denotes SNR,and is function of power transmitted by BS, noise and channel fading coefficients. For mmWave cellular system, the EE metric is given by:

$$\eta_{EE} = \sum_J \sum_I \sum_K B_k \mathbb{E}_r \left[ \mathbb{E}_h \left[ \frac{\log_2 \left( 1 + SINR_{j,i,k} \right)}{SNR_{j,i,k}} \right] \right] \left( 1 - P_{out,j}(R) \right), \quad (bit/J) \quad (9.6)$$

where SNR and SINR can be determined using (9.1) and (9.3), respectively. The EE metric indicates amount of data rate delivered per unit of system energy.

### 9.3.4 SSE and SEE Metrics of mmWave Cellular System

Spatial characteristics of mmWave cellular system is crucial in determining overall system performance. For example, propagation loss in the system is a function of system

162

dimensions, and affects SNR and SINR. Therefore, a study of SE and EE metrics is not enough for efficient design of a mmWave cellular system. The spatial metrics SSE and SEE given by (2.13) and (2.15), respectively, are more meaningful and must be considered [98]. Accordingly, these metrics are evaluated for macrocell as sum of spatial efficiencies of small cells in a macrocell area within a serving distance, $r$.

## 9.4   Evaluation of Efficiency Metrics of mmWave Cellular System

Monte Carlo simulations have been performed in MATLAB environment to evaluate SE, EE, SSE and SEE metrics in 28 and 73 GHz mmWave bands. In order to obtain reliable results, $10,000$ iterations have been conducted in the simulation. The efficiency metrics are investigated as a function of BS transmission power ($P_j$), BS serving distance ($d$), and SNR at MU. The steps used in simulations are given below:

1. The path loss for 28 and 73 GHz bands are calculated for LOS and NLOS links using (3.9) for each values of $P$ and $r$ using path loss model parameters given in Table 3.2.

2. SNR of MU is computed using (9.1), using fading coefficient $h \sim \mathcal{G}\ (v, 1/v)$. The parameters, $KT$, $B_k$ and $NF$, are given in Table 9.1.

3. For cellular system model shown in Figure 9.1, aggregated inter-cell and intra-cell interferences are obtained using (9.2).

4. The SINR is determined using (9.3) with $\sigma_k^2 = KTB_k$.

5. SE and EE metrics are computed using (9.5) and (9.6) with $P_{out}$ calculated using (9.4), see Figure 9.2.

6. The SSE and SEE metrics are computed using $\sum \frac{\eta_{SE,j,i,k}}{A_{j,i}}$ and $\sum \frac{\eta_{EE,j,i,k}}{A_{j,i}}$, respectively, with $A_{j,i} = \pi d_{j,i}^2$ the coverage area of small cell BS [43].

The following assumptions are used in Monte Carlo simulations:

1. Channel fading coefficients, $h_{i,j,k}$ in (9.1) and (9.2) are i.i.d random variables.

2. Transmission power, $P_i$ in (9.1), is identical for all small cell BSs.

3. Antenna gain, $G_i$ is same for all BSs, and similarly antenna gain, $G_k$ is same for all MUs.

4. Intercell interference is based on first tier of macrocells.

5. Intercell distance, $r_{i,j,k} = 3R + d$, intracell distance, $r_{i,k} = 2d$, represent severe case of interference for MUs in small-cells.

6. Macro cell radius $R = 500\ m$ is assumed and maximum serving distance of a small cell BS is set to $d = 100\ m$.

The mmWave cellular system parameters used in simulations are given in Table 9.1. Steps used in simulation to determine metrics are captured in flow chart shown in Figure 9.3.

**Table 9.1:** Parameters used in simulations of efficiency metrics of mmWave cellular system

| Symbol | Description | Value |
|--------|-------------|-------|
| $B_k$ | User bandwidth | 0.1 GHz |
| $P_i$ | Microcell BS transmission power | $-10$ dBm $-40$ dBm |
| $KT$ | Noise PSD | $-174$ dBm/Hz |
| $NF$ | Noise Figure | 6 dB |
| $d$ | Maximum microcell BS serving distance | 100 $m$ |
| $R$ | Macro cell radius | 500 $m$ |
| $J$ | Number of macrocells sharing entire spectrum | 7 |
| $I$ | Maximum number of micro BSs in a macro cell | $1/\rho$ |
| $K$ | Number of users for each microcell BSs | 20 |
| $\rho$ | Density of microcell BS in a macrocell | $\left(\frac{d}{R}\right)^2$ |
| $\varrho$ | Propagation environment density | $10^{-2}$ |
| $l_t$ | Antenna length of microcell BS | 0.1 $m$ |
| $l_r$ | Antenna length of MU | 0.005 $m$ |

## 9.4.1 Numerical Results: SE Metric

The SE metric of mmWave cellular system is is plotted in Figure 9.4 as a function of microcell BS serving distance, $d$, for LOS and NLOS links in 28 and 73 GHz bands with its transmission power fixed at 10 dBm. It is observed that a data rate of 1 T bits/s can be achieved in the system for $d = 1$ $m$. For case of LOS link with $d = 50$ $m$ at 73 GHz, 0.5 T bits/s is achieved in the system where number of microcell in each macrocell is 100 BS. Also, it is observed that SE metric is nearly decreased with rate $3.912 \times 10^9$ and $4.843 \times 10^8$ bits/s/m for LOS and NLOS, respectively, for both bands. The SE metric is also investigated as a function of BS power for $d = 45$ $m$ in Figure 9.5. It is observed that SE metric is enhanced as BS power is increased. For example, SE increases with rate of $2.55 \times 10^9$ bits/s/dBm for $-10 \le P_t \le 24$ dBm, for NLOS link in both bands. Also, it is noted SE metric is almost saturated for high values of BS power and there is
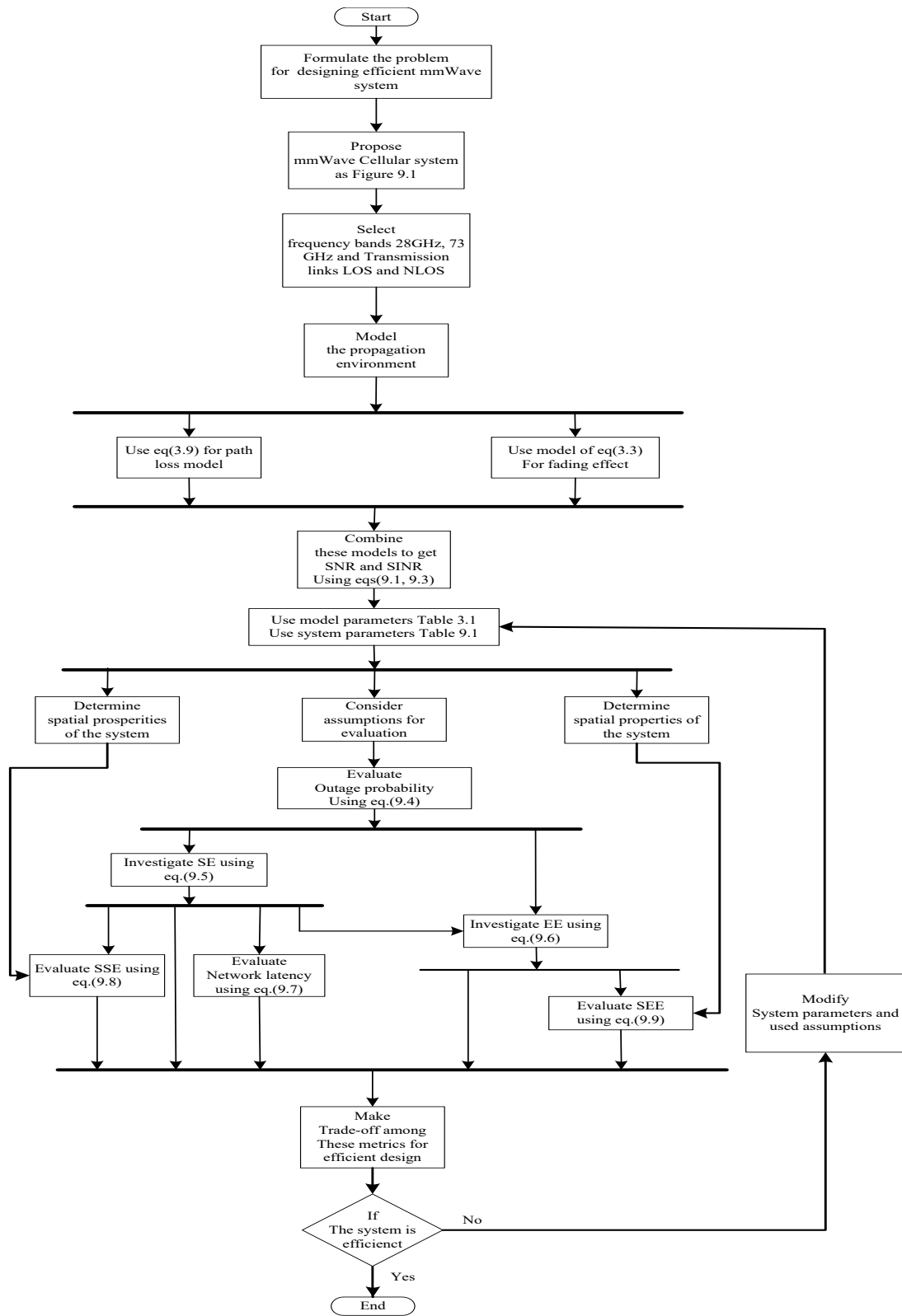
**Figure 9.3:** UML activity diagram for designing an efficient mmWave cellular system

no significant improvement for BS power $\geq 40$ dBm indicating for designing a spectrally efficient mmWave cellular system, BS power of 40 dBm is sufficient. The figure also illustrates superiority of 73 GHz band for LOS link in the system. For BS power of 40
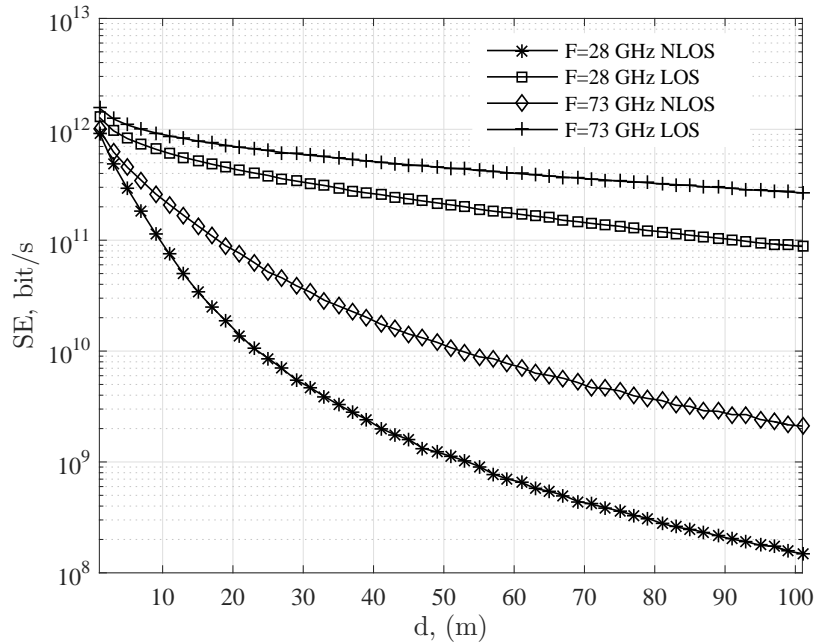


**Figure 9.4:** SE metrics of mmWave cellular system in 28 GHz and 73 GHz bands for NLOS and LOS links as a function of the maximum serving distance, $d$

dBm, both mmWave bands can be used to achieve dara rate in excess of 1 T bits/s. Since SNR at MU is function of BS power, receiver noise, fading and interference, SE metric of the system is examined for LOS link in 73 GHz band in Figure 9.6, as a function of both serving distance and SNR. It is noted that SE metric is an increasing function of SNR and deceasing function of $d$. Also, it is observed that as a function of $d$ SE metric exponentially decreases for low values of SNR; however, it gradually decreased for high values of SNR. The numerical results presented in this section are consistent with results presented in [68] and [110], where an analytical channel model is used. However, SE metrics obtained in this section are based on channel model obtained using real-world

167
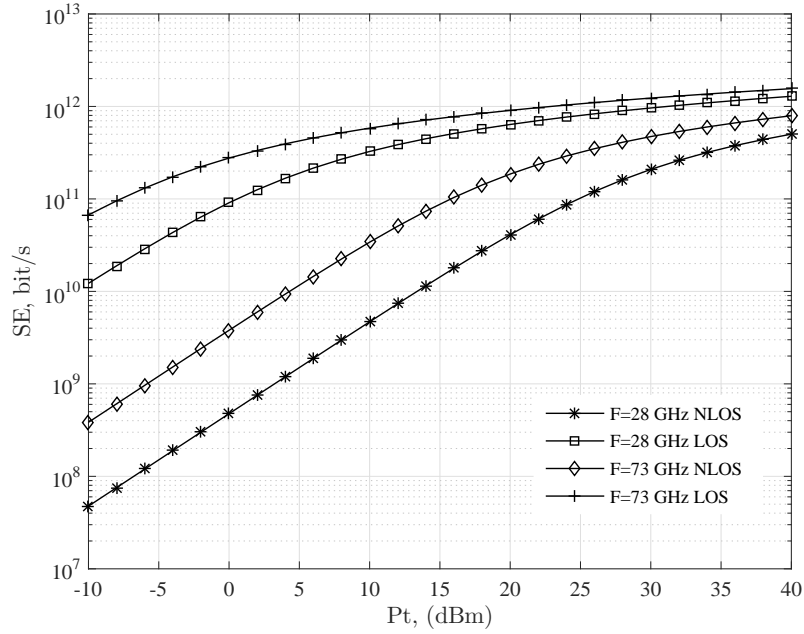
**Figure 9.5:** SE metrics of mmWave cellular system in 28 GHz and 73 GHz bands for NLOS and LOS links as a function of microcell BS power, $P$, ($d = 45\ m$)

filed measurements [61].
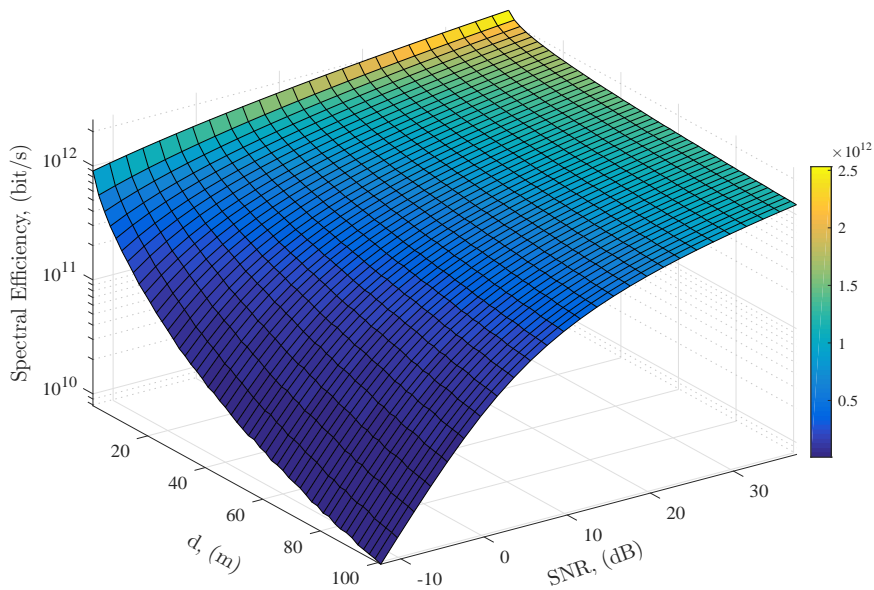


**Figure 9.6:** SE metrics of mmWave cellular system in 73 GHz band for LOS link as a function of $d$ and SNR

## 9.4.2 Numerical Results: EE Metric

The EE metric can be used for designing energy-efficient mmWave cellular systems and the metric depends on BS power. The EE metric is, therefore, a function of data rate, SNR at MU and BS serving distance. In Figure 9.7, EE metrics are plotted as a function of BS power for LOS and NLOS links in 28 GHz and 73 GHz bands. It is observed that 73 GHz band is less energy-efficient compared to 28 GHz band. Also, it is noted that EE metric decays with rate of $1.17 \times 10^9$ bits/J/dBm for a wide range of BS power. The
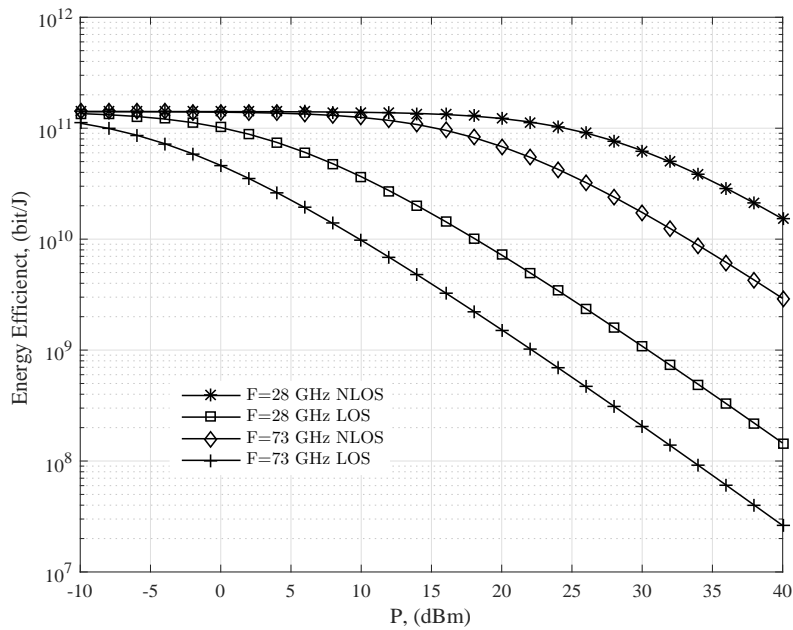


**Figure 9.7:** EE metrics for NLOS and LOS links in 28 GHz and 73 GHz bands, as a function of BS power

EE metric degrades as BS power is increased, indicating that cellular system becomes energy inefficient due to increased transmission power at BS. Figure 9.8 and Figure 9.9 show a comparison between EE metrics of 28 GHz and 73 GHz bands for LOS link as a function of both $d$ and SNR. It is observed from these figures that 28 GHz band can
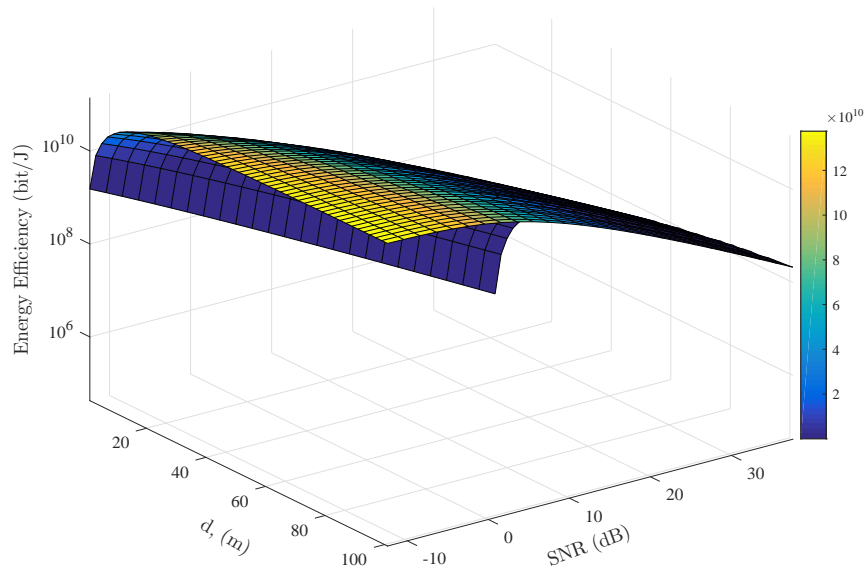
**Figure 9.8:** EE metrics of mmWave cellular system band for 73 GHz LOS link as a function of $d$ and SNR at MU
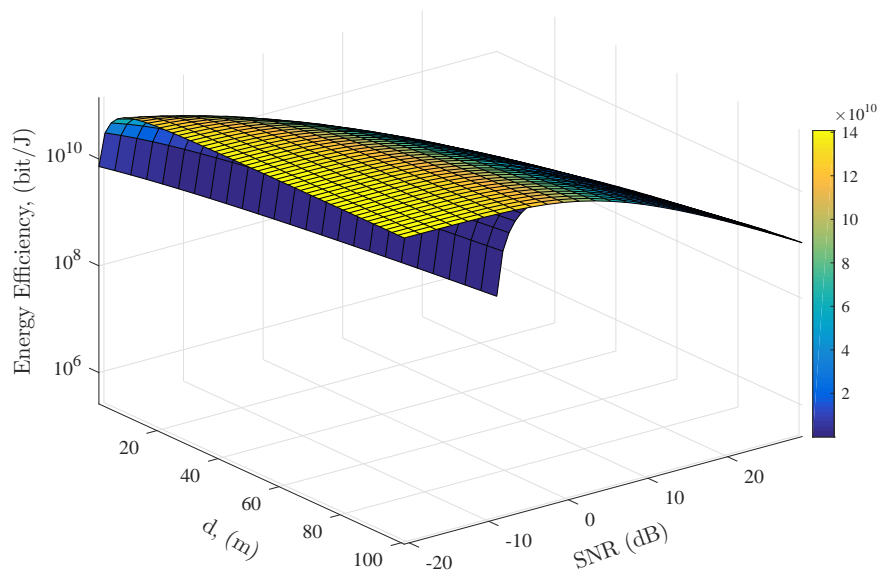


**Figure 9.9:** EE metrics of mmWave cellular system band for 28 GHz LOS link as a function of $d$ and SNR at MU

offer higher energy efficiency compared to 73 GHz band. This observation is useful in making a choice between two frequency bands in the design of energy-efficient design mmWave cellular system. Also, it is observed that SNR required at MU for LOS link in 73 GHz band is greater than that required for NLOS link in 28 GHz band. The EE metric improves for serving distance, $d$, up to 30 $m$, and becomes flat for $d > 30$ $m$. Therefore, in the design of efficient mmWave cellular system, it is important to consider trade offs among serving distance of microcell BS, its transmission power, and mmWave band to be deployed.

### 9.4.3   Numerical Results: System Latency

System latency or delay is a critical metric for real-time applications of a mmWave cellular system. Thus, system delay is examined as a function of cellular system parameters. While delay in a mmWave cellular system can be due to several factors, in this section, transmission delay between MU and its BS is of concern. For a given user bandwidth and information quantity $Q$, system delay $D$ is given by $D = Q/R_I$ where $R_I$ is number of bits/s delivered to a user in the system [77]. For the system shown in Figure 9.1, delay-per-bit for $k^{th}$ user, $D_k$, can be expressed as

$$D_k = \frac{Q_k}{B_k \mathbb{E}_r \left[ \mathbb{E}_h \left[ \log_2 \left( 1 + SINR_{j,i,k} \right) \left( 1 - P_{out,j}(R) \right) \right] \right]} \tag{9.7}$$

where $Q_k$ is quantity of information for for $k^{th}$ user, and $SINR_{j,i,k}$ is given by (9.3). The delay vs efficiency metrics of a mmWave cellular system is examined using Monte Carlo simulations of $D_k$ given in (9.7). The channel parameters given in Table 3.2 and

cellular system parameters given in Table 9.1 have been used in simulations of and $D_k$ is plotted as a function of BS power and user distance from its BS in Figure 9.10 and Figure 9.11, respectively. These figures show that LOS link in 73 GHz band achieves least delay compared to NLOS link in 28 GHz band. Also, it is noted that delay can be decreased by increasing BS power. For example, delay for $k^{th}$ user is less than 1 $ns/bit$ for BS power $\geq$ 20 dBm. However, the EE metric of the system rapidly decreases as BS power increases as shown in Figure 9.7. The delay of $k^{th}$ user in the system increases as it moves away from its BS as depicted in Figure 9.11. In contrast, SE metric of the system is reduced as user distance from its BS increases, indicating that EE and SE metrics are in conflict for a given user delay.
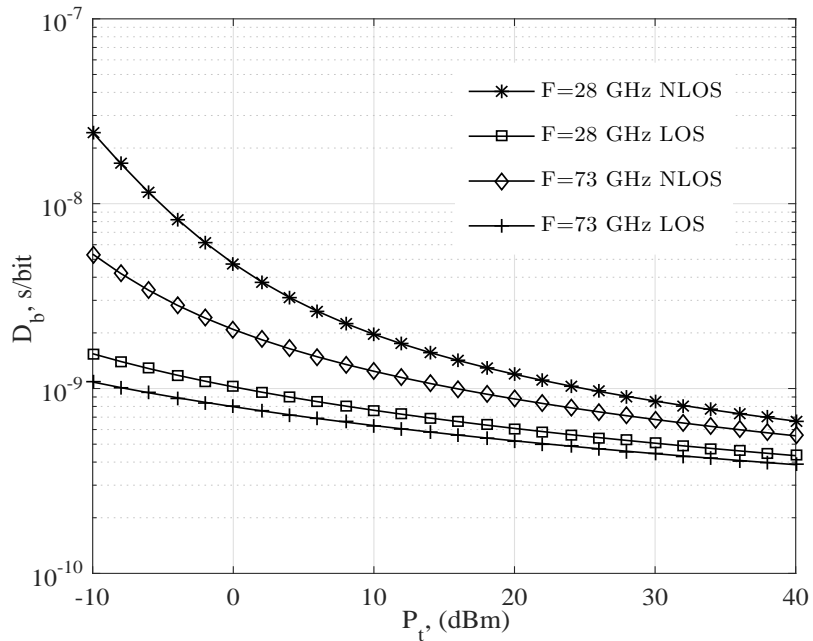


**Figure 9.10:** Delay of $k^{th}$ user in mmWave cellular system as a function of BS power
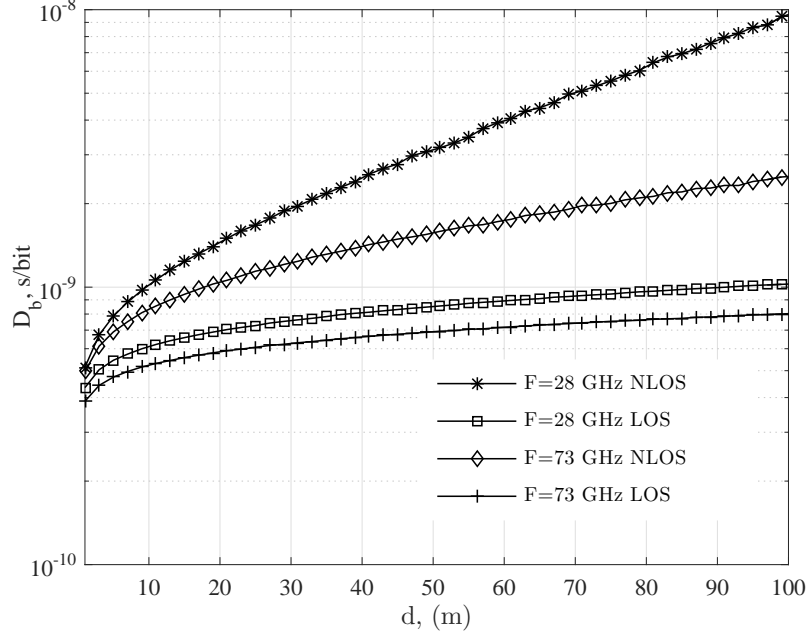
**Figure 9.11:** Delay of $k^{th}$ user in mmWave cellular system as a function of distance $d$

## 9.4.4   Numerical results: SSE Metric

The SSE metric is an indication of utilization of spectral resources per unit area of the cellular system. For mmWave cellular system shown in Figure 9.1, this metric is given by

$$\eta_{SS} = \sum \frac{\eta_{SE_{j,i,k}}}{A_{j,i}} \tag{9.8}$$

where $\eta_{SE_{j,i,k}}$ is SE metric of $k^{th}$ MU at $i^{th}$ BS in $j^{th}$ cell and $A_{j,i}$ is coverage area of $i^{th}$ BS in $j^{th}$ cell. The metric in (9.8) links SE metric of the system and its service area and is investigated as a function of $P_t$, $d$ and SNR at MU. In Figure 9.12, SSE metrics are plotted as a function of $d$. It is noted that SSE metric is a decreasing function of distance of user from its BS, since the area is proportional to $d^2$. Also, SSE metric is plotted as a function of $d$ and SNR in Figure 9.13. It is noted that for large coverage

area in a mmWave cellular system BS power required must be appropriately increased to achieve acceptable SSE metric.
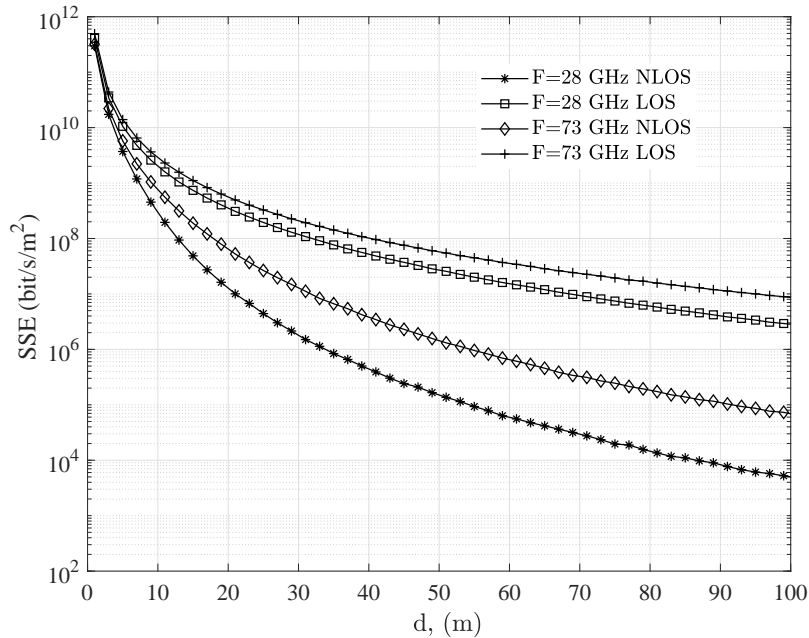


**Figure 9.12:** SSE metrics of mmWave cellular system as a function of BS serving distance, $d$

## 9.4.5 Numerical results: SEE Metric

The SEE metric characterizes area data rate per unit BS power and can be expressed as

$$\eta_{SE} = \sum \frac{\eta_{EE_{j,i,k}}}{A_{j,i}} \tag{9.9}$$

where $\eta_{EE_{j,i,k}}$ is given by (9.6) and $A_{j,i} = \pi d_{j,i}^2$ with $d_{j,i}$ serving distance. This metric provides an insight into the deployment options for optimum mmWave band utilization. The SEE metric is evaluated as a function of BS power and is shown in Figure 9.15 and the metric rapidly deteriorates as BS power increases; however, it maintains a certain

174
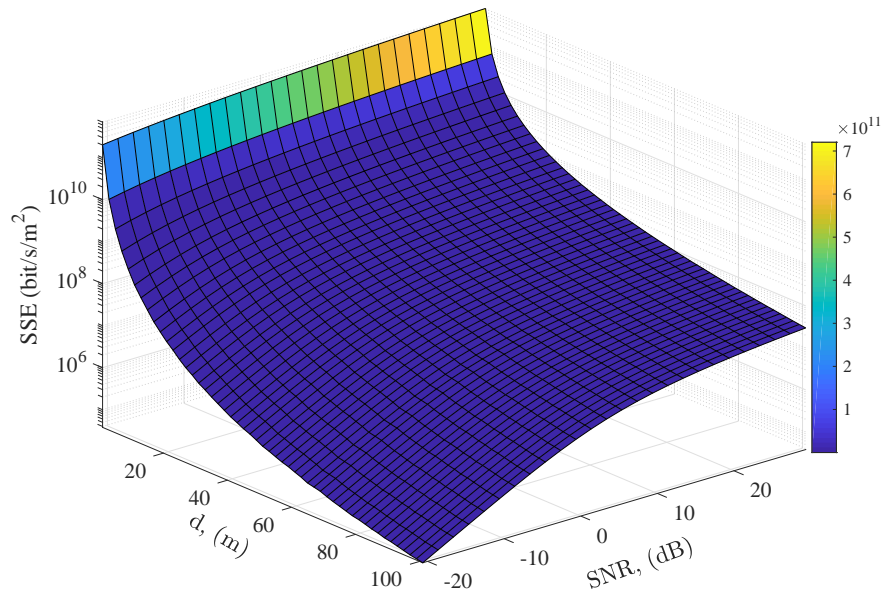
**Figure 9.13:** SSE metrics of mmWave cellular system (73 GHZ band) for LOS link as a function of $d$ and SNR at MU

level of performance for lower values of BS power. Also, it is observed that SEE metric decreases marginally as radius of small cell increases as shown in Figure 9.14. These results show conflict between SE and EE metrics as a function of BS power. For efficient design of mmWave bands a trade off between SSE and SEE metrics is inevitable. The 28 GHz band provides higher EE metric for BS power $P_t > 20$ dBm with acceptable SE metric. On the other hand, 73 GHz is superior in terms of SE metric; however, it performs poorly with respect to EE metric. As regards transmission environment, 28 GHz band superior compared to 73 GHz band for NLOS links, such as that in indoor cellular systems. However, 73 GHz band is more suitable for LOS links, such as that in outdoor cellular systems.
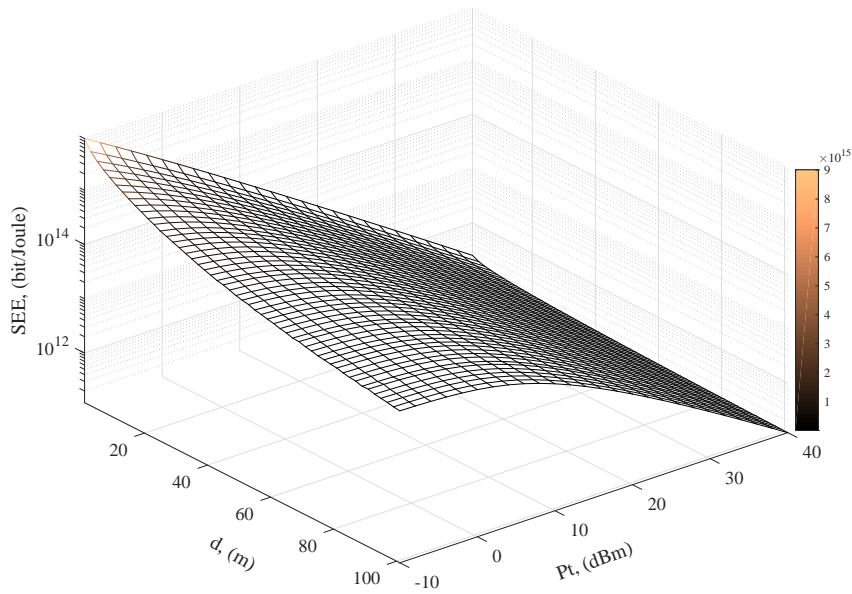
**Figure 9.14:** SEE metrics of mmWave cellular system (73 GHZ band) for LOS link as a function of $d$ and $P_t$

## 9.5 Chapter Summary

In this chapter, mmWave cellular systems are considered in which macrocells are overlaid with a number of smaller microcells. The channel models developed based on real-world field measurements available for LOS and NLOS transmission links have been used to derive expressions for SNR and SINR at MU in cellular system considering intercell and intracell interferences. A framework is presented for design of a mmWave cellular system using analysis of SE, EE, SSE, SEE and delay metrics of the systems. The metrics of the system have been obtained using Monte Carlo simulations, as a function of important system parameters for LOS and NLOS links in 28 GHz and 73 GHz bands. The investigation of metrics of the system as a function of BS power, SNR at MU, distance of MU from BS and type of links in the system is provided. The results show that SE
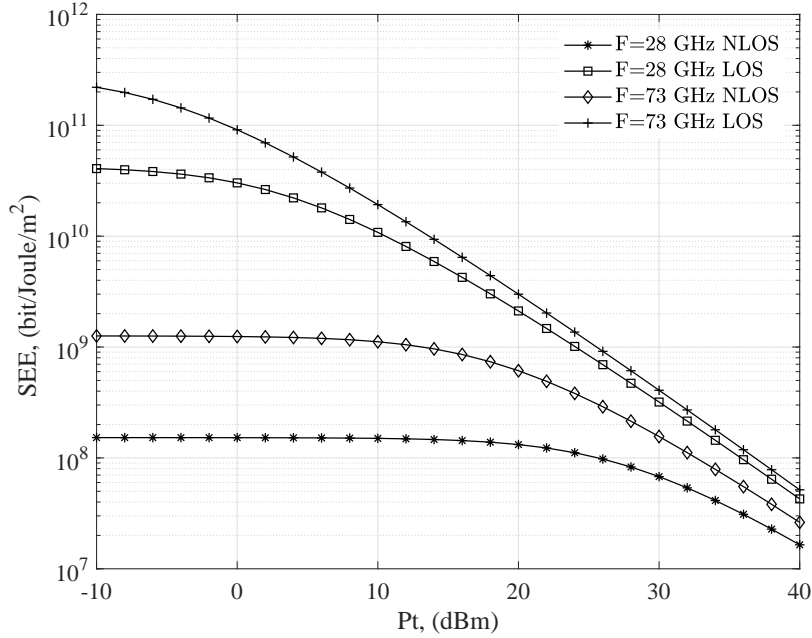
**Figure 9.15:** SEE metrics of mmWave cellular system (73 and 28 GHZ bands) for LOS and NLOS links

metric is always in conflict with EE metric with regard to BS power, and serving distance BS. The 28 GHz band is expedient for NLOS links in the system, and 73 GHz band is more appropriate for LOS links. The efficiency metrics are useful in standardization of mmWave cellular systems, as SE metric provides maximum data rates achievable and transmission ranges mmWave bands and EE metric provides insight into how to utilize energy resource of the system in cells as a function of data rate. It is noted that SE metric of the system is more sensitive to which of 28 and 73 GHz bands is used for NLOS link compared to LOS link. Regardless of whether link is LOS or NLOS in the system, 73 GHz band achieves higher SE metric compared to 28 GHz band. The rate of decay in SE metric is steeper for NLOS link compared to LOS link, as $d$ increases.

# Chapter 10

# Conclusions

## 10.1 Introduction

This Chapter summarizes contributions of this thesis and conclusions drawn from results obtained. Also, areas for further research in the light of future needs of spectral- and energy-efficient wireless communication and cellular systems are outlined. Chapter 2 presented fundamental definitions of performance metrics of communication and cellular systems such as EE, SE, SEE, SSE, coverage probability, and BER. Also, relationship between SE and mutual information of a communication system is discussed. It is demonstrated that there always exits trade-off between power and spectral resources of communication system. Upper bounds on SE and EE metrics of a communication system operating in AWGN are plotted to highlight trade-off between the two metrics. For efficient design of a communication system, sacrifice of one metric for the other is required. This aspect is explained using upper bounds on SE and EE metrics. In designing an efficient cellular system, roles of spatial metrics, SSE and SEE, are discussed using their basic definitions. The importance of power consumption model used in communication system on its EE and SE metrics is also illustrated. The quality of a communication system is expressed using its BER metric. This metric and its relationship to efficiency

metrics are discussed from the viewpoint designing an efficient digital communication system. All metrics described in this Chapter are used throughout the thesis for analysis and design of communication and cellular systems. In Chapter 3, wireless channel models used in the thesis are presented and discussed. In particular, Nakagami-$m$ model is used for modelling multipath fading channel and GK model is used to represent multipath fading coupled with shadowing channel. The statistical descriptions of these models are given and methods used to numerically simulate them in MATLAB environment are also given. These models are good for analysis and design of communication and cellular systems in microwave band, as parameters of models can be adjusted to fit a variety of real-world wireless channel environment. In order to describe mmWave channel behavior, two path loss models one for LOS and the other for NLOS paths in 28 and 73 GHz bands are presented and discussed. These models have been developed using extensive filed measurements and are widely used. In Section 10.2, a summary of contributions of thesis is presented, and in Section 10.3, suggestions for further research are also given.

## 10.2    Summary of Contributions

In Chapter 4, expressions for SE and EE metrics of an $M$-QAM system, over Nakagami-$m$ and GK channels, are derived in closed-form and are investigated as a function of parameters of both system and distributions representing fading and shadowing channels. The numerical results show that EE and SE metrics of system are sensitive to fading and shadowing effects over channel. For example, SE metrics for 16-QAM and 4-QAM systems in GK channel ($m = 1$, $c = 1$) are reduced by 35% and 30%, respectively,

compared to corresponding SE metrics for an AWGN channel. Similarly, EE metrics of 16-QAM system in Nakagami-$m$ ($m = 1$) and GK ($m = 1$, $c = 1$) channels decrease by 31% and 51%, respectively, compared to EE metric of an AWGN channel for same system. In designing an $M$-QAM system careful choice of one metric at the cost of other is inevitable. That is, to design an energy-efficient $M$-QAM system, a sacrifice of its spectral resources must be made. To design an energy-efficient $M$-QAM system, adaptive technique is proposed, in which system adjusts its level of modulation, $M$, based on estimated SNR over channel to achieve maximum EE metric. In this adaptive $M$-QAM system, its EE and SE metrics can be enhanced. For example, EE metric of adaptive system can be enhanced by nearly 8 times and SE metric by 1.4 bits/s/Hz, for $0 \leq$ SNR $\leq 5$ dB, compared to conventional 16-QAM system with both systems subject of severe fading and shadowing (GK channel with $m = 1$, $c = 1$). However, a price in terms of system complexity for adaptive system is inevitable.

In Chapter 5, BER metric of $M$-QAM system is derived in closed-form for GK channels using MGF approach. This metric is illustrated as a function of parameters of system and that of statistical distribution representing GK channel. Power Penalty (PP) required for an $M$-QAM system operating over GK channel relative to the same system operating over an AWGN channel is assessed and illustrated. For example, for a 64-QAM system operating over GK channel ($m = 1$, $c = 5$) to achieve same BER metric ($10^{-3}$) as that of 64-QAM system operating in AWGN channel, nearly 16 dB of additional power is required. An adaptive $M$-QAM system is therefore proposed that can improve BER metric of the system based on estimated SNR, for a set target BER. The system adjusts its level of modulation based on range of estimated SNR and tar-

get BER. An expressions for BER metric of adaptive system is derived using truncated MGF approach and is illustrated. It is noted that the proposed adaptive system assures target BER even when severe fading and shadowing conditions exist over channel (GK channel, $m = 1$, $c = 1$). The adaptive $M$-QAM system is robust to channel conditions and provides a performance superior to that of corresponding conventional system for GK channel. The outage probability of adaptive system is also derived for GK channel and is illustrated. It is observed that, for severe channel environment ($m = 1$, $c = 1$), adaptive system experiences high outage probability, $P_o \geq 10^{-1}$ for $0 \leq \text{SNR} \leq 25$ dB.

Chapter 6 investigated SE, EE and BER metrics of an $M$-CPFSK system over Nakagami-$m$ and GK channels. Closed-form expressions for these metrics have been derived by finding average mutual information of DCMC representing an $M$-CPFSK system. The SE and EE metrics are then examined as a function of modulation index, observation length of receiver, normalized bandwidth and SNR. Numerical results show that efficiency metrics deteriorate as fading and shadowing effects over the channel become severe. For example, SE and EE metrics of a 2-CPFSK system degrade by nearly 25% for severe multipath fading over the channel (Nakagami-$m$, $m = 1$) compared to corresponding SE and EE metrics of the same system in AWGN channel. Also, EE metric of a 2-CPFSK system becomes poorer by 55% when severe fading and shadowing exist over the channel (GK channel with $c = 2$ and $m = 1$) compared to EE metric of the same system in AWGN channel. However, multiple-symbol-observation receiver can be used in the system to make SE and EE metrics of the system less sensitive to fading and shadowing effects over the channel. For example, for $-10 \leq \text{SNR} \leq 0$ dB, SE metric can be doubled and EE metric tripled by using a 5-symbol receiver in a 2-CPFSK system

compared to using one-symbol receiver in the system. The improvement, however, comes at the cost of increased system complexity. The BER metric of 2-CPFSK system for GK channel is derived in closed-form and is illustrated as a function of receiver observation length and GK distribution parameters. Power penalties required for a 2-CPFSK system operating over Nakagami-$m$ and GK channels are evaluated and tabulated. It is worthwhile mentioning that in an $M$-CPFSK system the observation length of receiver can be used as an adjustable parameter based on channel conditions.

Chapter 7 provides a framework for designing an energy- and spectral-efficient cellular system. For three antenna configurations at BS, omni, $60^o$ and $120^o$, cellular system is analyzed using its SE, EE, SSE, SEE and coverage probability metrics. The co-channel interference, path loss and multipath fading are considered in the analysis of these metrics and closed-form expressions are derived and illustrated, as a function of SNR, cell radius, path loss exponent and parameter of fading distribution. Results have demonstrated that antenna sectorization is an effective technique to improve efficiency metrics of a cellular system. For instance, $60^o$ antenna system at BS can enhance SE and EE metrics by 58% and 107%, respectively, compared to that of omni system at BS for $R_d \leq 4$. Also, SSE and SEE metrics of cellular system can be enhanced by nearly three times with coverage probability reproaching to nearly unity. Also, it is noted that efficiency metrics of a cellular system do not improved for $R_d \leq 4$ and hence for designing an efficient cellular systems its dimensions have to be below this value of $R_d$. It can be concluded that sectorized antenna system at BS is the way to go for designing an energy efficient cellular system; however, sectorization increases complexity of the system.

In Chapter 8, analysis and design of efficient MU-MIMO cellular system using its

SE and EE metrics is presented assuming BS in the system is equipped with $\mathcal{M}$ antennas and employs MRC diversity receiver. In the analysis of such a system, path loss, cochannel interference and multipath fading and shadowing effects over the channel are considered. Both fading and shadowing are assumed independent and Gamma distributed. Closed-form expressions for uplink SE and EE metrics of MU-MIMO system at BS are derived using MGF approach and are illustrated as a function of user's transmitted power, normalized reuse distance, antenna array size at BS and number of users in each cochannel cell. Numerical results show that increasing array size at BS can effectively enhance efficiency metrics. For example, SE metric improves at the rate of 0.02 bits/s/Hz/antenna while EE metric by $4.22 \times 10^4$ bits/J/antenna for $R_d \leq 4$. It is observed that increasing the number of users in system reduces its SE and EE metrics due to increased cochannel interference from users, and hence, antenna array size at BS must be increased to maintain or improve system efficiency metrics. Also, it is observed that optimum range of reuse distance is $2 \leq R_d \leq 4$ for efficient design of a MU-MIMO cellular system.

Chapter 9 provided a framework for designing an efficient dense mmWave cellular system using its SE, EE, SSE, SEE and system delay metrics in 28 and 73 GHz frequency bands. The efficiency metrics are evaluated for LOS and NLOS links in the system as a function of power transmitted by BS, user's distance form BS and SNR at MU. Results show that SE metric of the system is more sensitive, for both 28 and 73 GHz bands, for NLOS link compared to LOS link. Regardless of whether link is LOS or NLOS in the system, 73 GHz band is spectrally efficient and 28 GHz band is energy efficient. It can be concluded that while 28 GHz band is expedient for indoor cellular systems, 73 GHz

band is appropriate for outdoor cellular systems. The behavior of efficiency metrics can provide are useful information towards standardization of mmWave cellular systems. Adapting system parameters according to SNR estimation over the channel is a capable method for designing a spectral- and energy-efficient communication systems. The BS antenna sectorization is an effective technique to improves overall energy efficiency of cellular system, but at the cost of increased complexity of the system. In MU-MIMO system, MRC diversity receiver is attractive for designing power efficient cellular systems. Also, increasing antenna array size of MIMO system can significantly improve efficiency metrics of the cellular system. Implementing ultra-dense cellular systems in mmWave bands is an operative solution for providing broadband wireless services with efficient energy consumption.

Overall, in this thesis, a modest attempt has been made to understand how efficiency metrics can be effectively used for designing communication and cellular systems. Although, in the thesis, efficient design and analysis of specific communication and cellular systems are considered, the results are useful in understanding how to trade-off among various metrics of these systems. The research presented can be used in reducing global warming and for sustainable development of energy-efficient systems.

## 10.3    Suggestions for Further Research

This thesis examined the problem of efficient design of communication and cellular systems, including MU-MIMO and mmWave bands cellular systems, using various metrics such as SE, EE, SSE and SEE metrics etc. A major concern for designers of cellular

184

systems is to provide users high data rate so that they can use new broadband services. This objective can be achieved using: *i*) small cell infrastructure, *ii*) huge available bandwidth in mmWave band, and *iii*) using very large number of antennas at BS. The small
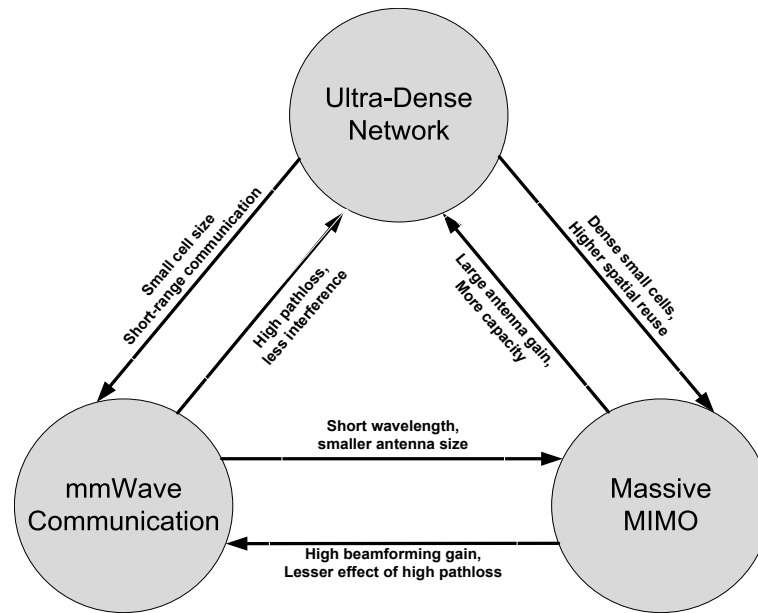


**Figure 10.1:** The symbiotic cycle of the three prominent next generation communication technologies

cell infrastructure can be realized using the concept of ultra-dense network by overlaying macrocell with large number of small cells. The objective thus is to serve each user by BS of single small cell, thereby increasing spectral and energy efficiencies of cellular system. In this approach, users and BSs suffer from severe co-channel interference. Therefore, investigation of uplink and downlink SE and EE metrics of such an ultra-dense system considering co-channel interference and channel effects is an important topic and deserves immediate attention. Providing large bandwidths to users in a cellular system requires a shift to mmWave frequency bands and small cell deployment in the system to overcome path loss and outage issues. The intercell and intracell interferences issue in such a system needs to be tackled effectively. This can be accomplished using massive

MIMO technology with BS equipped with a large number of antennas. Such a system has potential to increase spectral efficiency through the use of spatial multiplexing. At the same time, energy efficiency of the system can also be improved. The symbiotic relationship among the three technologies, mmWave communication, massive MIMO and ultra dense cellular system, is illustrated in Figure 10.1. The massive MIMO technology can be implemented in mmWave bands since wavelength scale is between 1 and 10 $mm$. Combining mmWave communication and massive MIMO technology is a key research trend for designing next-generation cellular systems. Thus, investigation of SE and EE metrics is essential for defining standards for such new systems. The wireless industry's 5G standard addresses demands of business and consumers for the next decade. The 5G is expected to be implemented in next-generation of cellular systems with assumed super-fast connectivity and higher data rates with more reliability. Such systems are going to be spectral- and energy-efficient. The ambitious metrics of 5G cellular systems are shown in Table 10.1 [111]. To achieve these performance metrics, 5G systems have to

Table 10.1: Performance metrics envisioned for 5G systems

| Performance metric | Expected value |
|---|---|
| Latency (ms) | 1 |
| SE (bits/s/Hz) | 10 |
| EE (bit/J) | 1/100 |
| Data rate (Gbps) | 20 |
| Traffic density (Mbits/s/m$^2$) | 10 |

use technologies identified in Figure 10.1. It is noted that mmWave communication and massive MIMO technologies are already candidates for 5G cellular systems [112]. In this system, energy consumption is of utmost importance and, thus, technologies have to be

found to make them energy-efficient.

In Chapter 6, $M$-CPFSK system over fading channel was considered. The observation interval $(n)$ in the receiver of the system plays a vital role in the determination of BER metric of the system. In Figure 10.2, BER vs. $n$ are plotted for SNR= $8, 9$ and $10$ dB, for a 2-CPFSK $(h = 0.715)$ system. It is observed that performance of the system improves as $n$ increases. Therefore, $n$ can be adapted in the system accordingly as channel conditions for maintaining certain level of BER metric in the system. Tis aspect needs further research as a function of modulation index, $h$, and level of modulation, $M$, in the system.
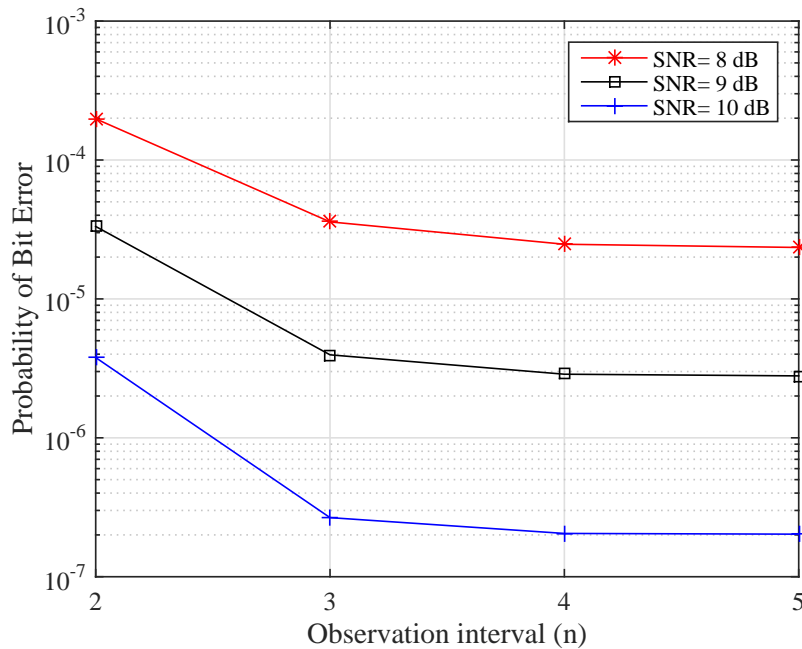


**Figure 10.2:** BER vs $n$ for 2-CPFSK system $(h = 0.715)$, for SNR= $8, 9$ and $10$ dB

Optimization of EE or SE metrics subject to certain constraints such as BER, delay, complexity etc. of the system is a research topic for further research.

From results obtained in this thesis, efficiency metrics are always in conflict. Thus, design

of communication systems that simultaneously satisfy both spectral and energy efficiency requirements can not be achieved. It is observed that sacrifice in one metric leads to significant gain in the other metric. Design of such systems based on weigthed efficiency metrics is open research topic using thesis results.

# References

[1] C. MacGillivray, V. Turner, L. Lamy, K. Prouty, and R. Segal, "Idc future scape: Worldwide internet of things 2017 predictions," in *IDC Web Conference*, 2016.

[2] C. V. N. Index, "Global mobile data traffic forecast update, 2016–2021 white paper, accessed on may 2, 2017."

[3] H. Taoka, "Views on 5G," *DoCoMo, WWRF21, Dusseldorf, Germany, Tech. Rep*, 2011.

[4] R. N. Clarke, "Expanding mobile wireless capacity: The challenges presented by technology and economics," *Telecommunications Policy*, vol. 38, no. 8-9, pp. 693–708, 2014.

[5] X. Ge, J. Yang, H. Gharavi, and Y. Sun, "Energy efficiency challenges of 5G small cell networks," *IEEE Communications Magazine*, vol. 55, no. 5, pp. 184–191, 2017.

[6] D. C. Kilper, G. Atkinson, S. K. Korotky, S. Goyal, P. Vetter, D. Suvakovic, and O. Blume, "Power trends in communication networks," *IEEE Journal of selected topics in quantum electronics*, vol. 17, no. 2, pp. 275–284, 2011.

[7] J. J. Conti, P. D. Holtberg, J. Beamon, A. M. Schaal, J. Ayoub, and J. T. Turnure, "Annual energy outlook 2014," *US Energy Information Administration, Washington DC*, 2012.

[8] A. S. Andrae and T. Edler, "On global electricity usage of communication technology: trends to 2030," *Challenges*, vol. 6, no. 1, pp. 117–157, 2015.

[9] S. Solomon, *Climate change 2007-the physical science basis: Working group I contribution to the fourth assessment report of the IPCC.* Cambridge university press, 2007, vol. 4.

[10] A. Fehske, G. Fettweis, J. Malmodin, and G. Biczok, "The global footprint of mobile communications: The ecological and economic perspective," *IEEE Communications Magazine*, vol. 49, no. 8, 2011.

[11] J. Church and A. Wilkins, "Wireless Competition in Canada: An assessment," 2013.

[12] M. Faccio and L. Zingales, "Political determinants of competition in the mobile telecommunication industry," National Bureau of Economic Research, Tech. Rep., 2017.

[13] I. Res.60-1. (2015) Reduction of energy consumption for environmental protection and mitigating climate change by use of ICT/radiocommunication technologies and systems. [Online]. Available: https://www.itu.int/pub/R-RES-R.60

[14] "Study on energy savings management (ESM)," 3rd Generation Partnership Project, Tech. Rep. 3GPP TR 32.826, March 2010. [Online]. Available: http://www.3gpp.org/ftp/Specs/html-info/32826.htm

[15] C. E. Shannon, "A mathematical theory of communication," *ACM SIGMOBILE Mobile Computing and Communications Review*, vol. 5, no. 1, pp. 3–55, 2001.

[16] G. J. Foschini, G. D. Golden, R. A. Valenzuela, and P. W. Wolniansky, "Simplified processing for high spectral efficiency wireless communication employing multi-element arrays," *IEEE Journal on Selected areas in communications*, vol. 17, no. 11, pp. 1841–1852, 1999.

[17] M. K. Karakayali, G. J. Foschini, and R. A. Valenzuela, "Network coordination for spectrally efficient communications in cellular systems," *IEEE Wireless Communications*, vol. 13, no. 4, pp. 56–61, 2006.

[18] M.-S. Alouini and A. J. Goldsmith, "Adaptive modulation over nakagami fading channels," *Wireless Personal Communications*, vol. 13, no. 1-2, pp. 119–143, 2000.

[19] A. J. Goldsmith and P. P. Varaiya, "Capacity of fading channels with channel side information," *IEEE Transactions on Information Theory*, vol. 43, no. 6, pp. 1986–1992, 1997.

[20] G. Ungerboeck, "Channel coding with multilevel/phase signals," *IEEE transactions on Information Theory*, vol. 28, no. 1, pp. 55–67, 1982.

[21] P. McIllree, "Calculation of channel capacity for m-ary digital modulation signal sets," in *Networks, 1993. International Conference on Information Engineering'93.'Communications and Networks for the Year 2000', Proceedings of IEEE Singapore International Conference on*, vol. 2.   IEEE, 1993, pp. 639–643.

[22] S. Wales, "Spectral efficiency of m-qam in frequency reuse radio systems," *IEE Proceedings I (Communications, Speech and Vision)*, vol. 139, no. 4, pp. 381–385, 1992.

[23] B.-E. Modulations, "Summary of definition, implementation, and performance," CCSDS 413.0-G-1 Green Book, Tech. Rep., 2003.

[24] H. Kwon and T. Birdsall, "Channel capacity in bits per joule," *IEEE Journal of Oceanic Engineering*, vol. 11, no. 1, pp. 97–99, 1986.

[25] L. Zhao, G. Zhao, and T. O'Farrell, "Efficiency metrics for wireless communications," in *Personal Indoor and Mobile Radio Communications (PIMRC), 2013 IEEE 24th International Symposium on*. IEEE, 2013, pp. 2825–2829.

[26] S. Verdú, "Spectral efficiency in the wideband regime," *IEEE Transactions on Information Theory*, vol. 48, no. 6, pp. 1319–1343, 2002.

[27] S. Khakurel, L. Musavian, and T. Le-Ngoc, "Trade-off between spectral and energy efficiencies in a fading communication link," in *Vehicular Technology Conference (VTC Spring), 2013 IEEE 77th*. IEEE, 2013, pp. 1–5.

[28] F. Heliot, M. A. Imran, and R. Tafazolli, "A very tight approximation of the siso energy efficiency-spectral efficiency trade-off," *IEEE Communications Letters*, vol. 16, no. 6, pp. 850–853, 2012.

[29] L. Zhao, J. Cai, and H. Zhang, "Radio-efficient adaptive modulation and coding: Green communication perspective," in *Vehicular Technology Conference (VTC Spring), 2011 IEEE 73rd*. IEEE, 2011, pp. 1–5.

[30] B. Rimoldi, "Design of coded cpfsk modulation systems for bandwidth and energy efficiency," *IEEE Transactions on Communications*, vol. 37, no. 9, pp. 897–905, 1989.

[31] A. Barbieri, D. Fertonani, and G. Colavolpe, "Spectrally-efficient continuous phase modulations," *IEEE Transactions on Wireless Communications*, vol. 8, no. 3, pp. 1564–1572, 2009.

[32] S. Cheng, M. C. Valenti, and D. Torrieri, "Coherent continuous-phase frequency-shift keying: parameter optimization and code design," *IEEE Transactions on Wireless Communications*, vol. 8, no. 4, 2009.

[33] TREND. (2017) Towards real energy-efficient network design, european network of excellence. [Online]. Available: http://www.fp7-trend.eu/content/links

[34] Y. Chen, S. Zhang, S. Xu, and G. Y. Li, "Fundamental trade-offs on green wireless networks," *IEEE Communications Magazine*, vol. 49, no. 6, 2011.

[35] F. Richter, A. J. Fehske, and G. P. Fettweis, "Energy efficiency aspects of base station deployment strategies for cellular networks," in *Vehicular Technology Conference Fall (VTC 2009-Fall), 2009 IEEE 70th.* IEEE, 2009, pp. 1–5.

[36] J. Peng, P. Hong, and K. Xue, "Energy-aware cellular deployment strategy under coverage performance constraints," *IEEE Transactions on Wireless Communications*, vol. 14, no. 1, pp. 69–80, 2015.

[37] J. Akhtman and L. Hanzo, "Power versus bandwidth-efficiency in wireless communications: The economic perspective," in *Vehicular Technology Conference Fall (VTC 2009-Fall), 2009 IEEE 70th.* IEEE, 2009, pp. 1–5.

[38] D. Tsilimantos, J.-M. Gorce, K. Jaffrès-Runser, and H. V. Poor, "Spectral and

energy efficiency trade-offs in cellular networks," *IEEE Transactions on Wireless Communications*, vol. 15, no. 1, pp. 54–66, 2016.

[39] J. Tang, D. K. So, E. Alsusa, and K. A. Hamdi, "Resource efficiency: A new paradigm on energy efficiency and spectral efficiency tradeoff," *IEEE Transactions on Wireless Communications*, vol. 13, no. 8, pp. 4656–4669, 2014.

[40] Y. Li, M. Sheng, C. Yang, and X. Wang, "Energy efficiency and spectral efficiency tradeoff in interference-limited wireless networks," *IEEE Communications Letters*, vol. 17, no. 10, pp. 1924–1927, 2013.

[41] A. M. Alam, P. Mary, J.-Y. Baudais, and X. Lagrange, "Energy efficiency-spectral efficiency tradeoff in interference-limited wireless networks with shadowing," in *Vehicular Technology Conference (VTC Fall), 2015 IEEE 82nd*. IEEE, 2015, pp. 1–5.

[42] J.-M. Gorce, D. Tsilimantos, P. Ferrand, and H. V. Poor, "Energy-capacity trade-off bounds in a downlink typical cell," in *Personal, Indoor, and Mobile Radio Communication (PIMRC), 2014 IEEE 25th Annual International Symposium on*. IEEE, 2014, pp. 1409–1414.

[43] M.-S. Alouini and A. J. Goldsmith, "Area spectral efficiency of cellular mobile radio systems," *IEEE Transactions on vehicular technology*, vol. 48, no. 4, pp. 1047–1066, 1999.

[44] Y. Kim, T. Kwon, and D. Hong, "Area spectral efficiency of shared spectrum

hierarchical cell structure networks," *IEEE Transactions on Vehicular Technology*, vol. 59, no. 8, pp. 4145–4151, 2010.

[45] X. Ge, B. Yang, J. Ye, G. Mao, C.-X. Wang, and T. Han, "Spatial spectrum and energy efficiency of random cellular networks," *IEEE Transactions on Communications*, vol. 63, no. 3, pp. 1019–1030, 2015.

[46] E. G. Larsson, O. Edfors, F. Tufvesson, and T. L. Marzetta, "Massive MIMO for next generation wireless systems," *IEEE Communications Magazine*, vol. 52, no. 2, pp. 186–195, 2014.

[47] D. Gesbert, M. Kountouris, R. W. Heath Jr, C.-B. Chae, and T. Salzer, "Shifting the MIMO paradigm," *IEEE signal processing magazine*, vol. 24, no. 5, pp. 36–46, 2007.

[48] G. Boudreau, J. Panicker, N. Guo, R. Chang, N. Wang, and S. Vrzic, "Interference coordination and cancellation for 4G networks," *IEEE Communications Magazine*, vol. 47, no. 4, 2009.

[49] T. L. Marzetta, "How much training is required for multiuser MIMO?" in *Signals, Systems and Computers, 2006. ACSSC'06. Fortieth Asilomar Conference on.* IEEE, 2006, pp. 359–363.

[50] Marzetta, Thomas L, "Noncooperative cellular wireless with unlimited numbers of base station antennas," *IEEE Transactions on Wireless Communications*, vol. 9, no. 11, pp. 3590–3600, 2010.

[51] H. Q. Ngo, E. G. Larsson, and T. L. Marzetta, "Uplink power efficiency of multiuser mimo with very large antenna arrays," in *Communication, Control, and Computing (Allerton), 2011 49th Annual Allerton Conference on.* IEEE, 2011, pp. 1272–1279.

[52] Ngo, Hien Quoc and Larsson, Erik G and Marzetta, Thomas L, "Energy and spectral efficiency of very large multiuser MIMO systems," *IEEE Transactions on Communications*, vol. 61, no. 4, pp. 1436–1449, 2013.

[53] Z. Liu, W. Du, and D. Sun, "Energy and spectral efficiency tradeoff for massive MIMO systems with transmit antenna selection," *IEEE Transactions on Vehicular Technology*, vol. 66, no. 5, pp. 4453–4457, 2017.

[54] H. B. Almelah and K. A. Hamdi, "On the Downlink Spectral Efficiency of ZF Beamforming over MIMO Channels in Multi-Cell Environments," in *Global Communications Conference (GLOBECOM), 2016 IEEE.* IEEE, 2016, pp. 1–6.

[55] W. Tan, S. Jin, and J. Yuan, "Spectral and energy efficiency of downlink MU-MIMO systems with MRT," *China Communications*, vol. 14, no. 5, pp. 105–111, 2017.

[56] H. B. Almelah and K. A. Hamdi, "Spectral efficiency of distributed large-scale mimo systems with ZF receivers," *IEEE Transactions on Vehicular Technology*, vol. 66, no. 6, pp. 4834–4844, 2017.

[57] Y. Li, P. Wang, F. Chen, G. Wang, and Y. Liu, "Simulation and analysis of millimeter-wave propagation characteristics in complex office environment," *Journal of Computer and Communications*, vol. 3, no. 03, p. 56, 2015.

[58] J. Wells, "Faster than fiber: The future of multi-G/s wireless," *IEEE microwave magazine*, vol. 10, no. 3, 2009.

[59] J. Ko, Y.-S. Noh, Y.-C. Kim, S. Hur, S.-r. Yoon, D. Park, K. Whang, D.-J. Park, and D.-H. Cho, "28 GHz millimeter-wave measurements and models for signal attenuation in vegetated areas," in *Antennas and Propagation (EUCAP), 2017 11th European Conference on.* IEEE, 2017, pp. 1808–1812.

[60] T. Bai, V. Desai, and R. W. Heath, "Millimeter wave cellular channel models for system evaluation," in *Computing, Networking and Communications (ICNC), 2014 International Conference on.* IEEE, 2014, pp. 178–182.

[61] M. R. Akdeniz, Y. Liu, M. K. Samimi, S. Sun, S. Rangan, T. S. Rappaport, and E. Erkip, "Millimeter wave channel modeling and cellular capacity evaluation," *IEEE journal on selected areas in communications*, vol. 32, no. 6, pp. 1164–1179, 2014.

[62] T. Bai and R. W. Heath, "Coverage and rate analysis for millimeter-wave cellular networks," *IEEE Transactions on Wireless Communications*, vol. 14, no. 2, pp. 1100–1114, 2015.

[63] W. Roh, J.-Y. Seol, J. Park, B. Lee, J. Lee, Y. Kim, J. Cho, K. Cheun, and F. Aryanfar, "Millimeter-wave beamforming as an enabling technology for 5G cellular communications: Theoretical feasibility and prototype results," *IEEE communications magazine*, vol. 52, no. 2, pp. 106–113, 2014.

[64] X. Wu, G. V. Eleftheriades, and T. E. van Deventer-Perkins, "Design and characterization of single-and multiple-beam mm-wave circularly polarized substrate lens antennas for wireless communications," *IEEE Transactions on Microwave Theory and Techniques*, vol. 49, no. 3, pp. 431–441, 2001.

[65] Y. P. Zhang and D. Liu, "Antenna-on-chip and antenna-in-package solutions to highly integrated millimeter-wave devices for wireless communications," *IEEE Transactions on Antennas and Propagation*, vol. 57, no. 10, pp. 2830–2841, 2009.

[66] C. Stallo, E. Cianca, S. Mukherjee, T. Rossi, M. De Sanctis, and M. Ruggieri, "UWB for multi-gigabit/s communications beyond 60 GHz," *Telecommunication Systems*, vol. 52, no. 1, pp. 161–181, 2013.

[67] T. Bai, A. Alkhateeb, and R. W. Heath, "Coverage and capacity of millimeter-wave cellular networks," *IEEE Communications Magazine*, vol. 52, no. 9, pp. 70–77, 2014.

[68] W. Tan, P. J. Smith, H. A. Suraweera, M. Matthaiou, and S. Jin, "Spectral efficiency of multi-user mmWave systems with uniform linear arrays and MRT," in *Vehicular Technology Conference (VTC Spring), 2016 IEEE 83rd.* IEEE, 2016, pp. 1–5.

[69] T. A. Khan, A. Alkhateeb, and R. W. Heath, "Energy coverage in millimeter wave energy harvesting networks," in *Globecom Workshops (GC Wkshps), 2015 IEEE.* IEEE, 2015, pp. 1–6.

[70] A. Mesodiakaki, F. Adelantado, A. Antonopoulos, L. Alonso, and C. Verikoukis,

"Energy and spectrum efficient user association in 5G heterogeneous networks," in *Personal, Indoor, and Mobile Radio Communications (PIMRC), 2016 IEEE 27th Annual International Symposium on.* IEEE, 2016, pp. 1–6.

[71] T. Levanen, J. Pirskanen, and M. Valkama, "Radio interface design for ultra-low latency millimeter-wave communications in 5G era," in *Globecom Workshops (GC Wkshps), 2014.* IEEE, 2014, pp. 1420–1426.

[72] Z. Wei, X. Zhu, S. Sun, Y. Huang, A. Al-Tahmeesschi, and Y. Jiang, "Energy-efficiency of millimeter-wave full-duplex relaying systems: Challenges and solutions," *IEEE Access*, vol. 4, pp. 4848–4860, 2016.

[73] R. G. Gallager, *Information theory and reliable communication.* Springer, 1968, vol. 2.

[74] G. Colavolpe, G. Montorsi, and A. Piemontese, "Spectral efficiency of linear and continuous phase modulations over nonlinear satellite channels," in *Communications (ICC), 2012 IEEE International Conference on.* IEEE, 2012, pp. 3175–3179.

[75] E. V. Belmega, S. Lasaulce, and M. Debbah, "A survey on energy-efficient communications," in *Personal, Indoor and Mobile Radio Communications Workshops (PIMRC Workshops), 2010 IEEE 21st International Symposium on.* IEEE, 2010, pp. 289–294.

[76] L. Zhang, H.-C. Yang, and M. O. Hasna, "Generalized area spectral efficiency: An effective performance metric for green wireless communications," *IEEE Transactions on Communications*, vol. 62, no. 2, pp. 747–757, 2014.

[77] J.-M. Gorce, R. Zhang, K. Jaffres-Runser, and C. Goursaud, "Energy, latency and capacity trade-offs in wireless multi-hop networks," in *Personal Indoor and Mobile Radio Communications (PIMRC), 2010 IEEE 21st International Symposium on.* IEEE, 2010, pp. 2757–2762.

[78] O. Waqar, M. A. Imran, M. Dianati, and R. Tafazolli, "Energy consumption analysis and optimization of ber-constrained amplify-and-forward relay networks," *IEEE Transactions on Vehicular Technology*, vol. 63, no. 3, pp. 1256–1269, 2014.

[79] W. Osborne and M. Luntz, "Coherent and noncoherent detection CPFSK," *IEEE Transactions on Communications*, vol. 22, no. 8, pp. 1023–1036, 1974.

[80] M. I. Khalil, "The effect of energy efficiency and spectrum efficiency on bit error rate for unidirectional relay networks," in *Black Sea Conference on Communications and Networking (BlackSeaCom), 2017 IEEE International.* IEEE, 2017, pp. 1–5.

[81] P. M. Shankar, *Fading and Shadowing in Wireless Systems*, 2nd ed. Springer Publishing Company, Incorporated, 2017.

[82] M. K. Simon and M.-S. Alouini, *Digital communication over fading channels.* John Wiley & Sons, 2005, vol. 95.

[83] H. Sajjad and M. Jamil, "Error Rate Performance of Multi-Hop Communication Systems Over Nakagami-m Fading Channel," 2012.

[84] I. S. Gradshteyn and I. M. Ryzhik, *Table of integrals, series, and products.* Academic press, 2014.

[85] A. Goldsmith, *Wireless Communications.* New York, NY, USA: Cambridge University Press, 2005.

[86] A. P. Prudnikov, Y. A. Bryčkov, and O. I. Maričev, *Integrals and Series of Special Functions.* Moscow, Russia, Russia: Science, 1983.

[87] [Online]. Available: http://functions.wolfram.com/PDF/MeijerG.pdf

[88] M. Di Renzo, F. Graziosi, and F. Santucci, "Channel capacity over generalized fading channels: A novel MGF-based approach for performance analysis and design of wireless communication systems," *IEEE Transactions on Vehicular Technology*, vol. 59, no. 1, pp. 127–149, 2010.

[89] L. Hanzo, S. X. Ng, W. Webb, and T. Keller, *Quadrature amplitude modulation: From basics to adaptive trellis-coded, turbo-equalised and space-time coded OFDM, CDMA and MC-CDMA systems.* IEEE Press-John Wiley, 2004.

[90] F. Xiong, *Digital Modulation Techniques, Second Edition (Artech House Telecommunications Library).* Norwood, MA, USA: Artech House, Inc., 2006.

[91] A. J. Goldsmith and S.-G. Chua, "Variable-rate variable-power M-QAM for fading channels," *IEEE transactions on communications*, vol. 45, no. 10, pp. 1218–1230, 1997.

[92] J. B. Anderson, T. Aulin, and C.-E. Sundberg, *Digital phase modulation.* Springer Science & Business Media, 2013.

[93] T. Schonhoff, "Symbol error probabilities for M-ary CPFSK: Coherent and non-coherent detection," *IEEE Transactions on Communications*, vol. 24, no. 6, pp. 644–652, 1976.

[94] M. K. Simon and D. Divsalar, "Maximum-likelihood block detection of noncoherent continuous phase modulation," *IEEE Transactions on Communications*, vol. 41, no. 1, pp. 90–98, 1993.

[95] M. C. Valenti, S. Cheng, and D. Torrieri, "Iterative multisymbol noncoherent reception of coded CPFSK," *IEEE transactions on communications*, vol. 58, no. 7, pp. 2046–2054, 2010.

[96] A. Lereim, *Spectral properties of multi-h phase codes.* Communications Research Laboratory, Faculty of Engineering, McMaster University, 1978.

[97] F. Babich and F. Vatta, "Effects of sectorization on cellular radio systems capacity with different traffic loads," *Wireless Personal Communications*, vol. 21, no. 3, pp. 269–288, 2002.

[98] H. Pervaiz, L. Musavian, and Q. Ni, "Area energy and area spectrum efficiency trade-off in 5G heterogeneous networks," in *Communication Workshop (ICCW), 2015 IEEE International Conference on.* IEEE, 2015, pp. 1178–1183.

[99] J. Chen, L.-C. Wang, and C.-H. Liu, "Coverage probability of small cell networks with composite fading and shadowing," in *Personal, Indoor, and Mobile Radio Communication (PIMRC), 2014 IEEE 25th Annual International Symposium on.* IEEE, 2014, pp. 1965–1969.

[100] F. Rusek, D. Persson, B. K. Lau, E. G. Larsson, T. L. Marzetta, O. Edfors, and F. Tufvesson, "Scaling up MIMO: Opportunities and challenges with very large arrays," *IEEE signal processing magazine*, vol. 30, no. 1, pp. 40–60, 2013.

[101] M. X. Gong, B. Hart, and S. Mao, "Advanced wireless LAN technologies: IEEE 802.11 ac and beyond," *GetMobile: mobile computing and communications*, vol. 18, no. 4, pp. 48–52, 2015.

[102] S. Shrivastava and R. Vannithamby, "Group resource allocation techniques for IEEE 802.16 M," May 19 2015, uS Patent 9,036,728.

[103] H. Ji, Y. Kim, J. Lee, E. Onggosanusi, Y. Nam, J. Zhang, B. Lee, and B. Shim, "Overview of full-dimension MIMO in LTE-advanced pro," *IEEE Communications Magazine*, vol. 55, no. 2, pp. 176–184, 2017.

[104] E. Björnson, L. Sanguinetti, J. Hoydis, and M. Debbah, "Optimal design of energy-efficient multi-user MIMO systems: Is massive MIMO the answer?" *IEEE Transactions on Wireless Communications*, vol. 14, no. 6, pp. 3059–3075, 2015.

[105] H. Q. Ngo, M. Matthaiou, T. Q. Duong, and E. G. Larsson, "Uplink performance analysis of multicell MU-SIMO systems with ZF receivers," *IEEE Transactions on Vehicular Technology*, vol. 62, no. 9, pp. 4471–4483, 2013.

[106] A. Bletsas, H. Shin, and M. Z. Win, "Cooperative communications with outage-optimal opportunistic relaying," *IEEE Transactions on Wireless Communications*, vol. 6, no. 9, 2007.

[107] K. A. Hamdi, "A useful lemma for capacity analysis of fading interference channels," *IEEE Transactions on Communications*, vol. 58, no. 2, 2010.

[108] M. Abramowitz and I. A. Stegun, *Handbook of mathematical functions: with formulas, graphs, and mathematical tables.* Courier Corporation, 1964, vol. 55.

[109] J. Choi, "Energy efficiency of a heterogeneous network using millimeter-wave small-cell base stations," in *Personal, Indoor, and Mobile Radio Communications (PIMRC), 2015 IEEE 26th Annual International Symposium on.* IEEE, 2015, pp. 293–297.

[110] A. Mesodiakaki, F. Adelantado, L. Alonso, M. Di Renzo, and C. Verikoukis, "Energy-and spectrum-efficient user association in millimeter-wave backhaul small-cell networks," *IEEE Transactions on Vehicular Technology*, vol. 66, no. 2, pp. 1810–1821, 2017.

[111] G. I. P. Association *et al.*, "5G Vision-The 5G Infrastructure Public Private Partnership: the next generation of communication networks and services," *White Paper, February*, 2015.

[112] N. Cardona, L. M. Correia, and D. Calabuig, "Key Enabling Technologies for 5G: Millimeter-Wave and Massive MIMO," *International Journal of Wireless Information Networks*, vol. 24, no. 3, pp. 201–203, Sep 2017. [Online]. Available: https://doi.org/10.1007/s10776-017-0366-z

# Curriculum Vitae

| | |
|---|---|
| **Name:** | **Abdulbaset Mustafa Hamed** |
| **Education:** | |

| | |
|---|---|
| **Ph.D.** | Department of Electrical and Computer Engineering |
| 2013 - 2018 | Western University, London, Ontario, Canada |
| *Major* | Communication Engineering |

| | |
|---|---|
| **M.Sc.** | Department of Electrical and Electronic Engineering |
| 2004 - 2008 | Tripoli University, Tripoli, Libya |
| *Major* | Communication Engineering |

| | |
|---|---|
| **B.Sc.** | Department of Electrical and Electronic Engineering |
| 1988- 1993 | Tripoli University, Tripoli, Libya |
| *Major* | Communication Engineering |

**Work Experience:**

- (1998-2006) Intelsat and Arabsat Satellite Earth Stations Communication Engineer, Head of National Satellite Services Department in Libyan Telecommunication Company, Tipoli, Libya.

- (2006-2011) Satellite Control Engineer Thales Alenia Space Company and Rascom-Star Company in RC1 and RQ1R Satellites Canas France, Gharaya Libya.

- (20011-2012) Lecturer, Courses in the area of Communication and Signal Processing, Tripoli University, Tripoli Libya.

- (2013-2017) Teaching Assistant, Digital Communication Systems, and Circuits and Systems, Western university, London, Canada.

**List of Publications:**

- .**Journal Articles**

  [1] Hamed, A., Alsharef, M. and Rao, R.K., "Analysis of Energy and Spectral Efficiency in Urban Shadowing Environment," IAENG International Journal of Computer Science, vol. 43, no.2, pp. 237-244, Jun 2016.

[2] Hamed, A., and Rao, R.K., "Spatial Spectral and Energy Efficiencies of Cellular Networks Limited by Co-channel Interference and Path Loss in Nakagami-$m$ Fading Environment," EURASIP Journal on Wireless Communications and Networking, vol. 2018, no.1, pp. 118-134, 2018.

[3] Hamed, A., and Rao, R.K., "Spectral and Energy Efficiencies in mmWave Cellular Networks for Optimal Utilization," Wireless Communications and Mobile Computing, Hindawi, vol. 2018, pp. 1-12 April 2018.

[4] Hamed, A., and Rao, R.K., "Energy and Spectral Efficiencies of $M$-CPFSK in Fading and Shadowing Wireless Channels," Physical Communication Journal, Elsevier, 2018, pp.1-9.

- **.Book Chapter**

  [1] Alsharef, M., Hamed, A., and Rao, R.K.,"Spectral Properties and Error Rate Performance of Digital Chirp Communication System." In The World Congress on Engineering and Computer Science, pp. 267-288. Springer, Singapore, 2015.

- **.Conference Papers**

  [1] Hamed, A., Rao, R.K. and Primak, S.L., "Adaptive multidimensional modulation over faded shadowing channels," Electrical and Computer Engineering (CCECE), 2014 IEEE 27th Canadian Conference on , vol., no., pp. 1-4, 4-7 May 2014

  [2] Hamed, A., Alsharef, M.,; Rao, R.K., "Bit Error Probability Performance Bounds of CPFSK over Fading Channels," Electrical and Computer Engineering (CCECE), 2015 IEEE 28th Canadian Conference, pp. 1329-1334, IEEE, May 2015.

  [3] Hamed, A.M., Alsharef, M.A, and Rao, R.K., "MGF Based Performance Analysis of Digital Wireless System in Urban Shadowing Environment," Lecture Notes in Engineering and Computer Science: Proceedings of TheWorld Congress on Engineering and Computer Science, pp. 679-684, 2015. <span style="color:red">Best Paper Award</span>

  [4] Alsharef, M., Hamed, A., and Rao, R.K., "Error Rate Performance of Digital Chirp Communication System over Fading Channels," Lecture Notes in Engineering and Computer Science: Proceedings of The World Congress on Engineering and Computer Science, 2015, pp. 727-732, 2015. <span style="color:red">Best Paper Award</span>

  [5] Hamed, A.M., Noorwali, A., and Rao, R.K., "Energy efficient adaptive transmission in generalized-K fading channel." Electrical and Computer Engineering (CCECE), 2016 IEEE Canadian Conference on, pp. 1329-1334, IEEE, 2016.

[6] Hamed, A.M.,; Rao, R.K., "Evaluation of Capacity and Power Efficiency in Millimeter-Wave Bands," The Society for Modeling and Simulation International, 2016 Summer Simulation Multi-Conference (SummerSim'16), pp. 1-6. IEEE, 2016.

[7] Hamed, A.M.,; Rao, R.K., "Bandwidth and Power Efficiency Analysis of Fading Communication Link," The Society for Modeling and Simulation International, 2016 Summer Simulation Multi-Conference (SummerSim'16), pp. 1-7. IEEE, 2016.

[8] Hamed, A.M.,; Rao, R.K., "Energy and spectral efficiency in cellular networks considering fading, path loss, and interference." In Electrical and Computer Engineering (CCECE), pp. 1-5. IEEE, 2017.

[9] Noorwali A., Hamed, A.M., Rao, R.K., "Modelling and Delay Analysis of Wireless HANs in Smart Grids over Fading Channels," Electrical and Computer Engineering (CCECE), 2016 IEEE 29th Canadian Conference, pp. 1-6, IEEE, 2016

[10] Shafter E., Hamed, A.M., Rao, R.K., "PAPR and BER performance analysis of OFDM system with multi-h CPFSK mapper." In Electrical and Computer Engineering (CCECE), 2017 IEEE 30th Canadian Conference on, pp. 1-4. IEEE, 2017.

[11] Hamed, A.M.; Sigiuk, H.,; Rao, R.K., "End-to-End Delay, Throughput, and Performance Analysis of Satellite-UMTS Telecommunication Networks," Electrical and Computer Engineering (CCECE), IEEE 28th Canadian Conference, pp. 1369-1373, IEEE, 2015